Implantable Antennas for Medical Wireless Telemetry Systems Operating in the 900MHz ISM Band

by

Md. Shahidul Islam

Dissertation submitted in fulfillment of the requirements

for the degree of

DOCTOR OF PHILOSOPHY

Department of Engineering

Faculty of Science

Macquarie University

Sydney, Australia

March 2014

ABSTRACT

Physiological signals in animals or humans, such as electrocardiogram (ECG), nerve activity, blood pressure, body temperature, need to be monitored continuously for various therapeutic and biomedical research purposes. Probably, rats are the most widely used animals in the laboratory experiments by the medical researchers to perform their research activities for the development of new drugs and treatment of diseases. They typically use wired systems to transmit biomedical data collected from various transducers to external monitoring or data-logging systems. These signal carrying wires through the skin often cause skin infections and restrict the freedom of rats in terms of their movement or socializing during the term of the experiment and hence weaken the value of the experiments. On the other hand, implantable medical devices for wireless biomedical telemetry systems have been emerging the market in recent years due to the availability of low-cost electronic chips such as RF modules. Few implantable wireless telemetry systems available in the market are inflexible and expensive while the wireless telemetry systems designed for free space link do not work when implanted, primarily because their antennas get detuned due to the presence of the skin and/or other body material.

To develop an implantable wireless biomedical telemetry system, a compact and efficient antenna is the most important and essential element of the system. However, the design and implementation of an electrically small implantable antenna is a challenging task, specifically, if it is implanted in a small animal such as a rat. Significant challenges exist in the UHF implementation because of the electromagnetic (EM) wave interactions with the surrounding biological tissue, complexity of the biological tissue, the need for antenna miniaturization, and power minimization of implantable device and biocompatibility

requirements. This dissertation presents the designs, implementations and validations of a few implantable planar inverted-F antennas (I-PIFAs). They all have full ground planes, as opposed to the partial ground plane of the original free-space antenna for a RFID system under development, to maximize the energy radiated out of the body and to minimize that into the body. Yet the developed antennas are much smaller than the original free-space antenna located on a RFID tag. The larger ground plane of RFID tag is utilised with the antenna ground plane to enhance the antenna performance. The antennas performances were evaluated by studying the bandwidth impedance, radiation pattern and input reflection coefficient characteristics inside the rat body model. To monitor a physiological signal (temperature) from rat skin remotely, one of the proposed antennas was attached with the implantable RFID tag circuit board. In addition, proximity feed technique was applied to the antennas for widening bandwidth (BW) as detuning of the operational frequency of the implanted antenna occurs due to the effect of bio-compatible coating material as well as rat tissue.

In order to get an idea on the range of detuning of an antenna because of its surrounding biological tissue environment, a preliminary experiment was conducted with a commercial antenna (ANT403-SP, Linx Technologies) in the 400MHz Medical Implant Communication Services (MICS) band. Two antenna feeds (co-planar, CPW and a micro-strip, MS) were designed and implemented for the antenna. A decrease in resonance frequency between 15% and 20% (400MHz to 320MHz) is found. It was also noted that, at a -10dB input reflection coefficient, the impedance bandwidth of the antenna was increased for both the feed schemes as a result of external (FR4 board and rat skin) loading.

Due to frequency shifting downwards with implantation, a series of I-PIFAs were designed, and simulated by commercial antenna simulation software (CST Microwave Design Studio). An UHF RFID system under development for free space was chosen and three I-PIFAs were fabricated to validate their functionalities for the implantable RFID telemetry system in the 900MHz Australian ISM band. At first, the RFID system was tested and it

worked well in free space in the UHF ISM band. However, the RFID system did not work at all once the RFID-tag PCB was covered with fresh rat skin samples collected from the Australian School of Advanced Medicine, Macquarie University, Australia. This initial investigation confirmed that the existing RFID-tag antenna is useless for an implantable system and motivated us to replace it with an implantable antenna with a larger BW so that the antenna can be functional in the desired UHF Australian ISM band. The fabricated antenna is compact with an approximate volume of 270mm^3 while the bandwidth is about 20%. The antenna was attached to a RFID-tag PCB, coated with MED 1134 (a medical-grade bio-compatible material) and placed under the fresh rat skin tissue. The implantable antenna was tested and the optimum RFID data reading range was determined to be 0.8m.

STATEMENT OF CANDIDATE

I certify that the work in this thesis has not previously been submitted for a degree nor has it been submitted as part of the requirements for a degree to any other university or institution other than Macquarie University.

I also certify that the thesis is an original piece of research and it has been written by me.

In addition, I certify that all information sources and literature used are indicated in the thesis.

. . . . . .

Md. Shahidul Islam

ACKNOWLEDGMENTS

Firstly, I am grateful to my parents who have shown me the light of this beautiful world and motivated me for study from my childhood. Secondly, I would like to express my gratitude to my principal supervisor, Professor Karu Esselle, for spending his invaluable time to review and feedback on my PhD thesis. He has reviewed my thesis even when he was on holidays. It would not have been possible to produce thesis without his kind support. His expertise in the field of antenna helped me a lot to complete my research. Definitely, he deserves my admiration as a person as well as my principal supervisor. I would also like to thank my associate supervisor, Professor Paul Pilowsky, for his important guidance from medical point of view and help to collect fresh rat skin samples for my project. My gratitude also goes to my adjunct supervisor, Mr. Dadid Bull, CEO of BCS Innovations, Sydney, Australia. He has provided his industrial expertise support towards my project, specifically, the RFID tag printed circuit board and identifying suitable biocompatible material for coating the implantable antenna. I am also grateful for his approval in funding some of my conference travel. I am also grateful to A/Professor Ladislau Matekovits from Politecnico di Torino University, Italy, for his review and support for my few research papers while he was a visiting research fellow at Macquarie University, Australia. My heartiest gratitude goes to Dr Keith Imrie, from the Department of Engineering, in proof-reading my thesis within a few days only. I appreciate his corrections since it has helped me towards my thesis preparation.

I am indebted to my wife Tahmina, my son Sakib and my daughter Samira for their patience and understanding my situation for not taking them for amusements during the holidays. I would like to thank my friends, Dr. Kashem Muttaqi, Dr. Dushmantha Thalakotuna, Dr Yogeshwar Ranga, Basit Ali Zeb, Ariful Huq, Debabrata Karmokar, Raheel Hashmi, Selim

Hossain, Syed Irfan and Syed Abbas for their help and support throughout my thesis. I also gratefully acknowledge the Macquarie University Research Excellence Scholarship (MQRES) given to me for three and a half years.

Contents

Chapter 7 Design, Fabrication and Measurements

Chapter 8 Conclusion and Future Work

List of Figures

Chapter 1

Introduction

1.1 Motivation

Implantable antennas for wireless bio-telemetry applications are attracting more attention among antenna researchers in recent years due to their ability to transmit physiological signals from the body of a human or animal to an external base station without wires passing across the skin. However, one of the greatest challenges is the miniaturisation of the antenna, specially, if it is to be implanted in a small animal, for example, in a rat, generally used by medical researchers in the laboratory. The planar inverted-F antenna (PIFA) is a potential candidate for implantable devices for bio-telemetry applications. PIFA is a low profile, compact antenna. It has gained significant attention from researchers and academia due to these advantages. However, a major drawback of the PIFA is its narrow operating bandwidth. Therefore, antenna researchers have developed several techniques recently to overcome this bandwidth limitation of the PIFA antenna. To overcome the narrowband drawback of PIFA, in this thesis all PIFA antennas have been designed with sufficient heights compared to radio-frequency identification (RFID) tag printed circuit board (PCB).

Another challenge in our RF telemetry system arises from the effects of the body material of experimental rats, such as skin, fat and tissue. The bandwidth of the PIFA antenna is reduced further in some cases, for instance, when the relative permittivity of the rat skin is increased. Of course, the relative permittivity and the conductivity of the rat's skin, fat and muscle are not constant all the time. Ageing, weather condition, stress

on its freedom etc. can change the relative permittivity and conductivity of rat's body tissues and ultimately can de-tune the resonance frequency of the implanted antenna.

During my PhD, few implantable PIFAs have been designed for a specific active (RFID) tag provided by our industry partner and one of them was fabricated and tested with the antenna covered by rat skin. Then a fabricated antenna was integrated to the RFID tag and the system was demonstrated with the new implantable antenna covered by rat skin. The functionality of the implantable PIFA antenna was validated by wirelessly monitoring the temperature, sensed by the RFID tag from a remotely located commercial RFID reader.

1.2 Implantable Wireless Bio-Telemetry

New technologies have been developed in the last decade to measure physiological parameters such as temperature, ECG, blood pressure in humans and laboratory animals. The rats are the most commonly used laboratory animals for pursuing medical research for testing and development of new medicine. However, majority of previous research had to be conducted using wired telemetry systems, limiting animal's mobility during the experiments. Although few wireless (implantable) medical telemetry systems are, commercially available, they are too expensive for most medical researches and they are not flexible. Therefore, in this PhD project, I aimed to convert a wireless telemetry system designed to work in air to an implantable wireless telemetry system, to enable medical researchers, to measure and monitor the physiological signals in the body of rats. The most challenging part of this project was to design and fabricate a small and suitable implantable antenna that will fit into the small area available in the sensor tag

provided by the industry partner. Smaller antenna size, variations in electrical properties of rat's body tissue, rat's behaviour and movement, size and weight of rats etc. imposed great challenges. ECG signal rate in rats terms of beats per minute (BPM) is higher than that of humans and as a results higher data rate is necessary for transmitting readings from the implanted unit to external monitoring unit. Fig. 1.1 shows the block diagram of the implantable bio-telemetry system.

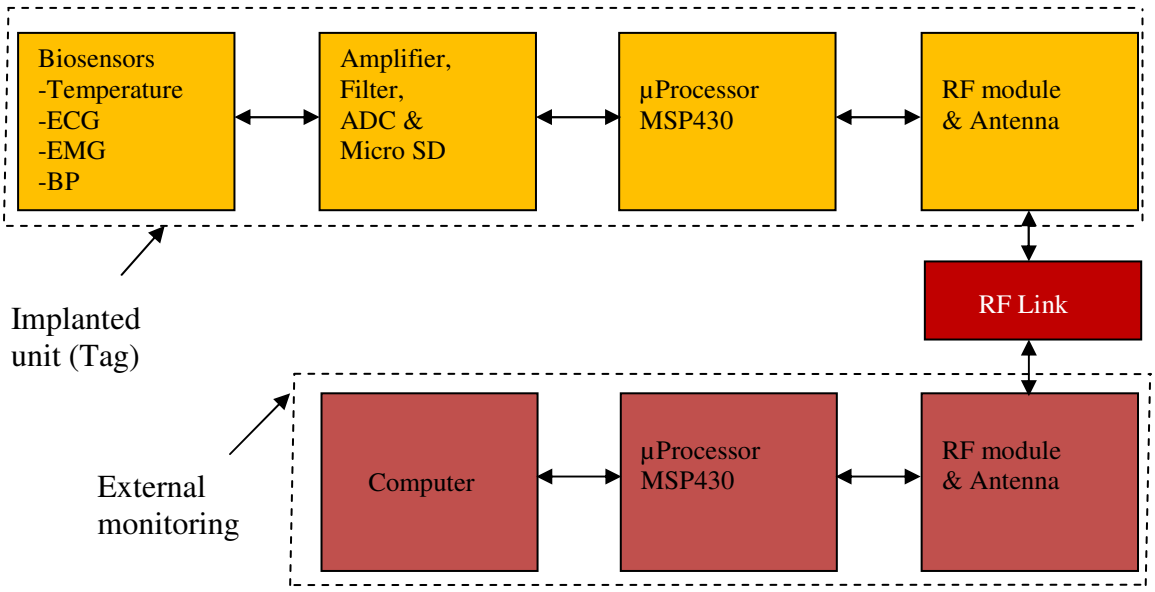

Fig. 1.1: Block diagram of an implantable bio-telemetry system

1.3 Goals of the Thesis

- To convert an existing active UHF RFID tag from Global Safety Solutions and Management Pty Ltd (GSSM Active Tag V1.0), developed for free space bio-telemetry applications by the industry collaborator, into an implantable RFID tag suitable for implantation in rats.
- To design miniaturized implantable antennas for the said bio-telemetry application and test some of them.

- To attach the fabricated antenna to demonstrate operation of the RFID tag for the wireless bio-telemetry system, with the tag kept under rat skin.

1.4 Organization of the Thesis

Chapter 2 is a literature review of recent implantable small antennas for RF bio-telemetry systems targeted for laboratory animals such as rats. Some wireless bio-telemetry systems are also described in this chapter. Link budget for an implantable wireless telemetry is presented at the end of the chapter.

In **Chapter 3**, frequency detuning study of a commercial antenna, when placed under rat skin is studied. A commercial antenna operating in the MICS band was selected and coplanar and microstrip feeds were designed to measure its return loss when it is covered by fresh rat skin samples collected from the research collaborators at the Australian School of Advanced Medicine.

Design and simulation results of a new implantable partially folded PIFA for Australian UHF ISM band are presented in **Chapter 4**. Parametric studies on the antenna and its surrounding environment parameters were conducted and provided in this chapter. Optimised values for few parameters obtained from parametric studies are also described.

Chapter 5 describes the designs of three implantable small PIFAs to be attached to the component-side of the RFID tag PCB provided for this project by the industry partner, BCS Innovations. Comprehensive parametric studies of the designed implantable antennas are also presented in this chapter.

The design and simulation results of a new implantable compact PIFA, to be attached to the ground-plane side of an RFID tag PCB, are given in **Chapter 6**. Results of antenna parametric studies and optimised simulation results are provided at the end of the chapter.

In **Chapter 7**, a new compact implantable antenna design is presented. Fabrication of its prototypes and their measured results are also presented. After attaching the new antenna to the RFID tag, the operation of the telemetry system was demonstrated, with the RFID tag placed under the rat skin. The temperature reading taken by the sensor in the tag was transmitted wirelessly to a remote RFID reader for this demonstration. The rat skin temperature result of the bio-telemetry system is also given after attaching the fabricated antenna with the RFID tag circuit board.

Finally, **Chapter 8** concludes the project descriptions and recommends possible future work.

1.5 Publications

Some works of the thesis have been published or accepted for publication. The list of published or accepted papers is provided below.

- **(2014) M. S. Islam**, Karu P. Esselle, David Bull, and Paul M. Pilowsky, "Antenna Design and Placement Options for an Implantable Wireless Medical Telemetry System," Proc. 2014 IEEE International Symposium on Antennas and Propagation (APSURSI), Tennessee, USA, July 2014 (accepted).
- **(2014) M. S. Islam**, Karu P. Esselle, David Bull, and Paul M. Pilowsky, "Implantable Compact Antennas for Wireless Bio-Telemetry: A Comparative Study," IEEE -

iWAT2014 International Workshop on Antenna Technology, March 2014, Sydney, Australia.

- **(2013) M. S. Islam**, Karu P. Esselle, David Bull, and Paul M. Pilowsky, "Making a Telemetry System Implantable: Challenges and Opportunities in Antenna Design," IEEE MTT-S IMWS -Bio 2013, RF and Wireless Technologies for Biomedical and Healthcare Applications, Dec 2013, Singapore .
- **(2013) M. S. Islam**, Karu P. Esselle, Ladislau M., David Bull, and Paul M. Pilowsky, "An Implantable PIFA Antenna with a J-Shaped Proximity Feed for RFID Telemetry," Proc.2013 IEEE International Conference on Applied Electromagnetics and Communications (ICECom), Dubrovnik, Croatia, October 14-16, 2013
- **(2013) M. S. Islam**, Karu P. Esselle, Ladislau M., David Bull, and Paul M. Pilowsky, "An Implantable Hilbert PIFA Antenna for an RFID- Based Telemetry System," Proc. 2013 IEEE International Conference on Electromagnetics in Advanced Applications (ICEAA), Torino, Italy, September 9-13, 2013.
- **(2013) M. S. Islam,** Karu P. Esselle, David Bull, and Paul M. Pilowsky, "An Implantable PIFA Antenna with Slotted Ground Plane," 13th Australian Symposium on Antennas, ASA 2013, Sydney, Australia.
- **(2012) M. S. Islam,** Karu P. Esselle, David Bull, and Paul M. Pilowsky ," Bandwidth enhancement of an implantable RFID tag antenna at 900 MHz ISM band for RF telemetry," IEEE 12th International Symposium on Communications and Information Technologies (ISCIT 2012), Australia, October 2012.
- **(2012) M. S. Islam,** Karu P. Esselle, David Bull, and Paul M. Pilowsky, "A Miniaturized Implantable PIFA Antenna for Indoor Wireless Telemetry," Proc. 2012 IEEE International Conference on Electromagnetics in Advanced Applications (ICEAA 2012), pp. 526-530, Cape Town, South Africa, 2-7 September 2012.

- **(2012) M. S. Islam,** Karu P. Esselle, David Bull, and Paul M. Pilowsky, "Design of an implantable antenna to acquire physiological signals from rats," Proc. 2012 IEEE International Symposium on Antennas and Propagation (APSURSI), ISBN978-1-4673-0462-7, paper no. IF15.13, Chicago, USA, July 2012.
- **(2011) M. S. Islam,** Karu P. Esselle, David Bull, and Paul M. Pilowsky," Effects of rat skin on the resonance frequency: An experiment with a commercial antenna for an implanted telemetry system," Proc. IEEE TENCON 2011, Nov 2011, Bali, Indonesia.
- **(2011) M. S. Islam,** Karu P. Esselle, David Bull, and Paul M. Pilowsky and Haichao Jing, "An Implantable RF Telemetry System for Rats: Design Issues" 12th Australian Symposium on Antennas, ASA 2011, Sydney, Australia.

Chapter 2

Background

2.1 Introduction

In this chapter, related works in the field of implantable antenna and wireless telemetry systems for small laboratory animals are reviewed. Challenges to implement such systems are highlighted with probable solutions are proposed by the author. Implantable wireless systems are a broad area of research and firstly we focus on this broad area. Secondly, we try to narrow down the literature review for our particular application that is, RFID-based wireless bio-telemetry in which RFID tag is to be implanted in a rat.

Generally, implantable wireless systems for small laboratory animals may be divided into two major units: Internal unit and external unit. The internal unit is implanted inside the body of the animal and external unit is located outside the body. Typical separation between the internal and external units is few centimetres to few metres. Internal unit may be powered by a battery implanted with the unit. The implanted battery may be re-charged using inductive coupling. The external unit is not so challenging compared to its internal counterpart. The internal unit usually consists of sensors to sense the vital signs from the body of small animals, a pre-amplifier to amplify low level vital signs (signals), a micro-processor, a micro-storage device, RF module and most importantly a miniature, light-weight, efficient antenna. The link between the units may be unidirectional or bidirectional as required by the application. Our proposed system is a bidirectional RF implantable system for laboratory rats. Whether the power to this

implantable unit is from coupling or from a small battery, the power consumption of the unit must be minimised.

The planar inverted-F antenna (PIFA) has attracted attention recently for several applications including mobile handsets and RF telemetry. It is a low-profile and compact antenna. Therefore, it is desirable for space-limited applications including implantable medical devices for small animals. In this study, one aim was to design a compact wideband PIFA antenna operating at 900MHz. It will be integrated to an existing RFID-based telemetry unit and will be implanted inside rats. Another aim was to assess antenna sensitivity to changes in the rat-body environment. Among small animals, rats are widely used in laboratory experiments where it is necessary to measure their physiological signals such as nerve activity, electrocardiography (ECG) waveforms, pH levels, temperature, blood pressure.

Antennas play an important role in any RF system. In telemetry, they make feasible transmitting and reception of signals between the implantable device and the external base station. Since the antenna needs to transmit captured physiological signals to an external unit such as an RFID reader, an efficient implantable antenna is essential for RF telemetry. In [1], a study of a capacitively-fed microstrip antenna element has been conducted to demonstrate a bandwidth enhancement. However, the size of the antenna is considerably large. Capacitive matching of microstrip patch antennas is described in [2], exploring the improvement of antenna performance. Another capacitively-coupled microstrip antenna is presented in [3] to minimize the antenna input port return loss so that maximum power transfer from the RF chip to the antenna is ensured. A PIFA antenna fed by electromagnetic coupling has been analysed in [4]. Its authors have elaborated the benefits of capacitively-coupled approach for designing PIFA antennas. The key benefits

of capacitively-coupled feed approach to a PIFA are bandwidth enhancement, compactness and easier input impedance matching capabilities. In [5], a broadband PIFA with capacitively-coupled feed is proposed for free-space applications. This paper demonstrated the possibility to increase the bandwidth of a PIFA antenna with capacitively-coupled feed over a conventional PIFA antenna. Although these publications have contributed significantly for the development of compact and efficient PIFA antennas, the inherent narrow-bandwidth limitation of PIFA antennas is still a challenging task, in particular, for implantable antennas. In [6], the permittivity and conductivity of rat skin have been measured and implantable antennas have been designed for medical wireless telemetry. Three rat samples have been used for measurements. Design of an implantable PIFA antenna to acquire physiological signals in rats has been described in [8] with antenna's surrounding environment model.

Rodents (small animals), particularly rats, are probably the most widely used in the laboratory. RF telemetry systems are desirable to extract and transmit physiological signals from their body to a base station, which is connected to computers of medical researchers who analyse these signals for different purposes, e.g. for the development of new drugs even for human treatment. A battery-less implantable blood pressure monitoring system for laboratory rats [7] has been designed and implemented. In [11], a portable telemedicine system is described for biomedical applications.

A space filling curve is defined as a continuous curve with the range of generally 2-dimensional square unit or 3-dimensional cube unit. Space filling curves such as Hilbert, Peano etc. have been recently utilized with planar inverted-F antenna for various applications including RFID telemetry systems [9-10]. Space filling curves are preferred

because they provide compactness to the PIFA antenna. Moreover, the operating frequency of the antenna can be changed with the number of iterations of the space filling curves while maintaining a fixed dimension. Hence, optimization of the antenna parameters could be performed which are important requirements to design PIFA for space-limited RFID telemetry applications. For instance, the thickness of the space filling curve trace and/or the dimension of the gap between two adjacent traces can be considered in the cost function as variables to achieve the desired antenna characteristics, as already reported in the literature [9-10]. The effectiveness of space-filling fractal geometry in lowering resonant frequency is presented in [9]. A down-sized printed Hilbert antenna [10] for UHF band provides usefulness of such space filling curve for designing PIFA antenna. Furthermore, design and implementation of implantable antennas [12-17] have been reported for telemetry applications in the recent years. One objective of my study was designing a compact Hilbert PIFA antenna operating at 900 MHz ISM band that can be interfaced with the-tag RFID-tag circuit board, I have been given by the industry partner. My implantable Hilbert PIFA antenna is to be implanted under the skin of experimental rats. This antenna design is novel in light of referenced implantable antennas since it is customized according to limited space available on RFID tag circuit board.

In recent years, several implantable and electrically small antennas have been designed and realized in wireless biomedical applications [18]–[22]. A dielectric loaded impedance matching for wideband implanted antennas has been presented in [23], in which a novel dipole antenna for implantable applications in ultra-wideband (UWB) is designed and numerically characterised. A miniature triple-band antenna for RF telemetry applications is presented in [15].

The main purpose of this dissertation is to design a compact implantable antenna to satisfy the space limitation on an existing RFID tag. After the illustration of the antenna physical and environment model, the reported results associated to an optimized geometry through a parametric study confirm the features of the proposed innovative geometry. However, design and implementation of an electrically compact implantable antenna is a major challenge due to the complex nature of rat's body tissues between the transmitter and receiver.

2.2 Challenges of Implantable Systems for Small Animals

Designing and fabricating miniature antenna, impedance matching at the body-air interface, overall size of the implantable unit, biocompatibility with the body tissue, power consumption by internal unit, surgical procedure, smallest range of the link between the internal and external units are the most challenging tasks accounted with the design of implantable systems for small animals. Some compromises are necessary on cost, quality of service, the size of the implantable unit and the range of the link. Heart beats of small animals such as laboratory rats is much higher (average, 250 beats per minute) than larger animals, for example cows. This sets a higher data rate transmission requirement through the wireless link. Therefore, it is a difficult task to achieve the optimum value at the same time for all the variables associated with the implantable systems. The overall volume of the implant must be small enough to accommodate under the skin of rat and thickness of the implant should not exceed 10mm. Bio-compatible insulation of the implant must be thin so that it will not contribute significantly to thickness of the implant. RF chip/modules often have different impedance rather than 50Ω input impedance of standard antennas and it needs to be transformed before connecting the antenna. Resonant frequency must be within the 900MHz ISM band.

Detuning effects due to coating and rat's body tissues must be considered. IEEE standard for radiation must be followed. Power consumption of the antenna should be small. Rat's body tissue model must take into account of the physical size of the rat.

Implanted antenna design has the following challenges to be faced.

- Characterization of antenna with a phantom or an equivalent solution similar to rats body tissue material.
- Design and implementation of low-profile antennas matched to the environment of the rats' body;
- Preference for simplified geometries for low-profile antennas implanted in the rats' body
- Estimation of the performance of indoor wireless link of the implanted antennas with consideration given to the maximum Effective Radiated Power (ERP) and Specific Absorption Ratio (SAR) limitations.

Table 2.1: A Comparison between MICS Specifications with the IEEE 802.15.4 Standard Used for WSNs [25]

Parameter	**MICS**	**IEEE 802.15.4**
Frequency	402-405 MHz	868 MHz (EU)
		916 MHz (US)
		2.4 GHz (Worldwide)
Bandwidth	300 KHz	62.5 KHz (for 2.4 GHz)
Data rate	>250 kbps	250 kbps (for 2.4 GHz)
Transmit power	25 μW	0.5 mW
Maximum link range	2 meters	10 meters

With the time constraint of the project, I mainly focused on the implantable RF systems. Medical Implantable Communications Service standard and IEEE 802.15.4 are widely used to implement implantable RF systems. A comparison between MICS specifications [25] with IEEE 802.15.4 standard used for wireless sensor networks is shown in Table 2.1. Of course, each of the two standards has some drawbacks compared to the other. Therefore, a trade-off is usually made for a particular application.

2.3 Implantable Antennas

Antenna is one of the essential components for RF systems. Some of them that are suitable for implantable RF systems are reviewed in this section in line with the system considered in our project. Reasons for wide variety of antenna types are the different requirements as:

- Operating frequency
- Power level (maximum voltage and current)
- Efficiency
- Bandwidth or operating frequency range
- Cost
- Size
- Gain.
- Technology.
- Applications.

2.3.1 Implantable Loop Antenna

In Fig. 2.1, an Implantable Small Loop Antenna [26] tag is proposed. It could be implanted under the skin of Steller's sea lions for tracking purpose. The author measured the impedance of the antenna using two types of housing: alumina and Acrylonitrile Butadiene Styrene (ABS). However, tissue simulating material was used for this measurement. Power loss measurement and impedance matching are also proposed to improve the efficiency of the antenna. The antenna has been tested in sea lion after interfacing with an RFID tag.

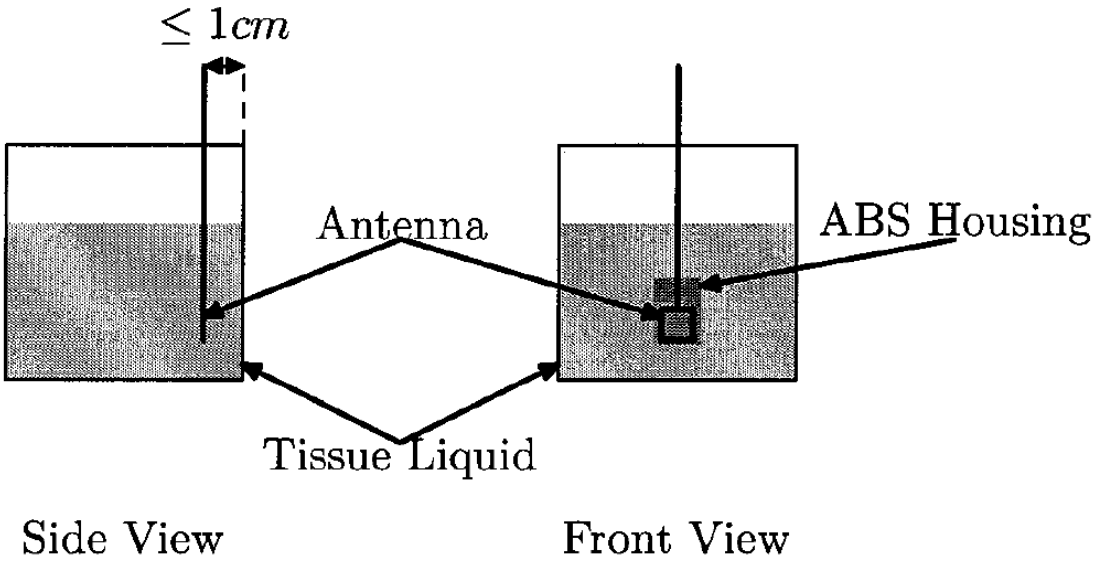

Fig. 2.1: An implantable small antenna and its housing [26]

Simplicity of the design and the transmission power efficiency improvement by the impedance matching slab on the skin are the advantages of this implantable loop antenna. However, the perimeter of the loop antenna (single turn) is 10cm which is quite large to be implanted in a small animal. Because of the single turn its radiation efficiency is low and placing matching slab on outer surface of the animal skin is not practical. Therefore, this type of loop antenna is not suitable to be interfaced in our RFID tag as the space for

antenna is limited (15mm×33mm). In addition, it is also not suitable to be implanted in a rat because of the size and weight of the rat.

2.3.2 Implantable Serpentine Antenna

Fig. 2.2 shows an implantable serpentine dualband antenna (400MHz and 2.4 GHz) with its operating environment (three-layer tissue model) whose parametric evaluation was performed within this human phantom [19]. A phantom consisting of three tissue layers (Fig. 2.2(b)),

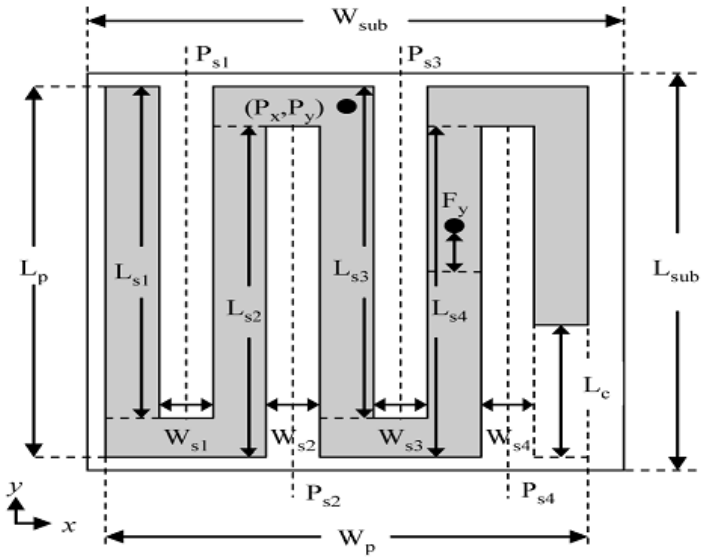

(a)

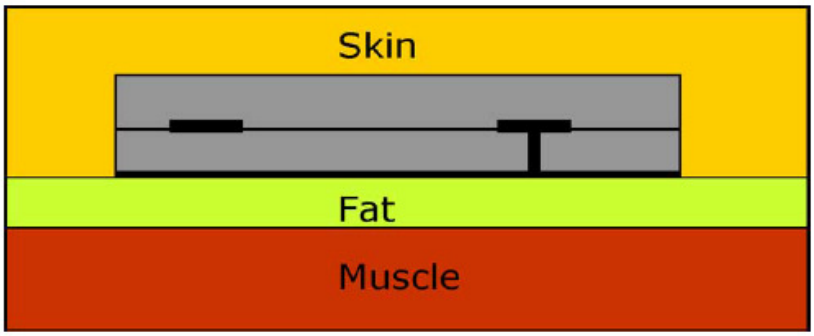

(b)

Fig. 2.2: An implantable dual-band antenna and its surrounding human tissue model; (a) Antenna geometry; (b) Skin-fat-muscle tissue model of human [19].

equivalent to human body tissues (skin, fat, and muscle) was developed to simulate the performance of the antenna (Fig. 2.2(a)) in the presence of these tissue layers. The overall size of the antenna is 23mm×23mm×2.5mm and this is still considered to be a large antenna for implantation in human body. In addition, there are sharp corners at various locations of this micro-strip implantable antenna. For a freely moving humans or animals, it is desirable that the antenna has round corners. Another expectation of the implantable antenna is the biocompatibility. Simulated results matched well with the measurement results. Model of the human body was used instead of testing within real human body. The antenna parameters were optimized by particle swarm optimization method.

2.3.3 Implantable Compact Patch Antenna

A novel 434 MHz compact patch antenna (Fig. 2.3) was proposed in [27]. The dimensions of the antenna is 130mm×130mm×2.97mm including the substrate and this antenna is intended to be implanted in human body. The antenna is slightly larger to be implanted in human compared to recently presented antennas in literature. The radiating patch is composed of a circular patch and an annular ring.

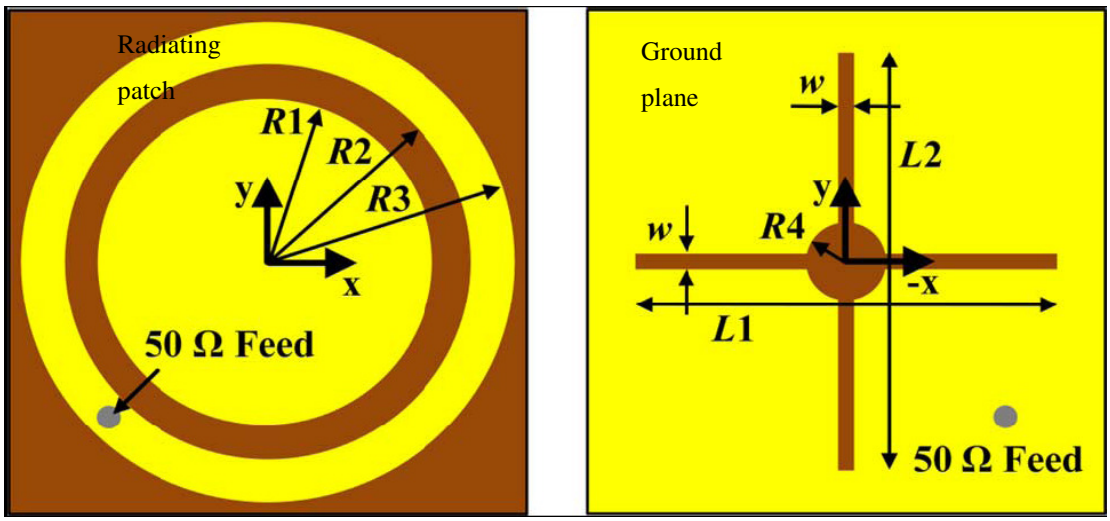

Fig. 2.3: A novel 434 MHz compact patch antenna [27]

2.3.4 Implantable Planar Inverted-F Antenna (PIFA)

In [28], a planar inverted-F antenna (PIFA at 402-405 MHz) for medical implant telemetry system (MITS) was proposed. The dimensions of the antenna were 39mm×30mm×9mm including the ground plane while the actual size (radiating element) of the antenna is 35mm×20mm. The antenna was attached to cardiac pacemaker in order to monitor cardiac beat.

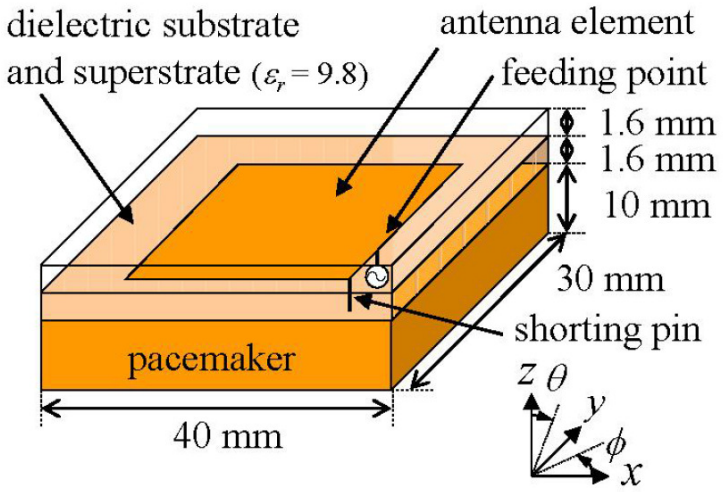

(a)

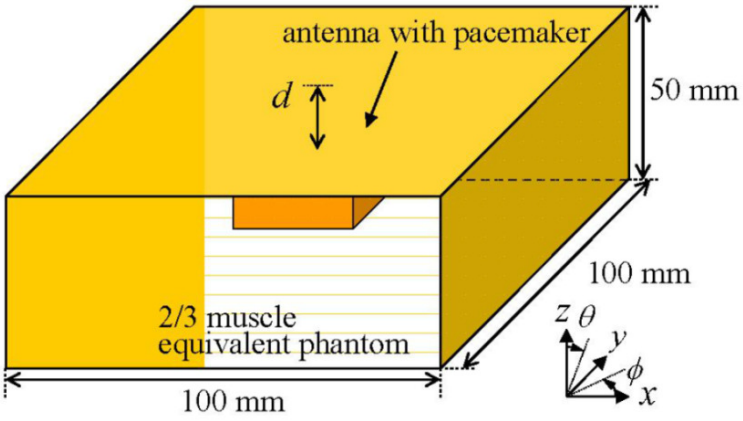

(b)

Fig. 2.4: Implantable PIFA: (a) Antenna and Pacemaker Model;
(b) Human Equivalent Model [28]

A 2/3 muscle-equivalent phantom model has been considered when the antenna was designed. In 2/3 muscle-equivalent phantom model, electrical constants of the body estimated from outside are equivalent to nearly 2/3 of the muscle tissue's electrical constants. It was shown that a communication link with the external equipment which is located within 6m distance and 104 degree of altitude may be established efficiently by this antenna. Fig. 2.4 shows PIFA and its pacemaker model as well as human equivalent model.

2.3.5 Implantable Folded Dipole Antenna

In Fig. 2.5 an implantable folded dipole antenna is shown [29]. The dimensions of the antenna are 20.3mm×0.8 mm ×0.8mm (Fig. 2.5(a)) and it is coated by a glass material with relative permittivity of 5.0.

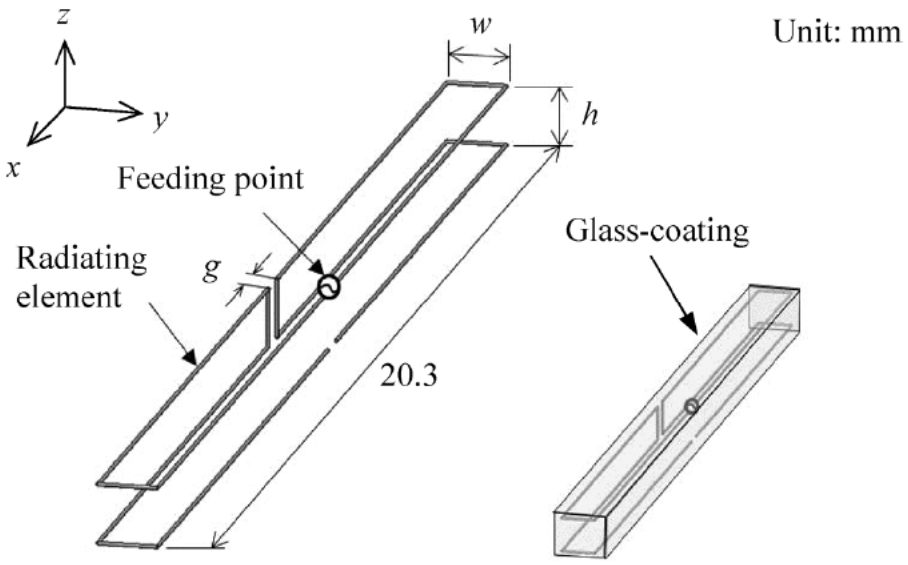

(a)

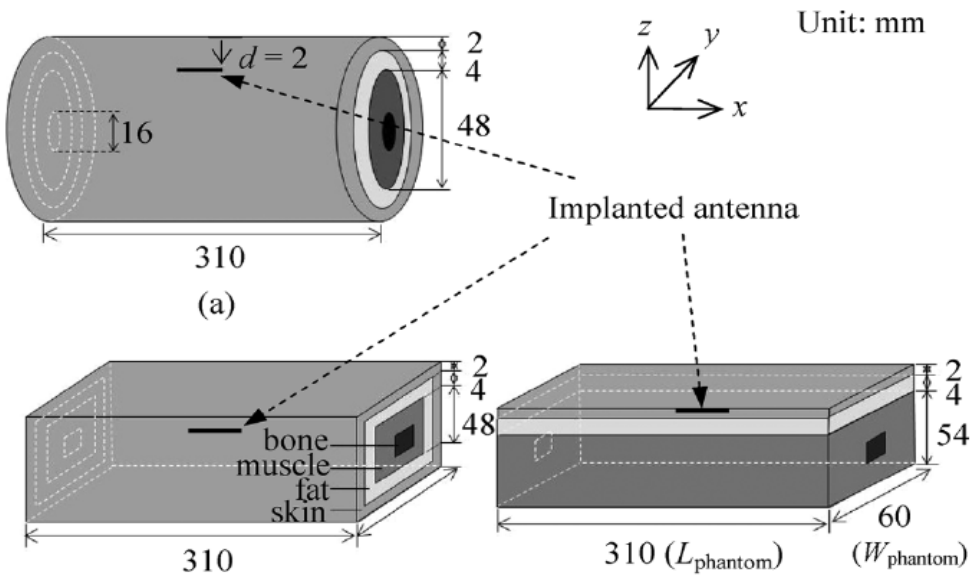

(b)

Fig. 2.5: Implantable Folded Dipole Antenna: (a) Antenna Geometry; (b) Antenna Surrounding Human Tissue Model [29]

Table 2.2: Parameters of the Link Budget [29]

Parameters	**Value**
Required Rx power: RP [dB]	-155.9
Bit error rate	1×10^{-5}
E_b/N_0 (ideal-PSK) [dB]	9.6
Required bit rate: *B*r [kbps]	7
Noise power density: N_0	4.04×10^{-21}
Boltzmann constant: k	1.38×10^{-23}
Ambient temperature T_0[K]	293
Available Rx power: AP[dB]	-125.1
Operation frequency: f [GHz]	0.953
Tx power: P_t [W]	2.5×10^{-5}
Tx antenna gain: G_t [dBi]	-35
Rx antenna gain: G_r [dBi]	0
Free space path loss: [dB]	44.06
Margin [dB]	30.8

This antenna surrounding human tissue model is shown in Fig. 2.5(b). The parameters of the link budget are presented in Table 2.2. This antenna has been designed to be operated in the 900MHz Japanese ISM band for the RFID based short-range communications. The link budget requirements have been fulfilled successfully by this antenna. Cylindrical and box type human tissue models were developed and the antenna parameters were simulated with these models.

2.4 Implantable RF Systems

RF systems for medical applications may be classified broadly non-implantable (in free space) and implantable. A number of RF systems may be found in the literature [30-47]. In implantable RF systems, medical data may be transmitted from implant to implant, implant to free space or vice versa. In the following sub-sections two implantable RF systems are discussed.

2.4.1 Reduction, Telemetry and Processing of Neural Data for Implantable System

A bidirectional implantable RF system has been tested on several sheep [30]. The block diagram of system is shown in Fig. 2.6. Neural data from the brain of the sheep, digitised by Digitising Head Stage Module (DHSM), was sent to the Implantable Central Module (ICCM). The implantable unit was powered up by induction coupling with the coils. The ICCM also has a FPGA for processing of data and a RF transceiver to link with base station, which is outside of the body of sheep. The base station is interfaced with a computer.

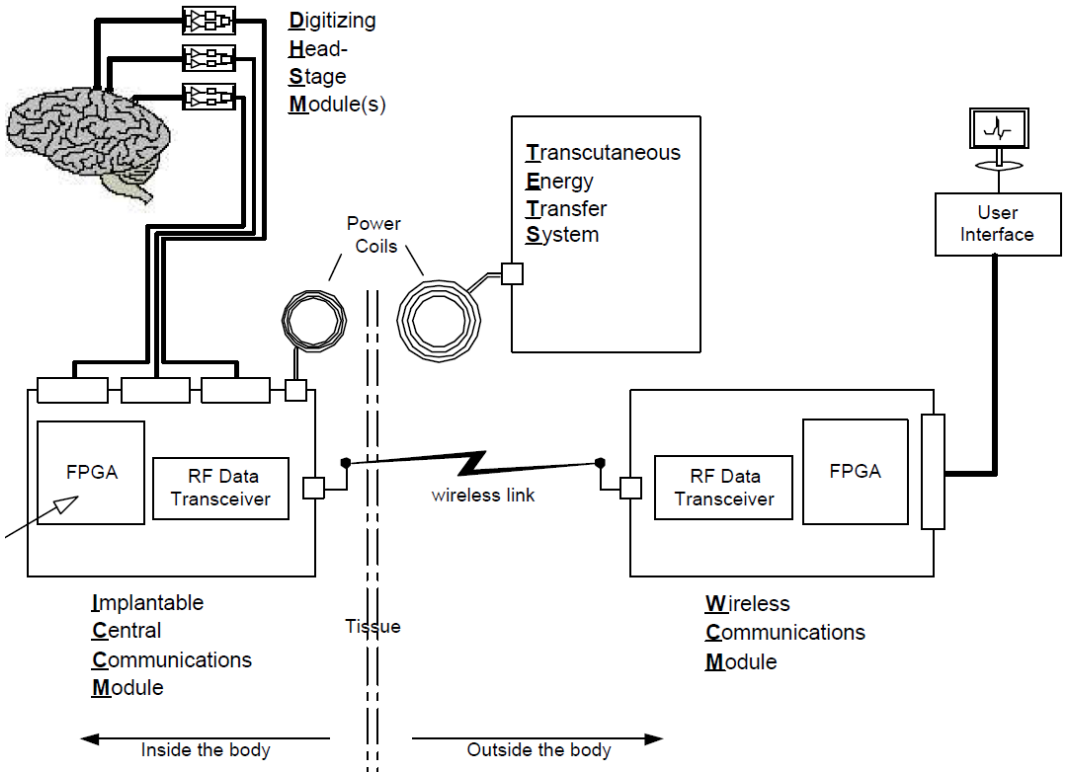

Fig. 2.6: A block diagram of the neural data acquisition system [30]

The limitation of this system is that implantable unit and base station must be very close to maintain the power supply for the implantable unit as there is no dc battery connected the implanted unit. In addition to this, alignment of the internal and external power coils must be matched properly to transfer maximum power to the implantable unit. This is one of the difficult tasks when the implanted animal is moving freely.

2.4.2 Implantable RF Blood Pressure Monitoring System

Fig. 2.7 shows a novel implantable RF blood pressure monitoring micro system for small laboratory rats [7]. The size of the laboratory rat cage is 20cm×10cm×10cm. The operating frequency of the RF link between the implantable unit and external unit is 433MHz. Although the absorption loss by the body material of rat is less at 433MHz, compared to 915MHz and 2.4GHz, the antenna size unit is larger. This is one of the

disadvantages of Medical Implantable Communication Service (MICS) standard when the implantable unit is used for small animal. The system requires for transmitter and receiver units to be placed properly at a fixed distance from each other with a constant RF power coupling coefficient. Due to the implantation of receiver unit inside the body of a freely moving laboratory rat, the received power by the implant will continuously change. Therefore, external unit controls the power level of implanted unit by an adaptive RF power controller.

The overall implant dissipates 300μW, which is transferred from the external unit. The limitation of the system is that the animal cage must be small enough to power up the implanted unit from the RF power coil placed under the cage. This limits the mobility of the laboratory rat. The blood pressure may be different if the mobility range of the rat is expanded.

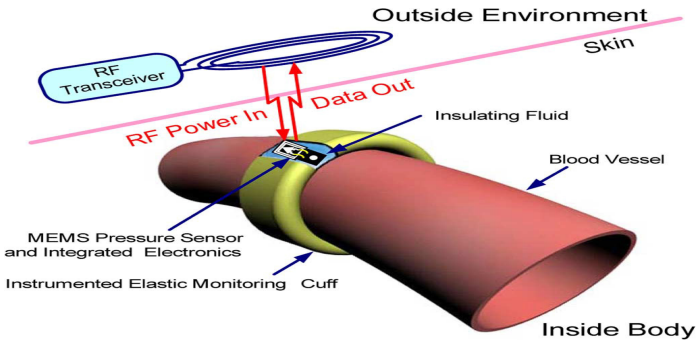

Fig. 2.7: Implantable RF blood pressure monitoring micro-system for laboratory rats [7]

In this system an elastic circular cuff is wrapped around a blood vessel of laboratory rats for real-time blood pressure monitoring. The cuff is made of soft bio-compatible silicone material as shown in Fig. 2.7. It is filled with bio-compatible insulating fluid with an immersed micro-electromechanical systems (MEMS) pressure sensor and integrated electronic system to detect a down-scaled vessel blood pressure waveform. An inductively coupled power transfer is performed in this system to power up

the implantable unit in a laboratory rat and characterized the blood pressure waveform by the system. The implanted unit consists of following components:

i. MEMS sensor interface circuitry
ii. analog-to-digital converter (ADC)
iii. system configuration and control unit, for signal conditioning and coding
iv. wireless data telemetry to an external receiver
v. an adaptive RF to DC power converter

Laboratory rats were chosen for the testing of prototype cuff implanted around the vessel size (1 mm in diameter). Experiments are conducted before and after the drug injection into the body of rats to characterize the miniature implantable monitoring cuff. The average heart rate of laboratory rat is 250 bpm. However, heart rate has increased to 330 bpm after 10min of the drug injection.

In summary, the authors presented a compact, lightweight, long-term, reliable bio-sensing implantable system with full-duplex RF telemetry capability to monitor real-time blood pressure from a "free" roaming rat housed in its home cage. The system also validated the capability of measuring blood pressure waveform with high fidelity.

2.5 Implantable Medical Devices

Implantable medical devices (IMDs) in biomedical applications [48-59] have been around for a long time, nearly a century. Biology and electronic engineering are the two main disciplines that should be considered when IMDS are designed and developed. Laboratory equipment such as X-ray, medical imagers, pacemakers is widely used for the analysis medical data in humans. Implantable pacemaker, which was developed by Wilson Greatbatch and William M. Chardack in the middle of last century, probably the

pioneer IMD successfully embedded into the human body. It is important to make implants more acceptable in general public in terms of cost and benefits. However, great advances in micro technology and nanotechnology have opened the door of miniaturised IMDs, for example, a device to be implanted in human eye for blind people, known as vision implant. Modern devices available today, have reconfigurable feature settings and functionalities. In addition, they maintain compact size with extremely low power consumption, at least for some applications, for instance, cochlear implant (hearing implant) [24]. Even, diagnosis of diseases is being addressed by the IMDs, for example, eye sight problem. Remote monitoring of physiological parameters such as temperature, blood pressure, ECG from humans body or animals may be extracted and transmitted to external devices by implantable systems.

2.6 Link Budget for Implantable Wireless Telemetry

It is essential to know some key parameters for the wireless communication link budget between an implantable device and the external base station. The proposed implantable antenna is assumed to be attached to an RFID (at 900 MHz ISM band) circuit board and to be used in an indoor environment. The link distance is assumed to be in the range of 1.0m and the input power requirement of the implantable antenna is 25×10^{-6}W according to ERC recommendation 70-3 [25]. The receiving antenna used to this link budget is assumed to be monopole. Receiver power requirement (R_x power) in dBW can be calculated as

$$Rx_{requiredpower} = \frac{E_b}{N_0} + kT_0 + B_r \qquad (2.1)$$

where, $\frac{E_b}{N_0}$ is the energy per bit to noise power density [dB], k is the Boltzmann constant [J/K], B_r is the bit rate [kbps], T_0 is the ambient temperature [K].

$$Rx_{requiredpower} = P_t + G_t + G_r - L_d \quad (2.2)$$

where, P_t is the transmitted power of the implantable antenna [dBW], G_t and G_r are the gains of implantable antenna and receiving antenna respectively in dBi, L_d is the total path loss [dB]. For example, when the gain of the implantable antenna is -18.0 dBi then wireless communication link will be maintained with external base station [25]. Therefore, link budget requirements must be accounted for when implantable antennas are designed for wireless telemetry.

2.7 Conclusion

A number of implantable antennas and wireless bi-telemetry systems were discussed. It was found from literature review [60-68] that one of the greatest challenges is to design a compact implantable antenna to be implanted in a small animal such as a rat. Low level physiological signals extractions and transmission from inside of the animal body to an out-of-body base station needs higher power to be transmitted compared to free space communication for the same T_x-R_x separation, since most of power transmitted by the implanted antenna is absorbed by animal tissues. Generally, human body phantom and tissue properties [69-71] are used for numerical calculations by computer simulations. Therefore, a link budget formula was described at the end of the chapter which is typically used to calculate predicted received power at the receiver.

Chapter 3

Frequency Detuning Study of an Existing Antenna under Rat Skin

3.1 Introduction

Antennas are crucial in the development of implantable RF telemetry system. Rat skin tissue has a very high dielectric constant (~40) and covering an antenna with rat skin is similar to loading the antenna with a superstrate having a high relative permittivity. The loading an antenna with a superstrate of high permittivity reduces the resonance frequency of the antenna. It is important to know at least approximately the extent of variation in the resonance frequency of the antenna due to rat skin before designing an antenna for an implantable system. Limited frequency shifting may be corrected using external tuning elements, but biological tissues could cause larger shifts that are beyond such correction. In this chapter, we study the extent of resonance frequency variation of a commercial antenna to decide whether this antenna can be implanted inside the body of rats for transmitting signals using the Medical Implant Communications Service (MICS) band (402-405MHz). Here variations in the resonance frequency of a commercial antenna (ANT403 SP1, Antenna Factor ^{TM}) [72] with and without covering by rat skin, are investigated. Microstrip (MS) feed and co-planar waveguide (CPW) feed schemes are designed to feed the antenna. In MS feed, a conducting strip is separated from the ground plane by a dielectric layer to carry electromagnetic (EM) signal while a CPW feed is a type of strip transmission line (a planar transmission structure) for conveying EM signal to antenna. The CPW feed technique consists of a flat conductive metallic strip of small

thickness, deposited on the surface of a dielectric substrate slab with two narrow slits ground planes running adjacent and parallel to the strip on the same surface. A comparative study of frequency shifting between MS feed and CPW feed of the antenna is highlighted in this chapter. Frequency shifting due to ageing effects of the rat skin has also been measured in this experiment when the antenna was covered by rat skin, which has an average thickness of around 2mm. Fresh rat skin samples were collected and stored in salt solution before, and after, measurements.

3.2 Chapter Contributions

The contributions of this chapter are:

- Design of MS and CPW feeds for a commercial antenna to be tested in rat skin
- Experimental setup to measure antenna parameters in free space and rat skin
- Understand ageing effect measurements of rat skin samples (collected from hospital) on MS-fed antenna covered by FR4 board and rat skin
- Antenna input reflection coefficient (S_{11}) measurements of MS-fed and CPW-fed antennas in free space as well as when covered by FR4 board and rat skin (Fig. 3.7)
- Transmission coefficient (S_{21}) measurement of the MS-fed antenna when covered by FR4 board and rat skin (Fig. 3.13)
- Experimental and quantitative demonstration of the extent of antenna detuning when placed under the rat skin
- Assessment of the effect of antenna detuning on the link budget in the MICS band

3.3 Background

Implantable RF bio-telemetry system has been emerged in the market recently for wireless bio-medical applications. However, compact size, cost-effective and customized implantable devices are still limited in the market and mostly used for experimentation on small animals such as rats [6, 7]. If wireless biotelemetry system test is successful on the laboratory animals and approved for implantation into human body or animals by the authority of a country then production of the implantable devices starts. Fig. 3.1 shows an implantable bio-sensing wireless biotelemetry system [7] test in laboratory rats. In this example, implantable device is placed subcutaneously in rat to extract and transmit physiological data from its body to a data acquisition system in free space. In this scenario, the implanted device is receiving RF input power from the external base station. However, an internal DC battery may be used to supply power to the implantable device. Of course, an implantable antenna is necessary to transmit biomedical data wirelessly to the base station in free space. The overall size of the implantable device must be small enough so that it could easily be implanted in a small animal. Hence the size of the implantable antenna must be compact and efficient. As detuning of operating frequency of an implantable antenna is unavoidable, it is important to know, at least approximately the extent of frequency detuning. Then an antenna could be designed to radiate at a higher frequency in free space first. When it is implanted it will resonate and radiate at the correct operating frequency.

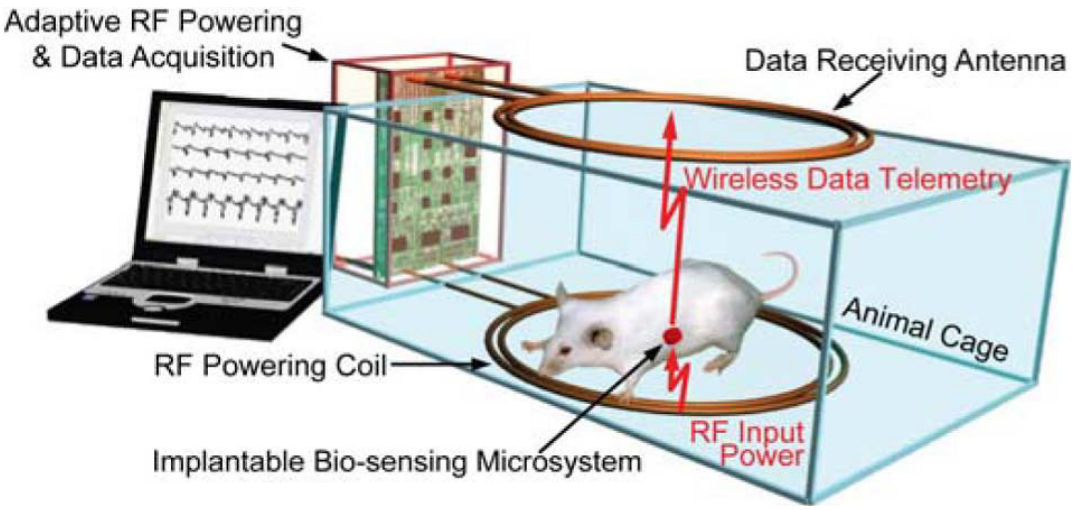

Fig. 3.1: An example of an implantable bio-sensing wireless biotelemetry system [7]

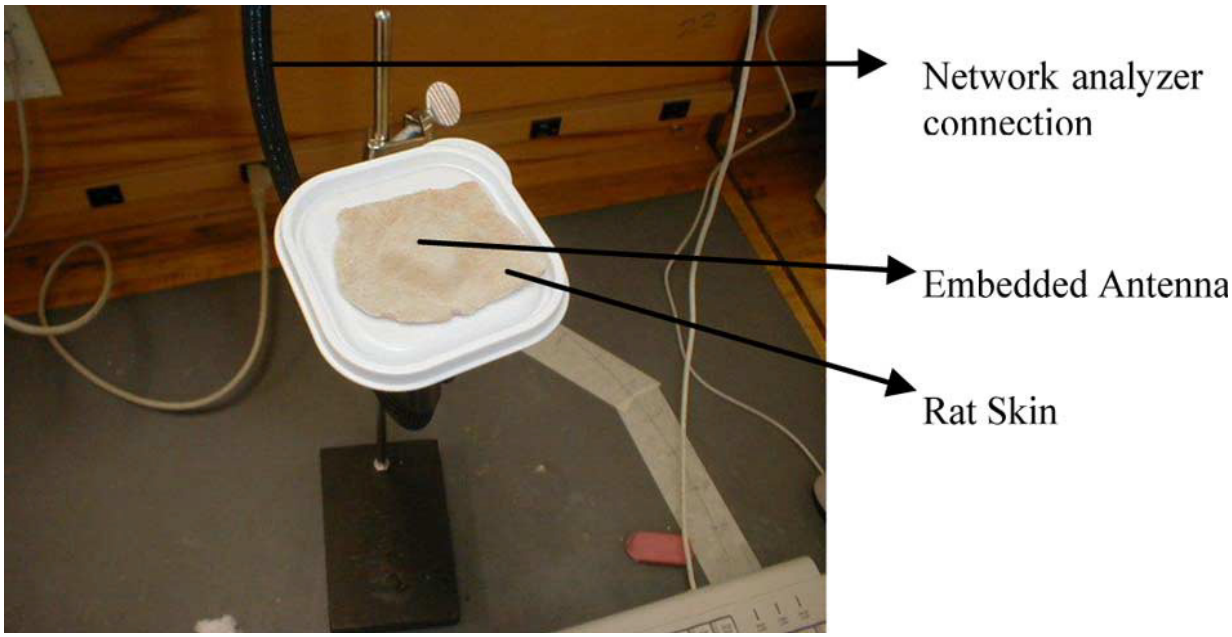

Fig. 3.2: Experimental setup to measure $S_{11}$of an implantable antenna when covered by rat skin [6]

An experimental setup to measure the return loss of an implantable antenna for medical wireless telemetry is shown in Fig. 3.2 where the antenna is placed under real rat skin. While the geometry of the designed antenna is shown in Fig. 3.3(a) the measured and simulated S_{11} of the implantable antenna [6] which covered by rat skin is illustrated in Fig. 3.3(b). This implantable antenna has been designed and implemented for dual-band operation (400MHz MICS and 2.4GHz ISM bands).

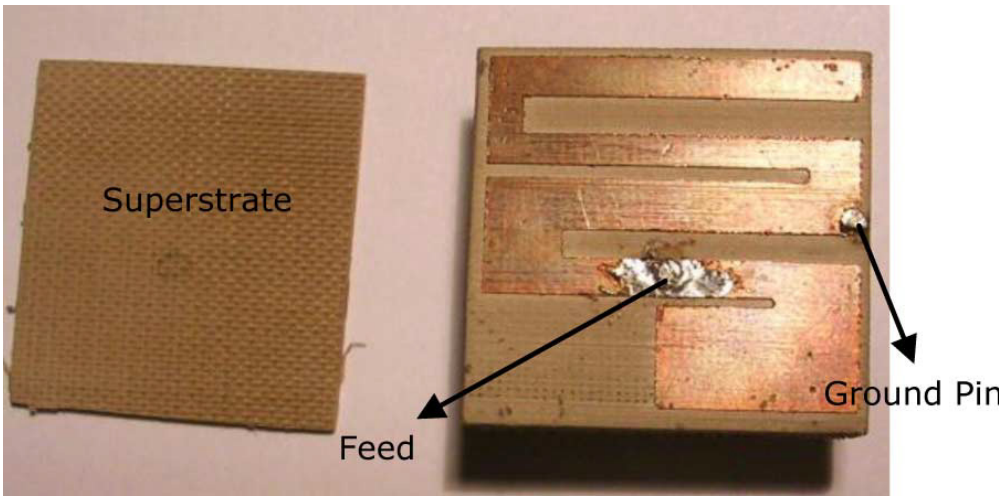

(a)

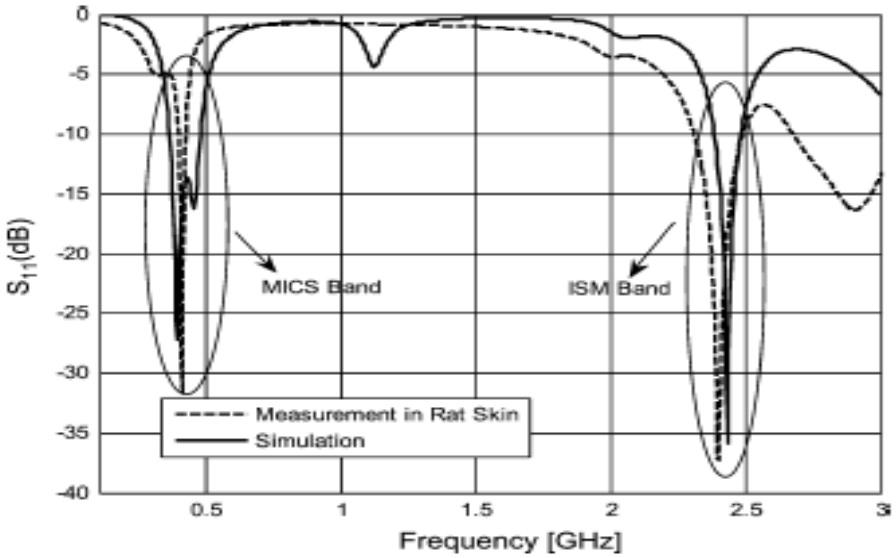

(b)

Fig. 3.3: Implantable antenna and its $|S_{11}|$ when covered by rat skin: (a) Fabricated dual-band antenna and (b) Measured and simulated input reflection coefficient ($|S_{11}|$) [6]

Before designing new antennas for implantable RFID tag provided by our industry partner, we tried to use available commercial small antennas to verify their suitability to use in our RFID tag PCB. The extent of resonance frequency detuning is studied on a commercial antenna operating at 400MHz MICS band due to the loading effect of rat tissue (skin and fat layers). The antenna is small to be attached on the RFID tag PCB and

can be easily implanted in laboratory rat for experimental purpose. The detailed description of the antenna is presented in the following section.

3.4 Antenna Geometry and Feed Design

Fig. 3.4 shows the geometry of the commercial antenna I investigated [72], and two feed designs I used to study the sensitivity of its resonance frequency. The dimensions of the ¼-wavelength grounded line planar antenna designed for free-space communication are 27.94mm×13.7mm×1.5mm.

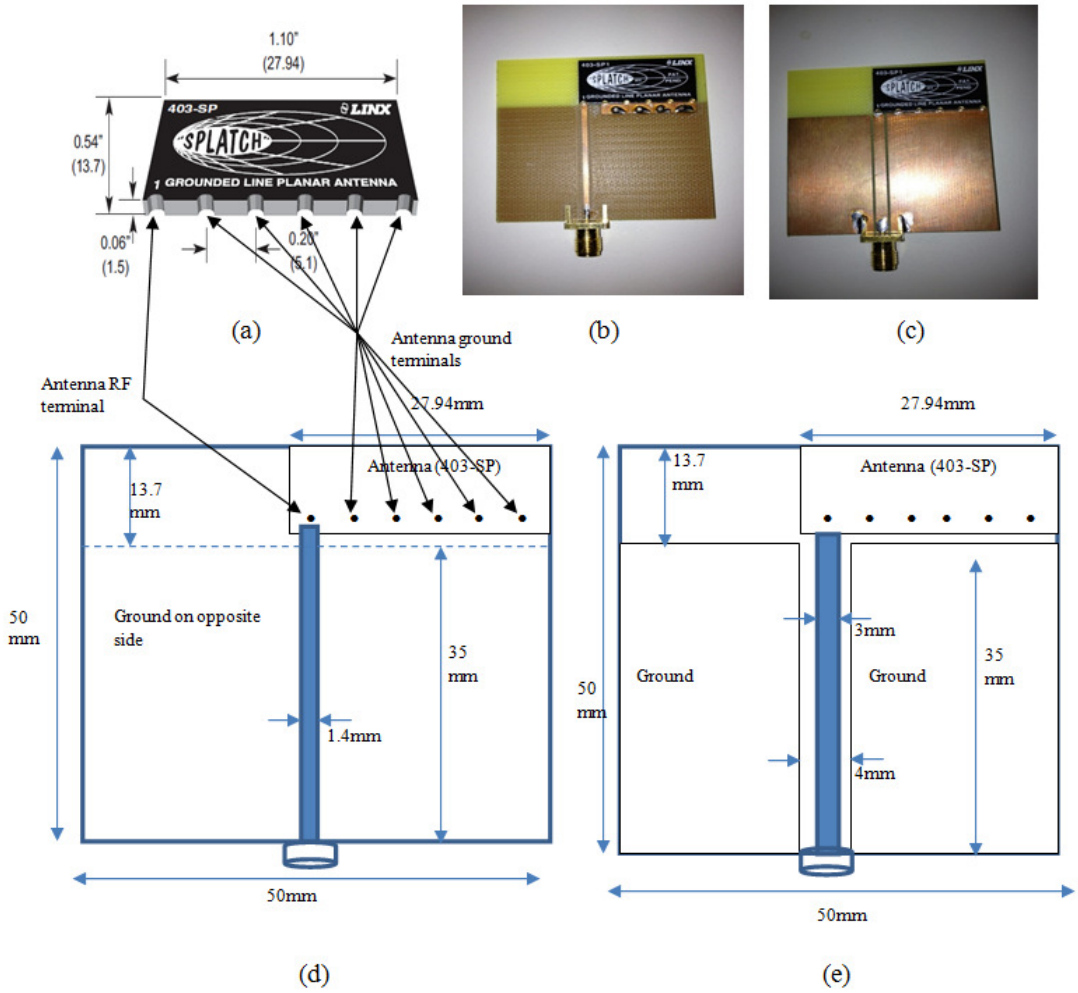

Fig. 3.4: ANT403-SP commercial antenna and two feed systems for it: (a) ANT-403-SP, (b) Fabricated MS feed, (c) Fabricated CPW feed, (d) MS feed design, and (e) CPW feed

According to the data sheet of the antenna, it is recommended that no ground plane or traces should be located under the antenna. The recommended 50Ω microstrip line feed (MS-feed) was designed by me and fabricated to feed the antenna. In addition, a 50Ω co-planar waveguide feed was designed and implemented, to compare the return loss between the two feeding techniques. The MS-fed antenna test board has a 1.4mm-wide microstrip line between the antenna and a 50Ω coax connector, on the upper surface of a 50mm×50mm FR4 board (Fig. 3.4(d)). The thickness of the FR4 board is 0.8mm. On the lower surface of the FR4 board, a 50mm×35mm partial ground plane is formed.

An FR4 board with the same area and thickness was used for the test board of the antenna with the co-planar waveguide (CPW) feed. The width of the central strip of the CPW is 3mm and the width of each CPW slot is 0.5mm. These dimensions ensure 50Ω matching with the commercial antenna. The antenna RF terminal is labeled as number 1 and there are 5 ground terminals as shown in Fig. 3.4(a). The gap between the RF terminal and the adjacent ground terminal is 5.1mm. The gap between any two adjacent ground terminals is also 5.1mm and all of them are connected to the ground planes. The MS feed and CPW feed are connected to the RF terminal of the antenna. The VNA is located closer to one of the walls and placed on a wooden table having a height of around 1m from the floor. The measurement was recorded for five days in a row and the variations of antenna parameters were monitored during this period.

3.5 Experimental Setup

Fig. 3.5 shows the experimental setup for S-parameter measurements. A Vector Network Analyzer (VNA) (HP 8720D) was used to measure the return loss (S_{11}) and the transmission coefficient (S_{21}) of the antenna. Calibration of the VNA was performed from

200MHz to 800MHz before any measurement is made. The anechoic chamber available is not suitable for such low frequencies and thus the measurement was conducted in a typical laboratory environment.

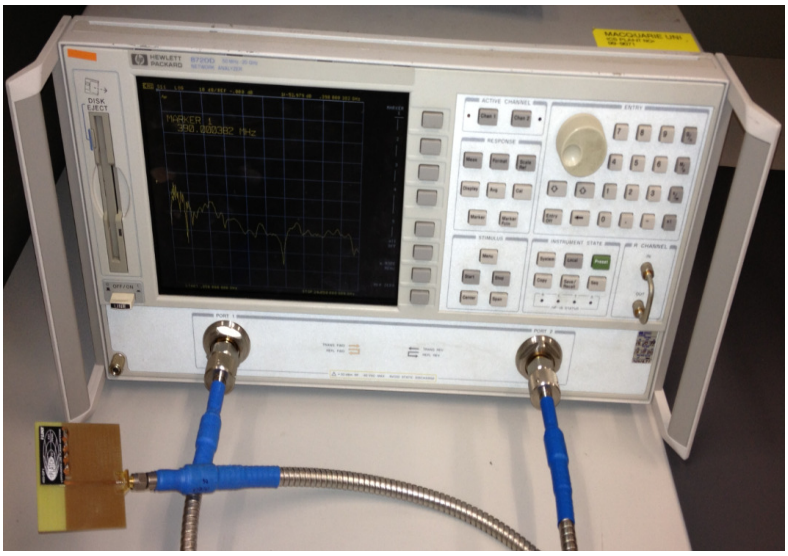

(a)

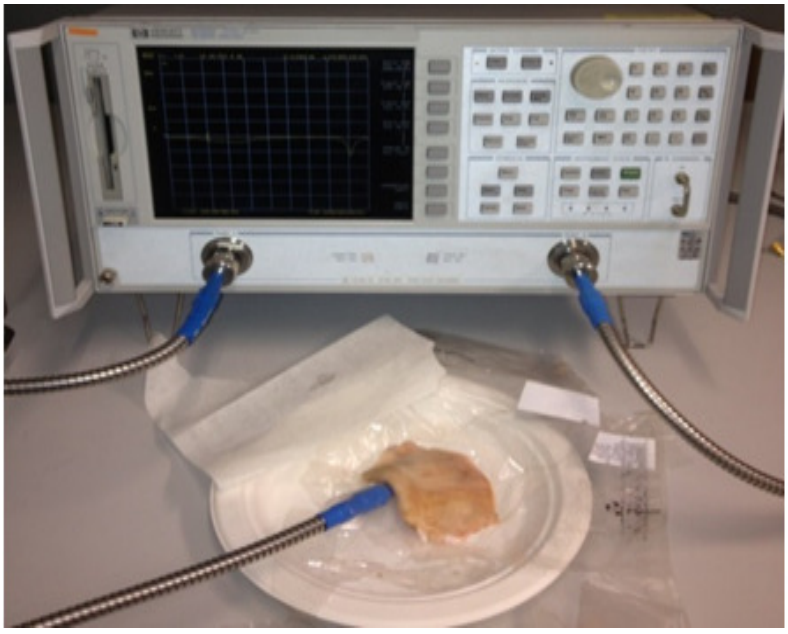

(b)

Fig. 3.5: Experimental setup: (a) S_{11} measurement without rat skin and (b) S_{11} measurement with rat skin

The size of the laboratory is approximately 10m×10m×4m with brick walls, floor and ceiling. There are several computers, oscilloscopes, signal generators, DC power supplies, VNAs etc. in this laboratory. Fig. 3.6 shows the placements of antennas and FR4 board for measuring S_{11} and S_{21}. The transmission coefficient, S_{21}, was measured by connecting the MS-fed antenna to port 1 (transmission port) of the VNA and the CPW-fed antenna to port 2 (reception port) of the VNA. The antennas are placed face to face and parallel to wooden table as shown in Fig. 3.6(c).The separation between the two antennas is approximately 5mm. The intension of this measurement is not to measure $|S_{21}|$ in the far field but to observe the resonant frequency shifting of the antenna due to rat skin loading. In addition, it also compares $|S_{21}|$ measured in free space. At first, the CPW-fed antenna is placed on the table with a sheet of A4- size transparent plastic used for education purposes. Secondly, the FR4 board is placed on top of the CPW-fed antenna and then the rat skin in a very thin transparent plastic packet is placed on it. Finally, the MS-fed antenna is placed on the rat skin. The reason for placing the FR4 board between the MS-feed antenna and the rat skin is to keep the resonance frequency above 300MHz. It is verified that, if the FR4 board is not placed between the CPW-fed antenna (transmitting antenna) and the rat skin, the resonance frequency is decreased at around 220MHz. It is also observed that interchanging two antennas between the VNA's ports to measure S_{21} has little effect on variations of resonance frequency.

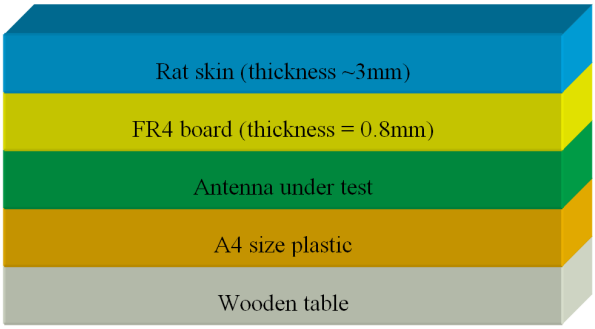

(a)

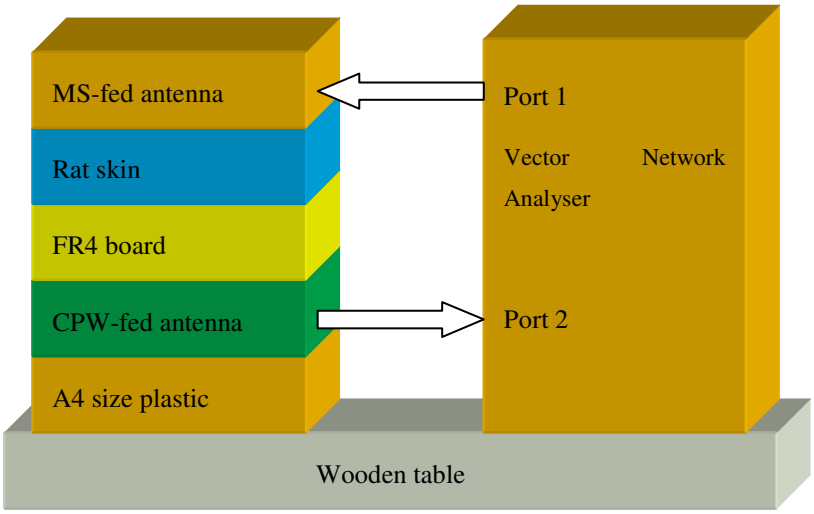

(b)

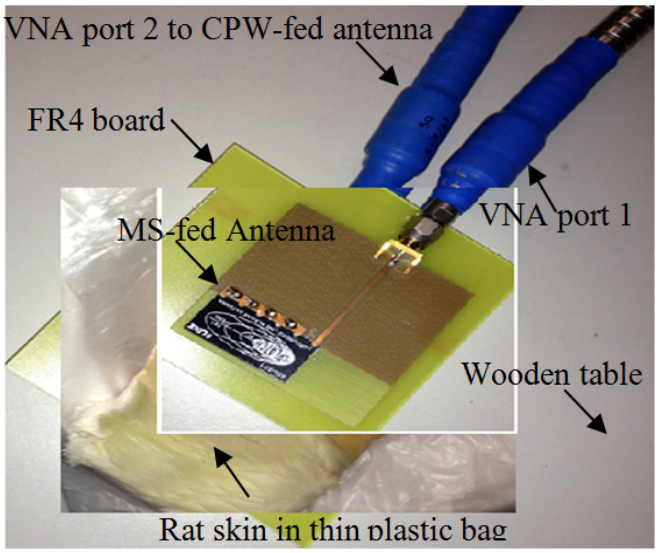

(c)

Fig. 3.6: Placements of items for measuring S_{11} and S_{21}: (a) S_{11} measurement (b) S_{21} measurement; (c) S_{21} measurement with antennas and rat skin sample placement

3.6 Return Loss and Transmission Coefficient Measurements

In this section, the measured return losses of the antenna are presented for the following cases:

Case I: Return loss of the antenna in free space,

Case II: Return loss when the antenna is covered by FR4 board, and

Case III: Return loss when the antenna is covered by FR4 board and rat skin.

3.6.1 Return Loss Measurements

Fig. 3.7 shows the return loss variations of the MS-fed antenna and the CPW-fed antenna. In Case I, the resonance frequencies of the MS-fed antenna and the CPW-fed antenna in free space are 395MHz (at -22dB) and 408MHz (at -16dB) respectively. It is observed that the resonance frequencies are slightly higher (13MHz) in the CPW-fed antenna and none of them are equal to the nominal resonance frequency mentioned in the commercial antenna data sheet. This is probably due to the fabrication tolerances of the feeding line. In Case II, when the antennas are covered by a FR4 board (thickness of 1.6mm), the resonance frequencies are shifted slightly down to 380MHz (at-20dB) and 400MHz (at -13dB), respectively. This is to be expected, as the FR4 board cover is acting as a superstrate on the antenna and its dielectric constant is higher (4.3) than that of air. Finally, in Case III, when the antennas are covered by rat skin placed on top of the FR4 board, the resonance frequencies decrease significantly to 335MHz (at -16dB) and 330MHz (at-14dB), respectively. In this case, the rat skin is acting as a second superstrate on top of the FR4 board, which is 1.6mm thick. However, this resonance frequency shift could be less if a thick FR4 board was used between the antenna and the rat skin. As a

result, the overall volume of the antenna under the rat skin would be increased, which is undesirable because of the small size of a rat.

The return loss is slightly larger for the CPW-fed antenna in all cases, whereas it increases moderately from Case I to Case III. The CPW-fed antenna shows a lower return loss than the MS-fed antenna when measured in free space (without covering by anything). For both antennas, a 15%-20% decrease in resonance frequency is noted. It is found that the 10dB return-loss bandwidth increases in both cases as a result of external (FR4 board and rat skin) loading.

The rat skin sample was preserved in a salt solution after the measurement to maintain the freshness of the rat skin sample. Fig. 3.8 shows the effect of ageing of the rat skin on the resonance frequency of the MS-fed antenna. From 9th Feb 2011 to 13th Feb 2011 (in 5 days) a resonance frequency change was observed and it was found that the resonance frequency decreased slightly during this period. However, it remained within the range of resonance frequencies from 320MHz (at -10dB) to 340MHz (at -16dB). It is also seen from the graph that $|S_{11}|$ is decreases slightly with ageing of the rat skin sample, although it was stored in a salt solution after the measurement. This result clearly indicates that a fresh rat skin sample will provide the return loss (16dB) as well as the resonance frequency. The resonance frequency with a fresh rat skin sample is closer to the MICS band than with an old rat skin sample. A high return loss from the antenna is always to be expected when it is covered by FR4 board and rat skin. They are acting as superstrates when placed on the antenna under test.

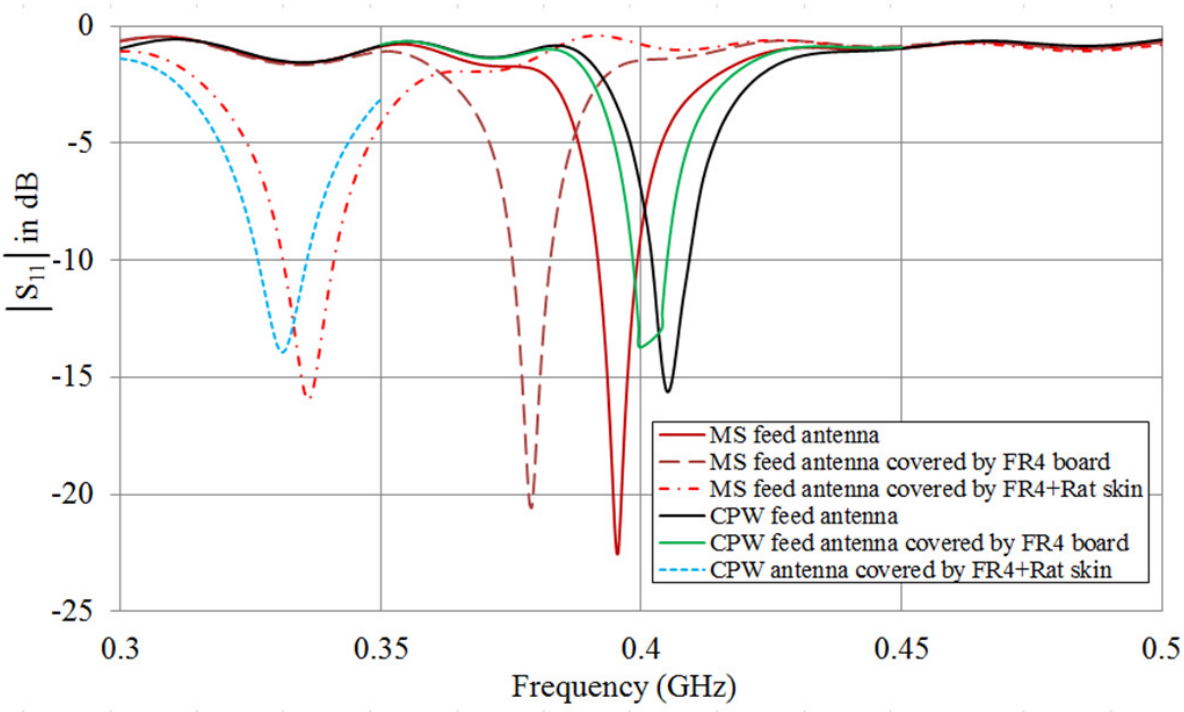

Fig. 3.7: Return loss variations of MS-fed and CPW-fed antennas

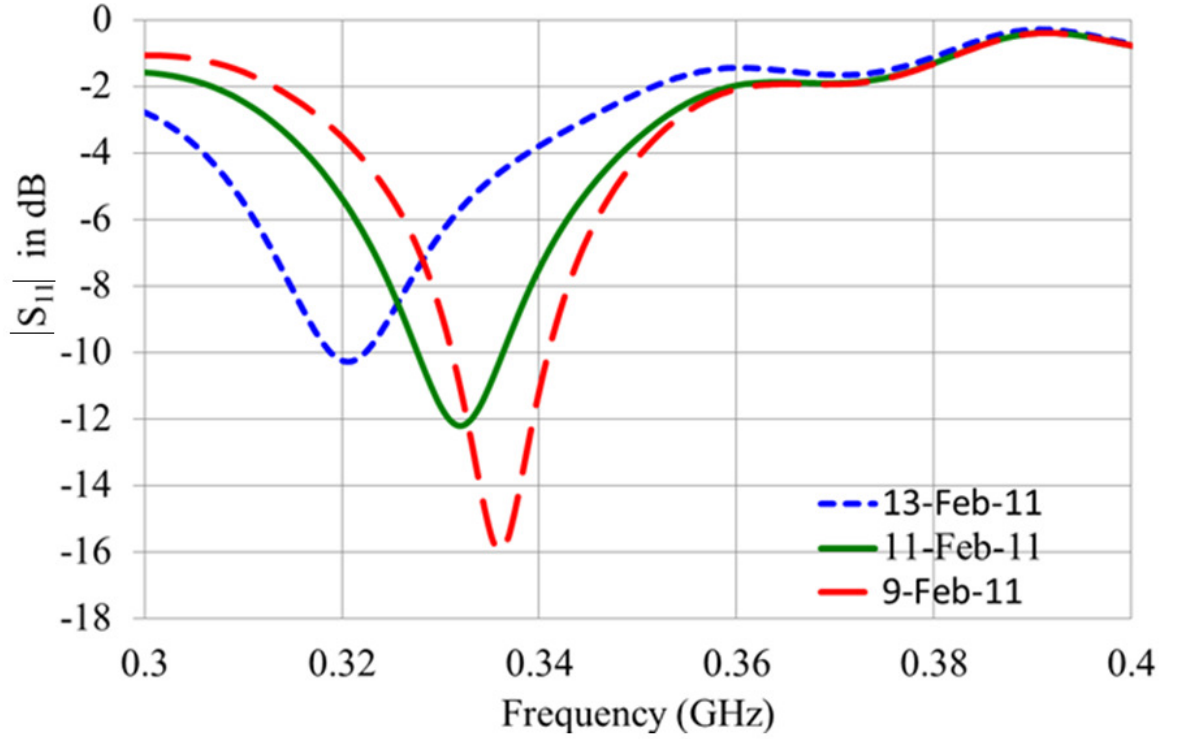

Fig. 3.8: Ageing effect of rat skin on MS-fed antenna covered by FR4 board and rat skin

In Fig. 3.9, the measured $|S_{11}|$ for the MS-fed antenna is shown when fresh rat skin sample was placed inside a very thin plastic bag and then the antenna was covered by it. The resonance frequency is detuned significantly. In this situation, the antenna is out of band and unable to communicate with 400MHz MICS band devices. Similarly, the resonance frequency is out of MICS band for the CPW-fed antenna when the rat skin is placed without an FR4 board between the antenna and the rat skin as shown in Fig. 3.10. In this scenario, there is more severe detuning of the resonance frequency, and again the antenna cannot be used with MICS band devices. Therefore, FR4 board is used in the measurements so that the antenna is still within the operating band. In Figs. 3.11 and 3.12, measured $|S_{11}|$ are presented with antennas inside the thin plastic bag, for MS-fed and CPW-fed antennas respectively.

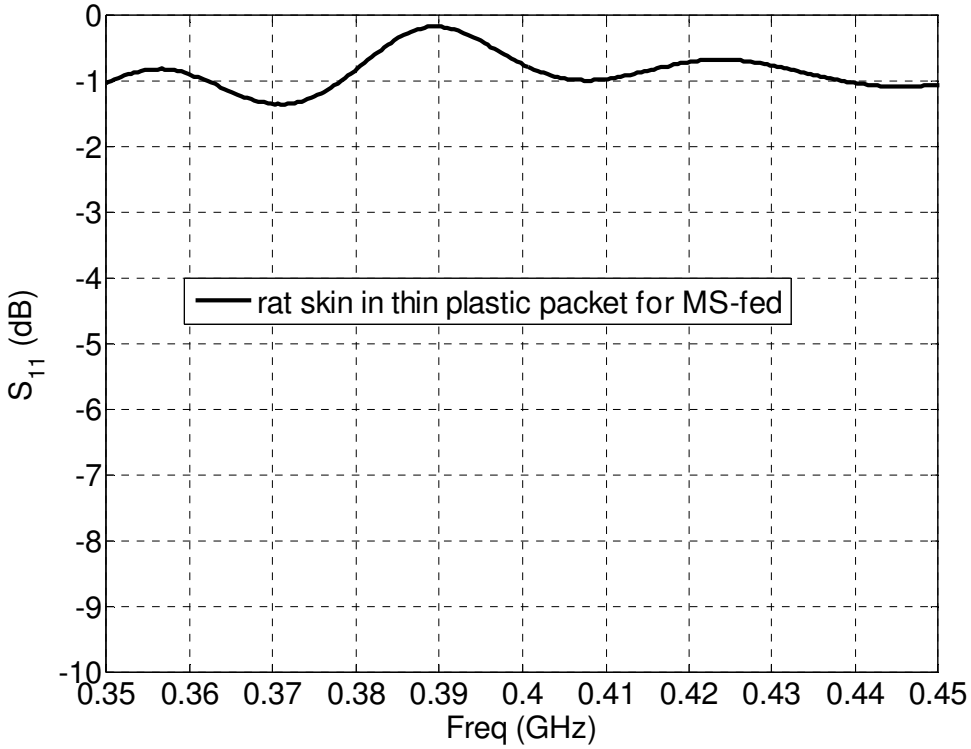

Fig. 3.9: $|S_{11}|$ for MS-fed antenna when covered by rat skin only

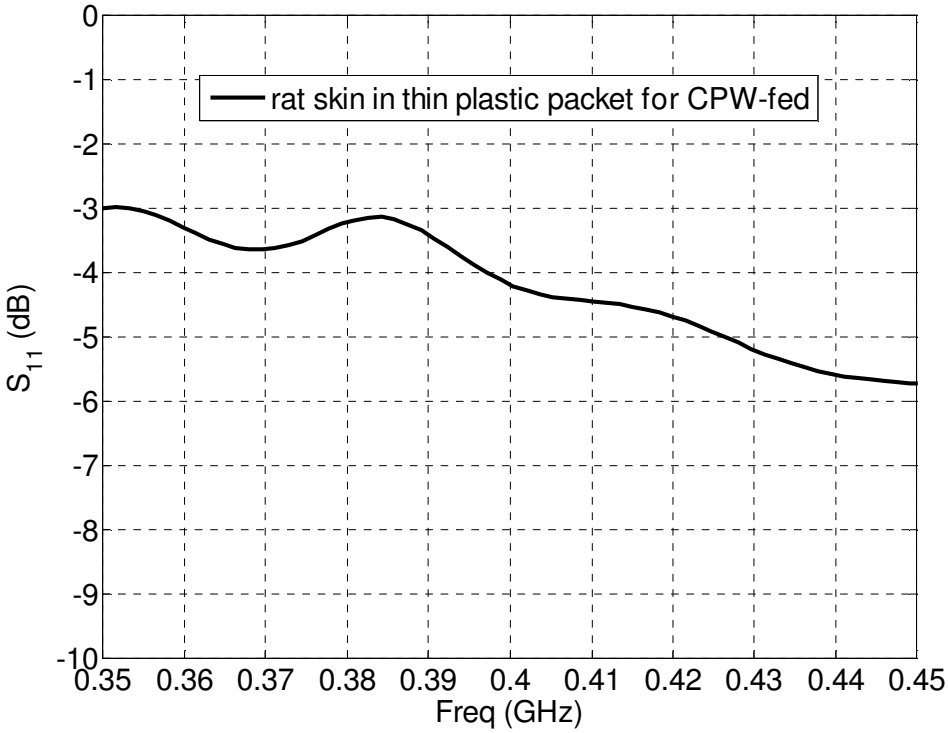

Fig. 3.10: $|S_{11}|$ for CPW-fed antenna when covered by rat skin only

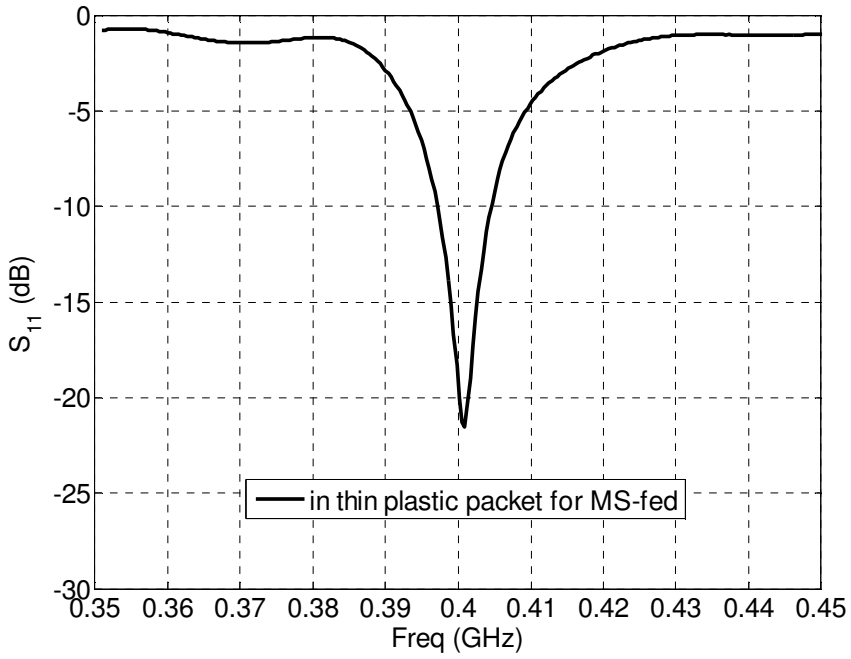

Fig. 3.11: $|S_{11}|$ for MS-fed antenna when covered by thin plastic packet only

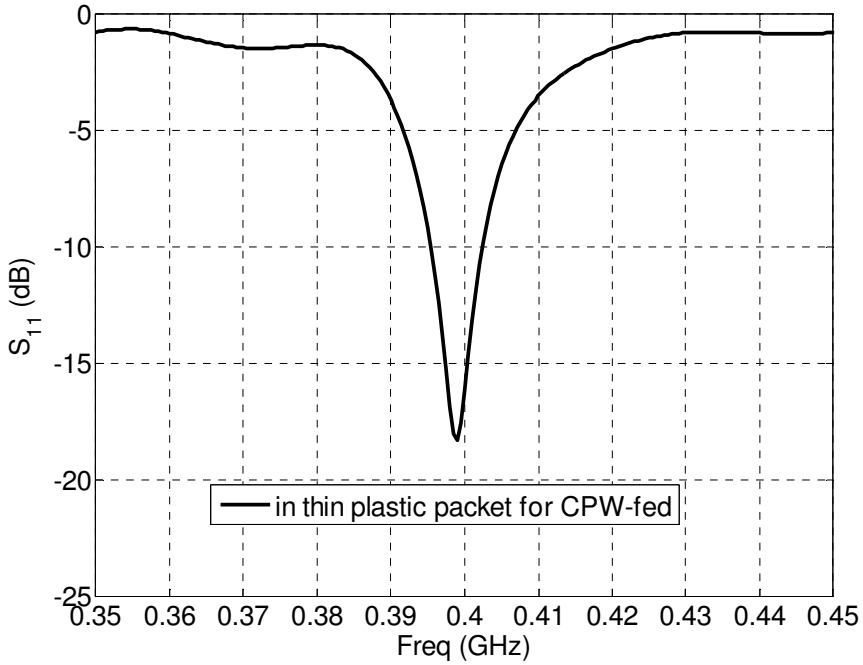

Fig. 3.12: $|S_{11}|$ for CPW-fed antenna when covered by thin plastic packet only

The results confirm that the plastic bag has little effect on the resonance frequency and it never goes below 397MHz. This plastic bag is used to protect the antenna from the conductive rat skin which can lead the antenna to be short-circuited. Generally, bio-compatible material is used for the conformal coating of the implantable device with the antenna. However, during this preliminary study, bio-compatible coating material was not available in the laboratory.

3.6.2 Transmission Coefficient Measurements

Fig. 3.13 presents transmission coefficient measurements ($|S_{21}|$) between the MS-fed and the CPW antennas. Fig. 3.13(a) shows $|S_{21}|$ measurement when one antenna is covered by the FR4 board and rat skin. The maximum power transfer occurs at around 318MHz. This clearly indicates that maximum power transfer does not occur close to the free-space resonance frequency of the antenna (~403MHz). It occurs close to the loaded resonance frequency (~318 MHz), which is far below the MICS band (402-405MHz), and the commercial antenna used for this experiment is not suitable for an implantable RF telemetry system. Similar results are expected for the CPW-fed antenna and, a $|S_{21}|$ measurement was not made on it. This suggests that customised antennas are required for implantable wireless telemetry, and that they must be tested before implanting inside the rat. An antenna should be designed with sufficient bandwidth that it will be within the desired operating band after detuning due to the dielectric loading of rat skin on the antenna. In Fig. 3.13(b), $|S_{21}|$ measurement in free space is shown. The maximum transmission coefficient is found to be approximately -27.56 dB at 403.4MHz. Transmission coefficient measurement is important as it predicts the available power to the receiving antenna. The maximum allowable effective isotropic radiated power (EIRP) by the implantable antenna for the MICS band is 25μW, allocated by Federal Communications Commission (FCC, USA). A low-power transmission requirement by the implantable antenna is essential to minimise the electromagnetic field radiation effect on the biological tissue so that no tissue damage occurs. Two types of feeds are tested to compare their performances.

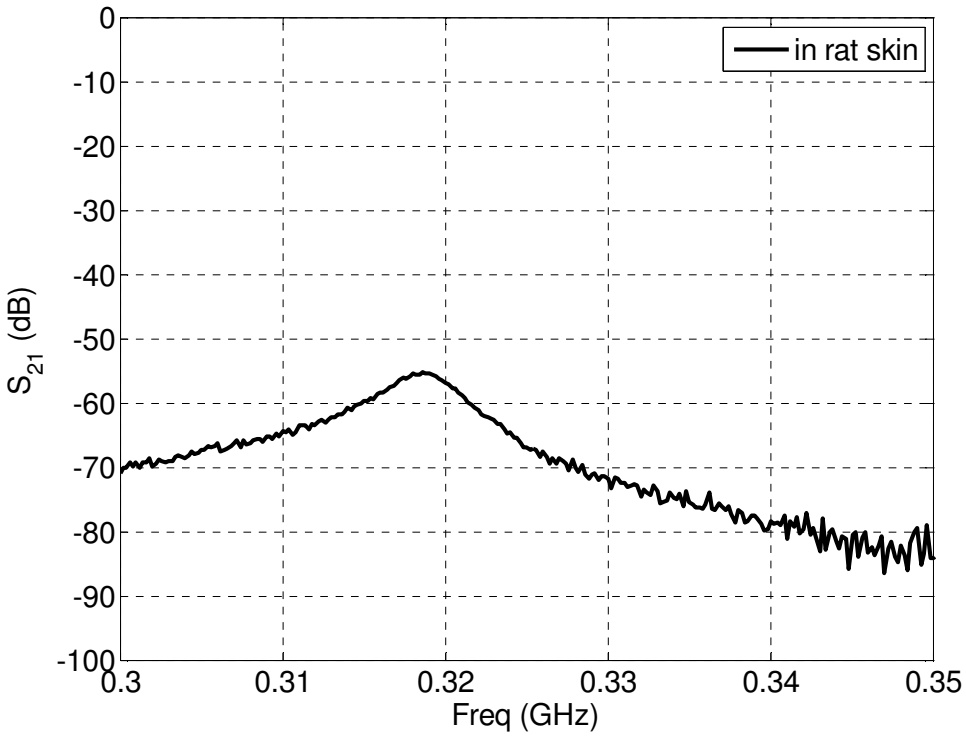

(a)

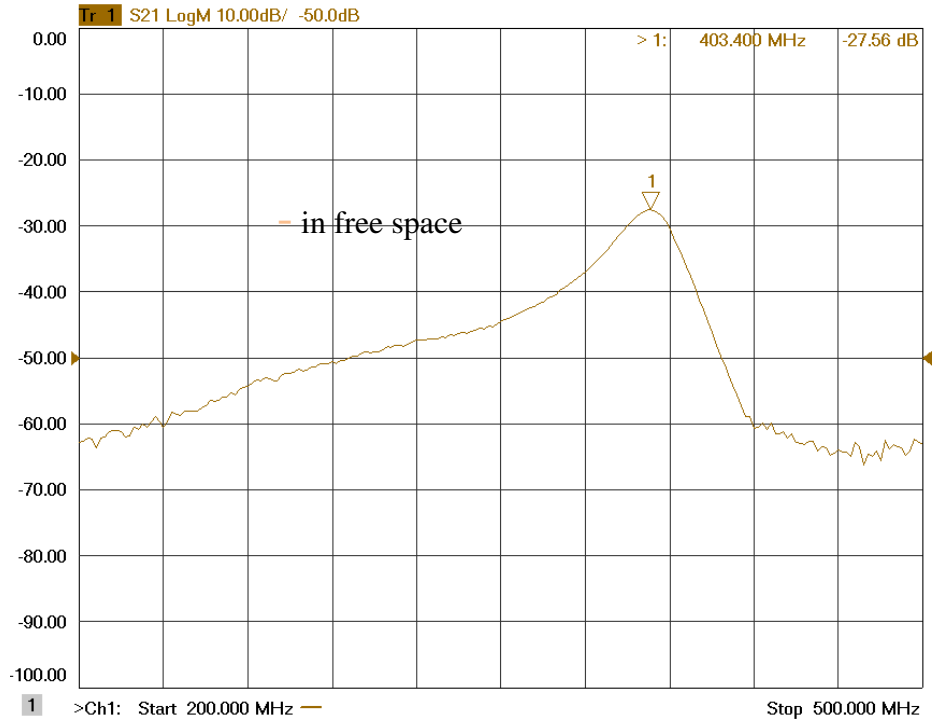

(b)

Fig. 3.13: Transmission coefficient ($|S_{21}|$) measurement; (a) CPW-fed antenna is covered by FR4 board and rat skin and MS-fed antenna is placed on top another FR4 board placed on rat skin; (b) Measured in free space

3.7 Conclusion

In this chapter, the variation of the antenna resonance frequency due to the effect of rat skin and FR4 board is discussed. MS-fed and CPW-fed antennas have been tested and it is clear that a 15%-20% decrease of resonance frequency can occur in both configurations. The effect of rat skin on transmission line was also observed but it was negligible compared to effect on antenna. This results suggest that, in order to maintain an efficient wireless link within a given operating frequency band, the implantable antenna must be designed for the implanted environment. Antennas designed for free space are detuned significantly and hence are not usable for such applications. In-vitro aging effects of rat skin also cause some variations in the antenna resonance frequency and return loss although these are minor. The transmission measurement ($|S_{21}|$) between two identical antennas also confirms that a large decrease in the optimal link frequency may occur when one antenna is placed inside the body of a rodent.

Chapter 4

Implantable Partially Folded PIFA Antenna for Australian UHF ISM Band

4.1 Introduction

In the previous chapter 3, the frequency detuning of a commercial antenna (ANT403 SP1, Antenna Factor ^{TM}, operating at 400MHz in free space), with and without rat skin over the antenna has been investigated. It was found from the investigation that this antenna, designed to operate in free-space is not suitable for an implantable system and designing a customised implantable antenna is an alternative solution. In addition, the Ultra High Frequency (UHF), the 900MHz Australian ISM band has been selected instead of 400MHz MICS band due to following reasons. First, an Australian company known as BCS Innovations has been working towards the development of a wireless telemetry system to extract physiological signals from the bodies of animals and human. Collaboration has been established between the Department of Engineering, Macquarie University and the BCS Innovations, Australia to develop a prototype of an implantable Radio Frequency Identification (RFID) device for laboratory rats. This existing RFID tag is operating well in free space in the 900MHz Australian ISM band but needs replacement of its antenna for the implantable RFID device. Second, the UHF band is a good candidate for RFID-based medical telemetry compared to its counterpart MICS band in terms of the wireless communication link range between an RFID tag and a reader. In addition, a high data rate can be supported between implanted and external devices. This

chapter presents a study of the antenna parameters of an implantable partially folded planar inverted-F antenna (PF-PIFA). Due to limited space for attachment of an antenna to the RFID tag, a PF-PIFA has been designed and simulated using commercial software, CST Microwave Design Studio. The PIFA configuration has been selected, due to its compact size, after a literature survey. In [73, 15], dual-band and triple-band implantable antennas have been presented for MICS (400MHz), ISM (2.4GHz) and UWB (3.1-10.6GHz) bands. A dielectric-loaded impedance matched antenna has been presented in [23]. This antenna has good impedance matching but the antenna is large due to the UWB bandwidth requirement. Several designs [5-6, 12] of implantable planar inverted F-antennas (PIFA) have been reported recently. The novelty of our PF-PIFA design is the folding of the open end of the radiating patch to act as a capacitor load plate which distinguishes it from referenced works. In addition, proximity feeding technique is applied to enhance the bandwidth.

4.2 Active RFID Circuit Board Description

Fig. 4.1 shows a photograph of the Global Safety Solutions and Management Pty Ltd (GSSM) active circuit board for which the proposed implantable antenna is designed to replace the existing antenna (operating well in free space communications). The overall dimensions of the circuit board are 60mm×33mm×1.6mm. It is constructed on a single-layer FR4 board substrate by placing the components on one side and a ground plane with an area of 33mm×22mm on the opposite side as shown in Fig. 4.1. It is located below the electronic components (RF chip, microcontroller etc.) between the battery (E) and antenna. It is seen from the circuit board that an area of approximately 15mm×30mm is occupied by the existing antenna. The proposed implantable antenna, therefore, has similar size as described later in this chapter.

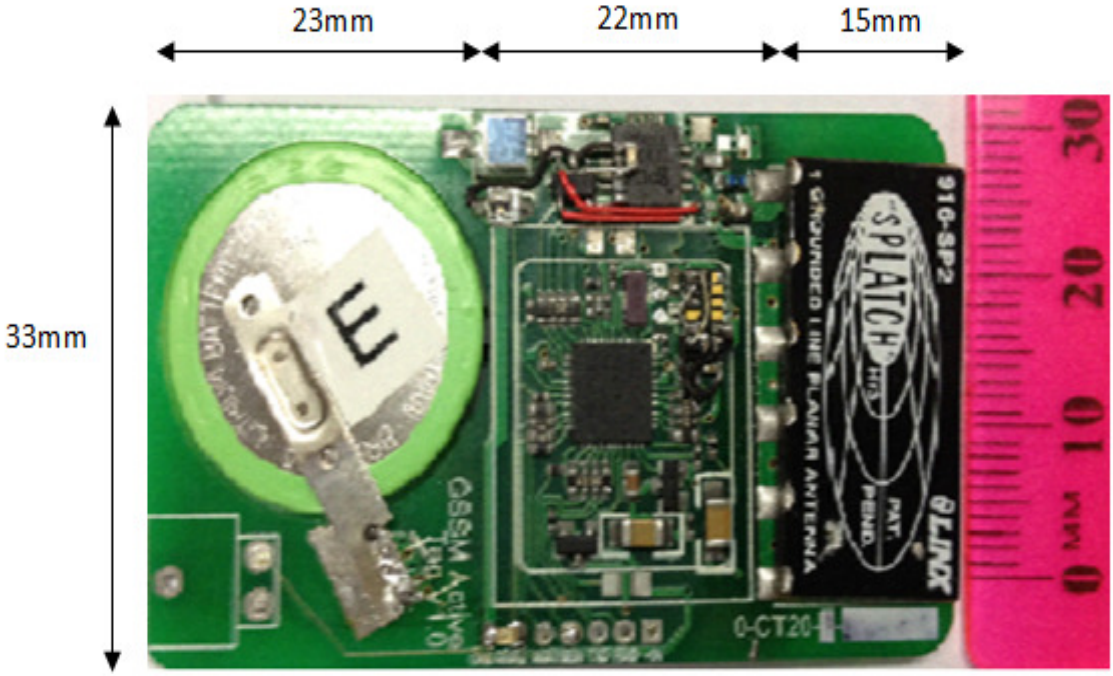

Fig. 4.1: GSSM active-tag circuit board with existing antenna [74]

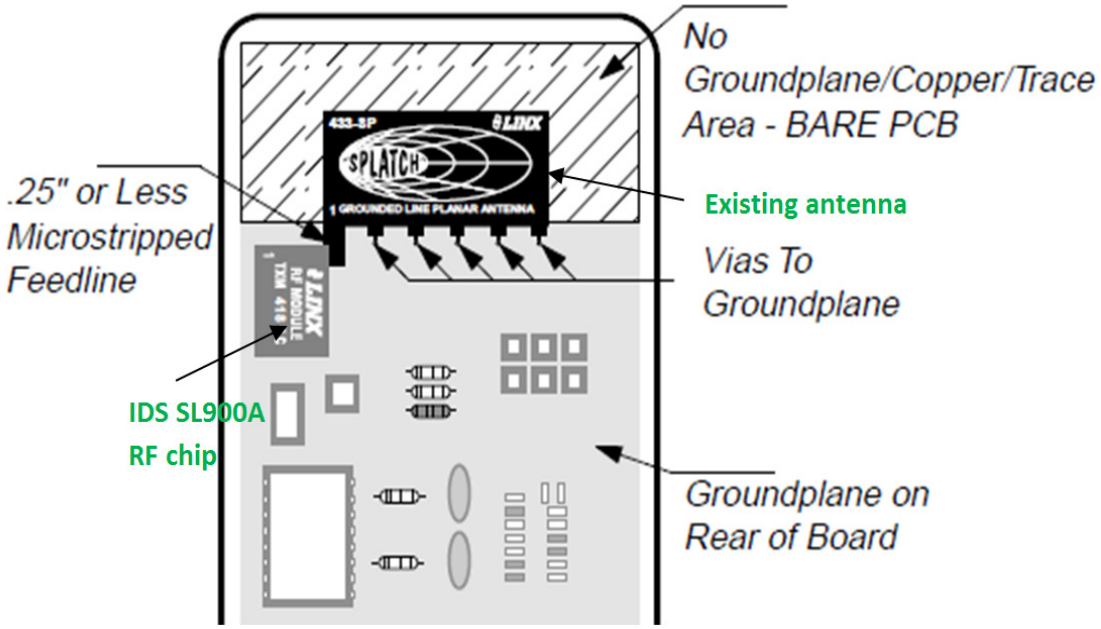

Fig. 4.2: Location of RF chip and antenna on GSSM active-tag circuit board [74]

In Fig. 4.2, the locations of the RF chip and the antenna on GSSM active tag circuit board [74] are shown. The RF chip and the existing antenna are connected by ≤3.85mm microstrip line. The ground plane (33mm×22mm) of the GSMM circuit board is connected to 5 ground pads of the antenna by vias. When this antenna is replaced by an implantable antenna, impedance mismatch as well as operating frequency detuning between the RF chip and the new antenna are expected. It is recommended by the manufacturer that no ground plane, copper and trace area should be located under the existing antenna. However, the proposed implantable antenna has its own ground plane to prevent the power flow into the rat's tissue. As a large ground plane is not possible on the component side of the circuit board, the antenna ground plane is connected to the larger ground plane of the RFID tag circuit board for optimum antenna bandwidth.

4.3 Antenna and RF-Chip Impedance Matching

The nominal input impedance of an antenna is generally 50Ω while the input impedance of the existing RF-chip (IDS SL900A) on the RFID tag is different (30-320jΩ at 900 MHz, according to the data sheet of the manufacturer). The antenna impedance is expected to vary somewhat from 50Ω with the tag in free space as well as in rat's body. A bio-compatible coating and the dielectric loading effect of rat's body tissue on the antenna of the tag will change the impedance considerably. As a result, the designed antenna which is conjugately matched with the RF-chip in free space is expected to detune from its operating frequency. According to the data sheet of the IDS SL900A RF-chip, its input impedance is 30-320jΩ (r = 321.4 and $\theta = -84.6^0$) at 900MHz which is significantly different from the antenna input impedance (50Ω). Therefore, the first task is to perform impedance matching of the antenna with the RF chip to provide the highest efficiency, maximum power transfer from the RF chip to the antenna and hence

maximum range between the RFID tag and the reader. The most common practice for antenna matching is to predict it at a -10dB reflection coefficient over the band of interest.

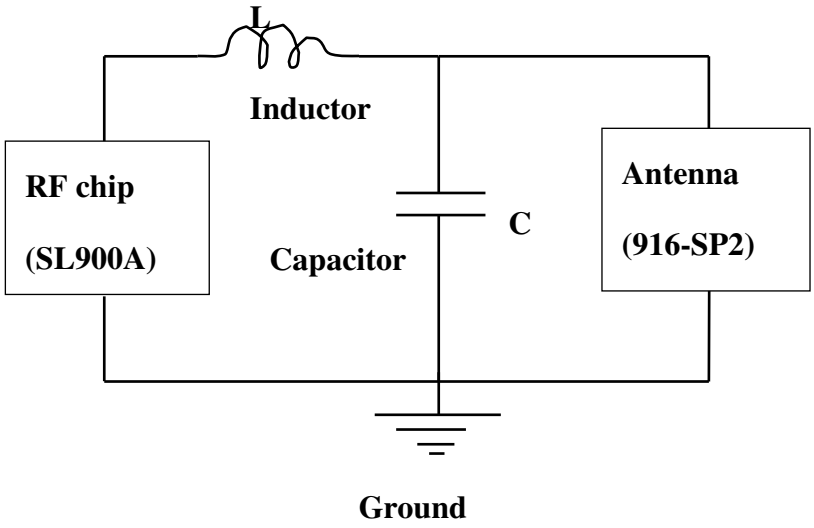

Fig. 4.3: Impedance matching of the antenna and RF chip [102]

The UHF band in this case is 915MHz-928MHz (Australia) as allocated in Australian radiofrequency spectrum allocations chart. A simple L-C network between the antenna and the RF chip may be used for impedance matching as shown in Fig. 4.3. Given complex source and load impedances and frequency, the component values were most conveniently calculated using the online matching-network circuit estimator.

4.4 Design Issues for Implantable RF Devices in Rats

Leading medical research groups around the world use rats and other animals, for the study of disease and normal physiology. Several projects conducted in the Australian School of Advanced Medicine (ASAM) focus on hypertension and cardiovascular disease, and the role of the central nervous system in regulating hypertension and

breathing. To date, the primary method of controlling hypertension in humans is the use of drugs. The pathway to approval of drugs for human use involves pre-clinical trials on animals such as rats. It is important not to compromise such trials by unnecessarily stressing the rats, which may happen if they are harnessed to monitoring equipment for extended periods. It would therefore be a major advance if we could devise implantable telemetry systems to extract, store and wirelessly transmit vital signals in rats to external monitoring stations. Commercial implantable RF telemetry systems (433MHz and 900MHz) currently available in the market for this purpose are limited, too expensive and less adaptive. A possible reason for this may be the insufficient effort and research made to address some design issues relevant to such systems, possibly as a result of resource limitations, limited expert advice and/or the urge to bring the product to the market. Although the complete implementation of an efficient implantable RF system is a challenging, long-term venture, in this section the relevant design issues that need to be addressed during the initial design phase of a cost-effective, small, low-power and adaptive RF telemetry system are discussed. In this RF system, the implantable device can wirelessly transmit at least the ECG, blood pressure (BP), renal nerve activity (RNA) and body temperature (BT) of rats in a regular fashion to an external base station. Ultimately, we anticipate that such a system would have a wider veterinary and clinical use.

The implanted device, developed to extract physiological signals from rat's body and transmit to nearby external base station, has a low-power RF transceiver, an UHF ISM band antenna, a microprocessor and a memory, and is powered by two AA batteries. With a power management system in the implantable module, operation for two months is expected. The external station, at a 1 to 2 metre range, may be networked through a

computer for data analysis, and for sending adaptive and configuration commands to the implanted unit. Both real-time and off-line data acquisition are considered, aided by a Micro SD storage in the implanted unit. Design issues are highlighted by the requirements of the researchers conducting such medical science experiments. The use of the maximum bandwidth available in the RF channels and possible compression of data needs to be considered.

Efforts have been made to reduce the size of an implantable antenna for freely moving experimental rats to be operated in the Industrial, Scientific and Medical (ISM) band (900MHz). Major requirements of antenna design as imposed by the application to rats as opposed to humans are: smaller antenna size, variations in electrical properties of the rat's body tissue, rat's behaviour and movement, size and weight. The ECG signal rate in terms of beats per minute (BPM) in experimental rats is higher than that of a human body and as a result higher data rate is necessary for transmitting data from an implanted unit to an external unit.

4.5 Antenna Design

In this section, design details of a partially folded implantable PIFA antenna are described. The background , antenna geometry and antenna surrounding environment model are discussed first followed by simulation results.

4.5.1 Background

Small size and low battery power consumption are the most important requirements when an implantable system is designed for small animals. The applications of such small antennas are widely found in biomedical RF telemetry systems as well as in radio frequency identification (RFID) systems. However, the greatest challenge is to

design a sufficiently small implantable antenna at a low frequency (below 1GHz). However, most of them focus on systems operating in the Medical Implant Communication Services (MICS) band (402-405MHz). Although the energy absorption in body tissue is less in the MICS band, the antenna size is quite large for a small animal such as a rat. Due to this and the availability of a commercial RFID device operating in free space in the 900MHz ISM band, a miniaturised and partially folded PIFA is proposed. The antenna is designed based on the theory reported in [5]. However, instead of using direct feed to the antenna reported in [5], a proximity feeding is applied and optimised to increase the bandwidth of the antenna.

4.5.2 Antenna Geometry

Fig. 4.4 shows the geometry of the proposed implantable antenna. This is called a partially-folded planar inverted-F antenna (PF-PIFA since the far end (from the feed point) is folded back clockwise after 18.2mm. The overall size of the antenna is 26mm×19mm×4.4mm including the ground plane. The antenna is fed by a feed plate located 2mm above the ground plane. A shorting pin (SP) is used to reduce the size of the antenna, as in a conventional PIFA. The location of this shorting pin is 5mm from the front edge of the ground plane and it connects vertically to the left edge of the radiating patch as shown in Fig. 4.4. A coaxial feed cable is connected from the bottom of the ground plane and the signal pin runs parallel to shorting pin from the ground plane to the feed plate.

The rectangular feed plate has dimensions of 26mm×10.5mm×0.2mm and its sides are parallel to the sides of the radiating patch. However, its left edge is shifted right by 0.7mm, from the left edge of the radiating patch. The thickness of all metal plates in the antenna is

0.2mm unless otherwise stated. A slot (15mm×0.5mm×0.2mm) parallel to the radiating patch is created on the patch to adjust the resonance frequency.

The partially folded part of the antenna is a capacitive plate/load (26mm×6mm×0.2mm) placed at 1.2mm above the top side of the ground plane. The gap between this plate and the feed plate is 1.7mm. An FR4 substrate (permittivity = 4.3) is considered in our design to achieve a reasonable bandwidth for RF telemetry between the implanted unit and a base station, which is in free space. CST Microwave Design Studio software is used to design the proposed antenna.

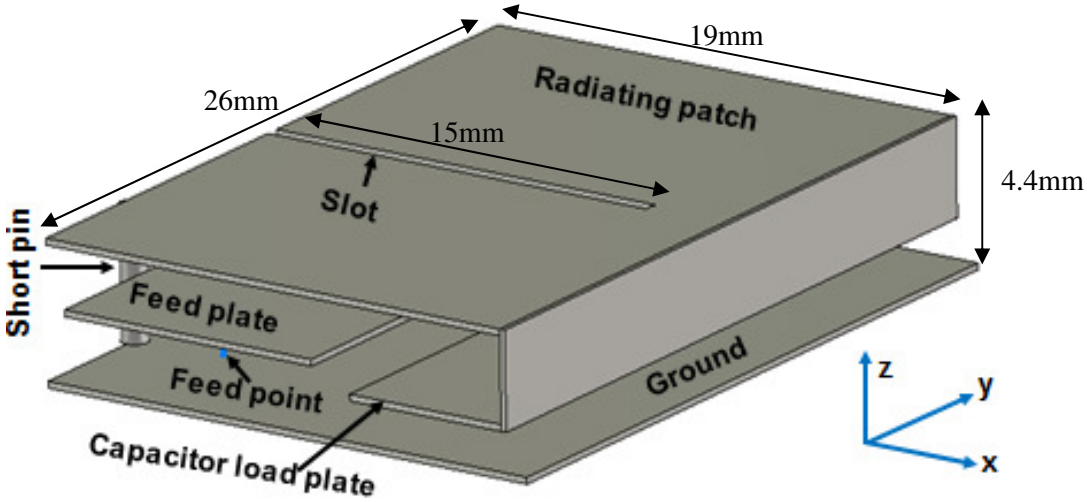

(a)

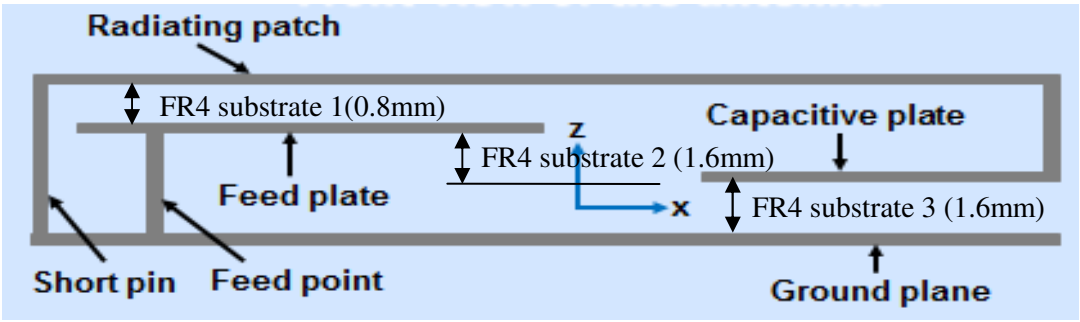

(b)

Fig. 4.4: Geometry of the proposed implantable antenna: (a) 3-D view; (b) Front view

Antenna dimensions summary:

- Overall dimensions: 26mm×19mm×4.4mm
- Slot size on patch: 15mm×0.5mm
- Feed plate size: 26mm×10.5mm
- Capacitive plate size: 26mm×6mm
- Substrate: FR-4 (dielectric constant=4.3)
- Substrate thickness: 4mm(1.6+1.6+0.8)

4.5.3 Antenna Surrounding Environment Model

In this section, we describe the simulation model employed for the design of the antenna, which is embedded in a rat's body. It is assumed that the radiating patch is just below the skin of the rat. Therefore, muscle is assumed to exist in all other five sides of the antenna, ignoring the fat layer. In addition to this, the implantable antenna needs to be encapsulated by a biocompatible material. Therefore, a thin layer (1mm) of coating is added to all six outer sides of the antenna. The simulation model is outlined in Fig. 4.5.

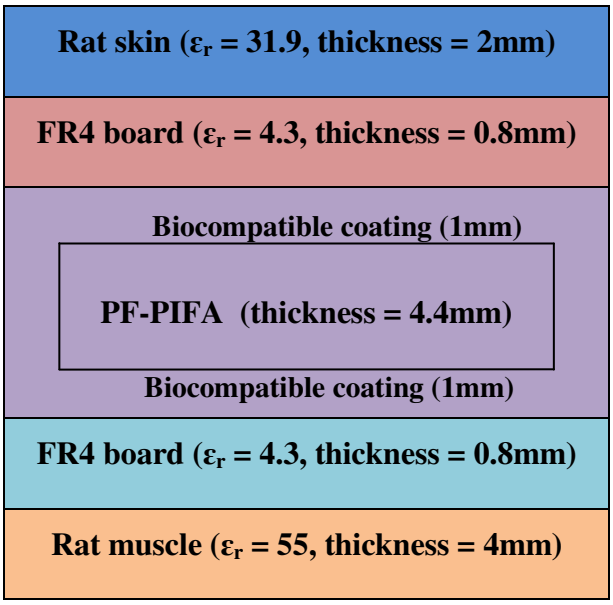

Fig. 4.5: The material layers of the simulation model

4.5.4 Simulation Results

Simulation results are presented in this section. Parametric analysis such as the relative permittivity of rat tissue, the feed plate area of the antenna to change the capacitance of the plate, the thickness of the rat skin on the radiating patch of the antenna, are applied in the simulation to determine their effects on antenna performance. The antenna parameters were determined by parametric optimisation. The dimensions of the antennas were truncated to the closest 0.1mm during optimisation. Fig. 4.6 shows the predicted input S11 magnitude of the PF-PIFA design. It is seen from the figure that the 10dB return loss bandwidth is 26MHz or 2.8%, from 895MHz to 921MHz. This bandwidth is sufficient for short-range implantable RF telemetry since the physiological signals of laboratory rats require relatively low data rates. The best value of the S_{11} magnitude is observed as -18dB at 908MHz. This is a promising result for such a small antenna. In Fig. 4.7, the real part of the antenna input impedance is presented. Here, the peak input resistance is found to be 45Ω which is close to the target 50Ω. Probably, this difference is due to the one decimal approximation to the antenna dimensions during optimisation. This one-decimal approximation is in line with the fabrication constraints of the antenna, since a tighter tolerance is practically difficult.

The imaginary part of the input impedance of the antenna is given in Fig. 4.8.Within the bandwidth of 895-921MHz, the input reactance swings between +4Ω and -35Ω. This value is slightly higher than expected, but acceptable because the antenna is still matched.

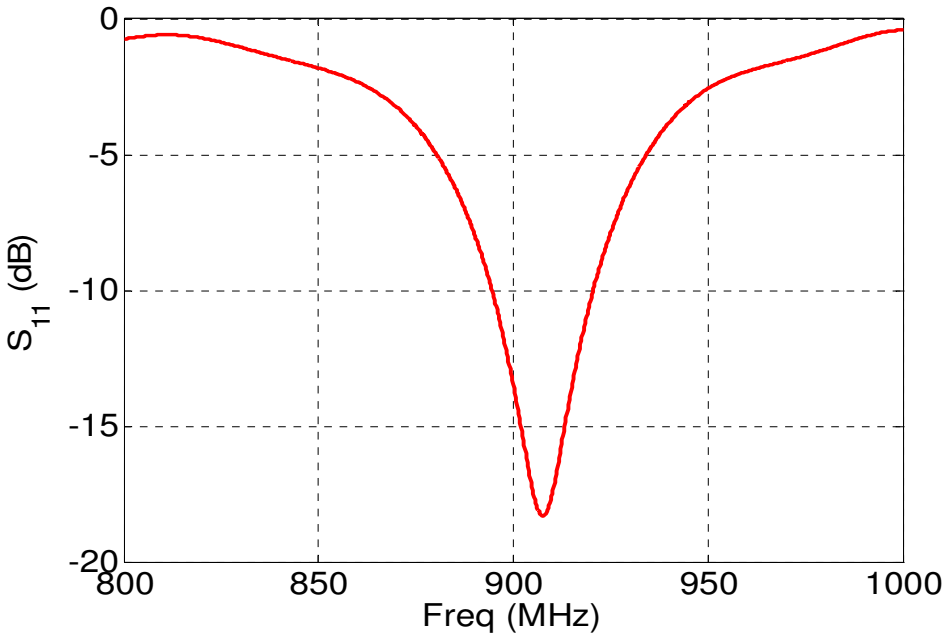

Fig. 4.6: Input S11 magnitude versus frequency

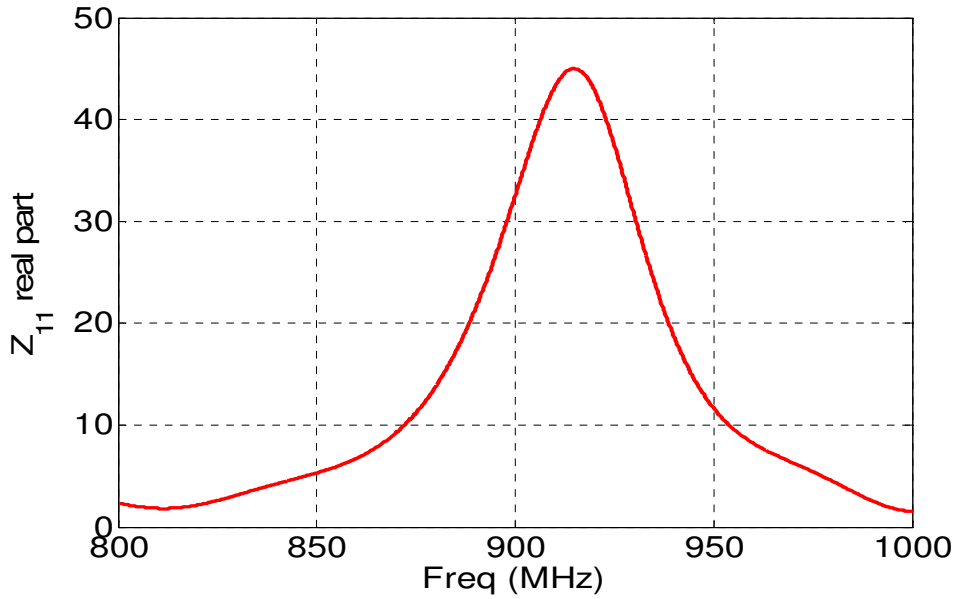

Fig. 4.7: Input resistance of the antenna in ohms

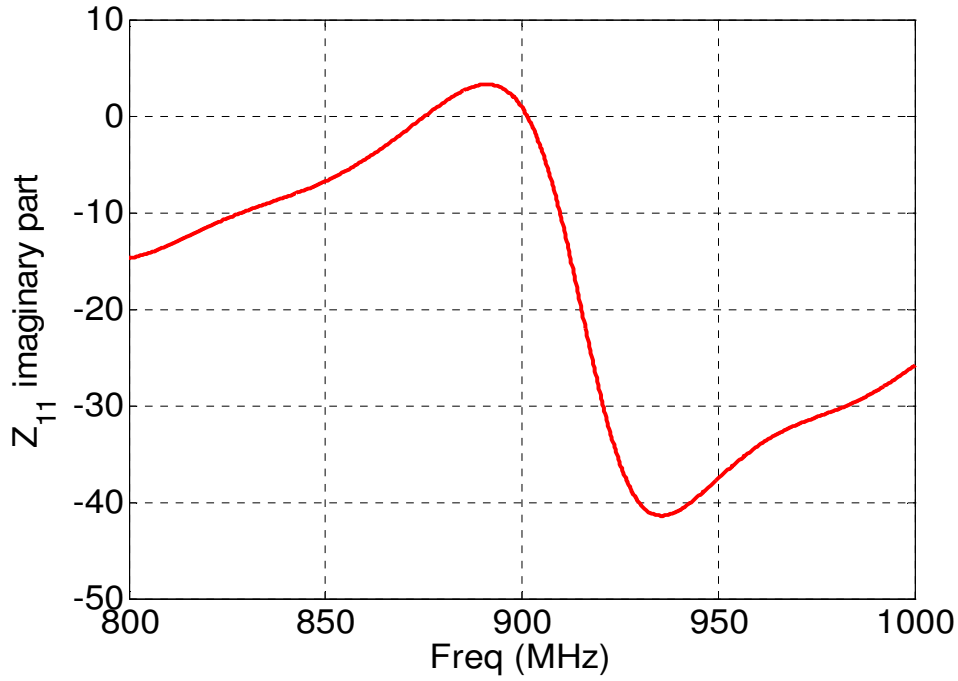

Fig. 4.8: Input reactance of the antenna in Ohms

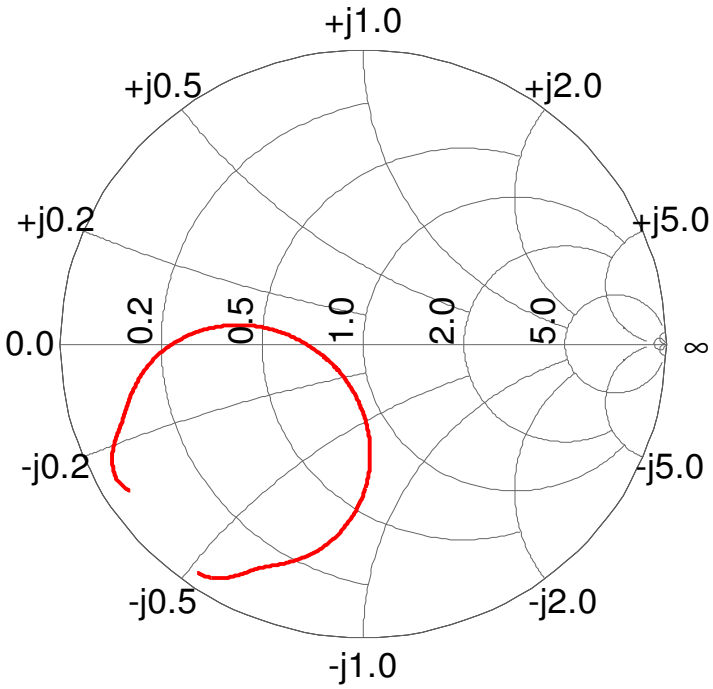

Fig. 4.9: Input impedance on Smith chart

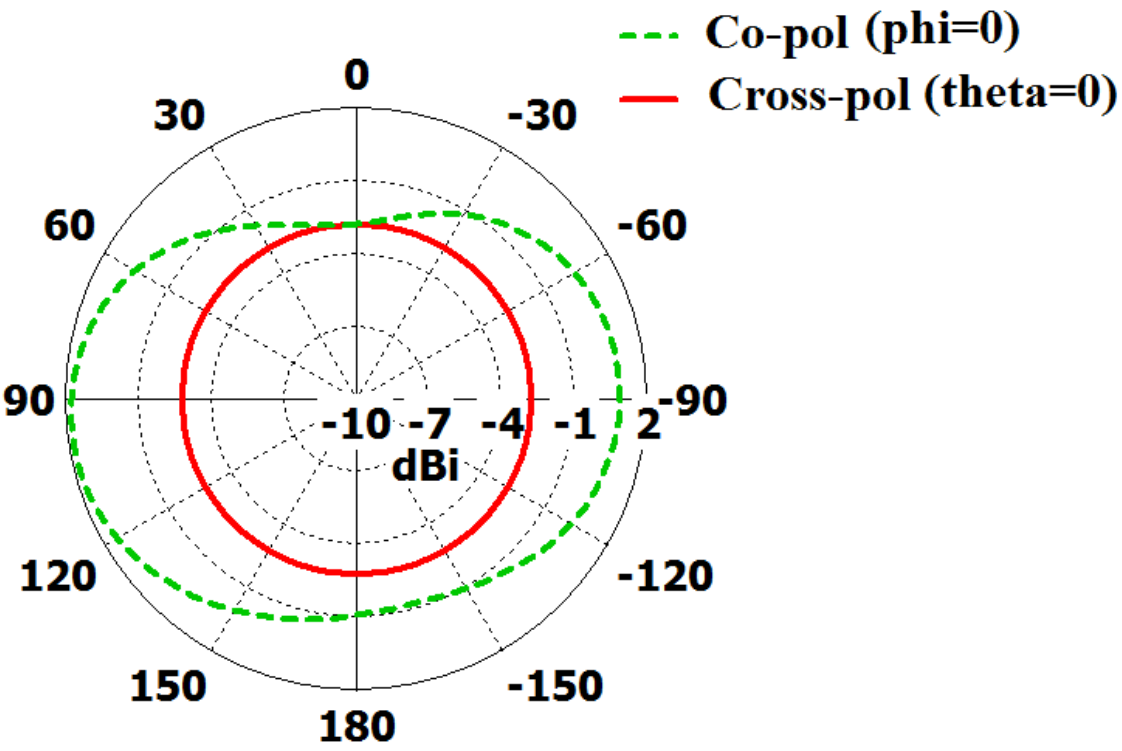

Fig. 4.10: Radiation pattern of the antenna

Fig. 4.9 shows the input impedance of the antenna on a Smith chart, for the frequency range from 800-1000MHz. In Fig. 4.10, the radiation pattern of the antenna is shown. It is found that the maximum radiation is approximately 2dBi when theta is 90 degrees and phi is zero degrees. The sensitivity of the antenna due to the relative permittivity variations of rat skin is reported in Fig. 4.11. Since it is known that the relative permittivity of rat skin changes due to various reasons such as the water contents, a parametric study was performed to observe the range of variation. It is also important to perform such a study to specify whether the resonance frequency will remain in the desired band or not.

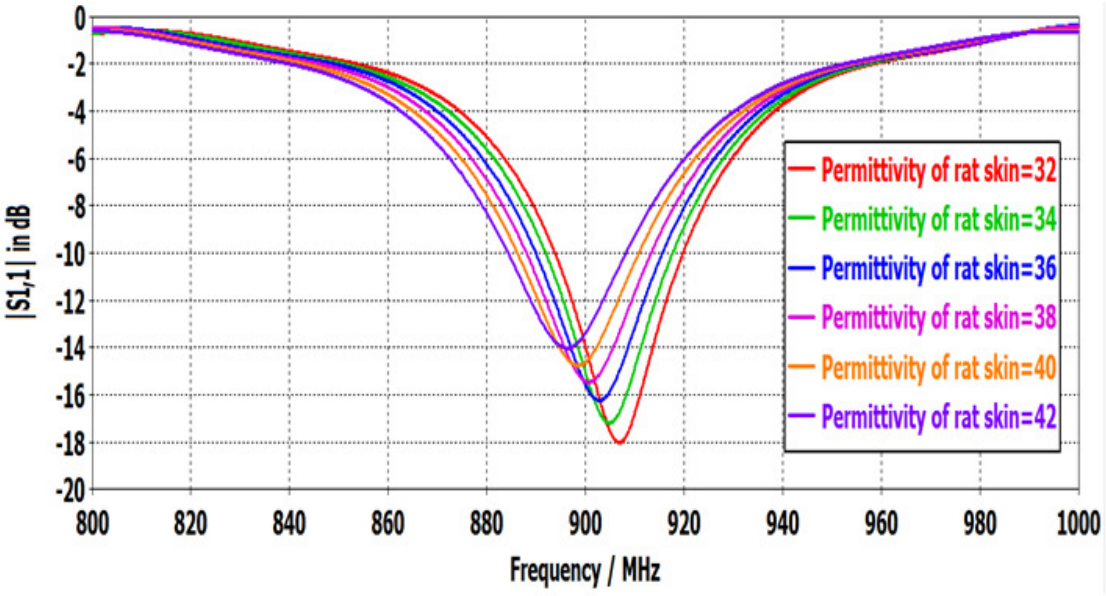

Fig. 4.11 Sensitivity of the antenna due to permittivity variations of rat skin

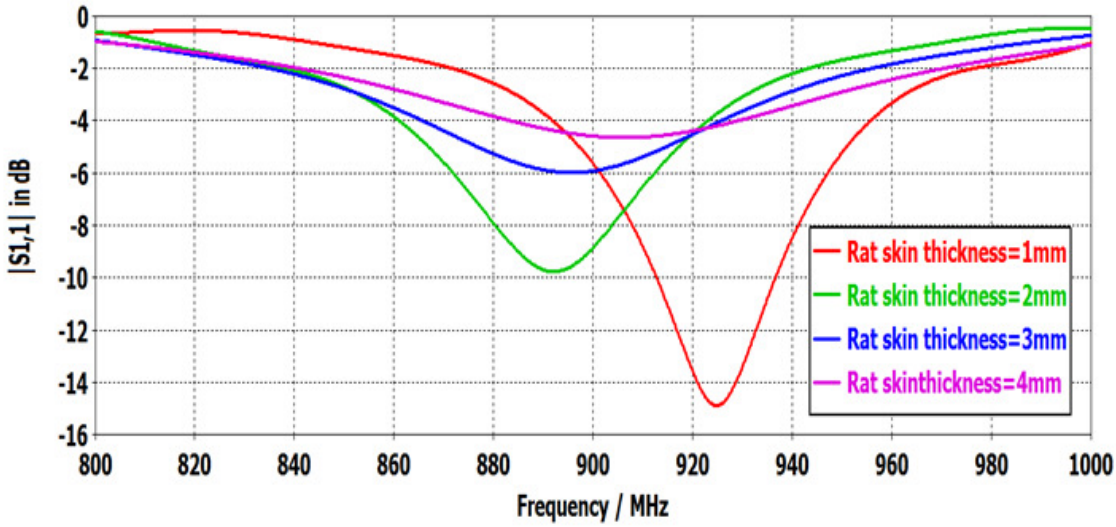

Fig. 4.12 Sensitivity of the antenna due to thickness variations of rat skin

Fig. 4.12 illustrates the sensitivity of the antenna to thickness variations of the rat skin on top of the antenna. The best value of return loss (-15dB) is obtained at 925MHz when the thickness of rat skin is 1mm. This confirms that sensitivity is huge for rat skin the thickness variation.

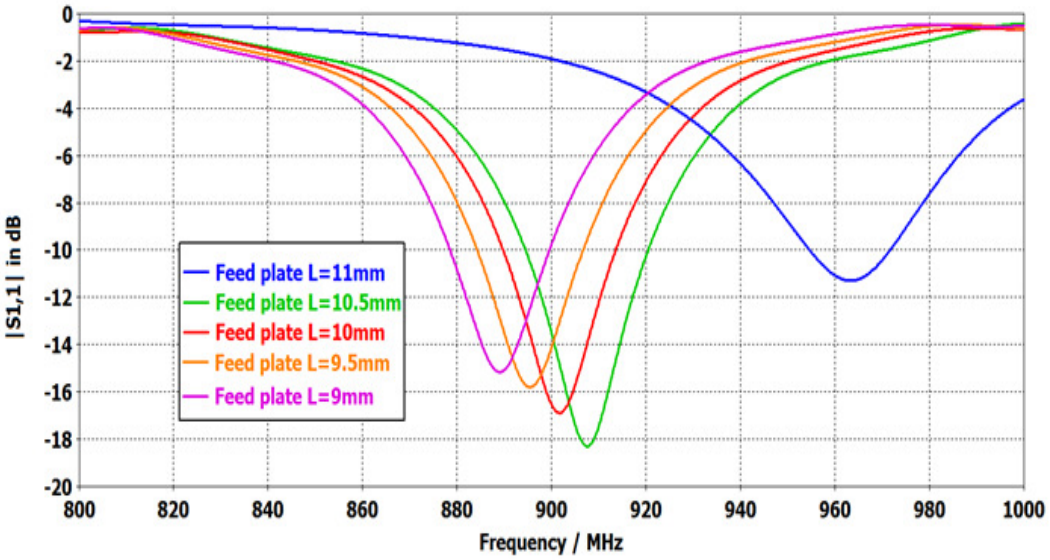

Fig. 4.13 Sensitivity of the antenna due to length variation of feed plate (increasing feed plate area) with 1.5mm-thick rat skin (relative permittivity 32)

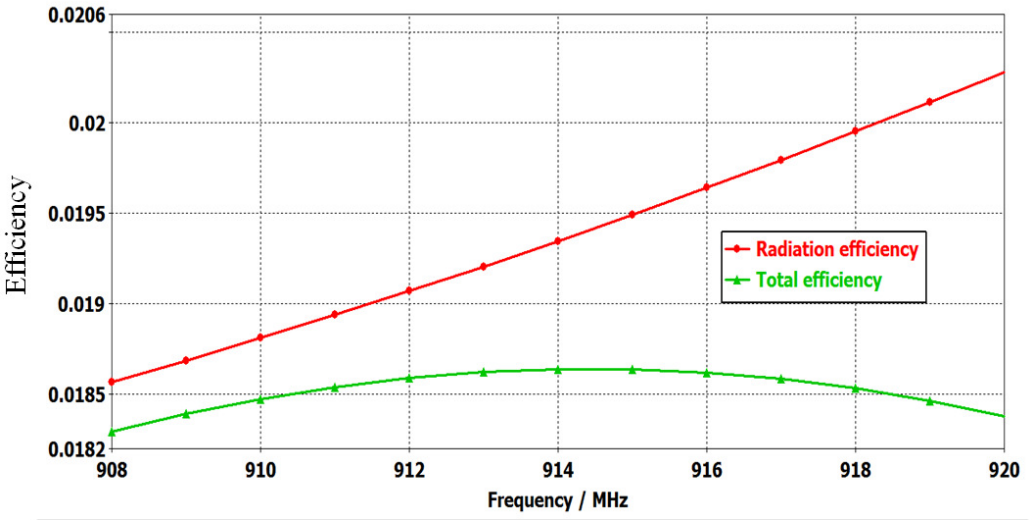

Fig. 4.14 Efficiencies of the antenna under 1.5mm thick rat skin with permittivity 32

In Fig. 4.13, the sensitivity of the antenna due to feed-plate length variation of the antenna is presented. The best value of return loss (-18dB) is obtained at 910MHz when proximity coupling feed-plate length is10.5mm. Fig. 4.14 shows the efficiencies of the

antenna when it placed below 1.5mm-thick rat skin with permittivity 32. This efficiency is a snapshot as the permittivity of rat skin is not a fixed quantity. It is clear from the figure that radiation efficiency (ratio of total power radiated by an antenna to the net power accepted by the antenna) and total efficiency (radiation efficiency multiplied by the impedance mismatch loss of the antenna, when connected to a transmission line or receiver) are closer at lower frequency, for example at 910MHz the efficiency of the proposed implantable antenna is approximately 1.8%.

4.6 Conclusion

The proposed PF-PIFA is small enough to be implanted under the skin of a rat. Its bandwidth is large enough for the wireless transmission of physiological signals in rats. A miniaturized partially folded planar inverted-F antenna (PF-PIFA) is proposed for a wireless physiological data acquisition system, being developed for small rodents including rats. The system operates in the Australian 900MHz ISM band (915-928MHz). The overall size of the antenna is $26\times19\times4.4mm^3$ and it has been designed to be implanted just under the skin of a rat. The 10dB return-loss bandwidth of the antenna is 2.8%, which is sufficient for this telemetry system. The RF link distance between the implanted and external antennas is assumed to be about 2m.

Chapter 5

Implantable PIFA Designs for RF Chip Side of the RFID tag PCB

5.1 Introduction

In the previous chapter, the design of a partially folded PIFA (PF-PIFA) for an implantable RFID tag PCB was presented and the antenna parameters were investigated. Although the predicted antenna bandwidth of PF-PIFA was good, the antenna size was still large in terms of the space available (33mm×15mm) on the RFID tag PCB to be implanted in a rat. Therefore, further investigations for implantable PIFAs were carried out to determine the possibility of achieving a smaller size but with reasonable antenna bandwidth. In this context, three compact implantable UHF PIFAs were designed and parametric studies were conducted. All of them are intended to be attached on the RF chip side of the RFID tag PCB and to be implanted under the skin of a rat. This RFID tag PCB has a micro-controller, an RF chip and an internal temperature sensor, as well as some lumped elements on the upper side (top) and a ground plane on the bottom side. Power to this implantable unit is supplied from a small button battery. Assessments of resonance frequency sensitivity due to changes in the surrounding antenna environments (biocompatible material and rat tissue) were performed.

5.2 Chapter Contributions and Background

5.2.1 Chapter Contributions

In this chapter, three compact PIFA designs are presented. Contributions of this chapter are:

- Smaller implantable PIFAs have been designed compared to the previous PF-PIFA
- Bandwidth enhancement for antenna designs 1 and 3
- Antenna efficiency improvement for antenna design 2
- Optimisation of antenna parameters through parametric studies of antenna designs 1, 2 and 3
- Utilisation of the RFID-tag ground plane in a combination with the antenna ground plane
- J-shaped proximity feed design for multilayered antenna design 3 to enhance the impedance matching
- Some of the content of this chapter has been published in [16, 75, 76]

5.2.2 Background

The preliminary antenna design presented in the previous chapter required more space than what is available for the implantable antenna and it led the designs of more compact antennas. However, some trade-off is necessary depending on the requirements and applications. For instance, reduction of antenna size often reduces the bandwidth and radiation efficiency of the antenna. As an implantable antenna intended for a small animal such as a rat or mouse must be small, low radiation efficiency is acceptable for the bio-telemetry application. This chapter presents three new implantable compact PIFA designs

and examines their performances to identify the trade-off for antenna parameters. All implantable antennas presented in this chapter are intended to attach on the components side of the RFID-tag PCB shown in Fig. 5.1. The maximum area available for the implantable antenna is 33mm×15mm on the component side of the RFID-tag PCB. This RFID-tag has a built-in temperature sensor to sense the body temperature from the animal/human, once implanted and one task of the implantable antenna is to transmit the recorded temperature to an external RFID reader. The RF module is also located on this side and the output impedance of the RF chip is transformed to ~50Ω using a lumped impedance transformer circuit so that any antenna with a 50Ω input impedance can be matched to the RF chip. The PIFA has an inherently narrow bandwidth and therefore capacitive feed techniques have been developed to enhance its bandwidth. In my designs 1 and 3, capacitive feeds are applied while in design 2 direct feed is applied.

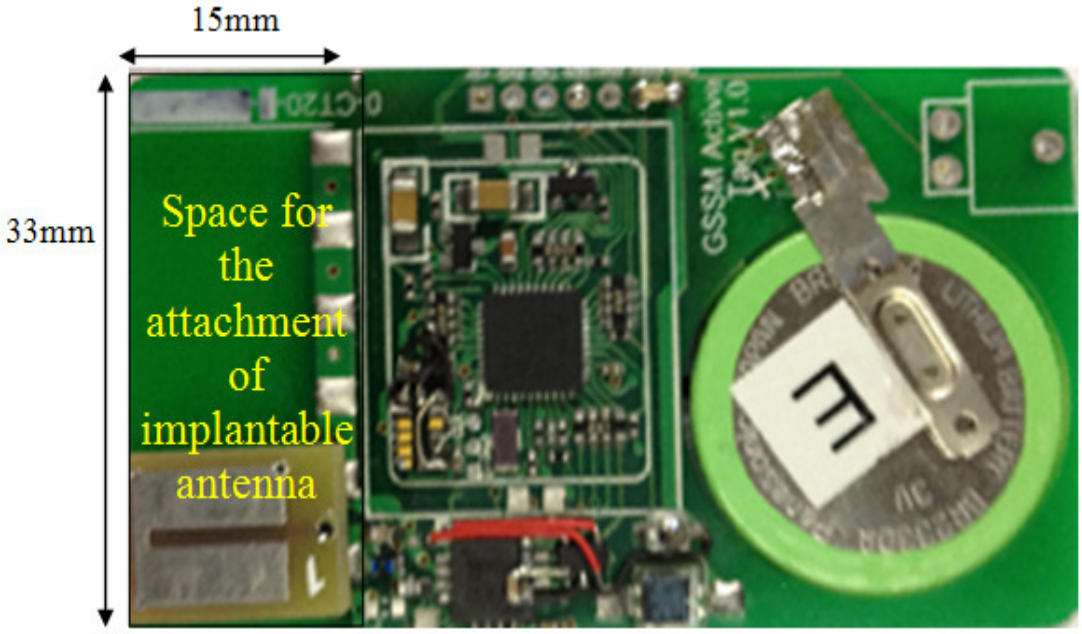

Fig. 5.1: Component side of the RFID-tag PCB showing space available for an implantable antenna

5.3 Implantable PIFA Design 1

The geometry of the designed PIFA Antenna 1 is shown in Figs. 5.2-5.4. The antenna parameters have been optimised by computer simulation using CST Microwave Design Studio software. The overall dimensions of the final design are 12mm×12mm×4mm. The area of the top radiating patch is 12mm×12mm. It is on a 0.8mm-thick Substrate-1 (RT5880LZ, dielectric const. = 1.96, loss tangent = 0.0019).

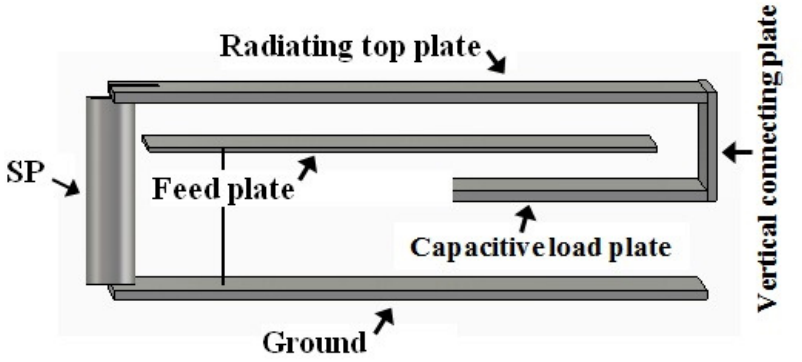

(a)

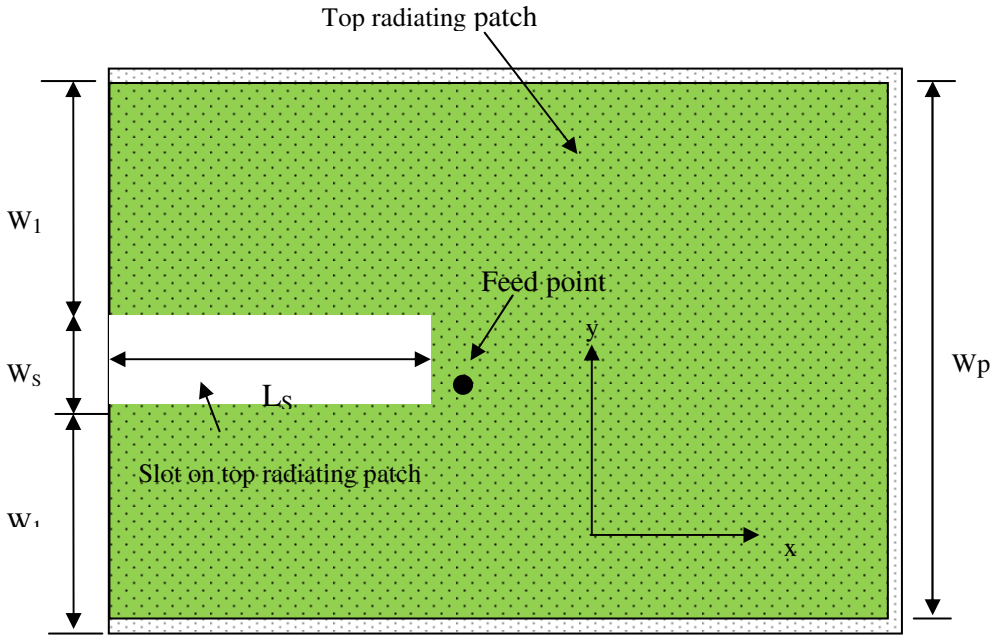

(b)

Fig. 5.2: Proposed Antenna 1 geometry: (a) 3D view; (b) Top view

A capacitively-coupled feeding plate is located on the lower surface of this substrate and its area is 9.5mm×12mm. There is a second Substrate-2 (RT5880LZ) below this feeding plate with the same thickness of 0.8mm. A capacitive load plate is located on the bottom surface of this second substrate. A third Substrate-3 (RT5880LZ) with a height of 1.6mm is on the ground plane of the antenna. The area of the ground plane is also 12mm×12mm. The top radiating patch and the capacitive load plate are connected by a vertical plate having the same width as the radiating patch (12mm). Its length has been optimised to 6mm by parametric optimization. Changing the area of this capacitive load plate will vary the capacitance between this and the ground plane. Such a change can be utilised for tuning the antenna resonance frequency. Feeding to the feed plate is performed from the bottom of the antenna using a via and the feed is located at x=3mm and y=5.5mm. A shorting pin (SP), located at x= 0, y=3, connects the radiating patch to the ground plane, and its height is 3.6mm. Table 5.1 shows the optimised antenna parameters of Antenna 1.

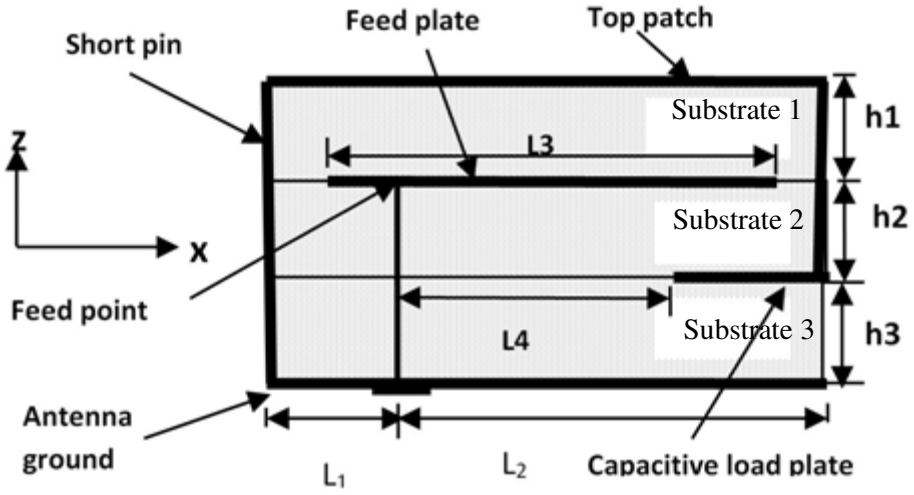

Fig. 5.3: Front view of the Antenna 1

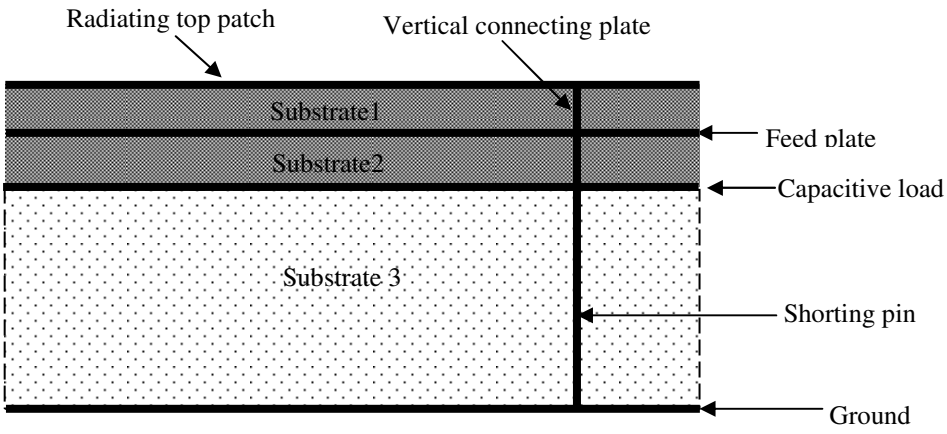

Fig. 5.4: Side view of the Antenna 1

Table 5.1: Optimised antenna parameters of Antenna 1

Optimized parameters of Antenna 1	**Symbol**	**Value (mm)**
Top radiating patch length	$L_1 + L_2$	12
Top radiating patch width	W_P	12
Top patch slot length	L_S	1
Top patch slot width	W_S	1
Feed plate length	L_3	9.3
Feed plate width	W_p	12
Ground plane length	$L_1 + L_2$	12
Ground plane width	W_p	12
Substrate-1 height	h_1	0.8
Substrate-2 height	h_2	0.8
Substrate-3 height	h_3	1.6
Short pin height	$h_1+h_2+h_3$	3.2
Feed point location	(x_F, y_F)	(3, 5.5)
Length of capacitive load	$L_2 - L_4$	6
Width of capacitive load	W_p	12

5.4 Model of Antenna 1 Surrounding Environment

The antenna's surrounding environment including the rat's body material needs to be modeled and included in the antenna design and optimisation process. The developed model for the rat tissue, surrounding the proposed implantable Antenna 1 is shown in Fig. 5.5. It is worthwhile to mention here that a biocompatible coating is also included in the model as it also has significant impact on the implantable antenna. The thickness as well as the relative permittivity of the biocompatible coating material play important role for the tuning the resonance frequency of the implantable antenna since it acts as the superstrate of the antenna.

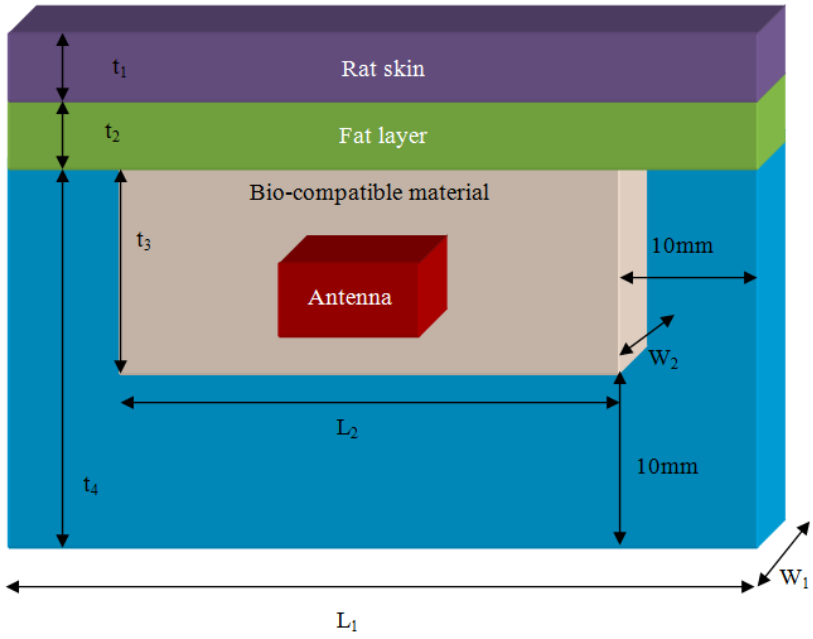

Fig. 5.5: Model of the Antenna 1 surrounding environment

The top layer of the model is skin and there is a fat layer below the skin. The antenna, enclosed by bio- compatible material (relative permittivity = 11.9), is placed under the fat layer. The rat's muscle covers the other sides of the enclosed antenna. Silicone is considered here as a suitable biocompatible material so that the antenna will not react with rat's body tissue. Table 5.2 shows the electrical parameters of the rat tissue

[6] of Antenna 1 while the surrounding environment parameters of Antenna 1 are shown in Table 5.3.

Table 5.2: Electrical parameters of rat tissue used for Antenna 1 [6]

Name of the rat tissue	Dielectric constant (ε_r)	Electrical cond. (σ), S/m
Skin	32	0.69
Fat	5.6	0.08
Muscle	58.8	0.84

Table 5.3: Surrounding Environment model parameters of Antenna 1

Surrounding environment model parameter of antenna 1	Symbol	Value (mm)
Rat's skin thickness on Fat layer	t_1	2
Fat layer thickness on silicone	t_2	2
Silicone box height	t_3	6
Skin layer length along X-axis	L_1	54
Skin layer width along Y-axis	W_1	54
Fat layer length along X-axis	L_1	54
Fat layer width along Y-axis	W_1	54
Muscle layer length along X-axis	L_1	54
Muscle layer width along Y-axis	W_1	54
Muscle height along Z-axis	t_4	16
Silicone box length	L_2	14
Silicone box width	W_2	14

5.5 Effects of Environment and Antenna Parameters on Antenna 1

In this section, we study the sensitivity of the antenna return loss and impedance bandwidth to antenna parameters (such as slot length) and environment parameters (such as skin permittivity). Figs. 5.6-5.8 illustrate the variation of antenna input matching with (i) slot length on the top radiating patch, (ii) area of the capacitive load plate, and (iii) permittivity of the substrates.

The effects of the antenna environment on its return loss are illustrated in Figs. 5.9-5.12. The relative permittivities of biocompatible material, rat skin, fat and muscle have been varied to observe the effects of those parameters on the antenna return loss. The main purpose of varying these parameters is to study to what extent the resonance frequency of the designed antenna will be detuned when its environment changes. Since the electrical parameters of biological tissues can change for several reasons such as, for example, the age of the rat, it is important to study this detuning and ensure that the antenna is matched in the operating ISM band under all operating conditions. Retuning of the resonance frequency of the antenna is not possible after implantation.

5.5.1 Effect of Slot Length of Radiating Patch on Antenna 1

In Fig. 5.6, the return loss of the antenna is plotted when the slot length (L_s) on the top radiating patch is changed between 1-5mm. It shows that increasing the slot length from 1mm to 5mm will decrease the resonance frequency approximately from 920MHz to 880MHz. While detuning of the antenna due to the variations of muscle, fat and skin layers is beyond the control of antenna designer, this slot length can be utilised to retune the resonance frequency within a certain range, for instance over the 880MHz to 920MHz

UHF band. Although the return loss is also changed due to slot length variation, it never goes below 10dB. This slot is cut along the centre line of the patch. The slot width is 1.0mm.

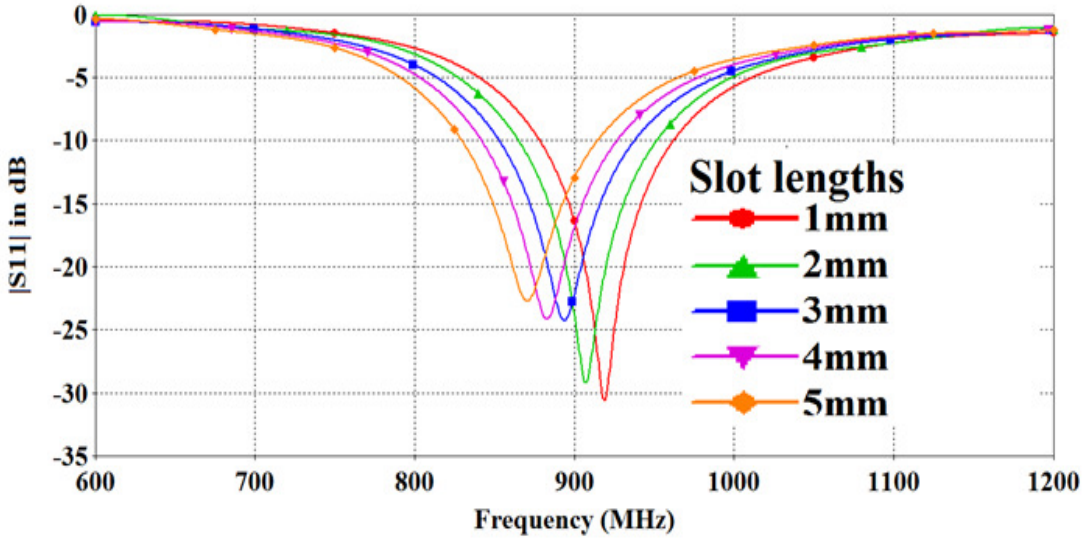

Fig. 5.6: Antenna 1 $|S_{11}|$ when the slot length on the top radiating patch is varied

5.5.2 Effect of the Capacitive Load Plate on Antenna 1

Fig. 5.7 shows the antenna return loss variation when the length of the capacitive load plate between the ground and the feed plate is varied between 3 and 7mm, by changing the capacitance of the load plate. At 10dB return loss, the resonance frequency decreases from 1010MHz to 890MHz with the increase of the plate capacitance. The width of the capacitive load plate is 12mm and hence the its area is varied from 3mm×12mm = 36mm^2 to 7mm×12mm = 84mm^2 . The height of this capacitive load plate is 1.6mm from the ground plane of the antenna. The minimum and maximum equivalent capacitances of the capacitive load plate can be easily determined by using the following formula:

$$\text{Capacitance, } C = \varepsilon_r \varepsilon_o \frac{A}{d} \qquad (5.1)$$

where ε_r is the relative permittivity of the substrate between the capacitive load plate and the ground plane, ε_0 is the permittivity of air, A is the plate area and d is the separation distance between the capacitive load plate and the ground plane. The variations of capacitance of the capacitive load plate due to the changes of plate length are:

$$C_{\min} = \varepsilon_r \varepsilon_o \frac{A}{d} = 4.3 \times 8.85 \times 10^{-12} \times (3 \times 12/1.6) \times 0.001\text{pF} = 0.856\text{pF} \qquad (5.2)$$

and

$$C_{\max} = \varepsilon_r \varepsilon_o \frac{A}{d} = 4.3 \times 8.85 \times 10^{-12} \times (7 \times 12/1.6) \times 0.001\text{pF} = 2.0\text{pF} \qquad (5.3)$$

From Fig. 5.7, it is evident that retuning of the implantable antenna is possible with a 10dB return loss for the band (915-928MHz) of interest by changing the area of the capacitive feed plate, which in turn changes the capacitance of the plate.

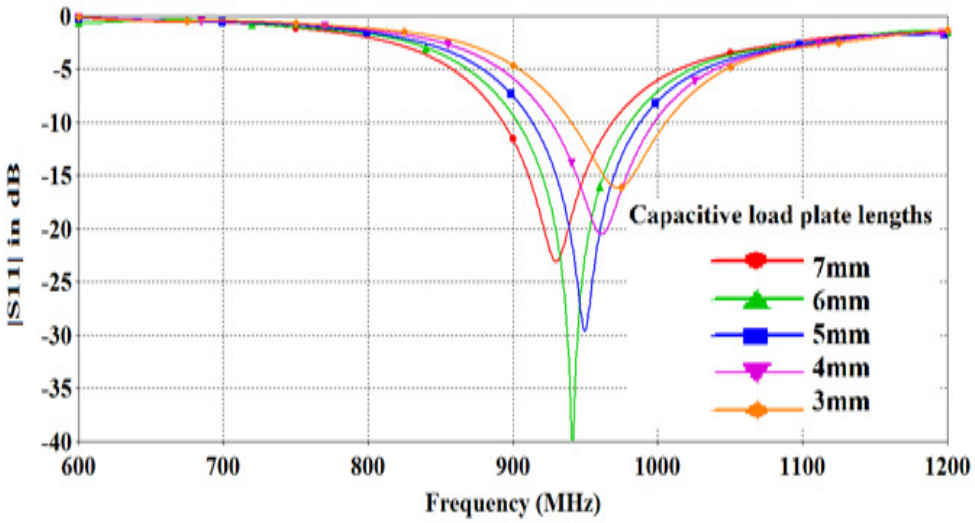

Fig. 5.7: Antenna 1 $|S_{11}|$ when the length of the capacitive load plate is varied along the x-axis

Calculating capacitances between ground plane and capacitive plate alone may not give the actual idea about the effect on the performance of the antenna. It is also

necessary to know the substrate used between these two plates. In addition, when the capacitance of the antenna is equal to inductance, optimum performance is obtained.

5.5.3 Effect of Substrate Permittivity on Antenna 1

The antenna return loss variations are shown in Fig. 5.8 when the relative permittivity of the substrate between the radiating patch and ground is varied, with a capacitive load plate length of 6mm. It is found that the resonance frequency decreases significantly, from approximately 920MHz to 750 MHz, with an increase of the substrate permittivity from 2 to 10. It is found that, with the best value (7mm) of capacitive load plate, the Australian UHF ISM band (915-928MHz) is covered when the permittivity of the substrate is 2. The permittivity of a particular substrate can change from one sample to another but that would be a much smaller change than this. Although a substrate with a high dielectric constant is typically used to reduce the size of the implantable antenna, it reduces the bandwidth of the antenna at the same time.

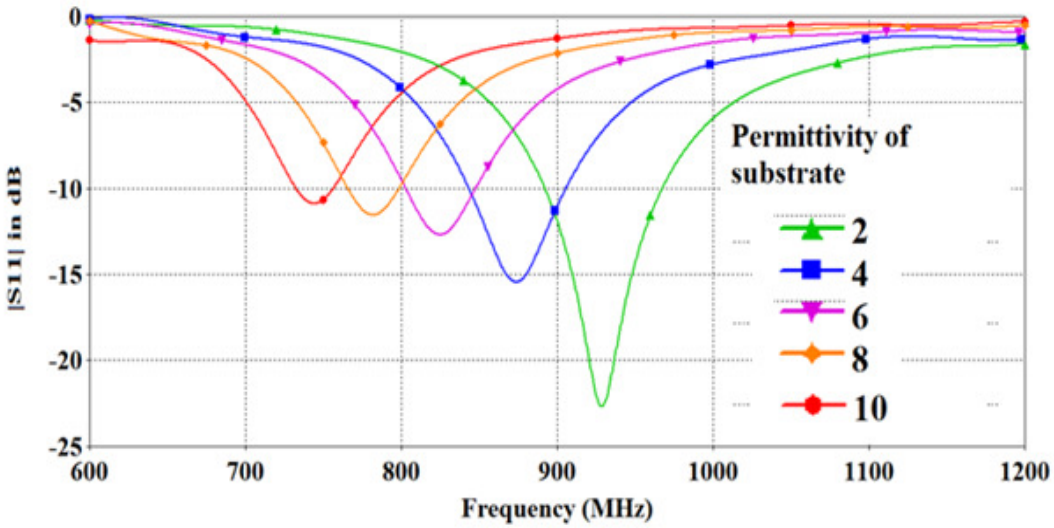

Fig. 5.8: Antenna 1 $|S_{11}|$ variation with relative permittivity of substrates 1, 2 and 3

The larger bandwidth is preferred for an implantable antenna, as the antenna might be detuned completely from the band of interest because of the effect of surrounding environment. If an implanted antenna is detuned completely, communication between the implantable device and the outside base station is lost and it is impossible to retune the implantable antenna from outside of the rat's body.

5.5.4 Effect of Biocompatible Coating Material on Antenna 1

In Fig. 5.9, the antenna return loss variation with the permittivity of the biocompatible coating (e.g. lossy silicone) is shown. This biocompatible material (such as silicone) acts as a superstrate of the antenna. When its permittivity is increased from 4 to 12, resonance frequency shifts down from 1140MHz to 920MHz.

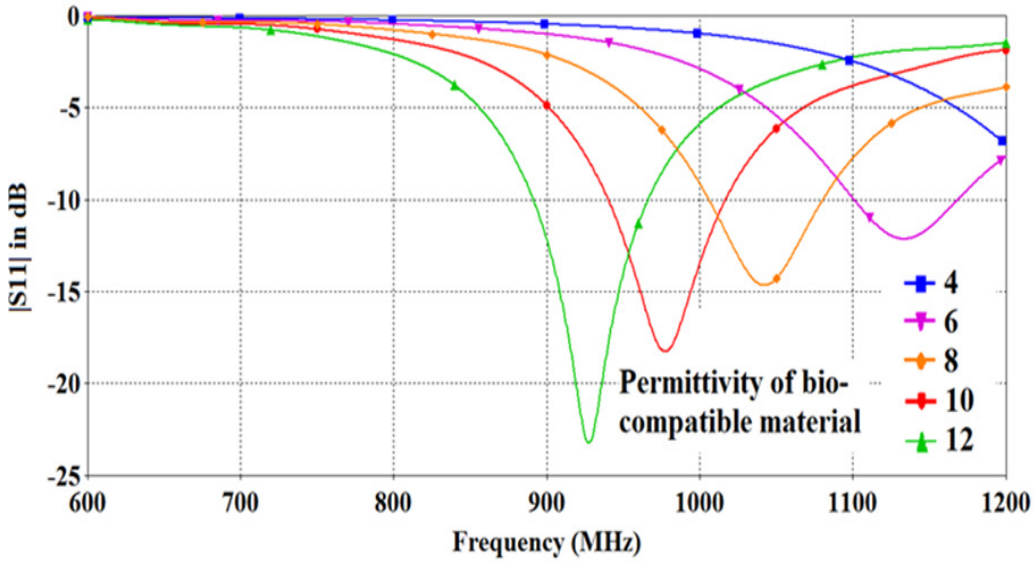

Fig. 5.9: Antenna 1 $|S_{11}|$ variation with the permittivity of the biocompatible coating

It is seen from the graph that optimum performance (23dB return loss at 920MHz) is obtained when the permittivity of the bio-compatible coating material is 12 with electrical conductivity, σ = 0.00025 S/m. However, a biocompatible coating material with such

high dielectric constant is difficult to achieve commercially. This material can be manufactured for coating an implantable device but it will be expensive since a special process is involved to prepare such material. It should be noted here that conductivity of the bio-compatible material also plays an important role in the performance of the antenna (although results are not shown with its variation). A significant resonance frequency detuning is observed due to the variation of the biocompatible material.

5.5.5 Effect of Rat Muscle on Antenna 1

The graph in Fig. 5.10 depicts the effect of rat muscle relative permittivity on the antenna return loss. In this case, the antenna resonance frequency decreases gradually, from 940MHz to 910MHz, when the muscle relative permittivity changes between 50 and 70 in steps of 5. The 900MHz UHF Australian ISM band of interest is covered for most of the variations except the extreme values of muscle permittivity.

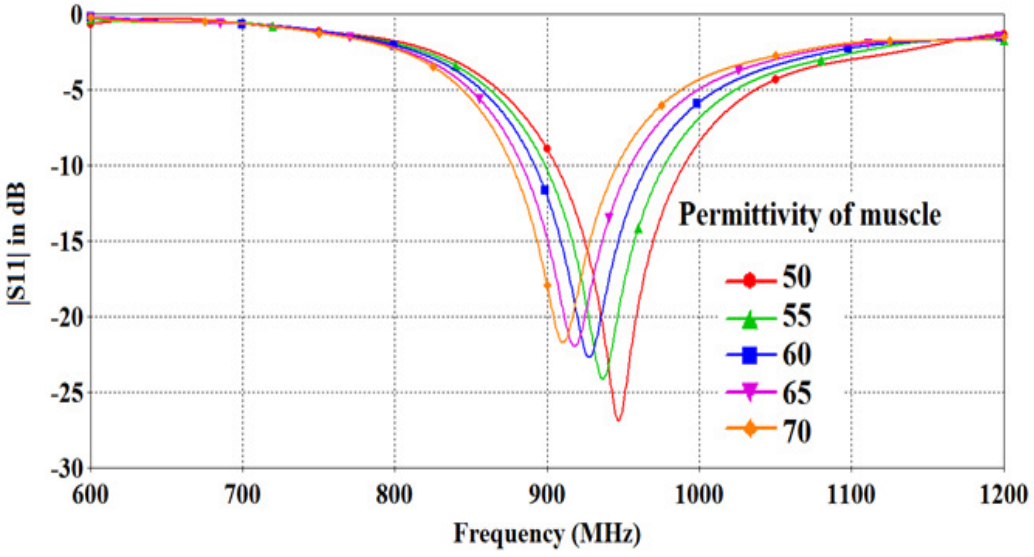

Fig. 5.10: The effect of muscle relative permittivity on $|S_{11}|$ of Antenna 1

From this result, it is clear that variation of muscle permittivity for the implantable device will not be a dominant factor if other antenna surrounding environment parameters are optimised. However, enough muscle volume must be considered for the antenna surrounding environment model since it affects the predicted radiation performance of the antenna. The location of the antenna with the implantable device is also an important factor. Generally, the proposed location for implantable device is just under the skin of the animal or human.

5.5.6 Effect of Fat Layer on Antenna 1

In Fig. 5.11, the effect of the relative permittivity of the fat on the antenna return loss is illustrated. It is found from the graph that the change in resonance frequency is negligible when the relative permittivity changes between 6 and 10. A bandwidth of approximately 90MHz (~10%) at 10dB return loss is preserved with variations of fat permittivity from 6 to 10. The permittivity of the fat layer can be changed for various reasons such as the weather condition and the age of the rat. This result also suggests that, in terms of antenna resonance frequency detuning, an implantable device can placed under the fat layer which is considered in the Antenna1 surrounding environment model.

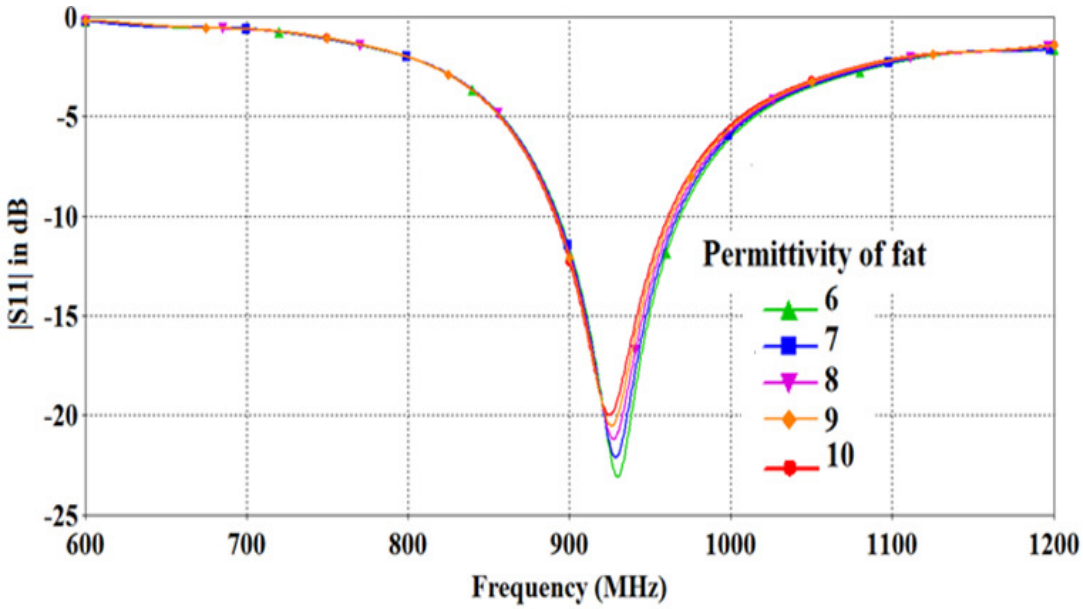

Fig. 5.11: The effect of fat relative permittivity on $|S_{11}|$ of Antenna 1

5.5.7 Effect of Skin Layer on Antenna 1

Fig. 5.12 shows the effect of relative permittivity of the skin on antenna return loss. Negligible shifting of the resonance frequency is noticed in this situation. The permittivity of the skin is varied from 30 to 40 in steps of 2 to study the detuning effect of Antenna 1. It is worthwhile to mention here that there are three superstrate layers on the antenna radiating patch: the bio-compatible coating layer (1mm thick), the middle fat layer (2mm thick) and the outermost skin layer (2mm thick). The stability of the resonance frequency is obtained by using the high-permittivity bio-compatible coating material (silicone with a relative permittivity of 11.9).

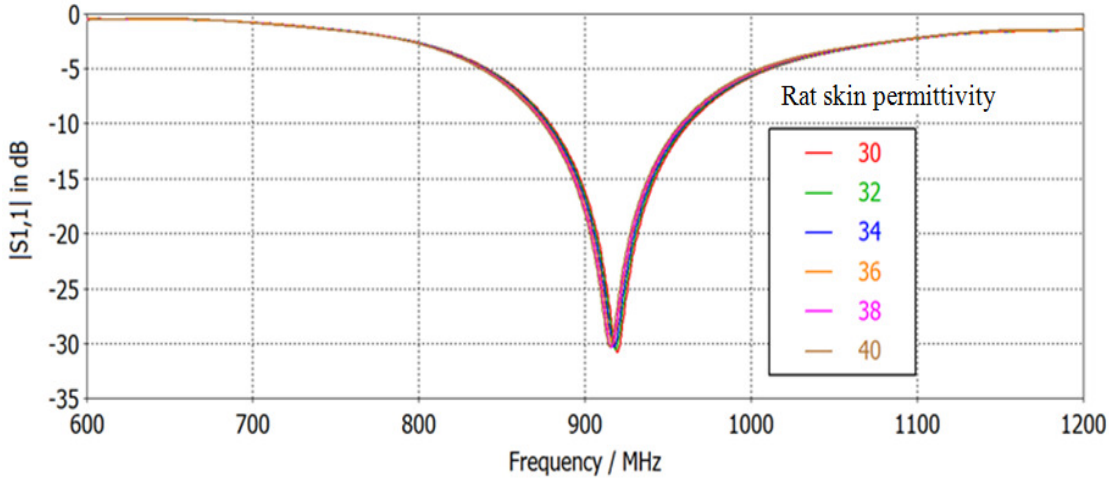

Fig. 5.12: The effect of rat skin permittivity on $|S_{11}|$ of Antenna 1

5.6 Optimised Simulation Results of Antenna 1

In this section, optimised simulation results for the Antenna 1 return loss, input resistance, input reactance, radiation efficiency, total efficiency and radiation pattern are presented (Figs. 5.13-5.17). The input reflection co-efficient of the proposed Antenna 1 is shown in Fig. 5.13. The optimised input reflection coefficient is found to be -30dB at 920MHz; that is, within the Australian UHF ISM band. The 10dB return-loss bandwidth of Antenna 1 is 9.2% (877-962MHz), which entirely covers the Australian UHF ISM band (915-928MHz). In Fig. 5.14, the input resistance of Antenna 1 is shown. An input resistance of 52Ω is obtained at 920MHz, confirming good impedance matching of Antenna 1. The reactance of Antenna 1 is plotted in Fig. 5.15, and it is evident from the figure that the reactance is within 1.0Ω and -3.0Ω in the Australian ISM band. It is known that the expected input reactance of an antenna should be zero for optimum performance of the antenna. Fig. 5.16 illustrates the radiation and total efficiencies of the designed Antenna 1. The radiation efficiency (0.4%) converges to total efficiency at 920MHz. The

radiated energy is mostly absorbed by the rat tissue and biocompatible material. As a result, a low radiation efficiency is achieved from the proposed Antenna 1. However, the literature suggests that such a low radiation efficiency is acceptable for implantable antennas for biomedical applications. The absolute directivity is plotted in Fig. 5.17, and the maximum directivity is 2.31dBi at 920MHz.

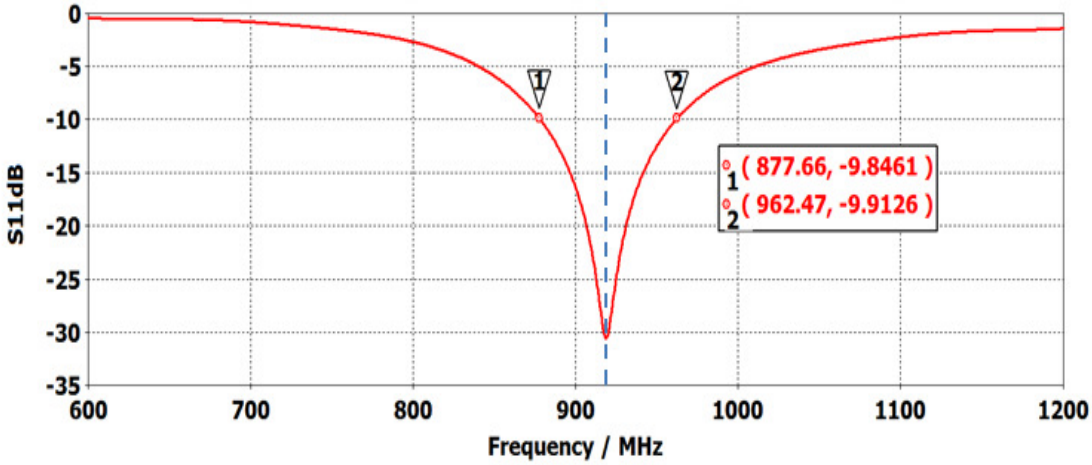

Fig. 5.13: Input reflection coefficient of Antenna 1

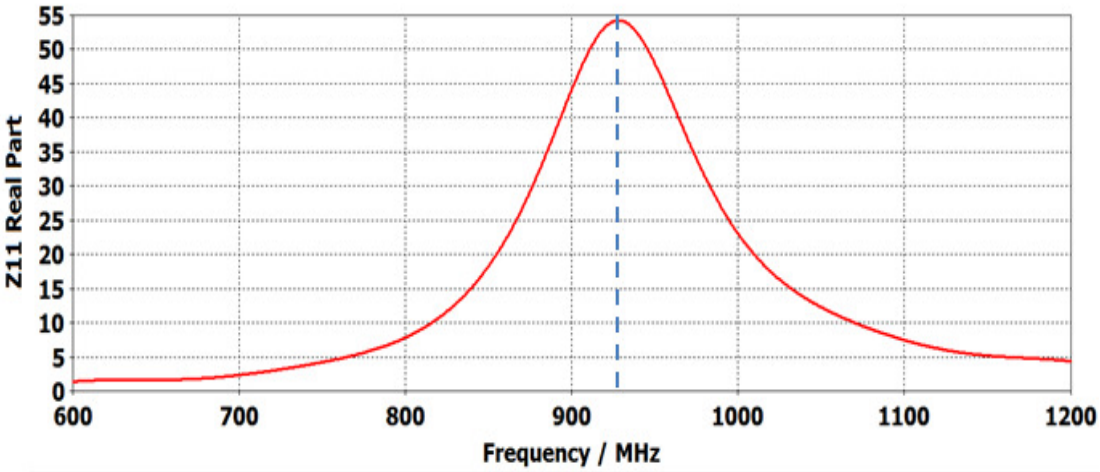

Fig. 5.14: Input resistance of Antenna 1

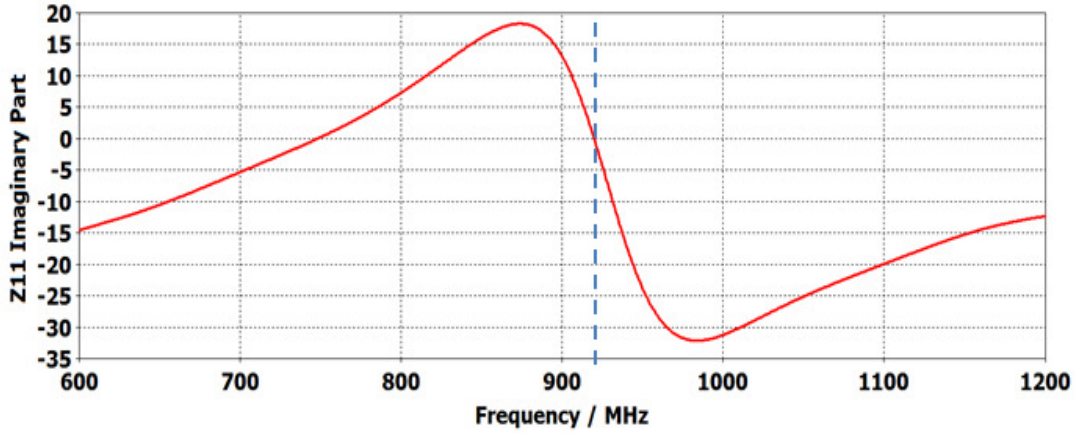

Fig. 5.15: Input reactance of Antenna 1

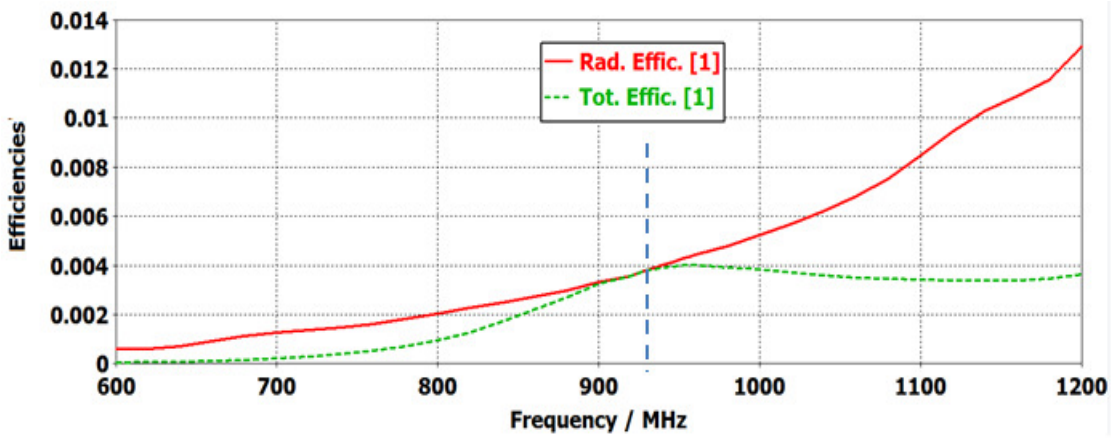

Fig. 5.16 Efficiency of Antenna 1

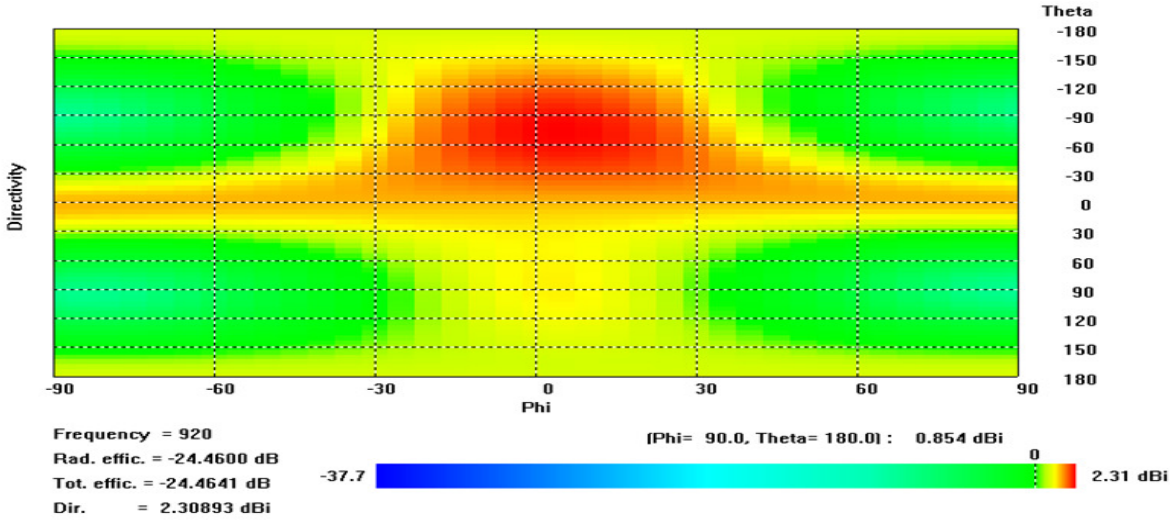

Fig. 5.17: Radiation pattern of Antenna 1

5.7 Implantable PIFA Antenna Design 2

The next antenna design is a second-order Hilbert PIFA. The geometry of this antenna resulting from the optimisation is shown in Figs. 5.18-5.19. The antenna parameters have been optimized by numerical analysis using CST Microwave Studio software. The overall metallic dimensions of the final Hilbert PIFA design are 25mm×25mm×7.6mm excluding the RFID ground plane and coating. The area of the top radiating patch (Hilbert curve) is 25mm×25mm. It is printed on a 5.6mm-thick (h_1) substrate (Rogers RO5880, dielectric constant, $\varepsilon_r = 2.2$). Although 5.6mm-thick Rogers RO5880 substrate is not commercially available, it can be constructed by a combination from substrates with the standard thicknesses of available substrates (3×1.6mm + 1×0.8mm = 5.6mm). A 3.2mm-thick (1.6mm+1.6mm) superstrate (Rogers TMM 10, dielectric constant = 9.2, loss tangent =0.0022) is placed on the top radiating Hilbert curve. Then the antenna is coated with a silicone (dielectric constant =11.9) which is a biocompatible material. The addition of superstrate in the antenna design 2 is to reduce the effect on the resonance frequency of the antenna due to the biocompatible layer. The antenna is fed through coax connector. The location of the feed point is x = 1mm from the left edge of the antenna ground plane and y = 7.8mm from the rear end of the Antenna 2 ground (Fig. 5.18). A shorting pin is used to further reduce the size of the proposed antenna, since its inductive behaviour compensates the capacitive nature of the Hilbert curve. It is connected between one end of the Hilbert curve and the ground (Fig. 5.18). The antenna ground is connected with the RFID circuit board ground (20mm×33mm) through five vias already located on the circuit board. The height and radius of each via connecting the two ground planes are 1.6mm and 0.5mm respectively.

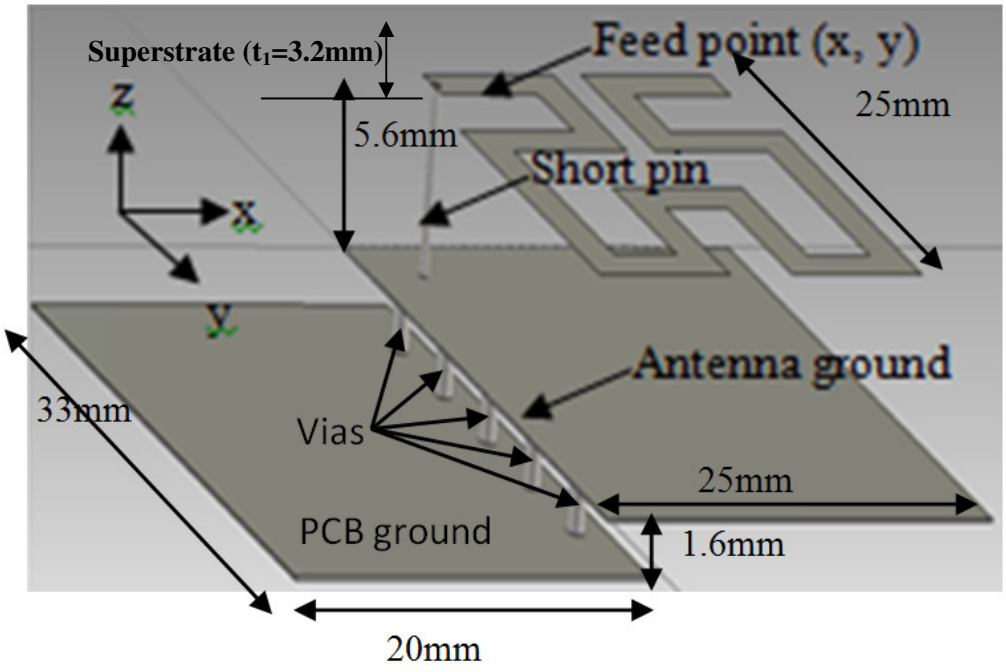

Fig. 5.18: 3D view of Antenna 2

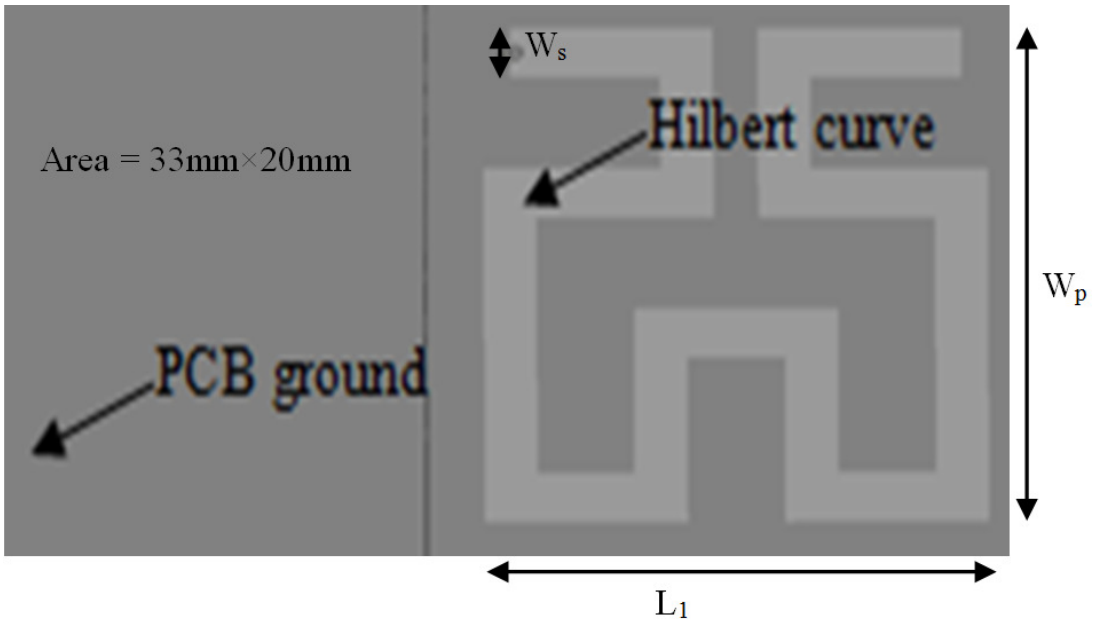

Fig. 5.19: Top view of Antenna 2

Table 5.4: Optimised Antenna 2 parameters

Optimized antenna 2 parameter	Symbol	Value (mm)
Top radiating patch length	L_1	25
Top radiating patch width	W_P	25
Trace width	W_S	2.2
Ground plane length	L_2	25
Ground plane width	W_1	25
Substrate height	h_1	5.6
Short pin height	h_2	5.6
Superstrate thickness	t_1	3.2

The antenna parameters have been studied, considering the surrounding media including the rat's body tissues. Moreover, a biocompatible coating layer inserted between the antenna and the rat's body tissue has also been considered in the analysis as described in the following section. The Antenna 2 parameters resulting after the optimisation processes are tabulated in Table 5.4.

5.8 Model of Antenna 2 Surrounding Environment

Because of the proximity of the different tissues to the antenna, the surrounding media need to be accurately modeled and included in the antenna design and optimisation process. Therefore, a model has been developed that considers the rat's body tissue which

surrounds the antenna. Additionally, a conformal coating involving a biocompatible material has been inserted around the antenna, as shown in Fig. 5.20, to facilitate its use in a bio-sensitive environment.

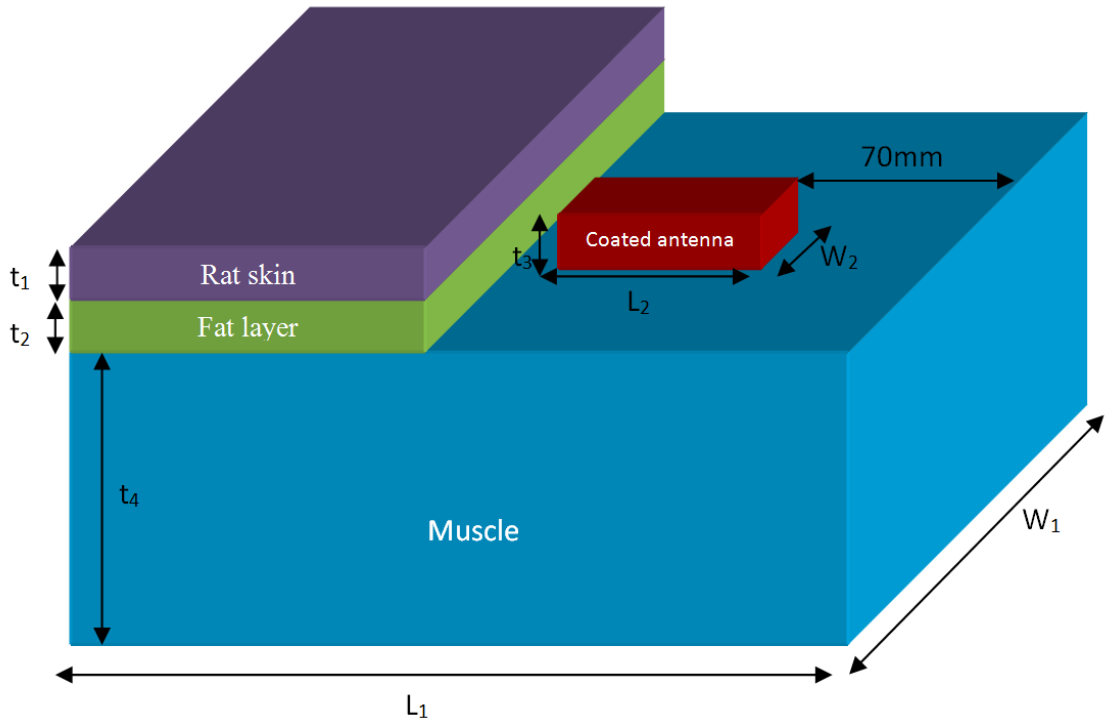

Fig. 5.20: Model of Antenna 2 surrounding environment

Hence, the antenna is contained within a block of biocompatible material which in turn is in direct contact with the biological tissues representing the actual working environment. The electrical properties of the rat's tissue for Antenna 2 are same as for Antenna 1 as mentioned earlier. The surrounding environment model parameters of Antenna 2 including the bio-compatible material (silicone with a dielectric constant of 11.9) are presented in Table 5.5.

Table 5.5: Antenna 2 environment model parameters

Environment model parameters of antenna 2	Symbol	Value (mm)
Rat skin thickness on fat layer	t_1	2
Fat layer thickness on silicone	t_2	2
Silicone box height	t_3	6
Skin layer length in X-axis	L_1	200
Skin layer width in Y-axis	W_1	60
Fat layer length in X-axis	L_1	200
Fat layer width in Y-axis	W_1	60
Muscle layer length along X-axis	L_1	200
Muscle layer width in Y-axis	W_1	60
Muscle height along Z-axis	t_4	56
Silicone box length	L_2	60
Silicone box width	W_2	35

It should be noted that thicknesses of rat skin and fat layers vary from rat to rat depending on the age of the rat. We assume that the rat is an adult (weight: 500-700g) and its length is 200-250mm excluding the length of tail. This assumption is made after consultation with researchers at the Australian School of Advanced Medicine, Macquarie University, Australia, who are investigating various physiological signals (blood pressure, ECG etc.) in rats.

The top layer of the model is skin and there is a fat layer below the skin. The antenna, enclosed by bio-compatible material, is placed under the fat layer. Rat muscle covers the other sides of the enclosed antenna. Silicone is considered here as a suitable biocompatible material so that the antenna will not damage rat tissue and at the same time the antenna will not be short circuited due to the conductivity of the tissue.

5.9 Optimised Simulation Results of Antenna 2

The optimised input reflection coefficient of the antenna is shown in Fig. 5.21. The two curves correspond to the conditions with and without connecting the antenna ground and PCB circuit board ground. It shows that the input reflection coefficient of the antenna is increased to -19.8dB without connecting the two grounds, from the previous value of -31dB when they are connected together through 5 vias. Fig. 5.22 represents the impedance of the antenna on a Smith chart. At f = 908MHz, the antenna input resistance is 50.03Ω and its reactance is -2.8Ω, which represents good matching. In Fig. 5.23, the radiation pattern of the antenna at the same frequency is illustrated. The maximum directivity of 3.3dB is observed for $\theta = 70^0$ and $\varphi = -50^0$.

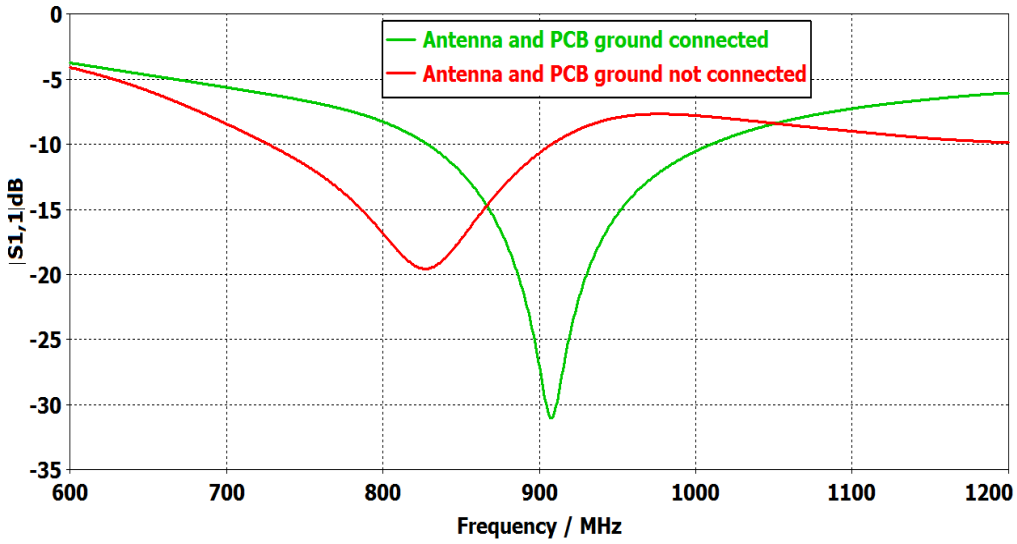

Fig. 5.21: Input reflection coefficient of Antenna 2

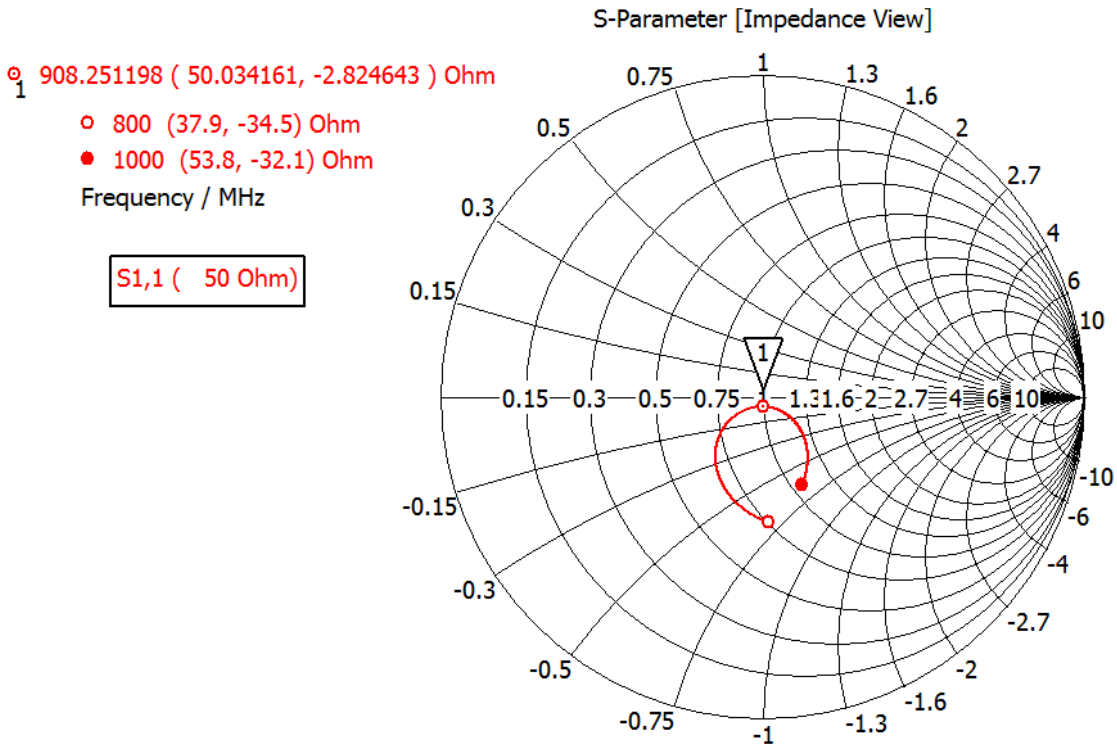

Fig. 5.22: Input impedance of antenna 2 on Smith chart

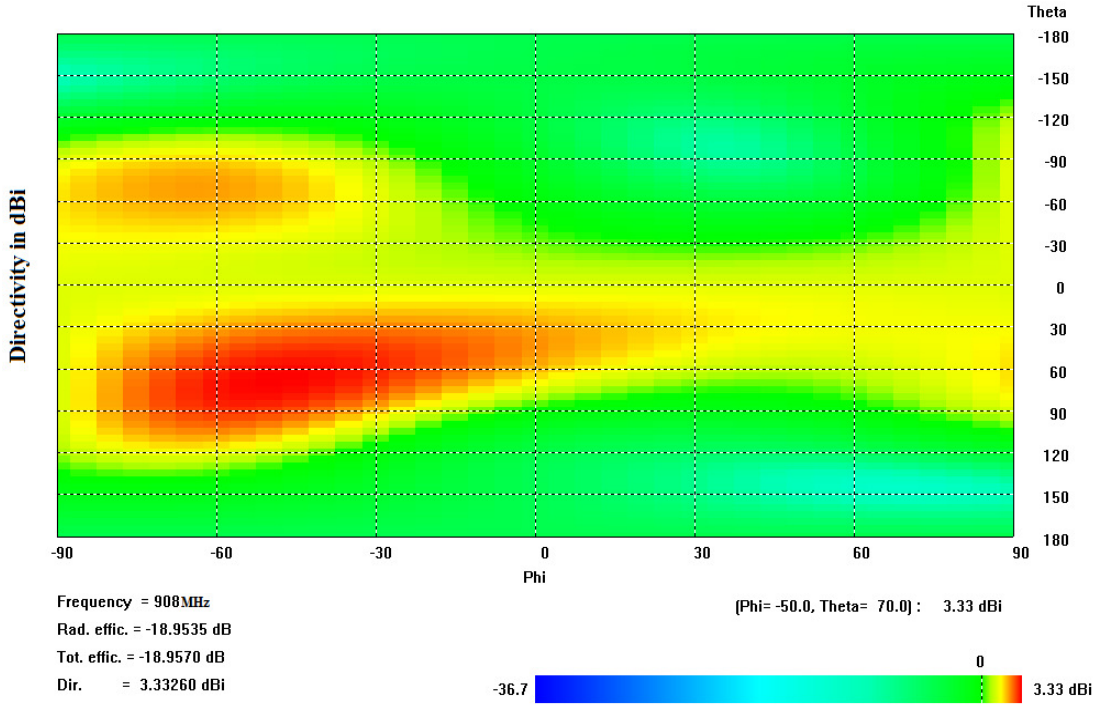

Fig. 5.23: Radiation pattern of Antenna 2

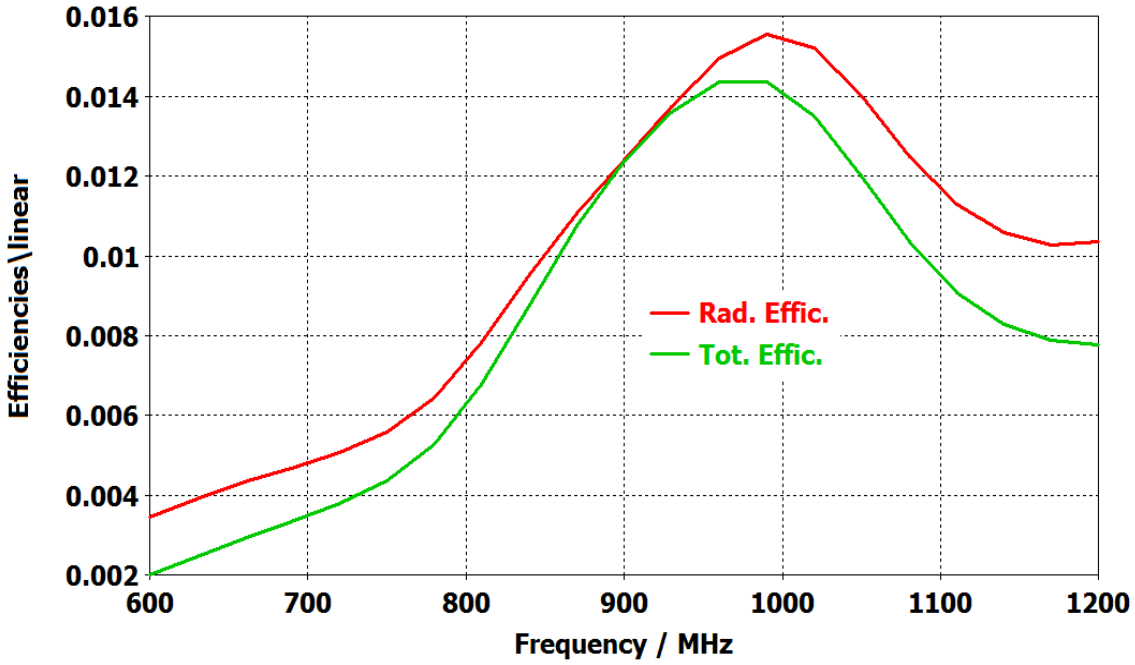

Fig. 5.24: Efficiency of antenna 2

The radiation and total efficiencies of the antenna are shown in Fig. 5.24. At 908MHz they are close to 1.3% which is significantly high for an implantable antenna. However, the overall size of this antenna is almost 2.2 times that of our previously designed antennas [7, 16-17]. In addition, the bandwidth of this Antenna 2 is 18.4% compared to our Antenna 1 bandwidth (8.5%).

5.10 Parametric Study of Antenna 2

Results of the parametric studies on Antenna 2 are shown in Figs. 5.25-5.36. The effect of relative permittivity of superstrate on the resonance frequency is illustrated in Fig. 5.25 when it was varied from 8 to 10 in steps of 0.5. It was found that the resonance frequency is ~908MHz (in the Australian UHF ISM band, 915-928MHz) when the permittivity is 9.2. A significant bandwidth (833-1000MHz) was also observed at -10dB

reflection coefficient when the permittivity is 9.2. With this permittivity value, the frequency of interest was completely covered. In Fig. 5.26, sensitivity of the resonance frequency of Antenna 2 is shown when permittivity of biocompatible coating material was varied. The relative permittivity of biocompatible coating material was varied from 2 to 4 in steps of 0.5 and no effect was observed on the resonance frequency. No effect was expected as a superstrate with high-permittivity and sufficient thickness (3.2mm) separated the coating material from the radiating patch of the antenna. In Fig. 5.27, the effect of relative permittivity of fat tissue of rat was presented when the fat permittivity was varied between 5 and 10 in steps of 1.0. The resonance frequency of the Antenna 2 was found almost stable at around 908MHz (10dB return loss) when permittivity of fat tissue was varied. The relative permittivity of muscle tissue of rat was varied between 50 and 70 in steps of 5 and the effect was shown in Fig. 5.28. Although a 10dB return-loss bandwidth of 167MHz (833-1000MHz) was obtained for the permittivity of 50 the resonance frequency was at ~908MHz. However, resonance frequency was found to be shifted slightly with the increase of muscle's tissue permittivity.

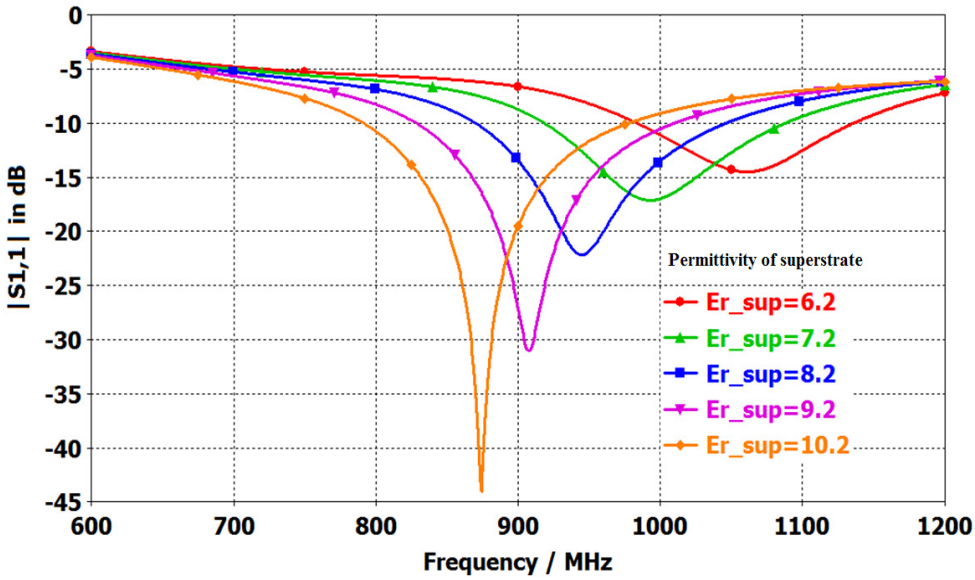

Fig. 5.25: $|S_{11}|$ of Antenna 2 when permittivity of superstrate is varied

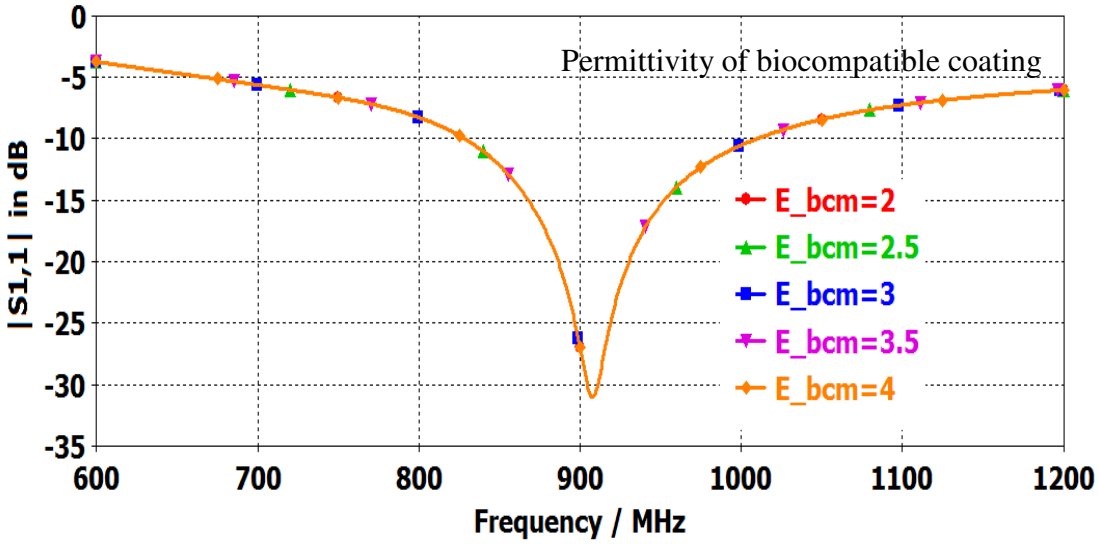

Fig. 5.26: $|S_{11}|$ of Antenna 2 when permittivity of biocompatible coating material is varied

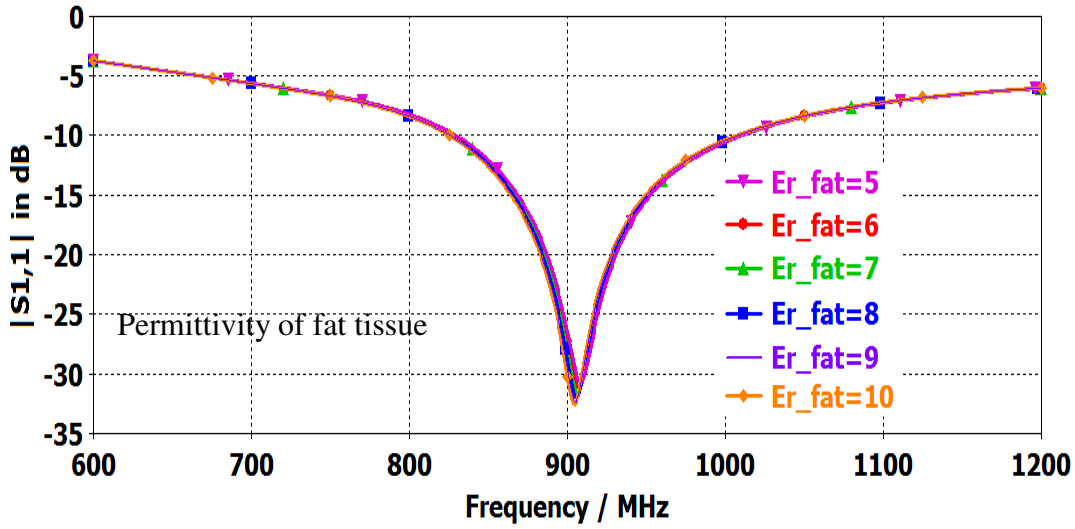

Fig. 5.27: $|S_{11}|$ of Antenna 2 when permittivity of fat tissue is varied

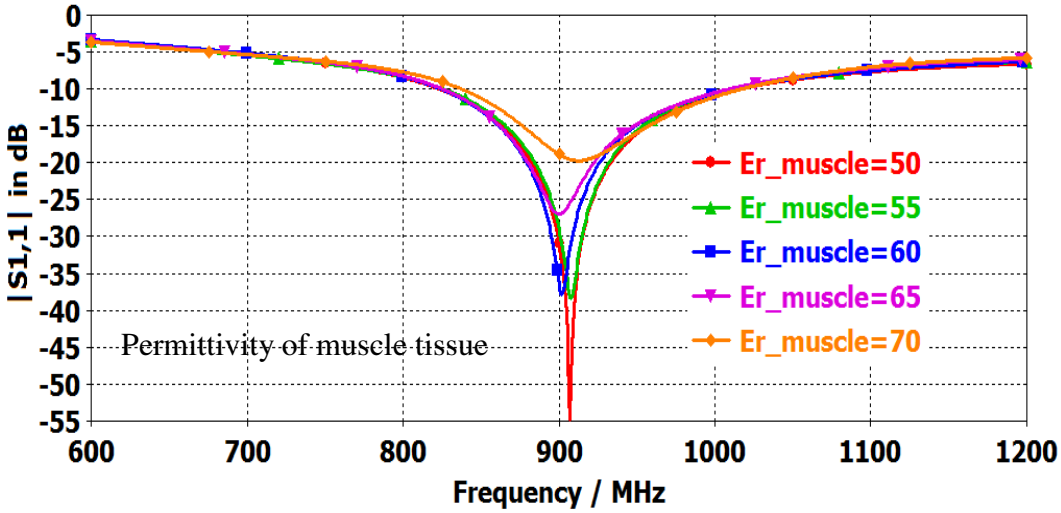

Fig. 5.28: $|S_{11}|$ of Antenna 2 when permittivity of muscle tissue is varied

In Fig. 5.29, the effect of permittivity of skin tissue of rat on Antenna 2 was shown when it was varied in the range of 30-40 in steps of 2. The resonance frequency was stable at around 908MHz (10 dB return loss). In Fig. 5.30, superstrate thickness variation effect on Antenna 2 was presented. The return loss was 31dB at a resonance frequency of ~908MHz when the superstrate thickness is 3.2mm.

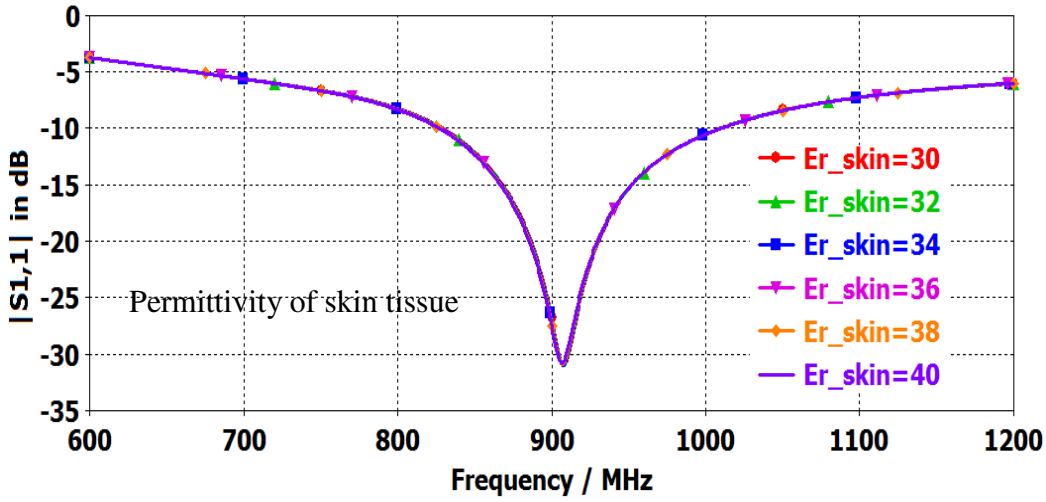

Fig. 5.29: $|S_{11}|$ of Antenna 2 when permittivity of skin tissue is varied

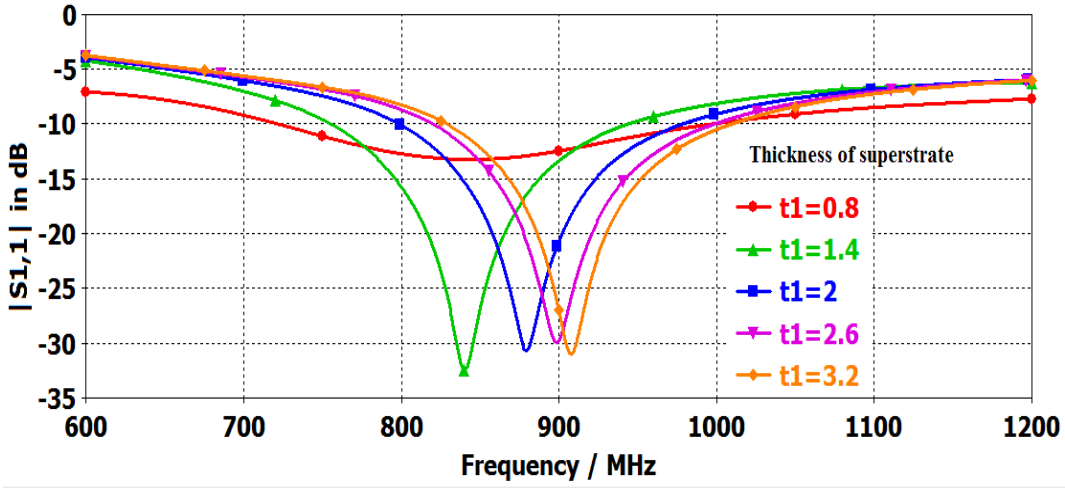

Fig. 5.30: $|S_{11}|$ of Antenna 2 when superstrate thickness (mm) is varied

In Fig. 5.31, the effect of biocompatible material thickness variation on Antenna 2 is illustrated. The resonance frequency remained fairly within the band of interest (915-928MHz) when the thickness of coating was varied between 0.5 and 2.0mm in 0.5mm steps. In Fig. 5.32, the effect of rat skin tissue thickness variation on Antenna 2 is given when it was varied from 0.5mm to 2.0mm in steps of 0.5mm. The range of resonance frequency detuning was found to be negligible. In Fig. 5.33, the effect of fat tissue thickness variation is investigated from 0.5mm to 2.0mm and similar effect due to rat skin thickness variation on the resonance frequency was found.

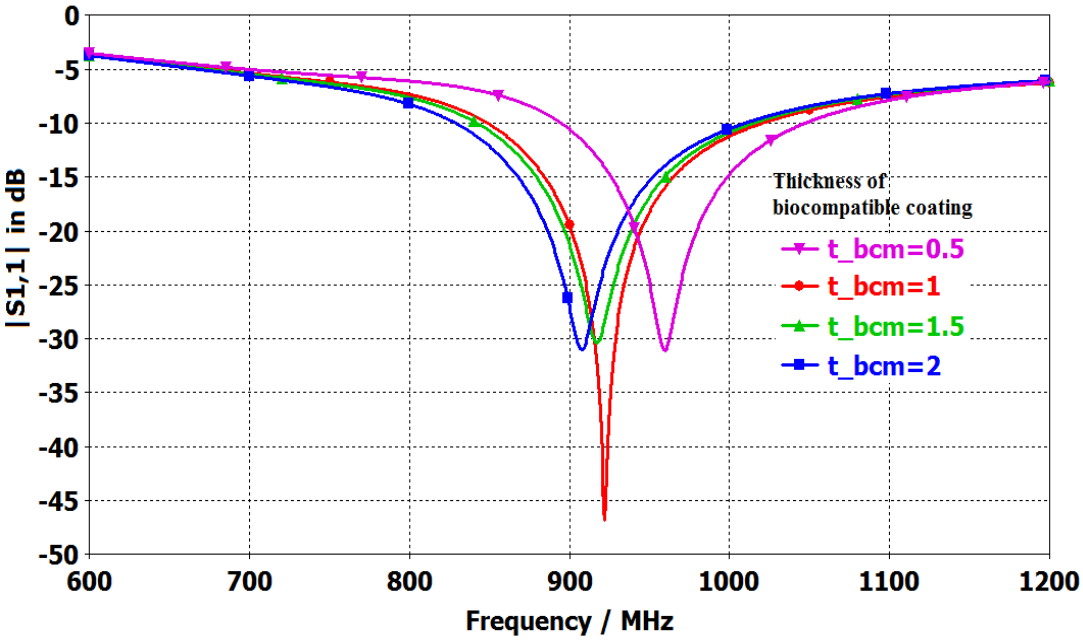

Fig. 5.31: $|S_{11}|$ of Antenna 2 when biocompatible material thickness (mm) is varied

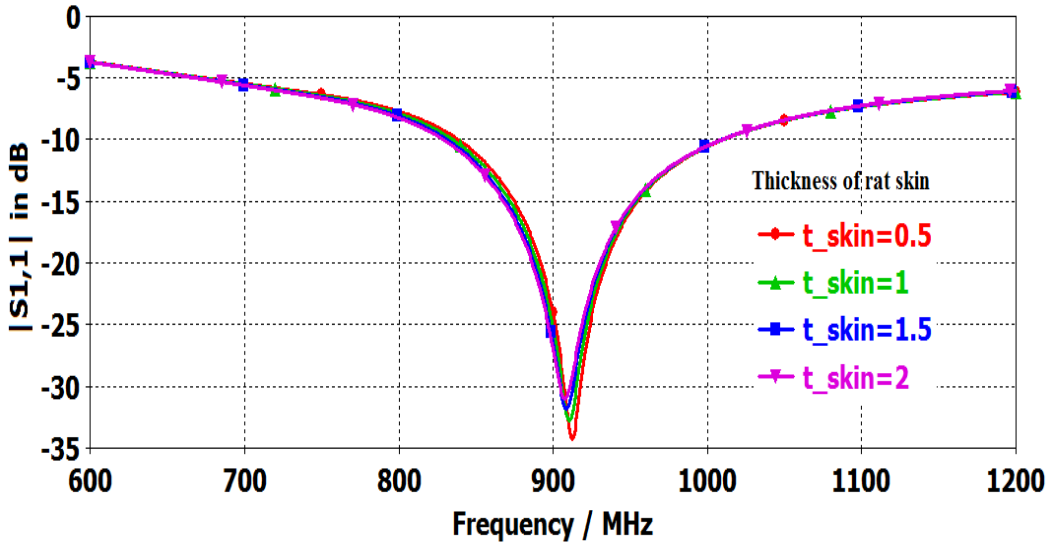

Fig. 5.32: $|S_{11}|$ of Antenna 2 when rat skin tissue thickness (mm) is varied

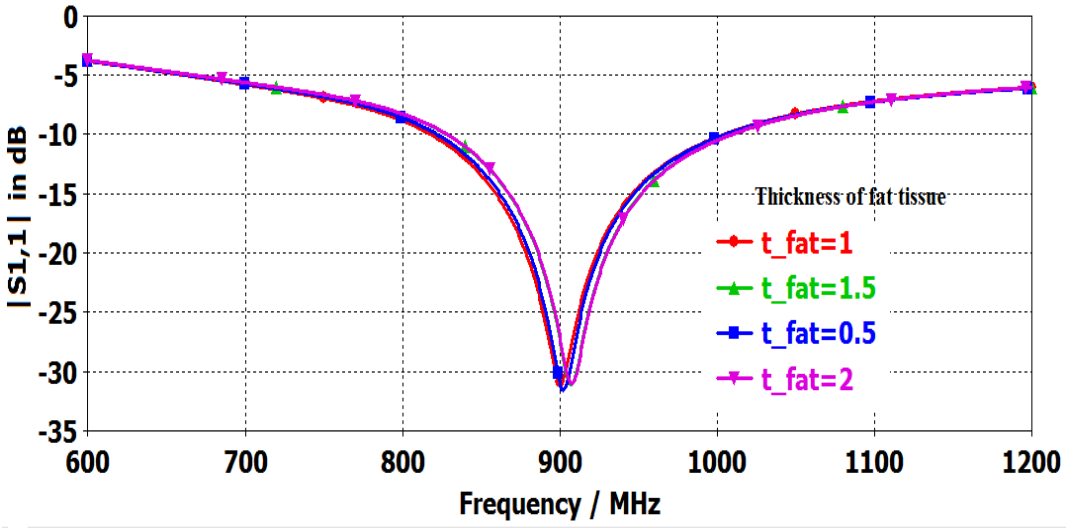

Fig. 5.33: $|S_{11}|$ of Antenna 2 when fat tissue thickness (mm) is varied

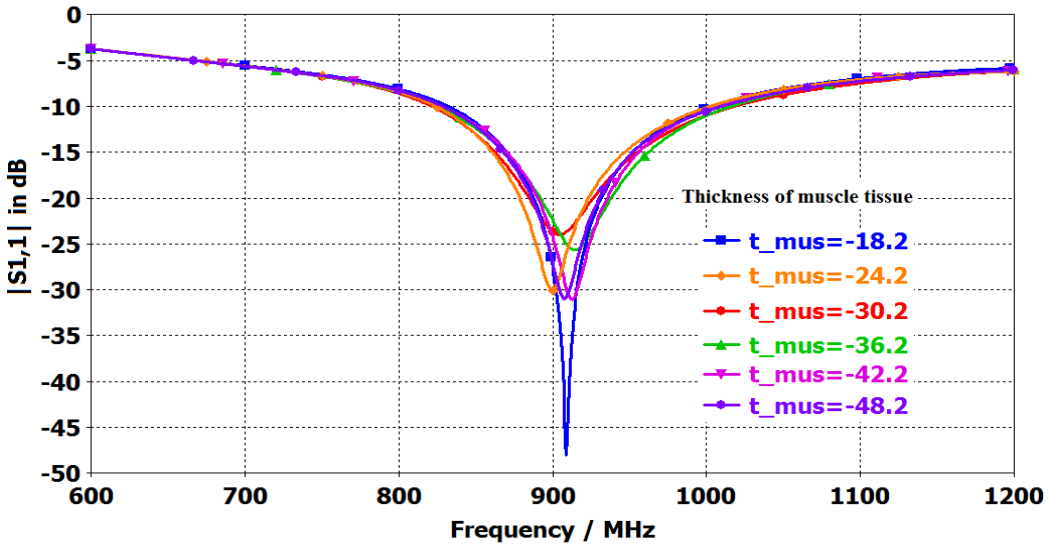

Fig. 5.34: $|S_{11}|$ of Antenna 2 when muscle tissue thickness (mm) is varied

The muscle tissue thickness variation (18.2-48.2mm) below Antenna 2 was considered and stable return loss (30dB) was obtained at ~908MHz when the muscle tissue thickness was more than 30.6mm (Fig. 5.34). The negative sign in the muscle tissue thickness value indicated that the variation is in –z direction. Thus it is important to consider enough muscle tissue below the antenna in the antenna environment model. In Fig. 5.35, Hilbert

curve strip width variation (2.0-4.0mm) of Antenna 2 was performed in steps of 0.5mm to observe its effect on the resonance frequency of the antenna. There was no effect on the resonance frequency with this antenna parameter variation and therefore the designed Antenna 2 is very stable on the strip width of this space filling curve.

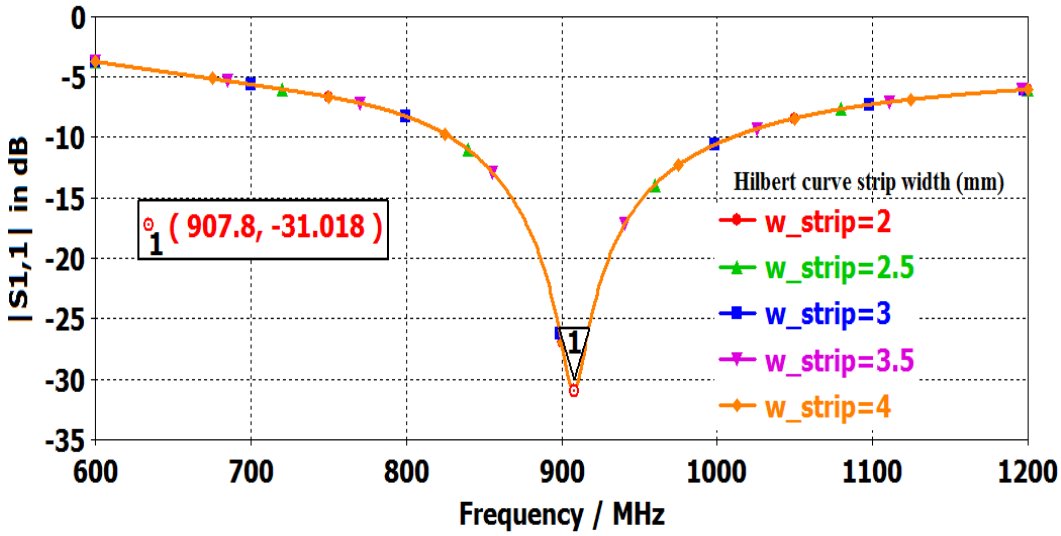

Fig. 5.35: $|S_{11}|$ of Antenna 2 when Hilbert curve strip width is varied

5.11 Implantable PIFA Antenna Design 3

The third antenna design is a J-shaped proximity-coupled PIFA. Fig. 5.36 shows the geometry of the proposed 4-layers antenna. The optimised overall dimensions of the antenna are 13.5mm×11mm×4.25mm. The dimensions of the upper and lower radiating patch are 13.5mm×3.5mm and 8mm×10.25mm, respectively. A slot was cut along the centre line of the lower patch to extend the current path, which in turn reduces the physical size of the antenna. The length and width of the slot are 9.5mm and 1.0mm, respectively. All the metals are printed on FR4 substrates (layers 1-4) with an estimated dielectric constant of 4.3. The thicknesses of Substrates 1, 2, 3 and 4 are 1.6mm, 0.8mm,

0.8mm and 0.8mm, respectively, including the printed copper layers. The bottom face of Substrate 1 is fully metallised and plays the role of a full ground plane. Its area is 12mm×8.5mm. Substrate 2 is located above Substrate 1, and a capacitive load plate with an area of 9.5mm×8mm is printed on its bottom face. The area of this capacitive load plate was optimised to fine tune the resonance frequency of the antenna. A J-shaped proximity feed line is printed on the bottom surface of Substrate 3, located above Substrate 2. Upper and lower radiating patches are printed on the top and bottom faces of Substrate 4, respectively. The upper and lower radiating patches are connected using two hollow cylindrical vias at the left edge of the geometry (Fig. 5.36(a)). Similarly, the capacitive load plate and the lower radiating patch are connected using two vias at the right edge of the structure, each of them having an outer radius of 0.25mm and an inner radius of 0.20mm.

The radius of each via has been optimised. A shorting pin with a height of 4.0mm is provided at the left corner of the antenna, to connect the lower radiating patch to the ground plane, and its radius is also 0.25mm. Hence this antenna belongs to the PIFA family. The height of the J-shaped feed plate is 2.4mm above the ground plane of the antenna. One end of this J-shaped feed plate is connected to the feed pin which is attached with the signal terminal. The height of the capacitive load plate from the ground plane is 1.6mm and it is located between the ground plane and the J-shaped proximity feed plate. An extra radiating patch is added on top of the slotted radiating patch, which distinguishes this antenna from our previous implantable PIFA antenna designs [16, 7, 17]. This extra upper radiating patch increases the length of the current path of the antenna and decreases the resonant frequency of the antenna. In addition, the J-shaped

proximity feed was designed to increase the impedance bandwidth of the antenna. The optimised antenna parameters for antenna design 3 are shown in Table 5.6.

Table 5.6: Optimised Antenna 3 parameters

Optimized parameters of Antenna 3	**Values in mm**
Upper radiating patch length (x-axis)	13.5mm
Upper radiating patch width (y-axis)	3.5mm
Lower radiating patch length (x-axis)	10.25mm
Lower radiating patch width (y-axis)	8.0mm
Slot length on lower patch (x-axis)	9.5mm
Slot width on lower patch (y-axis)	1.0mm
Radius of shorting pin and each via	0.25mm
Height of capacitive load plate (z-axis)	1.6mm
Ground plane length (x-axis)	12mm
Ground plane width (y-axis)	8.5mm
Shorting pin height (z-axis)	4.0mm
Proximity J-shaped feed height (z-axis)	2.4mm
Length of capacitive load plate (x-axis)	9.5mm
Width of capacitive load plate (y-axis)	8.0mm

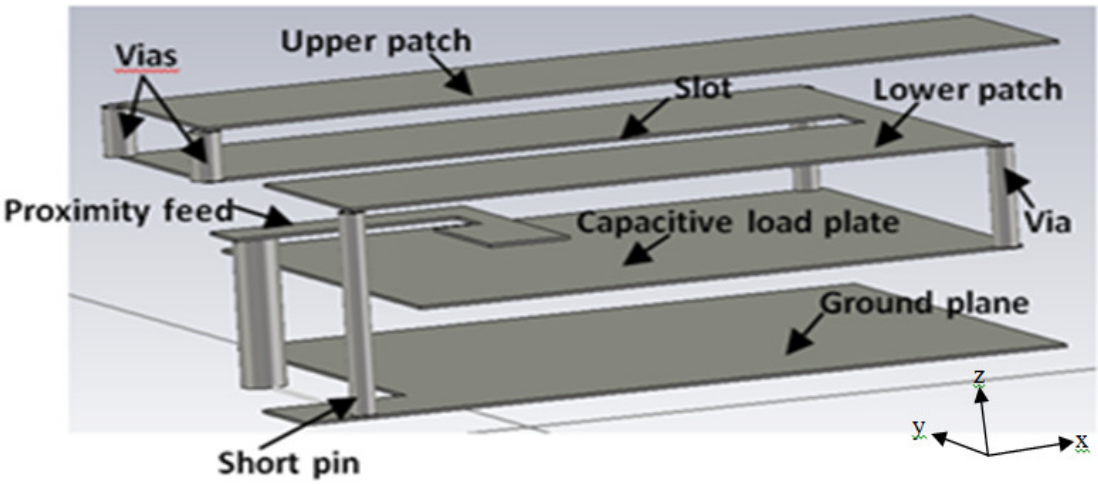

(a)

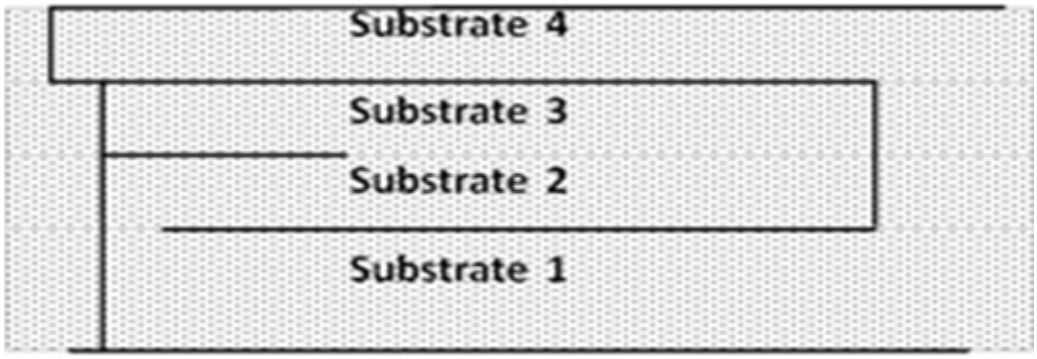

(b)

Fig. 5.36: Geometry of the proposed multilayer PIFA Antenna 3 with a J-shaped proximity feed: (a) 3D view and (b) Side view

5.12 Model of Antenna 3 Surrounding Environment

The antenna 3 operating environment has been modelled similarly to our previous model [8] and also shown in the previous two antenna designs in this chapter. However, some dimensions are different (as shown in Table 5.7) in the present model. It consists of 3-layers: skin-fat-muscle stratification and a bio-compatible material coating box surrounding the antenna. The coated antenna is located at an equidistant position from the

edges of the vertical sides of the muscle layer. The electrical properties of rat tissue for Antenna 3 are the same ones that were used in Antennas 1 and 2 previously. However, a different bio-compatible material (Silastic, dielectric constant = 3.01) is used for coating the Antenna 3 as well as the RFID circuit board. This is due to the availability of this material and its long-term stability as a biocompatible material.

Table 5.7: Surrounding environment model parameters of Antenna 3

Environment model parameters of Antenna 3	**Symbol**	**Value (mm)**
Rat skin layer thickness	t_1	2
Fat layer thickness	t_2	2
Muscle layer height	t_4	56
Muscle layer thickness below silastic box	$t_4 - t_3$	50.7
Skin, fat and muscle layers length	L_1	200
Skin, fat and muscle layers width	W_1	60
Silastic box length	L_2	16
Silastic box width	W_2	13.25
Silastic box height	t_3	5.3
Silastic box to muscle edge length	L_3	92

5.13 Optimised Numerical Results of Antenna Design 3

Parametric studies of the proposed antenna geometry have been carried out to achieve the optimised dimensions of Antenna 3. It is worthwhile to note here that, although it seems easy to perform parametric studies using commercial EM simulation software, in reality it is not the case for a low frequency implantable antenna to be operated at a bandwidth of only 1.4% (915-928MHz) as the resonance frequency may go out of the band of interest easily once implanted in animals. The optimised dimensions of the surrounding environment model parameters are given in Table VI. The electrical properties used in our environment tissue model are taken from [6].

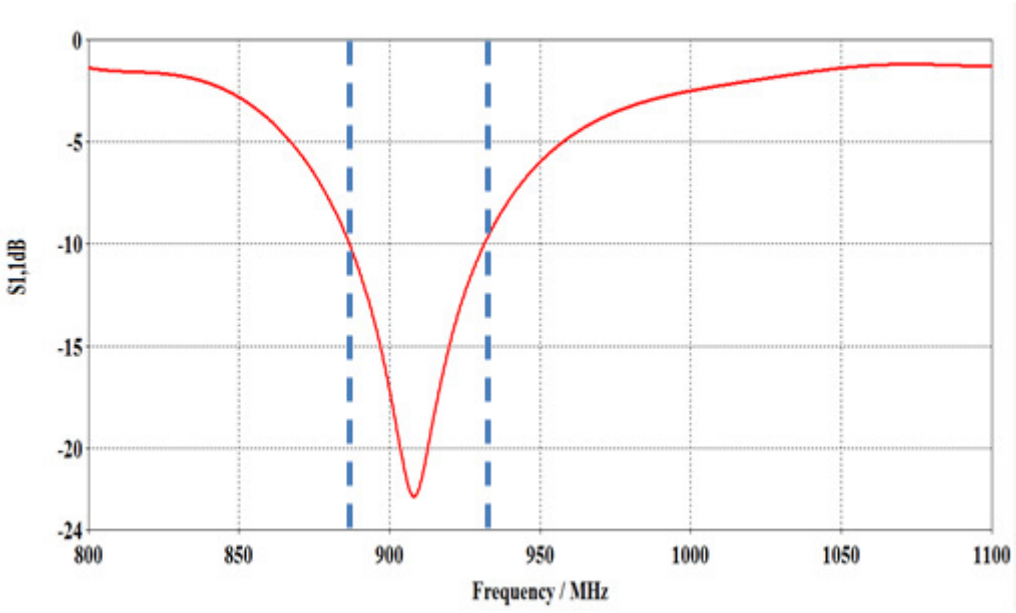

Fig. 5.37: $|S_{11}|$ vs. frequency for Antenna 3

The thickness of the bio-compatible material (Silastic) has been optimised to minimise the sensitivity to the tissue layers. The resulting antenna input return loss, input resistance, input reactance and radiation pattern are presented below. In Fig. 5.37, the antenna input reflection coefficient magnitude is presented. It is evident from the graph that a 10dB return-loss bandwidth of 50MHz (885-935MHz) that covers the Australian

ISM band is obtained. The return loss is a maximum (22dB) at 906MHz. The antenna input resistance as a function of frequency is shown in Fig. 5.38. It is found that at 906MHz the antenna input resistance is approximately 56Ω and the antenna return loss is 22dB.

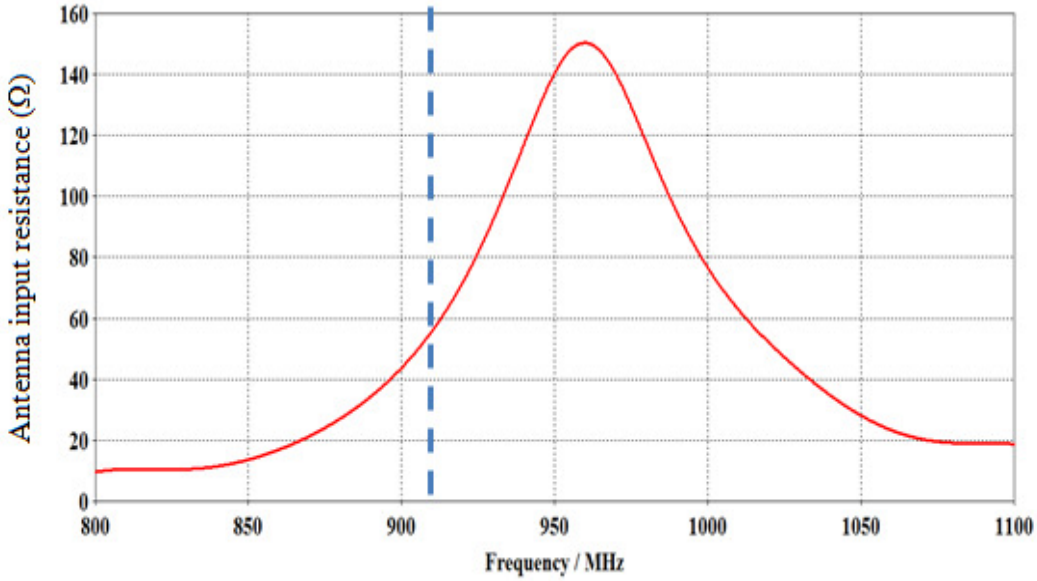

Fig. 5.38: Antenna 3 input resistance vs. frequency

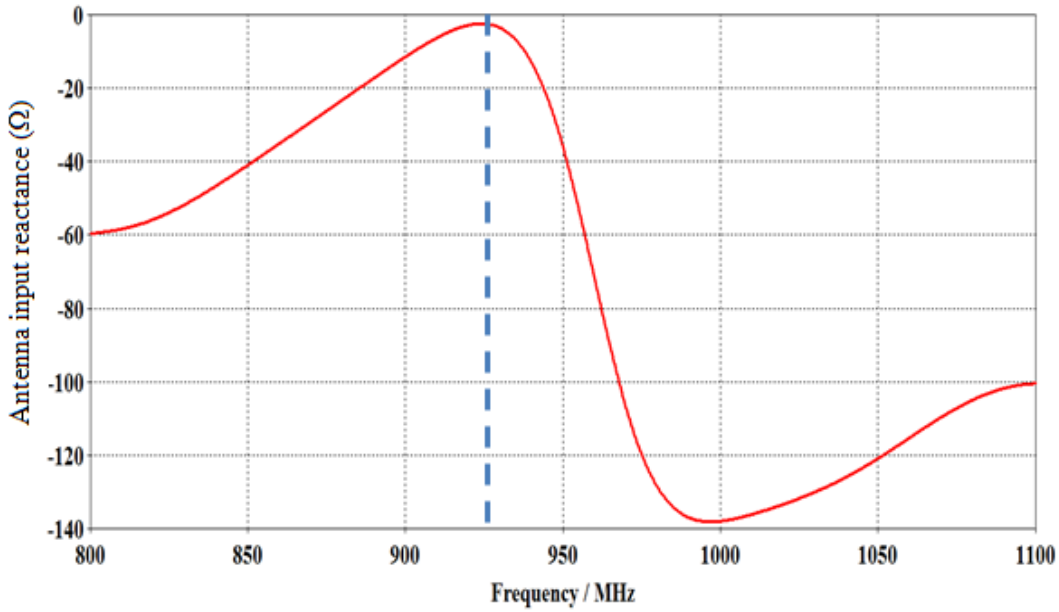

Fig. 5.39: Antenna 3 input reactance vs. frequency

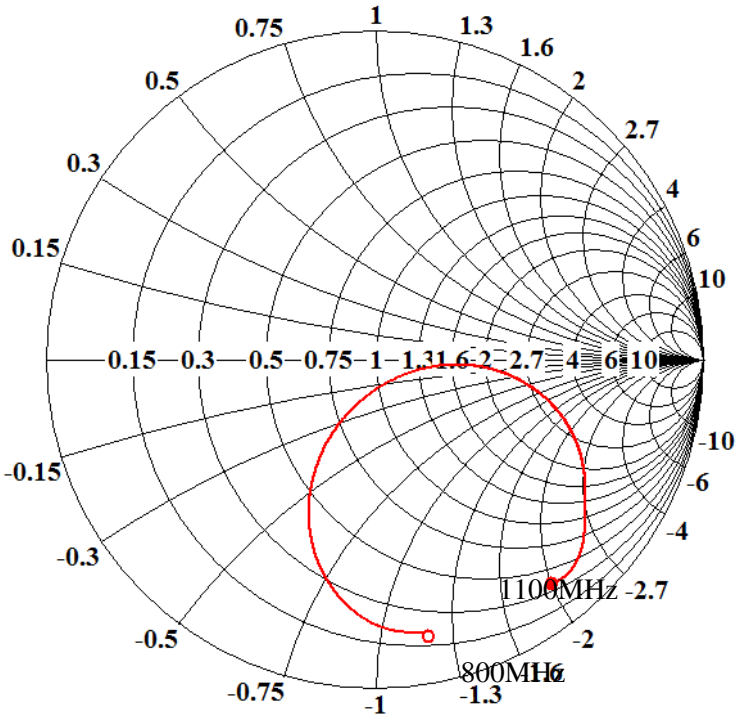

Fig. 5.40: Antenna 3 input impedance on Smith chart

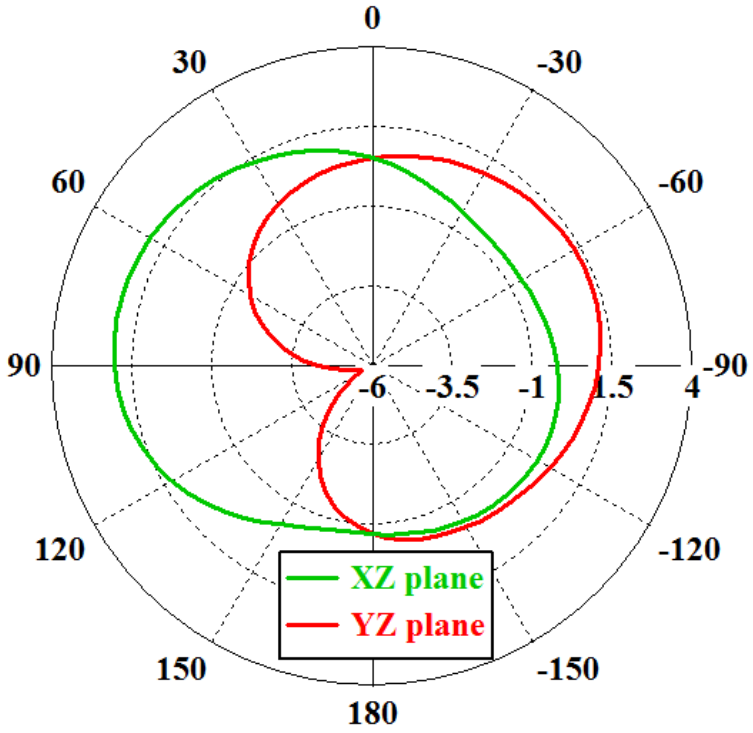

Fig. 5.41: Radiation pattern of Antenna 3

Fig. 5.39 represents the antenna input reactance as a function of frequency. We observe that the antenna input reactance converges to approximately zero ohm at around 925MHz. In Fig. 5.40, the antenna input impedance is shown on a Smith chart for the frequency range between 800MHz and 1100MHz. It is noticed that the locus of the impedance curve passes very close to the unity point at 906MHz. Finally, the antenna radiation patterns in the XZ and YZ planes are shown in Fig. 5.41. It shows that the maximum radiation is obtained outwards from the rat's body through the skin. However, an appreciable back radiation is also observed, but that is a trade-off that has to be made when designing such compact implantable antennas. The far-field absolute directivity in 2-D is shown in Fig. 5.42. The maximum absolute directivity is found as 2.93dBi at 900MHz. The radiation and total efficiencies of Antenna 3 (Fig. 5.43) are in good agreement, i.e. they converge at around 900MHz.

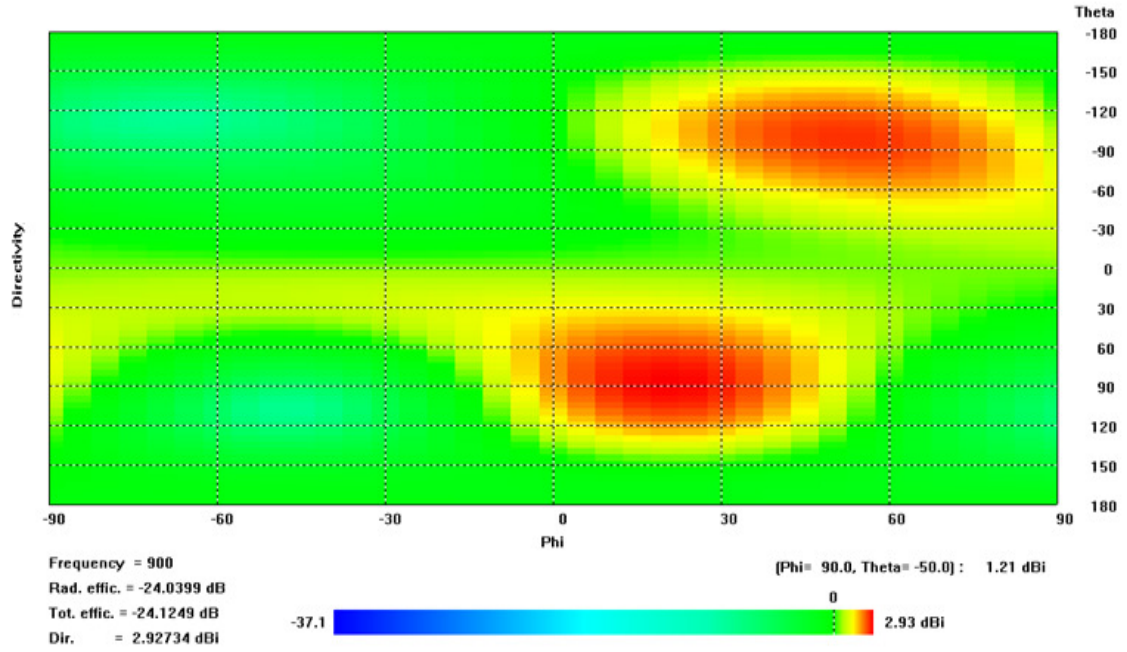

Fig. 5.42: Far-field absolute directivity in 2-D

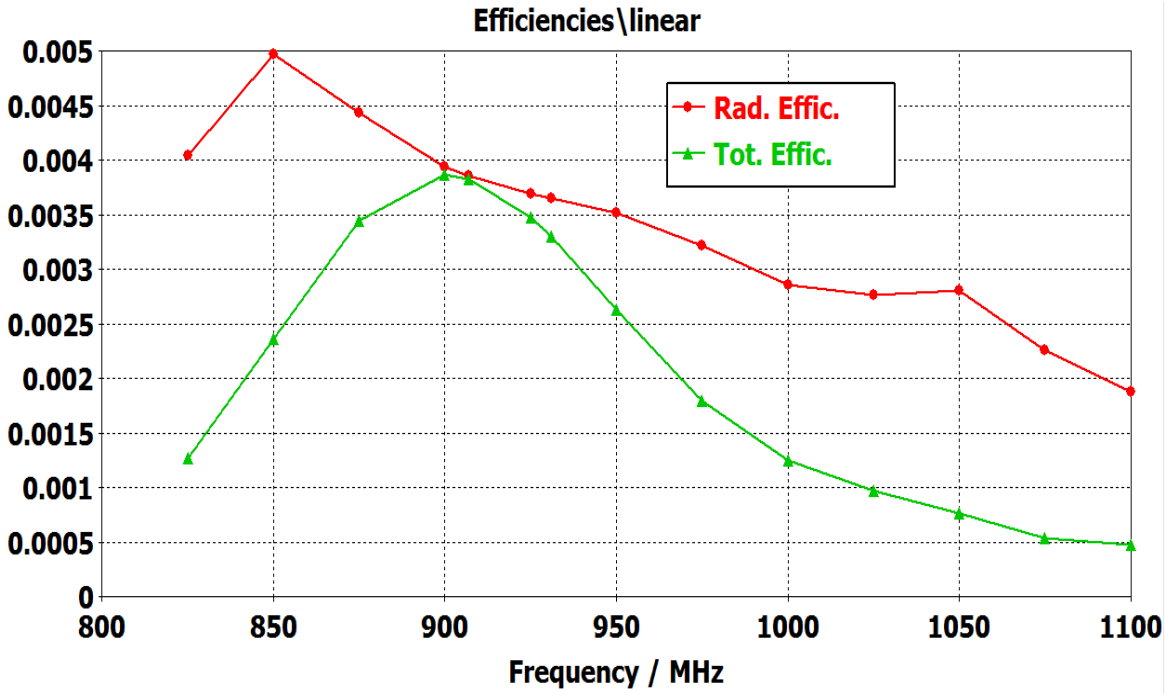

Fig. 5.43: Efficiencies of Antenna 3

Similar to designs of Antenna 1 and Antenna 2, Figs. 5.44-5.50 illustrate the results of the parametric studies on antenna design 3 parameters as well as on its surrounding environment parameters. Their brief descriptions are provided on each graph.

5.14 Parametric Study of Antenna 3

In Fig. 5.44, effect of biocompatible material thickness variation on antenna 3 was illustrated. The resonance frequency remained fairly within the band of interest (915-928MHz) at 10 dB return loss when the thickness of biocompatible coating (Silastic, dielectric constant = 3.0 at100KHz) was 1.0mm. When the thickness was varied between 1.0mm and 3.0mm in 0.5mm steps the resonance frequency was out of the band of interest and no BW was found at 10dB return loss.

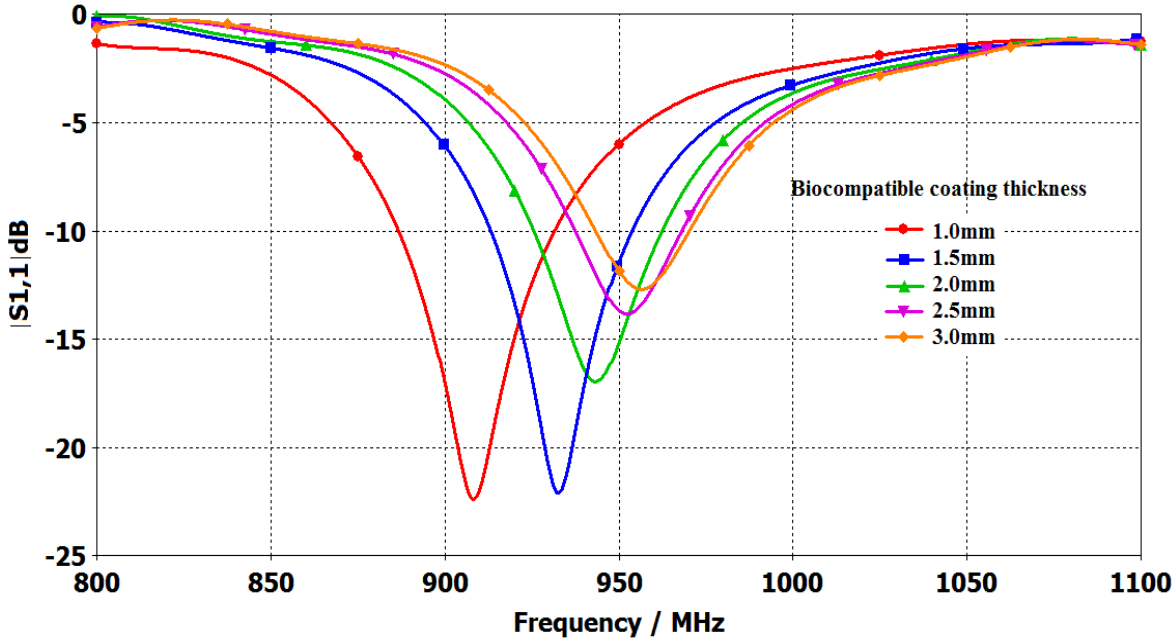

Fig. 5.44: $|S_{11}|$ of Antenna 3 when thickness (t) of bio-compatible coating material is varied

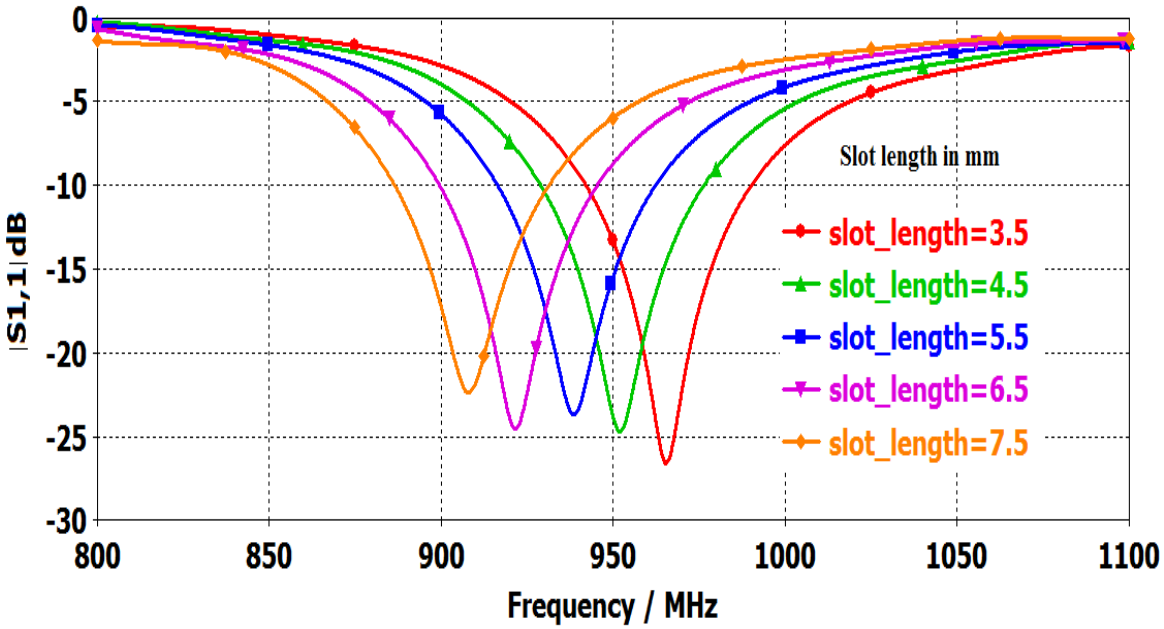

Fig. 5.45: $|S_{11}|$ of Antenna 3 when slot length on the radiating patch is varied

In Fig. 5.45, the return loss of the antenna was plotted when the slot length on the top radiating patch was varied between 3.5-7.5mm. It was found that increasing the slot

length from 3.5mm to 7.5mm will decrease the resonance frequency approximately from 965MHz to 915MHz. This slot length can be utilised to retune the resonance frequency of the implanted antenna within a limited range if detuning of the antenna due to the variations of muscle, fat and skin layers occurs. Although the return loss also changed due to slot length variation, it was always greater than 10dB with a sufficient 10dB return-loss (~100MHz). The resonance frequency was in the range of the target bandwidth with the slot length value of 7.5mm.

In Fig. 5.46, the return loss of the antenna was plotted when the gap between capacitor load plate and shorting pin was varied from 2.5mm to 3.0mm in steps of 0.25mm. It was found that increasing the gap from 2.5mm to 3.0mm will decrease the resonance frequency approximately from 946MHz to 926MHz. This gap also can be utilised to retune the resonance frequency of the implanted antenna within a limited range if detuning of the antenna due to the variations in the surrounding model parameters.

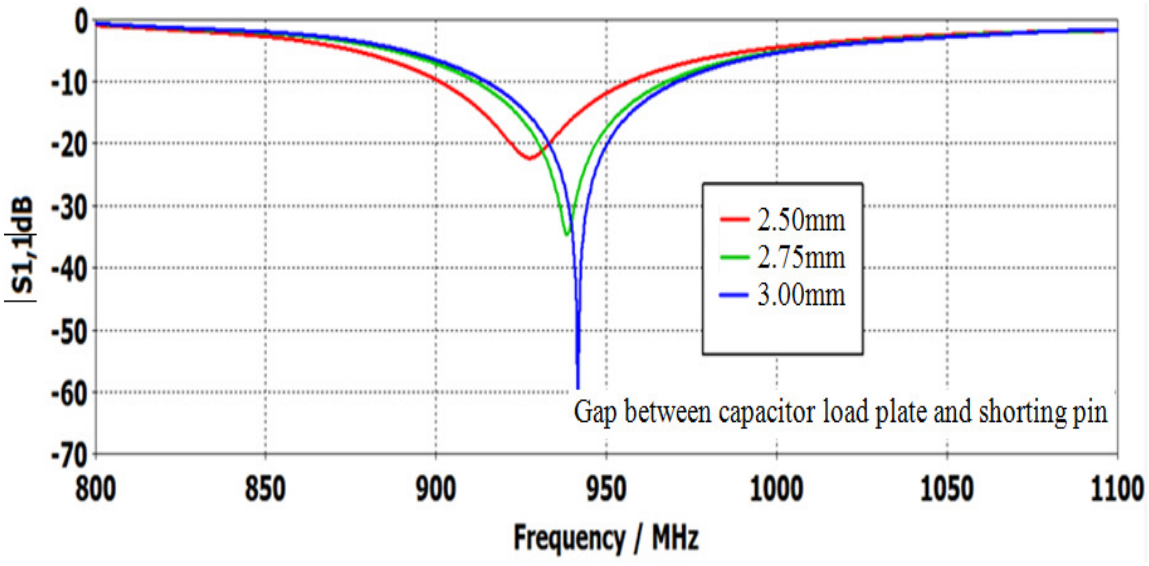

Fig. 5.46: $|S_{11}|$ of Antenna 3 when gap varied between capacitor load plate and shorting pin

The best value for the return loss was found to be nearly 55dB at 946MHz when the gap was 3mm, but it was out of the band of interest. The gap of 2.5mm between capacitor load plate and shorting pin for antenna design 3 provided the desired operating frequency with a bandwidth of 50MHz.

The return loss as function of frequency of the antenna 3 was plotted (Fig. 5.47) when length of J-shaped proximity feed plate was varied along the x-axis from 3.5mm to 4.5mm in steps of 0.5mm. It was found that increasing the length of J-feed plate from 3.5mm to 4.5mm will decrease the resonance frequency slightly (946MHz to 943MHz). This length can be utilised to match the impedance of the implanted antenna within a limited range if required. The resonance frequency was out of the band of interest for each length variation, however, at 10dB return loss, the target Australian ISM band (915-938MHz) was covered by the obtained bandwidth (914-970MHz).

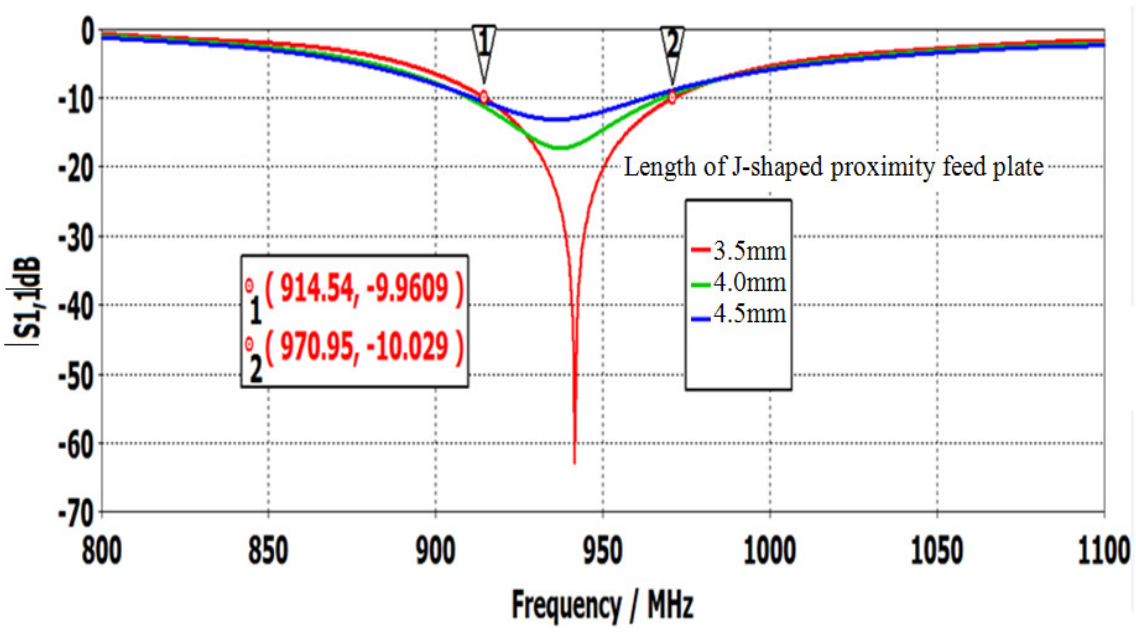

Fig. 5.47: $|S_{11}|$ of Antenna 3 when length of J-shaped proximity feed plate is varied along x-axis

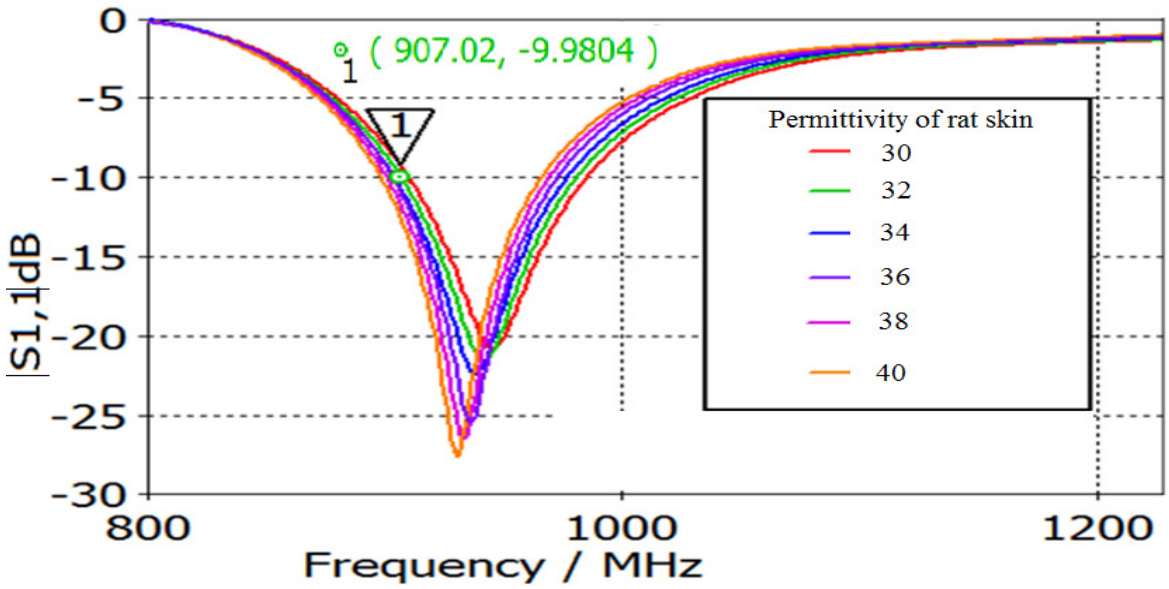

Fig. 5.48: $|S_{11}|$ of Antenna 3 when permittivity of skin tissue is varied

In Figs. 5.48-5.49, the effects of relative permittivities of skin and muscle tissues of rat were presented when (for skin, variation is 30-40 and for muscle, variation is 50-70). The resonance frequency of the Antenna 3 was found almost stable at around 920MHz (10dB return loss) when permittivities of rat tissues were varied.

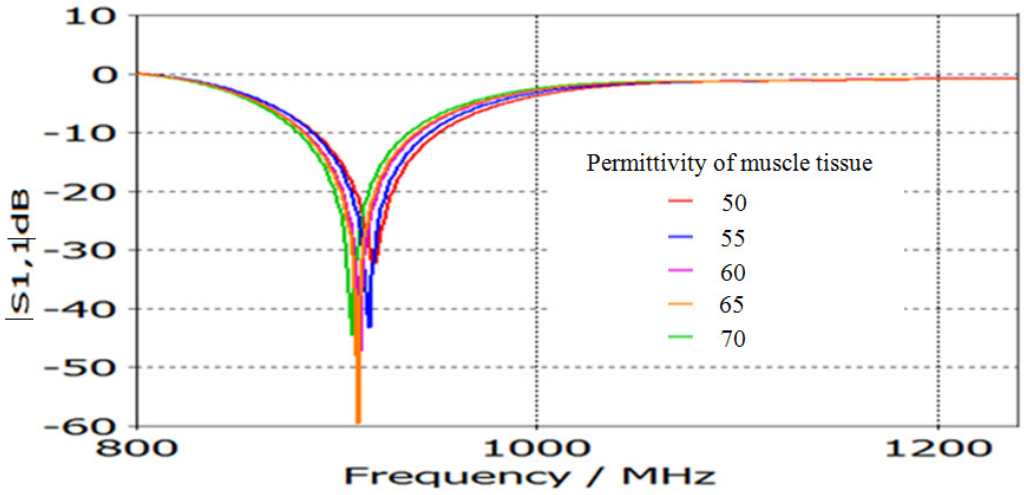

Fig. 5.49: $|S_{11}|$ of Antenna 3 when permittivity of muscle tissue is varied

In Fig. 5.50, the effect of biocompatible coating material on the Antenna 3 resonance frequency was illustrated when relative permittivity of material was varied between 2.5 and 3.5 in steps of 0.2. The resonance frequency was decreased from 925MHz to 890MHz and $|S_{11}|$ of the antenna was also decreased gradually at value of -17dB. The thickness of rat skin on top of the coating material was varied in the range of 2mm to 6mm and the effect on Antenna 3 resonance frequency is shown in Fig. 5.51. A little effect was found and optimum $|S_{11}|$ of the antenna was -35dB at 915MHz. Fig. 5.52 shows the sensitivity of Antenna 3 resonance frequency when the upper radiating patch length was varied from 8mm to 12mm in steps of 1.0mm. The resonance frequency shifted down to 900MHz from 925MHz with this length variation range (8mm-12mm). The $|S_{11}|$ of the Antenna 3 was found to be -20dB at 900MHz while it was -40dB at 925MHz.

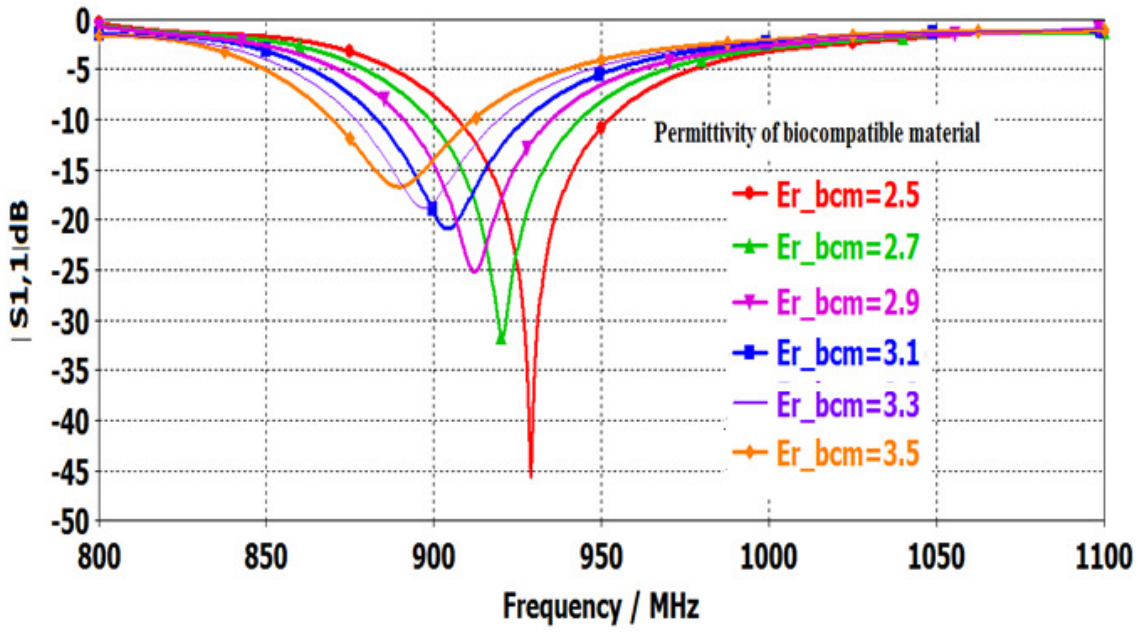

Fig. 5.50: $|S_{11}|$ of Antenna 3 when permittivity of biocompatible coating material is varied

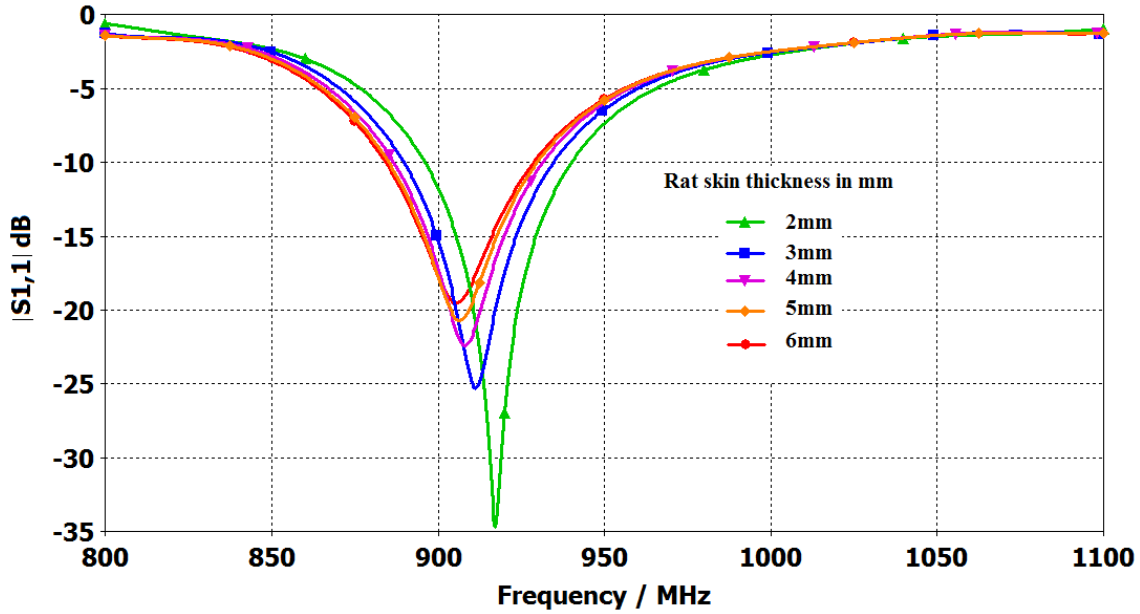

Fig. 5.51: $|S_{11}|$ of Antenna 3 when rat skin thickness is varied

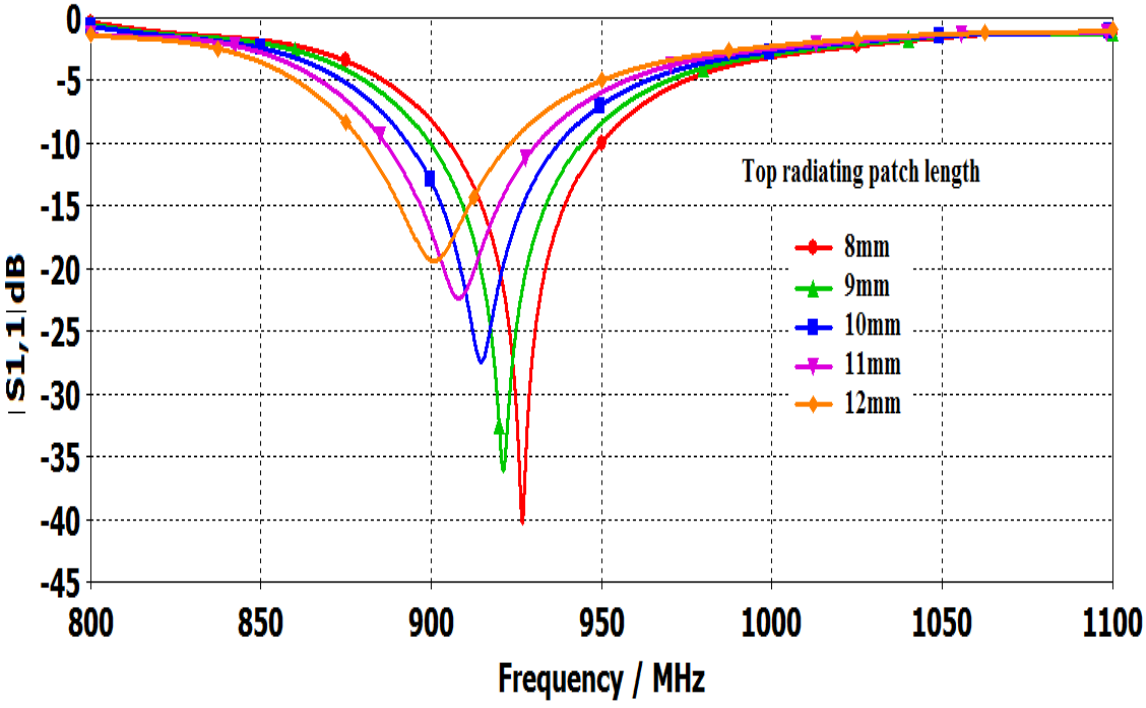

Fig. 5.52: $|S_{11}|$ of Antenna 3 when top radiating patch length is varied

5.15 Performance Comparison of Antenna 2 and Antenna 3

In this section, we compare the return losses, input impedances, radiation patterns and radiation efficiencies of Antenna 2 and Antenna 3. In Fig. 5.53, return losses ($|S_{11}|$) are compared. The maximum return loss of Antenna 2 is 30.8dB at 909MHz while it is 22.7dB for Antenna 3 at 920MHz. Although the resonance frequencies of the antennas are within the band of interest (915-928MHz), a 11MHz frequency shift is observed between the two resonance frequencies. Antenna 2 has a significantly wider 10dB return loss bandwidth of 167MHz, compared to 50MHz bandwidth of Antenna 3. Fig. 5.54 compares the input impedances between Antenna 2 and Antenna 3. The resistances of Antenna 2 and Antenna 3 are 53Ω (Fig. 5.54(a)) at 920MHz and 49.8Ω (Fig. 5.54(b)) at 908MHz, respectively. The reactances of Antenna 2 and Antenna 3 are -6.7Ω (Fig. 5.54(a)) at 920MHz and -2.8Ω (Fig. 5.54(b)) at 908MHz, respectively.

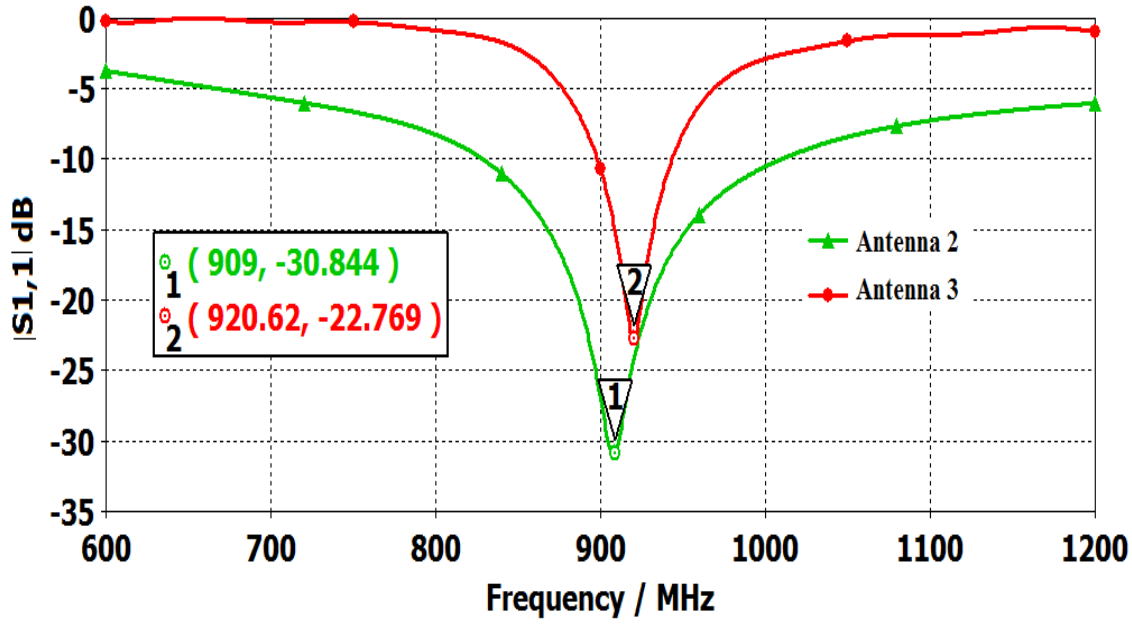

Fig. 5.53: $|S_{11}|$ of Antenna 2 and Antenna 3

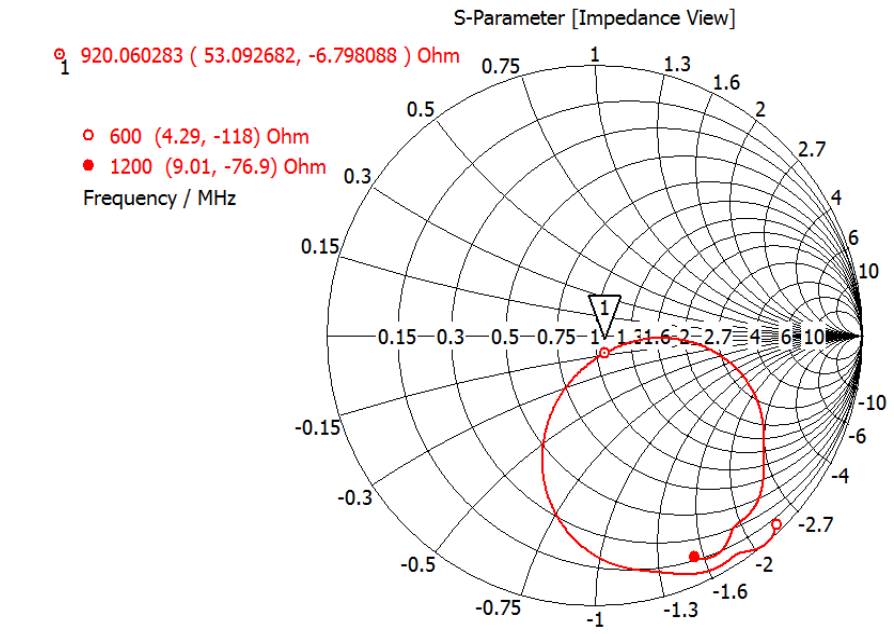

(a)

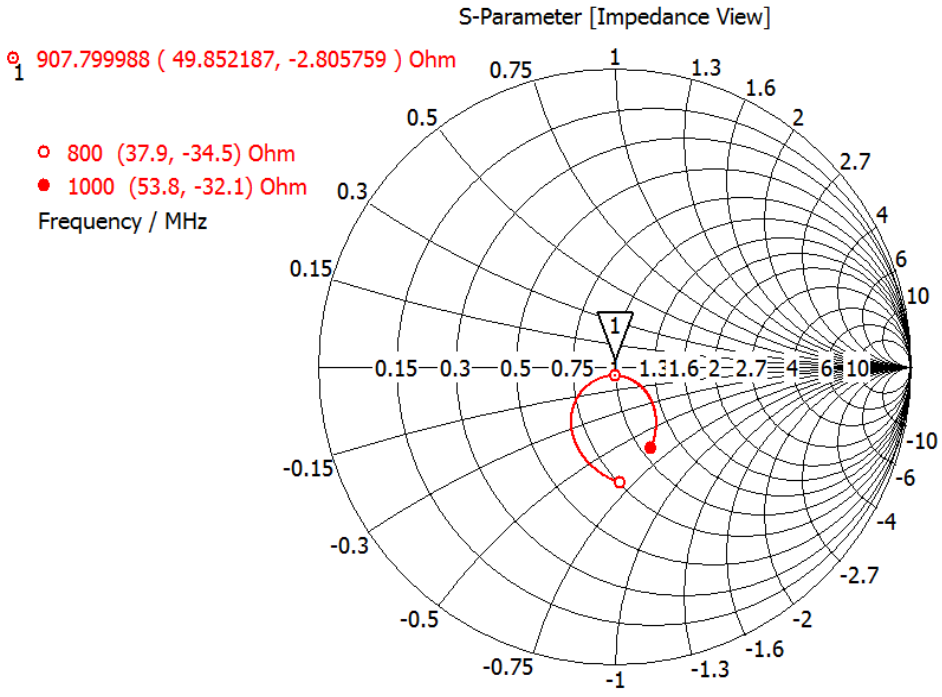

(b)

Fig. 5.54: Input impedances of Antenna 2 and Antenna 3: (a) Antenna 2; (b) Antenna 3

Radiation patterns of Antenna 2 and Antenna 3 at 900MHz are illustrated in Fig. 5.55 On φ = 0° plane, the maximum directvity of Antenna 2 is found to be 2.5dBi when θ = 45° while it is 2.1dBi for Antenna 3 when θ = 75°. On φ = 90° plane, the maximum directivities of Antenna 2 and Antenna 3 are 2.0dBi (θ = 60°) and 1.2dBi (θ = -65°), respectively. The absolute peak directivity of Antenna 2 is 3.4 dBi in φ = -45° , θ = 65° direction. For Antenna 3, it is 2.9dBi in φ = 20° , θ = -90° direction. Finally, Fig. 5.56 compares the radiation efficiencies. The efficiencies of Antenna 2 and Antenna 3 are 1.3% and 0.38%, respectively in the centre frequency (921.5MHz) of the Australian UHF ISM band (915-928MHz). A summary of antenna sizes, bandwidths and radiation efficiencies of the two antennas is presented in Table 5.8.

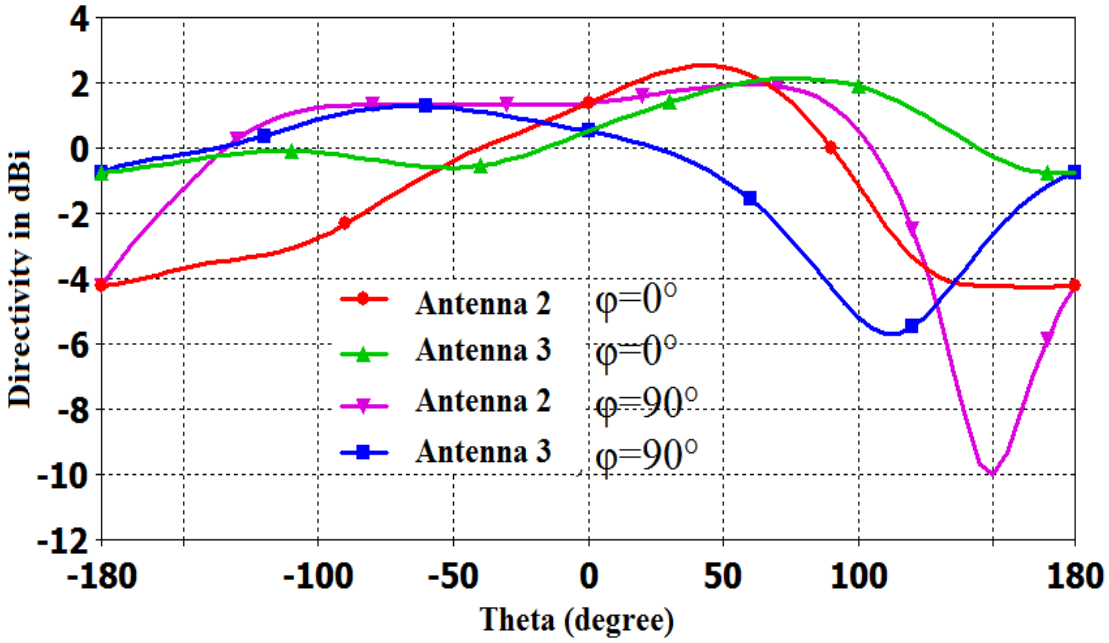

Fig. 5.55: Radiation pattern cuts of Antenna 2 and Antenna 3 at 900MHz on φ = 0° and φ = 90° planes

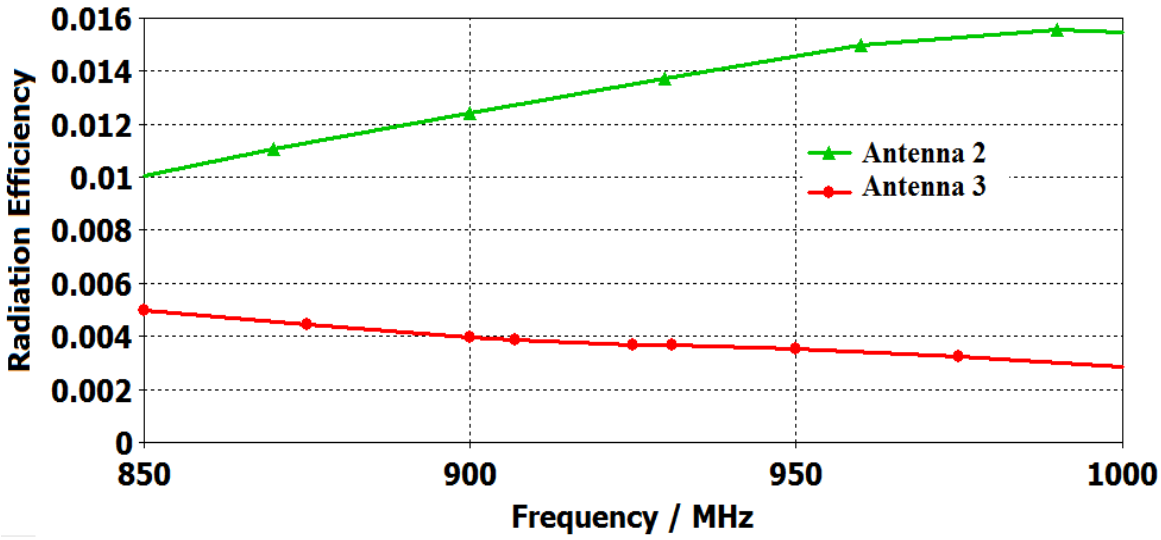

Fig. 5.56: Radiation efficiencies of Antenna 2 and Antenna 3

Table 5.8: Summary of antenna 2 and antenna 3 parameters

Antenna	**Antenna Volume (cm^3)**	**Antenna Area (mm^2)**	**10 dB return -loss Bandwidth (MHz)**	**Radiation Efficiency**
Antenna2	6.27	25×33 (coated: 27×34)	18.4% (833-1000)	1.3%
Antenna 3	0.63	13.5 ×11 (coated: 14.5 ×12)	5% (885-935)	0.38%

A 10dB return-loss bandwidth of 18.4% (833-1000MHz) is found for Antenna 2 which is much larger than the Australian UHF ISM band of interest. The predicted bandwidth of the much smaller Antenna 3 is approximately 5% (885-935MHz) but it also comfortably covers the band of interest. The maximum radiation for both the antennas is outwards through the skin which is desirable to reduce significant absorption loss by

biological tissues. Thus, either of the implanatble Antenna 2 and Antenna 3 can be used for implantable bio-telemetry by attaching them to an RFID-tag but Antenna 3 has a significant advantage in compactness at the expense of radiation efficiency.

5.16 Comparison of Designed Antennas and a Reference [29] Antenna

In order to evaluate the performance of each designed antenna, a comparison is made between all three antennas as well as with a reference antenna from the recent research in the field of implantable miniaturised antennas. Table 5.9 shows the comparison of the designed implantable PIFAs and a reference antenna [29]. The reference antenna is an implantable folded dipole type and coated with transparent glass material (dielectric constant = 5) and designed to be injected (implanted) into human body by a syringe It is observed that although bandwidth is larger, the radiation efficiency of the reference antenna [29] is poor compared the designed implantable Antennas 1, 2 and 3. This is the trade-off of the design. The largest size of the Antenna 2 ensures the highest radiation efficiency. The impedance bandwidth of Antenna 2 is 1.3% (833MHz-1000MHz). This Antenna 2 (25mm×25mm×7.6mm) needs extra space (~10mm length extension) on the RFID-tag PCB. The extension of PCB length may be compensated by cutting the PCB from the far end which is reserved for button battery and a smaller-radius button battery may be used near to the proposed Antenna 3. The space allocated for the current button battery on the RFID-tag PCB is quite large (23mm×33mm) compared to the size (60mm×33mm) of the RFID-tag PCB, more than one-third of the size of the PCB. The radiation efficiencies of antenna designs 1 and 3 are almost same (~0.4%). However, the bandwidth of antenna design 1 is larger (bandwidth = 9.2%) than that of antenna design 3 (bandwidth = 5%). Their overall sizes are also nearly identical (~576mm^3 and 631mm^3).

Table 5.9: Comparative Studies of Designed Antennas and Reference Antenna [29]

Antenna	Antenna size (mm^3)	Resonance Frequency (MHz)	Bandwidth	Radiation Efficiency
Antenna design 1	$12\times12\times4mm^3$	919.5MHz	9.2% (877-962MHz)	0.4%
Antenna design 2	$25\times25\times7.6mm^3$	908MHz	18.4% (833-1000MHz)	1.3%
Antenna design 3	$13.5\times11\times4.25mm^3$	910MHz	5% (885-935MHz)	0.38%
Reference antenna [29]	$20.3\times0.8\times0.8mm^3$	953MHz	16.2% (850-1000MHz)	0.15%

5.17 Conclusion

In antenna design 1, the effects of some antenna parameters, environment model parameters and bio-compatible layer permittivity on the antenna return loss have been investigated. It is found that possible variations in rat's tissues do not have a significant effect on antenna matching and bandwidth. Hence the designed antenna should operate well if those parameters change for any reason. Within the reasonable range the antenna return loss is more sensitive to some antenna parameters, and to the biocompatible layer permittivity. Significant variations are observed when the dielectric constants of substrate and silicone are changed over a wide range. Lesser variations are observed with the patch slot length and the capacitive load plate length. This sensitivity can be exploited to retune

the antenna if it is detuned, for example, due to additional packaging or attaching it to a RF circuit board, which could have a larger ground plane. The bandwidth of the antenna is predicted at around 9.2% (877-962MHz) with a return loss of 10dB, which is promising for the 900MHz ISM band. However, the radiation efficiency of the antenna is low (0.4%). As the antenna bandwidth under predicted conditions is much greater than the bandwidth of the ISM band, the antenna will continue to operate well even when the operating environment changes.

The resonance frequency of the Antenna 2, implantable Hilbert PIFA, detunes due to the presence of the dielectric bio-compatible coating around the antenna. The effect of the connection of the antenna to the RFID-tag PCB ground plane has been investigated. It was found that for a better impedance matching, the two ground planes must be connected. A 10dB return-loss bandwidth of 18.4% (833-1000MHz) was found which is adequate for the Australian UHF ISM band.

Finally, an implantable PIFA antenna with a J-shaped proximity feed has been designed for 900MHz ISM band and the key antenna parameters have been studied. Despite the compact size of the antenna the predicted10dB return-loss bandwidth is greater than 5% (885-935MHz). The maximum radiation of the antenna is outwards from the rat's body; this is desirable to avoid significant body absorption loss. Thus, the antenna can be used with our existing RFID circuit board in which the RF chip is matched to 50Ω.

Chapter 6

Implantable PIFA for Ground Plane Side on RFID Tag PCB

6.1 Introduction

The RFID tag PCB that has been considered to be implanted in a laboratory rat has two spaces available for the antenna: one is on the component side and the other is on the ground plane side. In the previous chapter 5, the designs and parametric studies of three implantable PIFA antennas for the component side of the RFID tag PCB board were described in detail. In this chapter, design and parametric studies of an implantable antenna for the ground plane side of RFID-tag PCB are presented. Since the antenna and RFID-tag PCB ground planes are on the same side and adjacent, an optimised partial ground slot was created between them.

6.2 Chapter Contributions and Background

6.2.1 Chapter Contributions

The contributions of this chapter are:

- Design of an implantable antenna to be attached on the ground plane side of the commercial RFID-tag PCB
- Creating a slot between the implantable PIFA antenna and RFID-tag grounds to improve the performance of the antenna and study its effect on the antenna. This slot has been optimised with parametric study.

- Investigation of the sensitivity of the antenna for various antenna parameters and its surrounding environment parameters.
- Understand the effect of the ground plane of the commercial RFID-tag PCB on the antenna performance in terms of input reflection coefficient, efficiency and radiation pattern

6.2.2 Background

The ground plane side of the commercial RFID tag PCB is shown in Fig. 6.1, and its larger ground plane is fortunately adjacent to the space available for an implantable PIFA, shown by the red coloured contour. As ground plane of our designed PIFA is smaller, we have increased the bandwidth by combining the RFID circuit board ground plane with the antenna ground plane. To achieve this bandwidth enhancement, a ground slot technique has been applied.

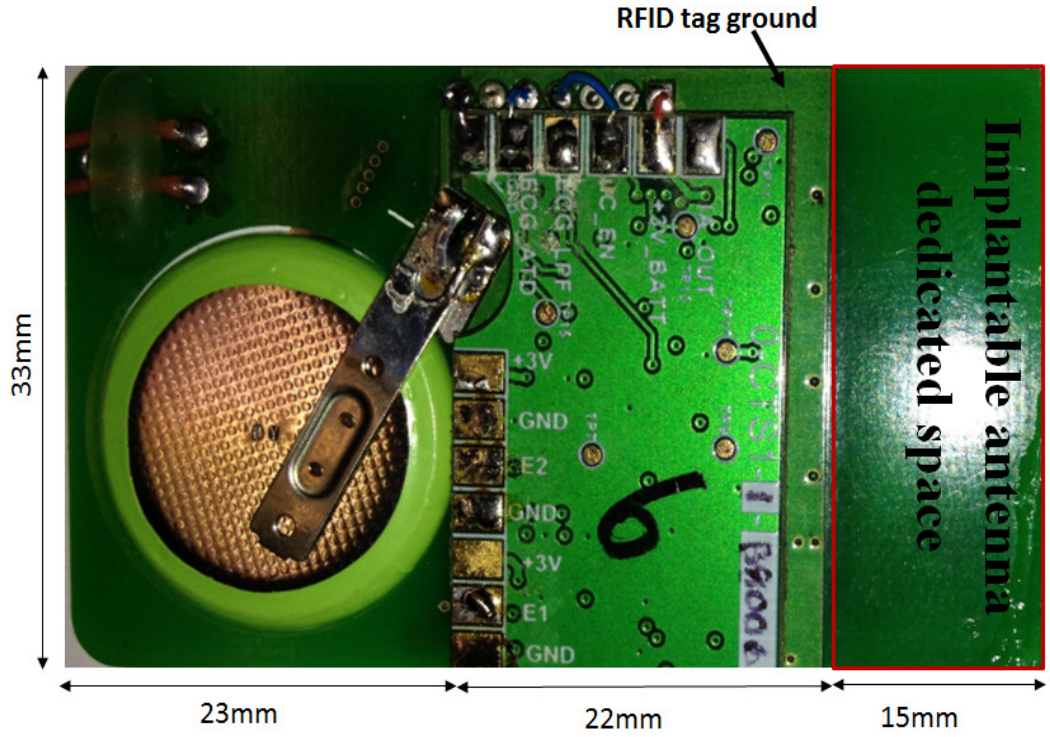

Fig. 6.1: Ground plane side of the implantable RFID tag PCB

A number of PIFAs [20, 77-82] have been reported recently. In [20], two PIFAs have been designed and characterised for biotelemetry applications in the Medical Implant Communications Services band (MICS) at 402-405MHz. Mutual coupling effects have been presented in [77] for a MIMO terminal with an array of PIFAs; each PIFA has the dimensions of 15mm×8mm in free space. However, the ground plane of the PIFA array is significantly larger (100mm×50mm×0.8mm) since it is designed for use with modern mobile phone sets. A frequency tuning method has been reported in [78] for a PIFA to cover the GSM bands (GSM850, GSM900 and GSM1800) as well as the PCS1900 and UMTS bands. A compact PIFA with a capacitive load and a capacitive feed has been proposed in [79] for application with dual-band operation of mobile phones. In [80], low-profile PIFA array antennas for UHF RFID tags are described extensively, including the possibility of using micro-strip line for input impedance matching to a RF module. Modifying the ground plane with slots on it and its effect on the performance of PIFAs is described in [81]. Bandwidth enhancement has also been demonstrated in [82] by inserting a single slot on the ground plane of a PIFA antenna. Like PIFAs, antennas with fractals and space-filling curves [83-100] have also gained attention among the antenna researchers recently because of their compactness features.

The PIFA is widely used in space-critical applications. A shorting pin mechanism makes the PIFA a quarter wave-length long electrically but much smaller physically. Generally, in a PIFA, a parallel radiating patch is separated from a finite ground plane and various techniques such as inserting a proximity feed and cutting slots (on the patch, the ground plane or both) are applied to enhance the bandwidth of the antenna. The resonance frequency of a PIFA operating in the free space can be expressed as:

$$f_r = \frac{c}{4(\sqrt{\varepsilon_r})(L+W)} \tag{6.1}$$

where L and W are the length and width of the radiating patch, c is the speed of light and ε_r is the relative permittivity of the material sandwiched between the radiating patch and the ground plane. Using the above equation, the free-space resonance frequency of our antenna is calculated so that we can estimate the decrease of resonance frequency when it is implanted into the body of a rat. A rough estimate is obtained by applying this technique. It is found that around one-fourth of the free-space resonance frequency is obtained once the antenna is under the rat skin. This is the basis of our PIFA antenna design for the 900MHz ISM band.

6.3 Implantable RFID Tag Antenna Design

We have designed an implantable compact PIFA for the RFID tag [101] provided by our industry partner [102]. This antenna has been custom designed to be interfaced (i.e. impedance matched) with the RF module (900MHz ISM band) of the RFID tag which is known to work in free space. Our proposed antenna is based on the investigation reported in [81], where it was shown that by creating appropriate slots on the ground plane one could improve the bandwidth of a PIFA antenna. In our research, a ground slotted PIFA antenna has been designed and simulated to optimize the bandwidth of the antenna. In particular, we aimed to enhance the bandwidth of the antenna by strategically connecting the antenna ground plane with the ground plane of the existing RFID tag, which operates at 900MHz, so that the device would operate well under the skin of a freely moving experimental rat. To find the optimum attachment of the two ground planes, we

performed computer simulations with a ground slot of variable length between the two ground planes. Electrical properties such as the permittivity and conductivity of biological materials that are required for the simulation were taken from [20].

Fig. 6.2 shows the geometry of our proposed PIFA antenna. In our design, we have considered the RFID active tag that operates in free space. The dimensions of the RFID circuit board (FR-4, ε=4.3, loss tangent =0.025) is 60mm×33mm×1.6mm and its ground plane area is 23mm×33mm. The ground plane area of our PIFA antenna is 9.5mm×33mm and it is partially connected to the ground plane of the RFID tag to increase the bandwidth of the antenna. However, a slot is maintained between the two ground planes to optimise the bandwidth of the antenna. The optimum dimension of the slot between the two grounds was found to be 24mm×1mm. This ground slot optimisation is possible by varying the width of the antenna ground plane and the length of the copper strip connecting the two grounds. There is no option to change the dimension of the ground plane of the RFID tag PCB. The size of the radiating patch is 11mm×13mm with a resonance frequency tuning slot at the centre of the patch along the y-axis. This tuning slot on the radiating patch is optimised and the length and width of the slot are 9.5mm and 3mm, respectively.

The FR4 substrates used in our design have dielectric constant, $\varepsilon_r = 4.3$ and loss tangent, $\tan\delta = 0.025$ unless otherwise stated. A capacitive feed plate is inserted between the top radiating patch and the antenna ground plane. The height of this feed plate is 2.4mm from the antenna ground and the height of the top radiating patch from it is 1.6mm. A microstrip feed line is connected to the feed point and it is traced below the antenna ground plane. The optimised length and width of the microstrip feed line are 10mm and 3mm, respectively.

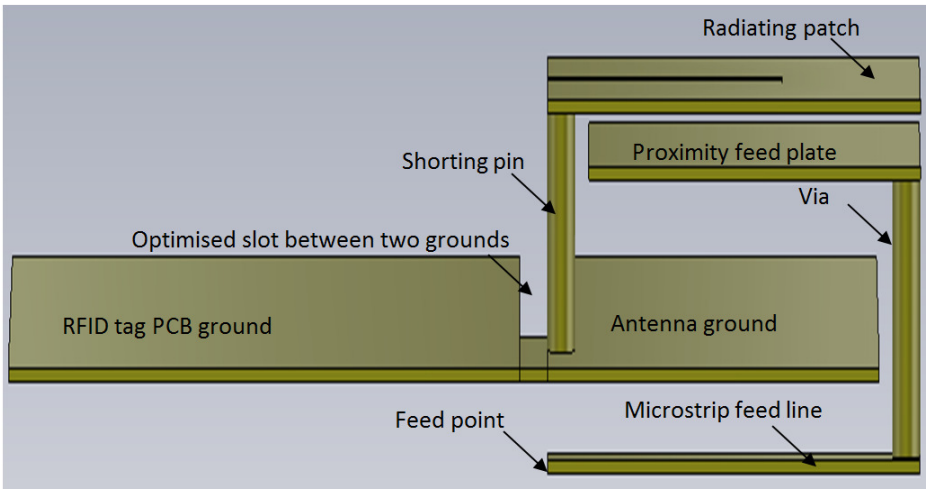

(a)

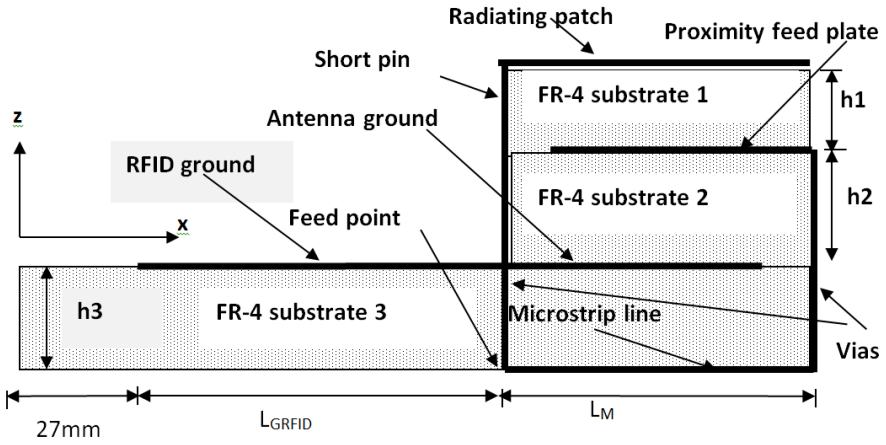

(b)

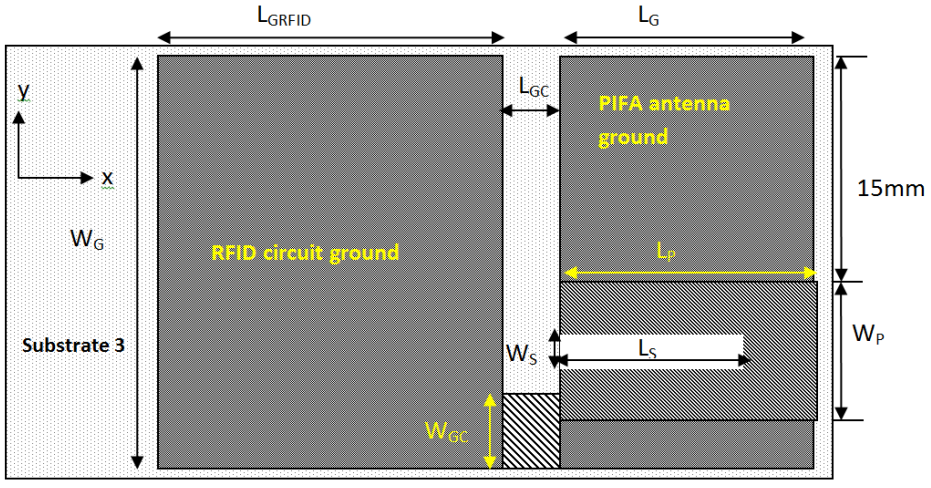

(c)

Fig. 6.2: Proposed implantable PIFA antenna: (a) 3D view, (b) Side view, and (c) Top view

A shorting pin with an optimised radius of 0.5mm is attached between the front left corner of the radiating patch and the antenna ground to reduce the size of the antenna. The antenna design parameters are given in Table 6.1.

Table 6.1: Optimised parameters of the designed antenna

Name of the parameter	Symbol	Value (mm)
Upper radiating patch length	L_P	11
Upper radiating patch width	W_P	13
Upper patch slot length	L_S	9.5
Upper patch slot width	W_S	3
Feed plate length	L_F	9.5
Feed plate width	W_F	13
Ground plane length	L_G	9.5
Ground plane width	W_G	33
Microstrip line length	L_M	10
Microstrip line width	W_M	3
FR-4 substrate 1 height	h_1	1.6
FR-4 substrate 2 height	h_2	2.4
FR-4 substrate 3 height	h_3	1.6
Ground connector length	L_{GC}	1
Ground connector width	W_{GC}	9
Short pin height	h_1+h_2	4
Feed point location	(x_F,y_F)	(0, 4)
RFID circuit ground length	L_{GRFID}	23
RFID circuit ground width	W_{GRFID}	33

In Fig. 6.2(a), a 3D view of the proposed implantable PIFA antenna is shown. The front view of the proposed PIFA antenna is shown in Fig. 6.2(b). The thick black lines are the copper metal parts of the antenna. Three FR4 substrates are stacked together. On the top surface of FR4 Substrate 1, the radiating patch is placed. The feed plate is placed at its bottom surface. The antenna ground plane is placed between Substrate 2 and Substrate 3. The RFID ground plane is placed on Substrate 3 as well. The widths of the two ground

planes are both 33mm. The shorting pin connects the upper most radiating patch and the antenna ground plane. One of the vias connects the feed plate to the microstrip line while the other via passes through Substrate 3 to make the ground point available at the bottom side of Substrate 3. The heights of FR4 Substrates 1, 2 and 3 are 1.6mm (h_1), 2.4mm (h_2) and 1.6mm (h_3), respectively. Although 2.4mm thick FR4 substrates are not available commercially, it can be constructed by combining 1.6mm and 0.8mm thick FR4 substrates. Fig. 6.2(c) shows the top view of antenna.

6.4 Model of the Antenna Environment

A model of the antenna operating environment has been created. It represents the biological material of a rat as shown in Fig. 6.3. At first, the antenna and the RFID tag are enclosed by a biocompatible material (silicone, ε=11.9, σ=0.00025) with a maximum 1mm thickness.

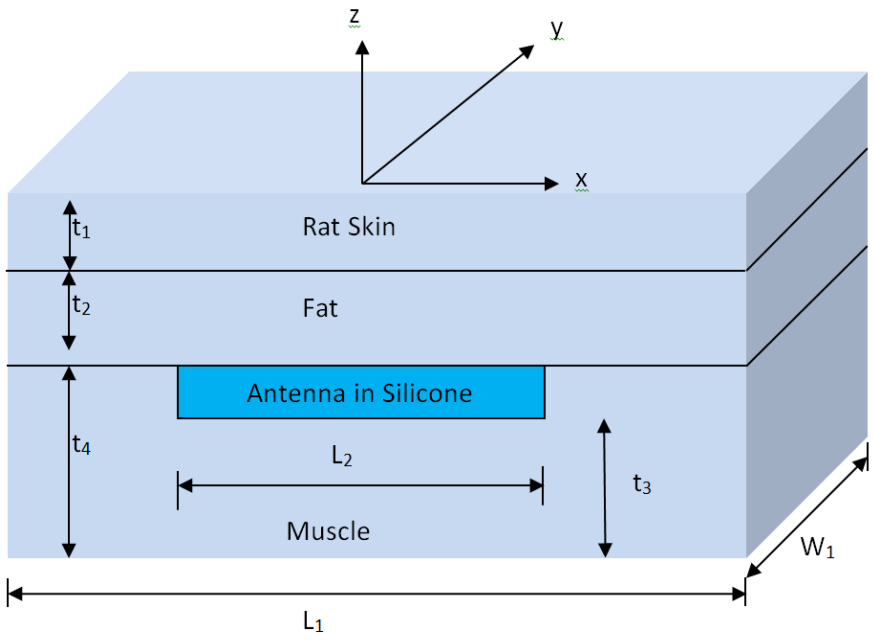

Fig. 6.3: The model of the antenna operating environment

Table 6.2: Antenna Environment Parameters

Name of the parameter	**Symbol**	**Value (mm)**
Rat's skin thickness on fat layer	t_1	2
Fat layer thickness on silicone	t_2	2
Silicone box thickness	t_3	7.8
Skin layer length along X-axis	L_1	103
Skin layer width along Y-axis	W_1	75
Fat layer length along X-axis	L_1	103
Fat layer width along Y-axis	W_1	75
Muscle layer length along X-axis	L_1	103
Muscle layer width along Y-axis	W_1	75
Muscle thickness along Z-axis	t_4	19.6
Silicone box length	L_2	62
Silicone box width	W_2	35

This is on the outer surface of the antenna structure and RFID circuit board. It produces a brick-shaped insulated implantable RFID tag. Then it is embedded into the muscle of a rat allowing 20mm in all directions except the top side which is covered by a fat layer (2mm). The upper most layer is the skin (2mm) of the rat. In our model, we have considered 2mm thickness for both the fat and skin layers since the simulation results confirm a negligible effect on the antenna performance even when their thickness is

further increased. Similarly, a 20mm thickness for the rat's muscle was assumed around the implantable RFID tag when the simulation was conducted. The depth or thickness of the muscle below the insulated implantable RFID tag is also 20mm. Table 6.2 lists the values of the environment variables. The antenna return loss, impedance bandwidth, impedance matching and radiation patterns have been obtained from our simulations with and without connecting the antenna ground with the RFID circuit ground. The model of the antenna operating environment has been included in these simulations, to represent the rat's body material. The electrical properties of the biological tissues, as shown in Table 6.3, are used in the simulations, and their values are taken from the graphs shown in Figs. 6.4-6.5 [6].

Table 6.3: Electrical Properties of Biological Tissues

Name of Tissue	Dielectric Constant (ε_r)	Electrical Conductivity (σ) S/m
Rat skin	32	0.69
Fat	5.6	0.08
Muscle	58.8	0.84

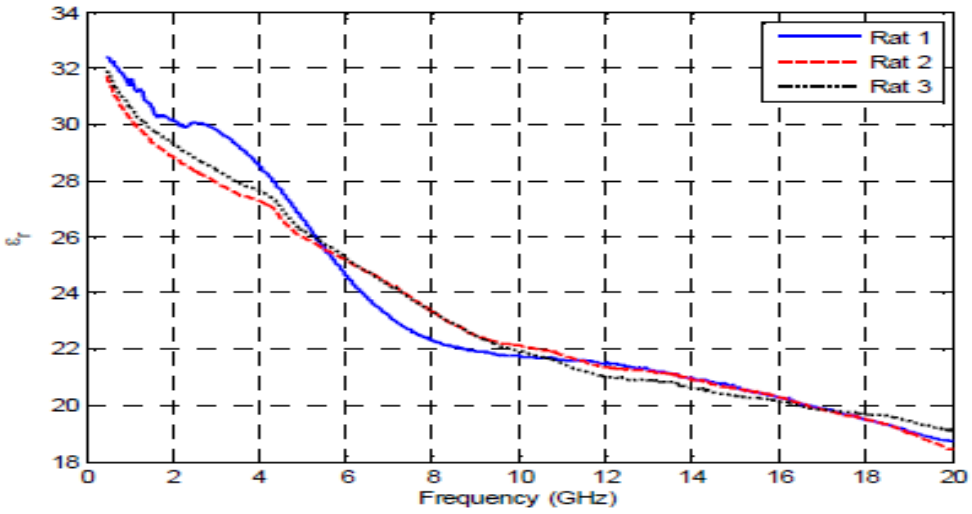

Fig. 6.4: Relative permittivity of rat skin [6]

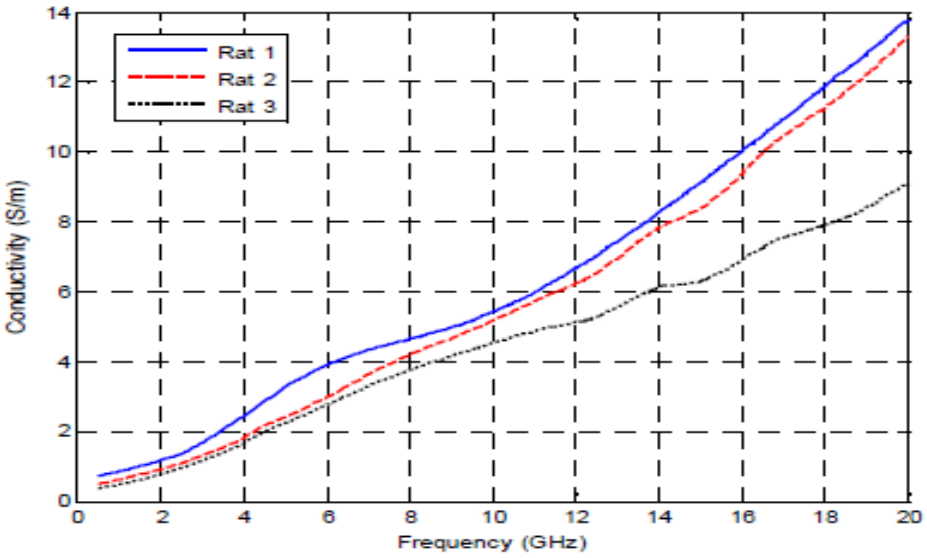

Fig. 6.5: Conductivity of rat skin [6]

6.5 Parametric Study of the Implantable Antenna

Parametric studies of the proposed implantable PIFA antenna were conducted by varying different antenna parameters and the surrounding environment parameters. The parametric study results are shown from Fig. 6.6 to Fig. 6.26. Some antenna parameters and the surrounding environment parameters are varied for the parametric studies and a brief description of each parametric study is provided in this section. The following parameters are considered to observe their effects: Width of microstrip feed line, radius of shorting pin, thickness of surrounding bio-compatible coating, thickness of surrounding fat layer, length of feed plate, width of feed plate, length of ground slot, width of ground slot, length of slot on radiating patch, slot width on radiating patch, length of surrounding tissue layers, thickness of surrounding muscle layer and relative permittivity of surrounding bio-compatible coating.

6.5.1 Variation of radius of shorting pin

The shorting pin location of the proposed antenna is shown in Fig. 6.6 and the radius of the shorting pin is varied from 0.1mm to 0.5mm. The height of the shorting pin is 5.6mm. The input matching of the antenna is improved from -22.6dB to -31.9dB (Fig. 6.7) as the radius of the shorting pin is increased from 0.1mm to 0.5mm respectively. The frequency tuning of the antenna is improved within the band of interest (Australian UHF ISM band, 915-928MHz). There is no change of the bandwidth of the antenna.

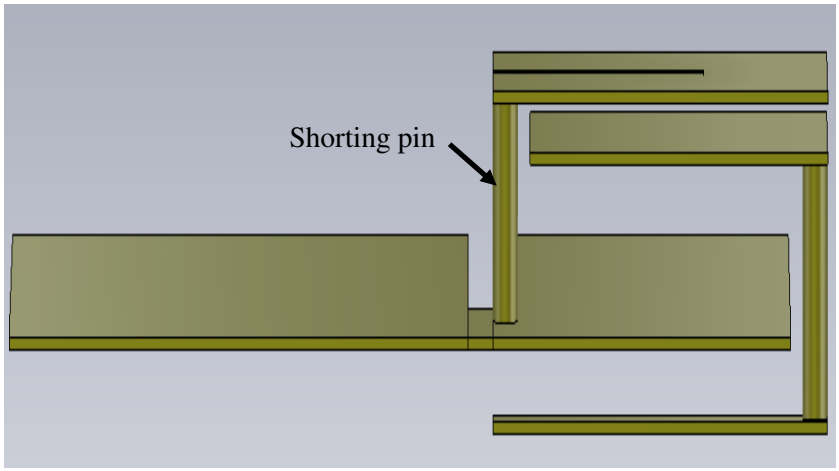

Fig. 6.6: Shorting pin location on the proposed implantable PIFA

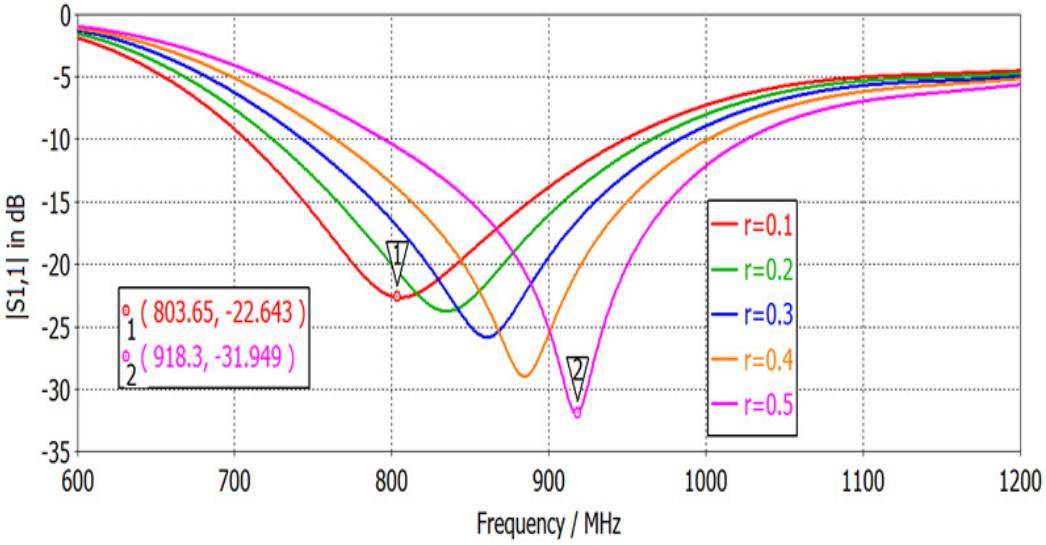

Fig. 6.7: $|S_{11}|$ vs. frequency when radius of shorting pin is varied

6.5.2 Variation of thickness of bio-compatible coating

The bio-compatible coating material applied to the surrounding environment model for our antenna is lossy silicone with a dielectric constant of 11.9 and a conductivity of 0.000025S/m. This material has a higher conductivity than other bio-compatible material, which has a dielectric constant of about 3.0 but acts as insulation for the antenna. When the thickness of the silicone is increased over the range of 1mm-3mm the effect of rat tissue on the antenna decreases and the antenna performance degrades (-31.9 to -13.4dB) as seen from Fig. 6.8. The resonance frequency shifted down from 918.3 MHz to 873.6MHz as thickness increases from 1.0mm to 3.0mm.

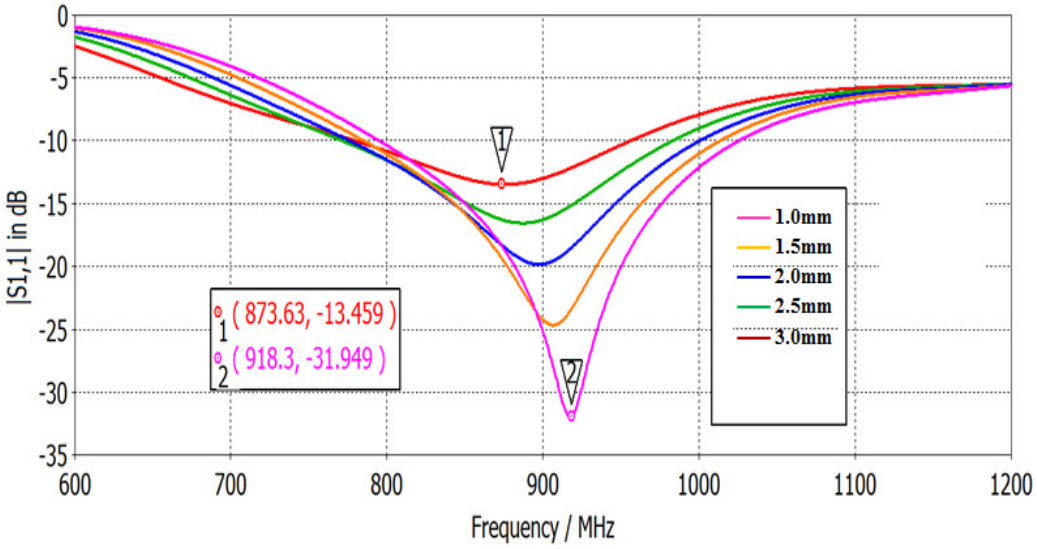

Fig. 6.8: $|S_{11}|$ vs. frequency when thickness of bio-compatible coating is varied

6.5.3 Variation of fat tissue thickness (t_2)

In order to determine the effect of the fat tissue thickness on the performance of the proposed antenna, the fat tissue thickness was varied between 0mm and 2mm (Fig. 6.9). In this case, 0mm fat tissue thickness means there is no fat layer on top of the bio-

compatible material of the antenna and the skin layer touches the silicone coating. The thickness of the skin layer is maintained as 2mm all the time when the fat layer thickness is varied. It is clear from Fig. 6.9 that a slight frequency shift (increases from 914.3 to 917.3 MHz) of the antenna occurs and the optimum input reflection coefficient is achieved at 917.3MHz. The antenna bandwidth is improved from 180MHz (820MHz-1000MHz) to 200MHz (800MHz-1000MHz) when the fat tissue thicknesses are 0mm and 2mm respectively. It is also found that there is no further improvement of the antenna performance when the fat thickness is increased from 1.5mm to 2mm at a-30dB input reflection coefficient.

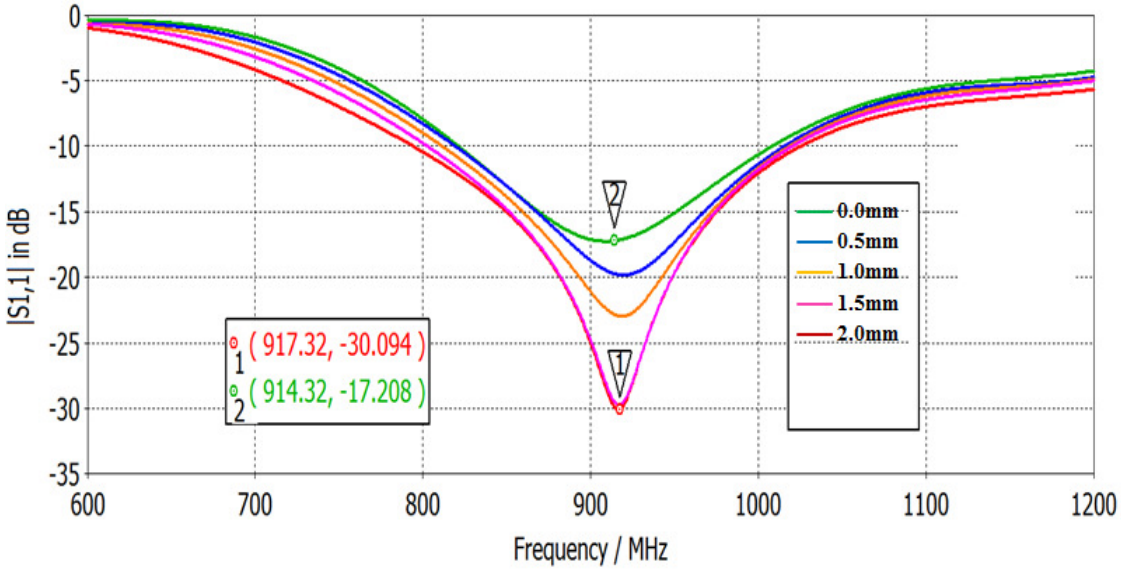

Fig. 6.9: $|S_{11}|$ vs. frequency when thickness of fat layer is varied

6.5.4 Variation of proximity feed plate length (L_F)

The proximity feed plate location is shown in Fig. 6.10; one end is connected to a cylindrical vertical pin known as a via. The open end of the proximity feed plate is varied which in turn changes the length. When the length is increased from 8mm to

12mm the input reflection coefficient is improved from -21.2dB at 900.9MHz to -30.1dB at 916.7MHz as shown in Fig. 6.11. The BW of the antenna is increased from 200MHz (800MHz-1000MHz) to 210MHz (800MHz-1010MHz) when the length of the feed plate is increased from 8mm to 12mm (optimised length).

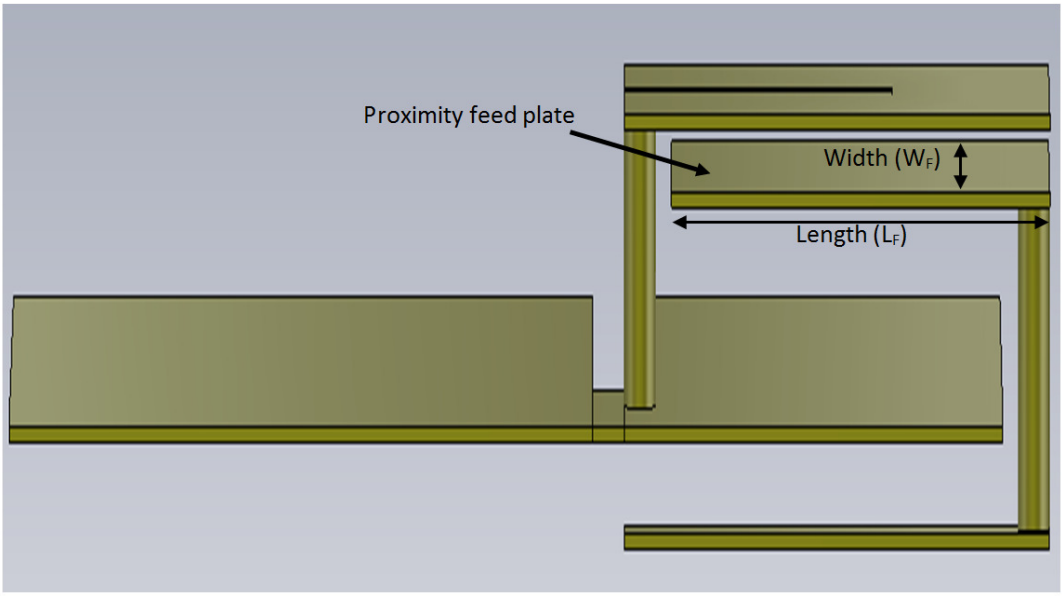

Fig. 6.10: Proximity feed plate location on the proposed implantable PIFA

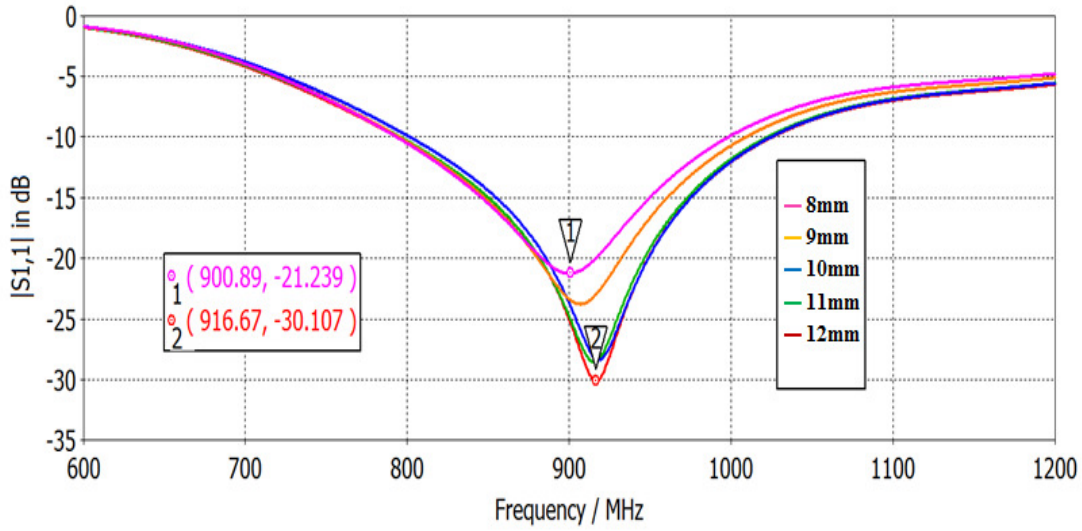

Fig. 6.11: $|S_{11}|$ vs. frequency when length (L) of feed plate is varied

6.5.5 Variation of proximity feed plate width (W_F)

The effect of the feed plate variation on the resonance frequency is shown in Fig. 6.12. In Fig. 6.10, the proximity feed plate location is shown. The width (W_F) of the proximity feed plate is varied between 9mm to 13mm. When the width is increased from 9mm to 13mm the input reflection co-efficient is improved from -21.2dB at 905.7MHz to -30.0dB at 917.9MHz. The bandwidth of the antenna is increased from 200MHz (900MHz-1000MHz) to 205MHz (800MHz-1005MHz) when the width of feed plate is increased from 9mm to 13mm (optimised width).

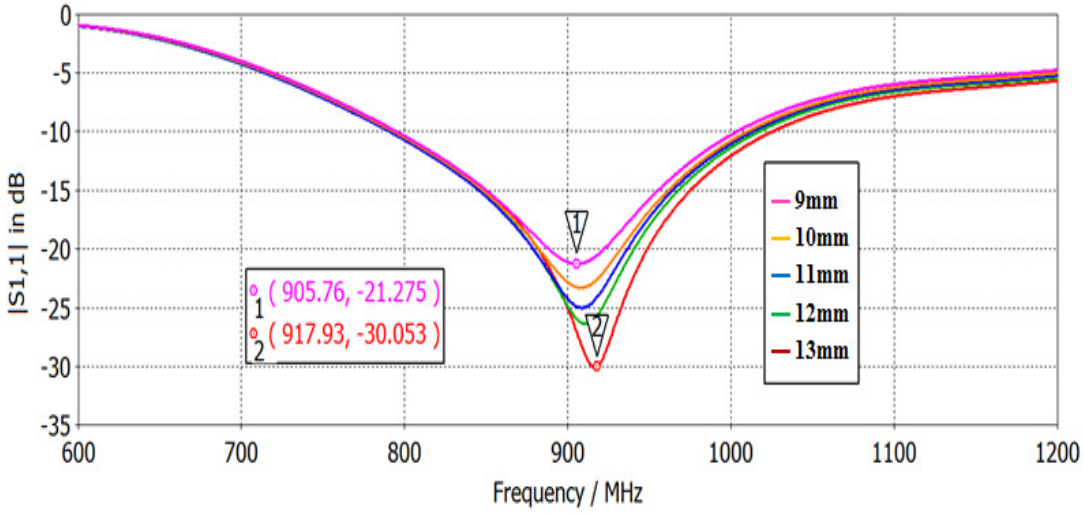

Fig. 6.12: $|S_{11}|$ vs. frequency when width (W) of feed plate is varied

6.5.6 Variations of length and width of ground slot

The slot between the RFID tag PCB ground and the antenna ground is shown in Fig. 6.13. The length and width of the ground slot is varied to see their effects on the performance of the antenna. First the length of the ground slot is varied from 8mm to 28mm and its effect is observed as shown in Fig. 6.14. The resonance frequency of the

antenna is 850MHz when the slot length is 8mm.The optimised slot length is 20mm at a 25dB return loss and the resonance frequency of the antenna is found to be 914.8MHz. The bandwidth covered with this optimised ground slot length is 230MHz (790MHz-1020MHz).

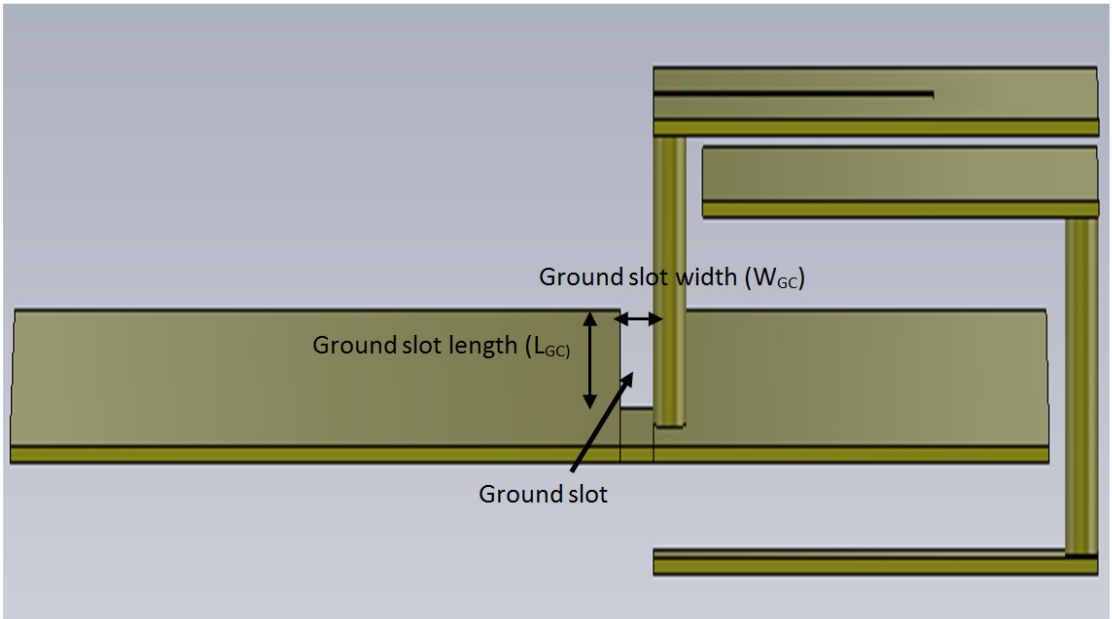

Fig. 6.13: Ground slot location on the proposed implantable PIFA

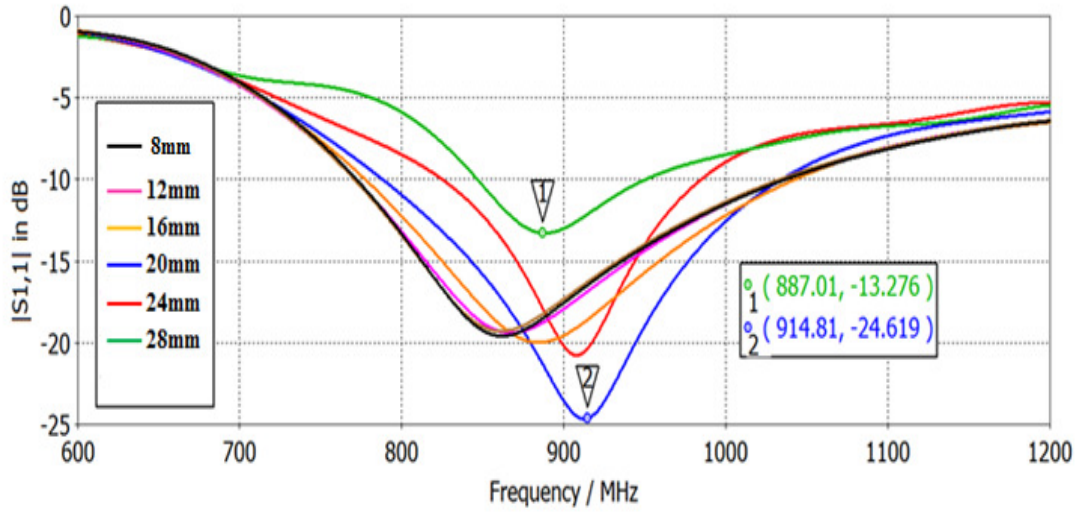

Fig. 6.14: $|S_{11}|$ vs. frequency when the length of ground slot is varied

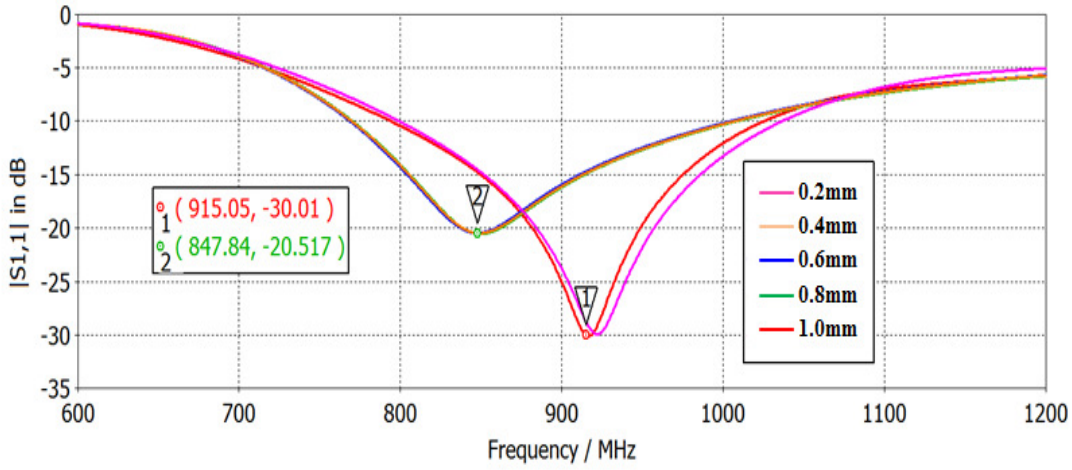

Fig. 6.15: $|S_{11}|$ vs. frequency when the width of ground slot is varied

Secondly, keeping the optimised ground slot length fixed (20mm), the width of the slot is varied between 0.2mm to 1.0mm and its effect is presented in Fig. 6.15. The best value of the input reflection coefficient of the antenna is found to be -30dB with the optimised ground slot width of 1.0mm. However, with ground slot width of 0.2mm the antenna reflection coefficient is very close to the best value. The resonance frequency lies within the Australian UHF ISM band and the bandwidth is 230MHz (800MHz-1030MHz).

6.5.7 Variations of length and width of slot on radiating patch

A slot is cut on the radiating patch of the antenna and its location is shown in Fig. 6.16. Its length and width are varied in the ranges of 2.5mm to 10.5mm and 1.0mm to 3.0mm, respectively. The responses to the length and width variations of the slot on the radiating patch are shown in Figs. 6.17-6.18. It is evident from Fig. 6.17 that the sensitivity of the antenna return loss is more due to length variations of the slot than to its width variations (Fig. 6.18). The resonance frequency shifted down from 982.8MHz to 917.7MHz when the slot length was increased from 2.5mm to 10.5mm.

Thus, this slot can be utilised for retuning the antenna to a desired frequency range if it is detuned due to some reason. The optimised value of the slot length on the radiating patch is 10.5mm at 917.7MHz (30dB return loss) while the optimised slot width is 1.0mm at 918MHz (30 dB return loss).

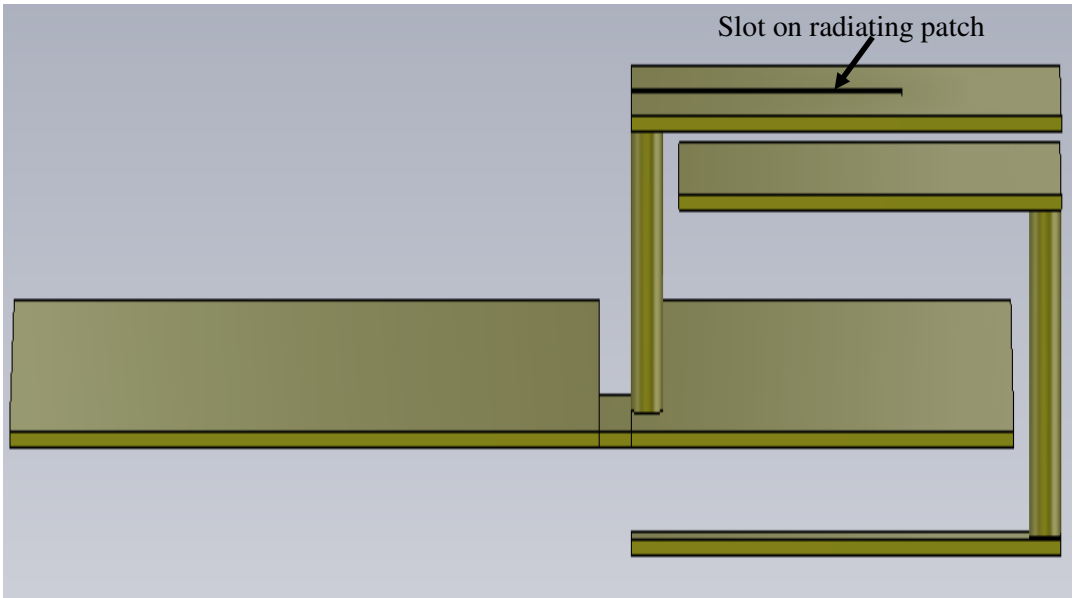

Fig. 6.16: Location of the slot on the radiating patch of the proposed implantable PIFA

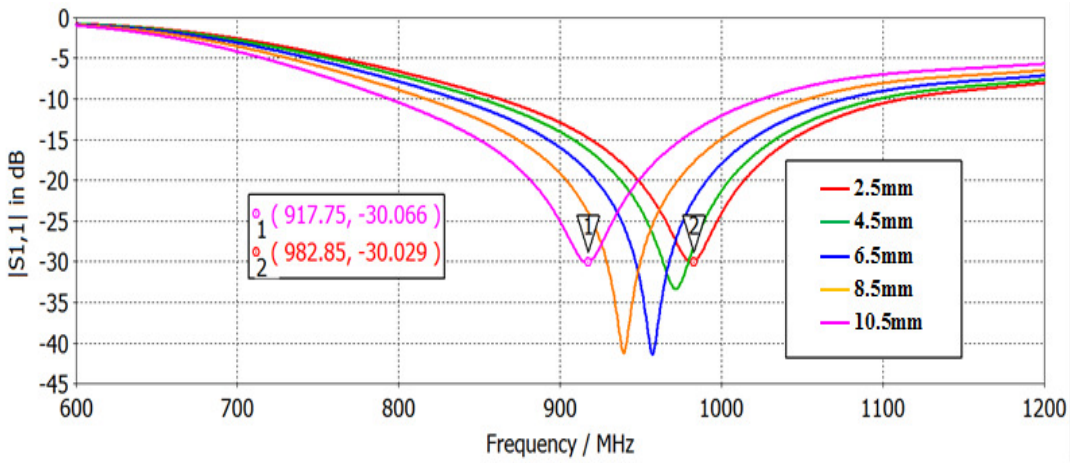

Fig. 6.17: $|S_{11}|$ vs. frequency when patch slot length is varied

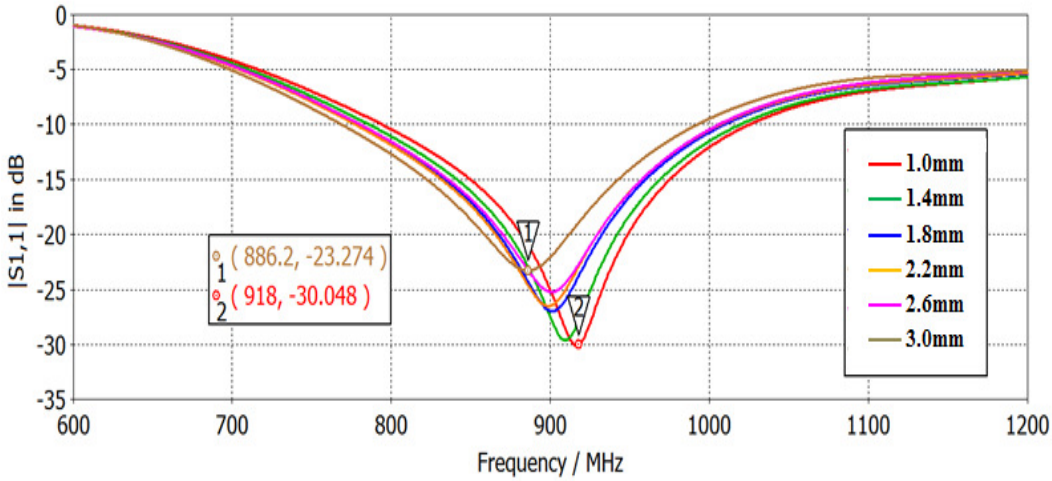

Fig. 6.18: $|S_{11}|$ vs. frequency when the patch slot width is varied

6.5.8 Variation of length of tissue layers

The weight and size of the rat may increase when the antenna is already implanted in the rat. Therefore, the length of rat tissue (muscle, fat and skin) is varied from 100mm to 200mm to determine the effect on the antenna input reflection coefficient. No effect on the antenna performance is found with variation of the rat tissue as shown in Fig. 6.19.

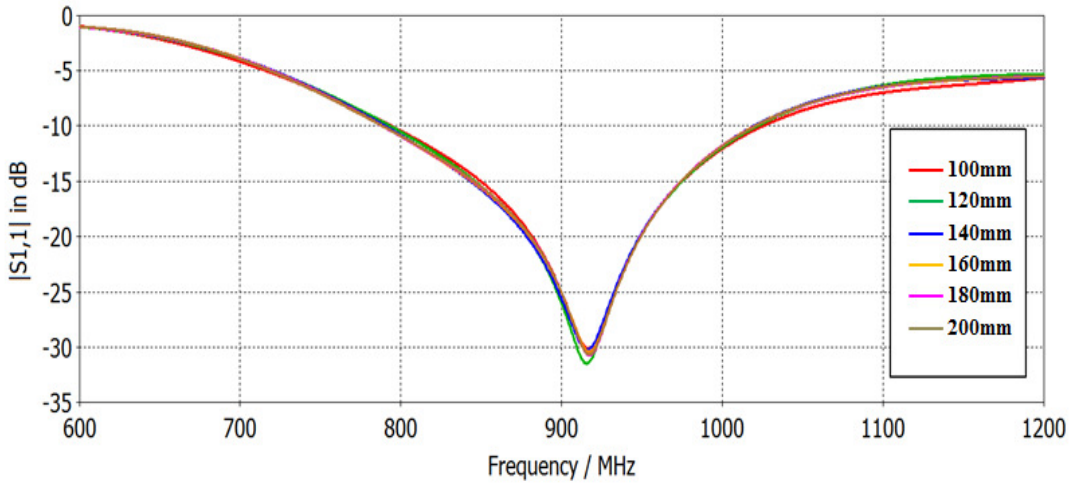

Fig. 6.19: $|S_{11}|$ vs. frequency when length of tissue layers is varied simultaneously

6.5.9 Variation of thickness of muscle tissue

The thickness of the rat muscle tissue may change when the antenna is already implanted in the rat. Therefore, the thickness of the rat muscle tissue is varied from 15mm to 55mm below the antenna to observe its effect on the antenna input reflection coefficient.

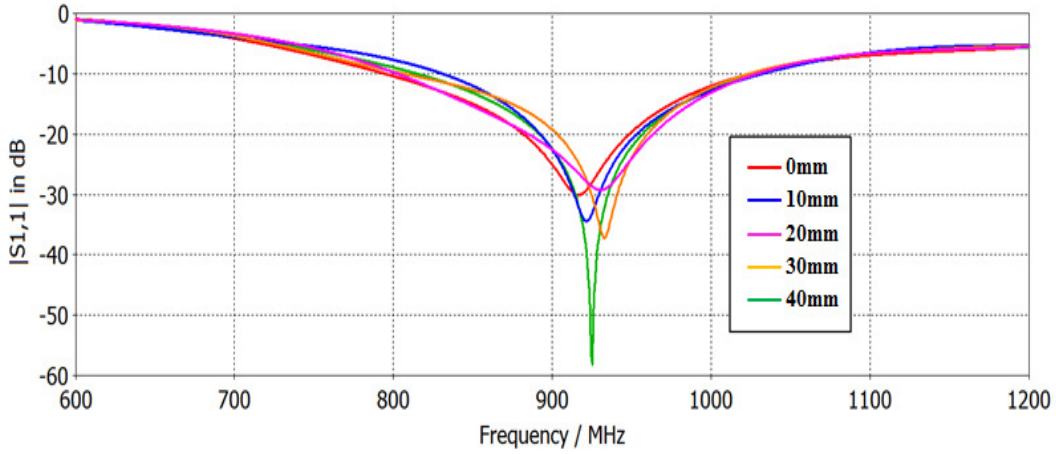

Fig. 6.20: $|S_{11}|$ vs. frequency when thickness of muscle layer below antenna is varied

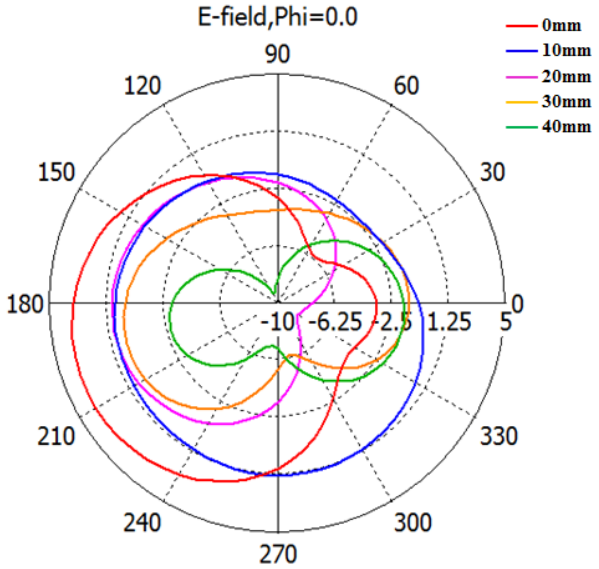

Fig. 6.21: E-field (φ=0) in XZ plane when thickness of muscle below antenna is varied

Although there is shift of the resonance frequency, the antenna performance is improved. The best value of the return loss is found to be 50dB at 920MHz as shown in Fig. 6.20 when the thickness of muscle layer below the antenna is 55mm. The effects on E-field, antenna efficiency and radiated power due to rat muscle tissue thickness variations are illustrated in Figs. 6.21-6.23, respectively.

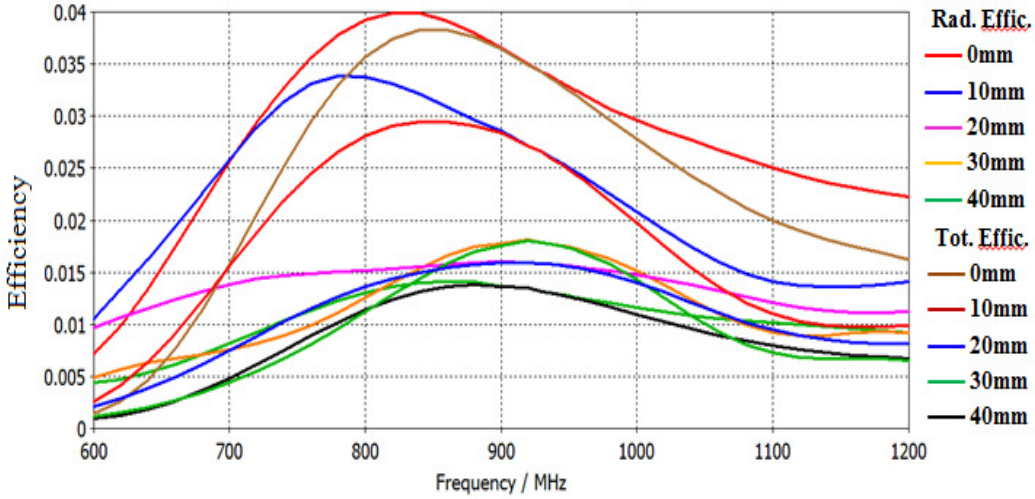

Fig. 6.22: Efficiency when thickness of muscle layer is varied

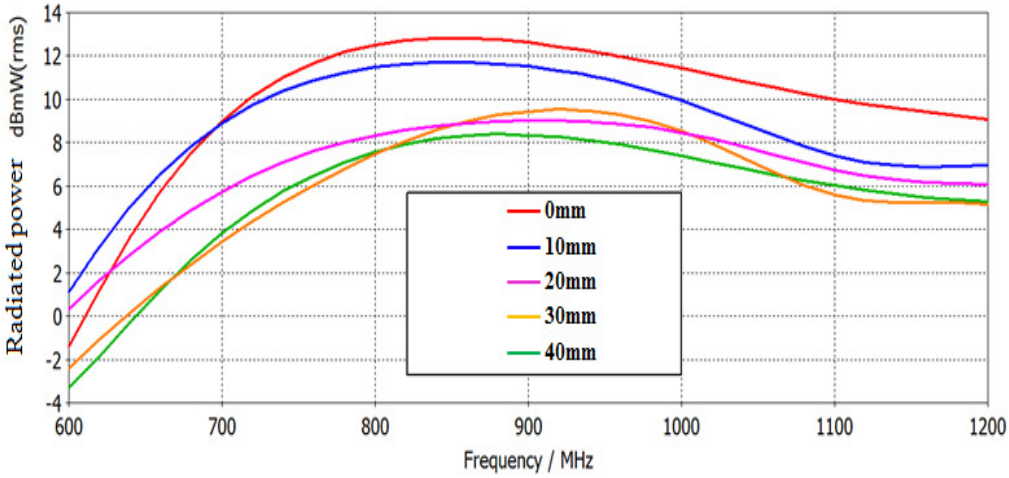

Fig. 6.23: Radiated power when thickness of muscle layer is varied

6.5.10 Variation of relative permittivity of biocompatible coating

The implantable device must be coated with the bio-compatible material before being placed inside an animal such as a rat to isolate it from the body tissue. In this section, the effect of this biocompatible coating material is studied by changing its relative permittivity between 2 and 12 as shown in Fig. 6.24. A significant frequency detuning of the proposed antenna is found, i.e. the frequency is shifted down to 912.8MHz at a relative permittivity of 12 from 1150MHz at a relative permittivity of 4. The optimum input reflection coefficient of the proposed antenna is -36.2dB at 947.2MHz and the BW is approximately 210MHz (~22%) at a 10dB return loss.

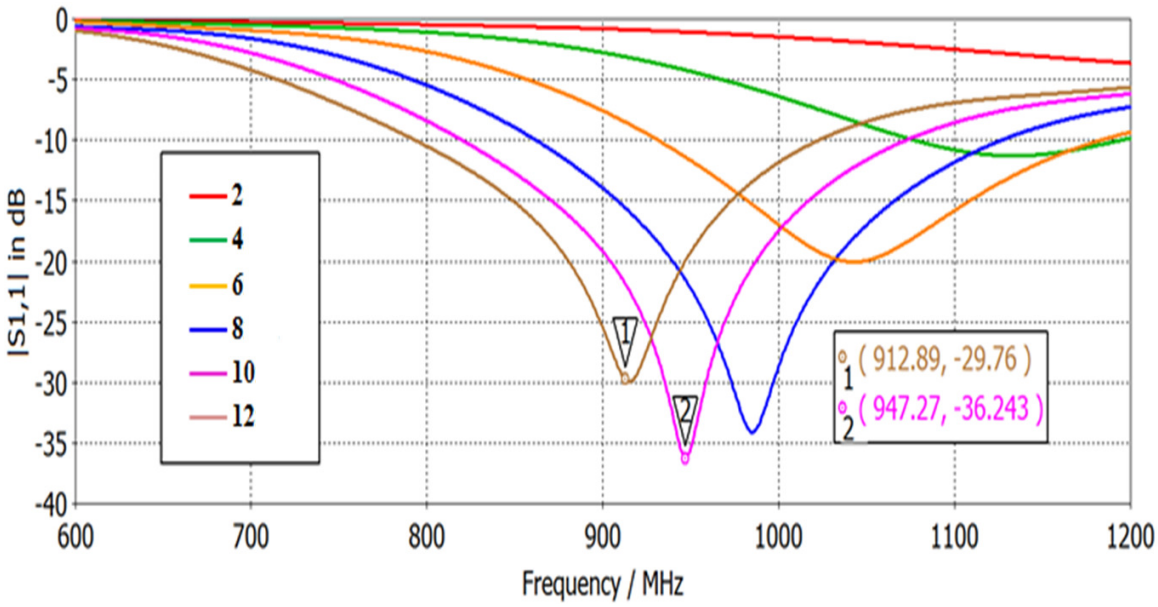

Fig. 6.24: $|S_{11}|$ vs. frequency when relative permittivity of bio-compatible coating is varied

6.6 Creating an Optimised Slot between Antenna and RFID tag PCB Grounds

In this section, we present our implantable PIFA (11mm×13mm×5.6mm) with a slotted (optimised) ground plane, operating in the 900MHz Australian ISM band, custom designed for implantation under the skin of a rat. It is possible to connect the RFID tag PCB board larger ground to the designed PIFA ground simply by soldering them since they are on the same side of PCB. However, because creating slot on the ground can improve the performance [82], a slot between two grounds was created and optimised. The main purpose of this was to further enhance the bandwidth of the PIFA. The antenna bandwidth was enhanced further (Fig. 6.25) by partially connecting the antenna ground plane to the RFID circuit ground plane, leaving an optimised slot between them. The antenna operating environment was modeled and included when the antenna was simulated and optimised. Our results show that the directivity (Fig. 6.26) of the antenna also improves with the slotted ground connection. It is also found that the directivity as well as the return loss of the PIFA improved significantly with the optimisation of the slot on the RFID ground. The direction of maximum radiation is exactly normal to the radiating patch of the designed PIFA after the slot is optimised. The return loss of the antenna has been increased by about 7.0dB at 927MHz with the optimised slot on the ground plane. Thus, by designing an optimum slot on the RFID ground plane, one can improve the implantable antenna performance for space limited applications. The design details of a PIFA with ground slots to improve the performance can be found in [17, 81].

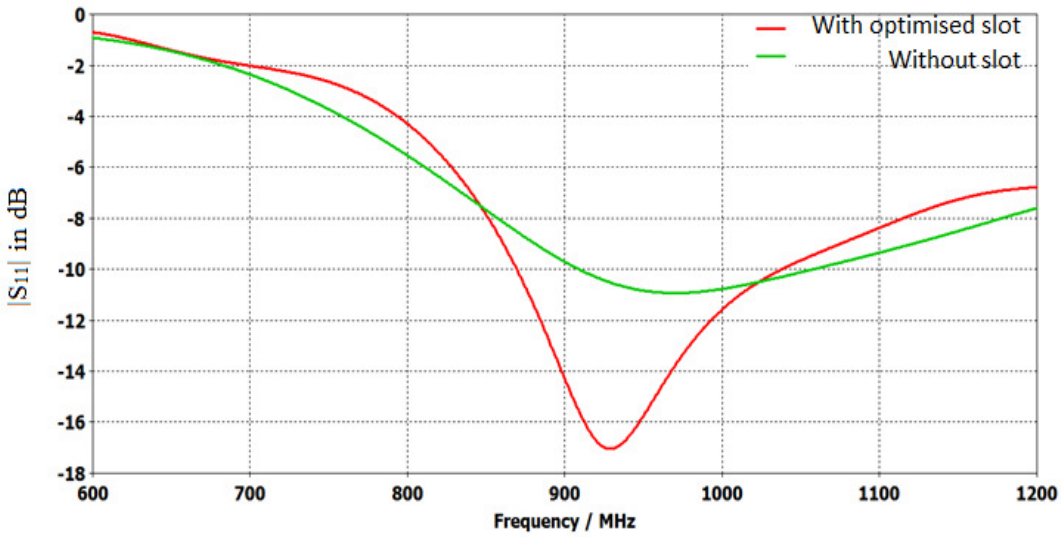

Fig. 6.25: $|S_{11}|$ vs. frequency with and without ground slot

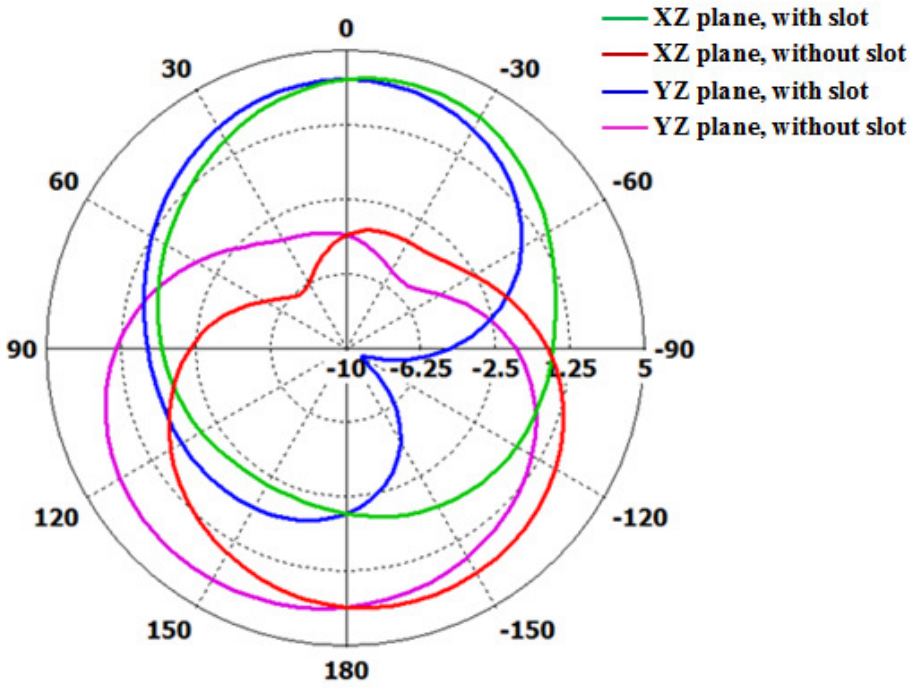

Fig. 6.26: Antenna radiation pattern with and without ground slot

6.7 Optimised Results and Discussions

We have performed computer simulations with the antenna surrounding environment model presented earlier in this chapter to obtain the following antenna parameters: (i) antenna input return loss, (ii) antenna input resistance, (iii) antenna input reactance, and (iv) antenna directivity. In all simulations, we have plotted the results with and without connecting the RFID tag ground and antenna ground plane together. A slot between these two grounds have been optimised (length and width) before plotting the graphs.

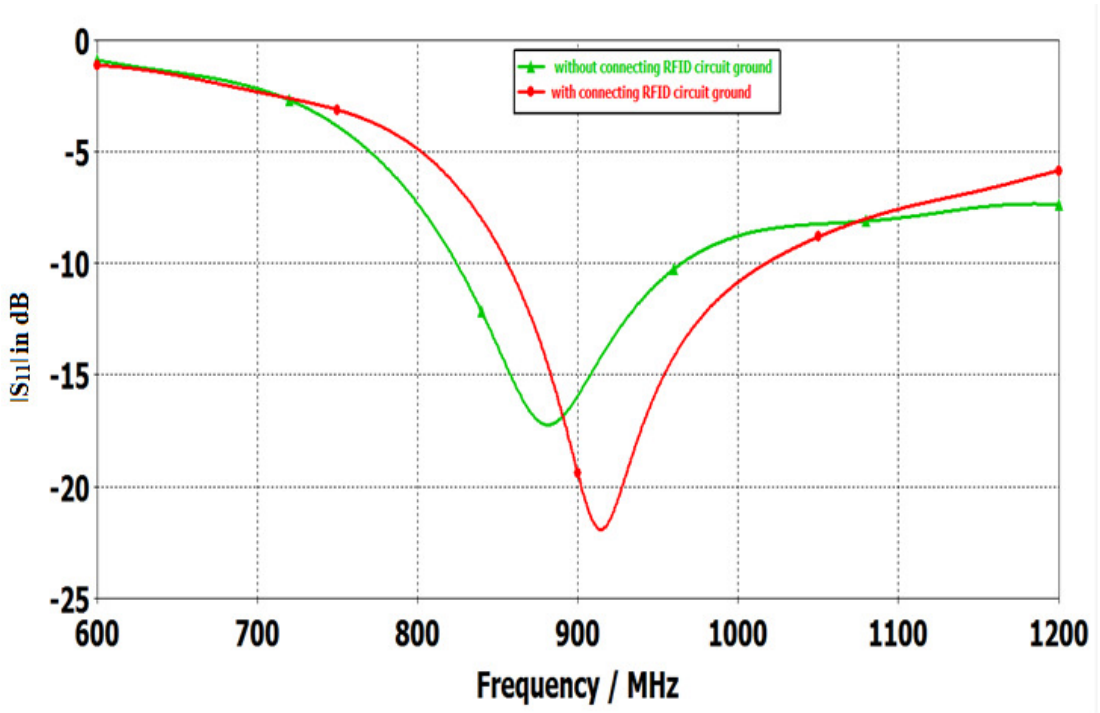

Fig. 6.27: $|S_{11}|$ vs. frequency of the antenna, with and without antenna ground connection to the RFID tag PCB ground

In Fig. 6.27, the antenna input reflection coefficient is presented with and without the RFID tag ground attached to the PIFA ground. It is evident from the graph that the bandwidth as well as the return loss improves when they are connected together. In addition to this, better matching is observed in the 900MHz ISM band.

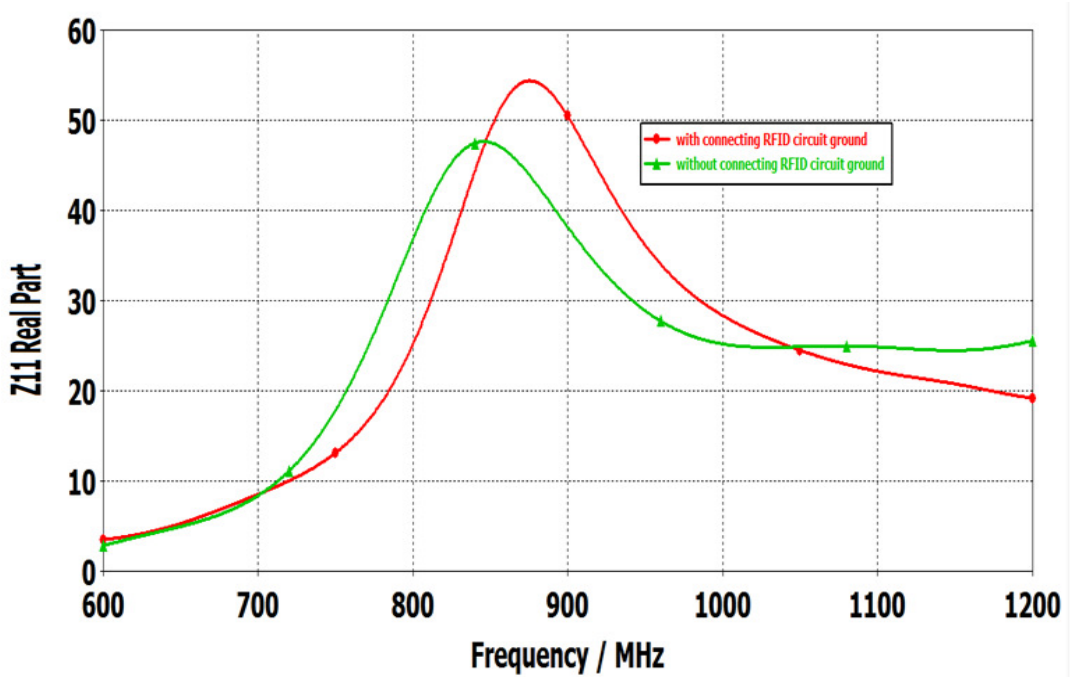

Fig. 6.28: Antenna input resistance vs. frequency with and without connecting the antenna ground to the RFID tag PCB ground

The antenna input resistance vs. frequency with and without connecting the ground plane of the RFID tag PCB is shown in Fig. 6.28. It is found that at 900MHz the antenna input resistance is exactly 50Ω when the antenna ground is connected to the ground plane of the RFID tag PCB while it is below 40Ω when they are not connected. In Fig. 6.29, the antenna input reactance vs. frequency with and without connecting the antenna ground to the ground of the RFID circuit is shown. We notice that the antenna input reactance converges to approximately zero at around 920MHz but it is well above zero when the antenna ground plane is not connected to the ground plane of the RFID circuit.

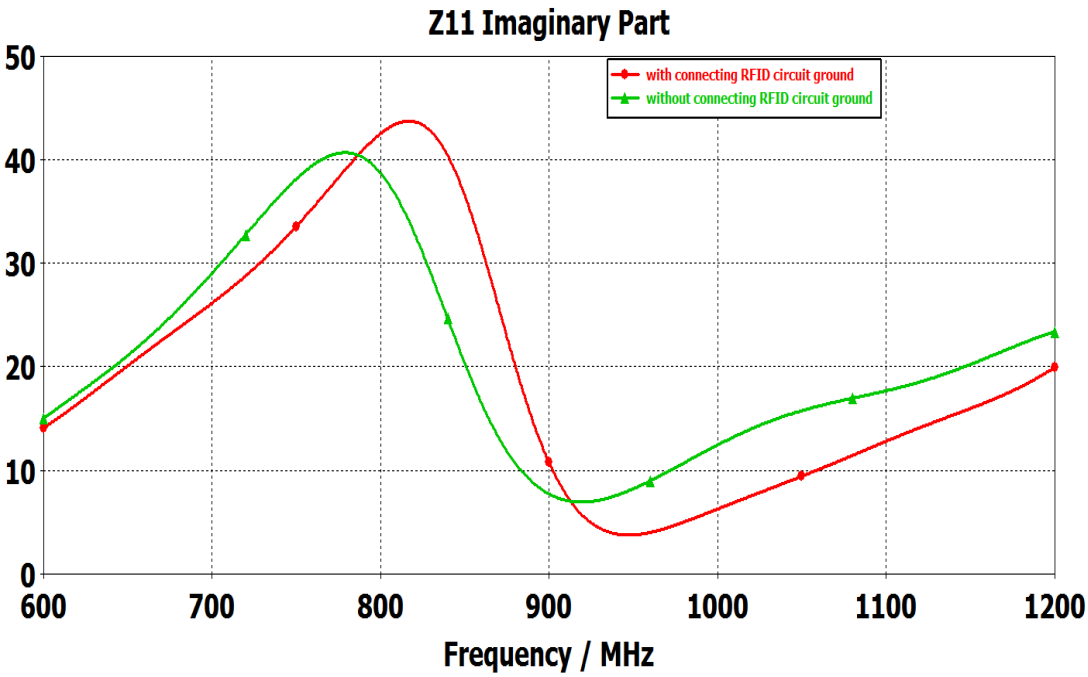

Fig. 6.29: Antenna input reactance vs. frequency with and without connecting the antenna ground to the RFID tag PCB ground

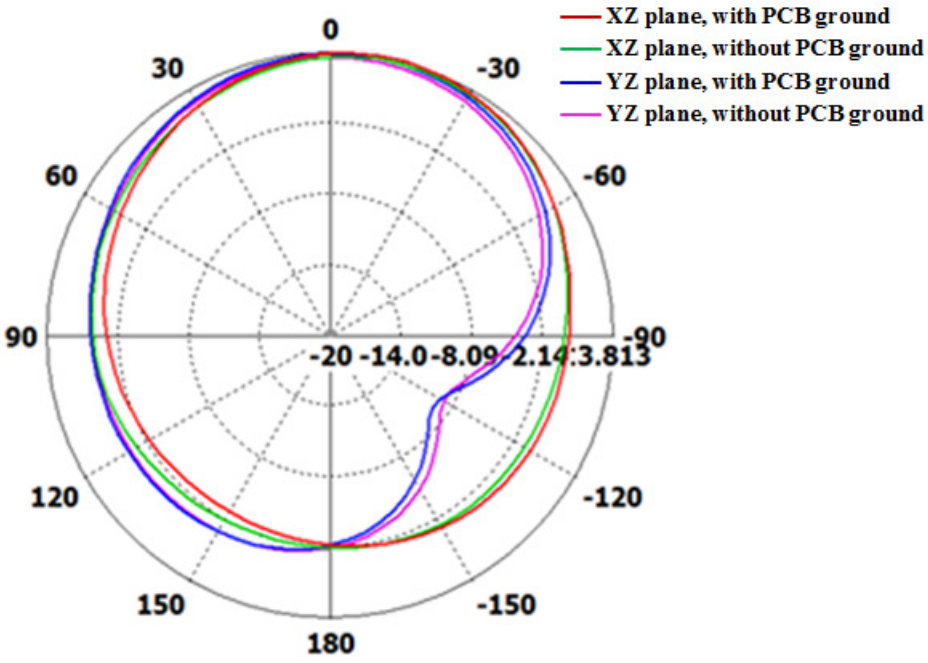

Fig. 6.30: Antenna radiation pattern on two planes with and without connecting the antenna ground to the RFID tag PCB ground

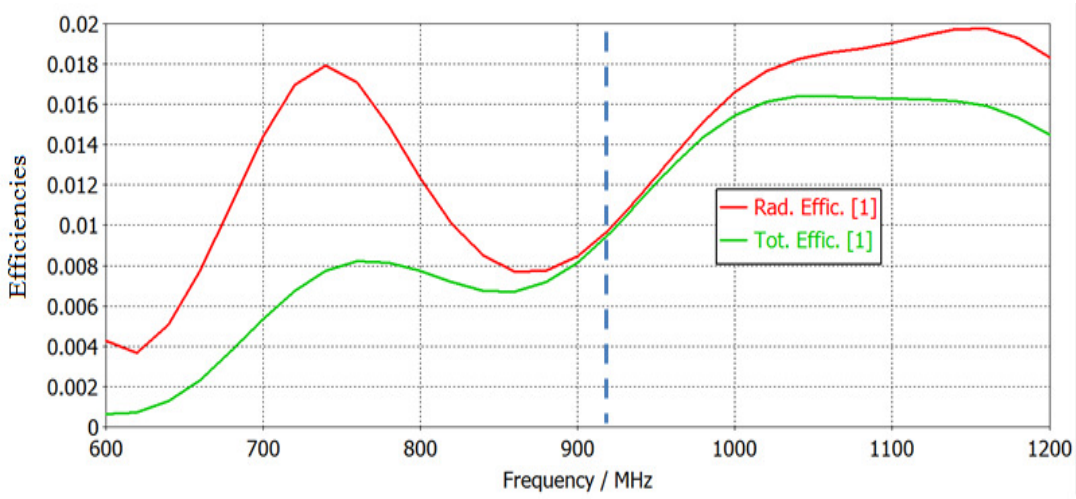

Fig. 6.31: Efficiencies of the proposed antenna for ground plane side of RFID tag PCB

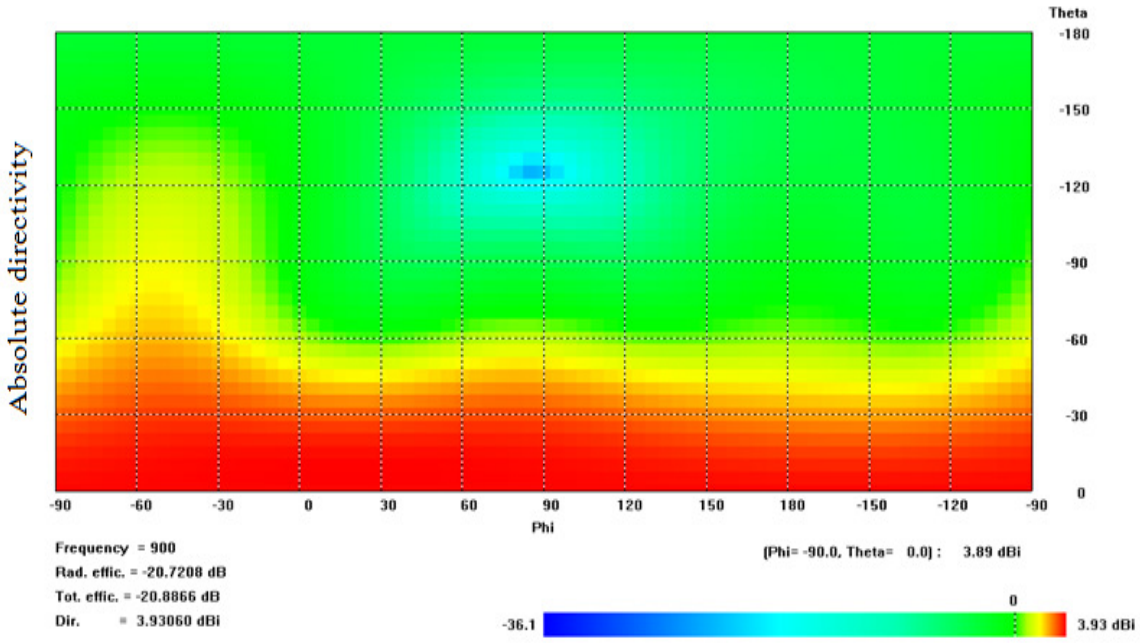

Fig. 6.32: Absolute directivity of the proposed antenna for ground plane side of RFID tag PCB

The radiation pattern of the antenna, with and without connecting the antenna ground to the ground of RFID tag PCB, is presented in Fig. 6.30. It shows that the maximum directivity is obtained in the z-direction, i.e. outwards from the rat's body through the skin, which is the desired direction. Therefore the loss of RF energy due to absorption by

the lossy rat tissue is reduced, as the RF signal passes through thin rat skin tissue. In Fig. 6.31, the radiation and total efficiencies of the proposed antenna for the ground plane side of RFID tag PCB are presented. The efficiencies of the proposed implantable PIFA are approximately 1% at about 920MHz. As an implantable antenna, this result is very good when high losses in rat tissue are considered. The far-field directivity of the proposed antenna is shown in Fig. 6.32. It is found that the maximum directivity is exactly outward through the rat tissue i.e. perpendicular to the radiating patch of the antenna. The far-field peak directivity is predicted to be 3.93dBi for the designed antenna.

6.8 Conclusion

An implantable compact PIFA, that is suitable to be attached on the ground plane side of the RFID tag PCB, was designed and simulated to investigate the antenna parameters. It is observed that the bandwidth is enhanced when the ground plane of the antenna is partially connected to the ground plane of the RFID circuit, leaving an optimised slot between them. The directivity of the antenna also improved when this is done. Thus, we can utilize the ground plane of the RFID tag to improve antenna performance when an implantable antenna is designed. Parametric studies were conducted and their results are presented to illustrate the sensitivity of the antenna to various antenna parameters as well as its surrounding environment parameters.

Chapter 7

Design, Fabrication and Measurements

7.1 Introduction

In the previous chapters, a series of implantable PIFAs were designed and comprehensive investigations of the sensitivities of their resonance frequency to antenna parameters and their surrounding environment were performed. In this chapter, the design, fabrication and measurement details of two new implantable PIFAs are presented. Since the proximity couple-fed implantable PIFA (I-PIFA) has a wider bandwidth, the possibility of maintaining the operating frequency of the antenna within the band of interest (915MHZ-928MHz, Australian ISM band) is higher, even when it is detuned by the rat tissue or biocompatible coating. However, this was not achieved in the first fabrication as the measurement results ($|S_{11}|$) showed the resonance frequency to be at 1150MHz, which was outside the Australian UHF ISM band. The antenna was then modified by increasing the length of the radiating patch and the new design was fabricated. The modified implantable PIFA was coated with NuSil's MED-1134 biocompatible coating material and the input reflection coefficient measurement was performed again under rat skin. The modified antenna with the RFID tag, placed under the skin of a rat, was found to be operating in the desired UHF band.

In the last decade, various RFID-tags and antennas [103-111] have been designed and implemented for the RFID communications. One of the major goals of this thesis is to

design and fabricate an implantable antenna to be attached to an UHF RFID tag and transmit the extracted physiological signals from the body of a rat to an external RFID reader connected to a computer. A small implantable antenna is essential for interfacing with the RF chip of the RFID-tag PCB. Since the space is limited on the selected RFID tag PCB, a compact PIFA (9.25mm×8mm×3.2mm) was designed (Fig. 7.1) and fabricated (Fig. 7.6). The implantable antenna was coated with a biocompatible material, Sylgard (dielectric constant = 2.7). After the attachment of the coated antenna to the RF chip of the RFID-tag PCB, the input reflection coefficient ($|S_{11}|$) was measured and it was found that the resonance frequency was at around 1150MHz (Fig. 7.13), far above the 900MHz ISM band. The predicted $|S_{11}|$ shown in the same figure indeed shows that the resonance frequency of the antenna is close to 900MHz if it is coated with a higher-dielectric (dielectric constant = 3.9) biocompatible material. Since this higher-dielectric biocompatible material was not commercially available at the time of this thesis, an alternative solution was to retune the antenna by increasing the length of the top radiating patch. Re-designed antenna was fabricated and coated with a readily available bio-compatible material and $|S_{11}|$ was measured again under the skin of a rat. These measurements confirm that the final antenna operates well in the Australian ISM band when it is attached to the RFID tag, and placed under the skin of rat. Finally, the operation of the RFID tag with the new antenna was demonstrated by transmitting the temperature between the tag and RFID reader when tag is placed under the rat skin.

7.2 Chapter Contributions

The main contributions of this chapter are:

- Design and fabrication of a miniaturised implantable PIFA antenna to be attached on the component- side of the RFID-tag PCB.
- Investigation of the effects of rat tissue on the return loss and resonance frequency of the implantable antenna. This was because high-permittivity biocompatible material was assumed in the antenna design process.
- Measurement of antenna prototypes in free space without coating, in free space with biocompatible coating and under rat skin.
- Retuning an implantable antenna to the Australian UHF ISM band when it is detuned due to the readily available biocompatible material (MED 1134).
- Demonstration of the operation of the telemetry system by transmitting temperature reading from the RFID tag to the RFID reader, with the new antenna prototype interfacing to tag circuit and the tag is covered by rat skin.
- Measurement of the read range of the new RFID telemetry system.

7.3 Antenna Design with Its Surrounding Environment

Fig. 7.1 shows the geometry of the designed implantable antenna. The 3D views and side view of the antenna are shown in Fig. 7.1(a), 7.1(c) and 7.1(b), respectively. The overall optimised dimensions of the antenna are 9.25mm×8.0mm×3.2mm. The area of the top radiating patch is 9.25mm×8mm with a slot of length of 8.0mm at the center line along the length of the radiating patch. The width of the slot is 1.0mm. It is printed on a 0.8mm-thick FR4 (Substrate 1) with an estimated dielectric constant of 4.3.

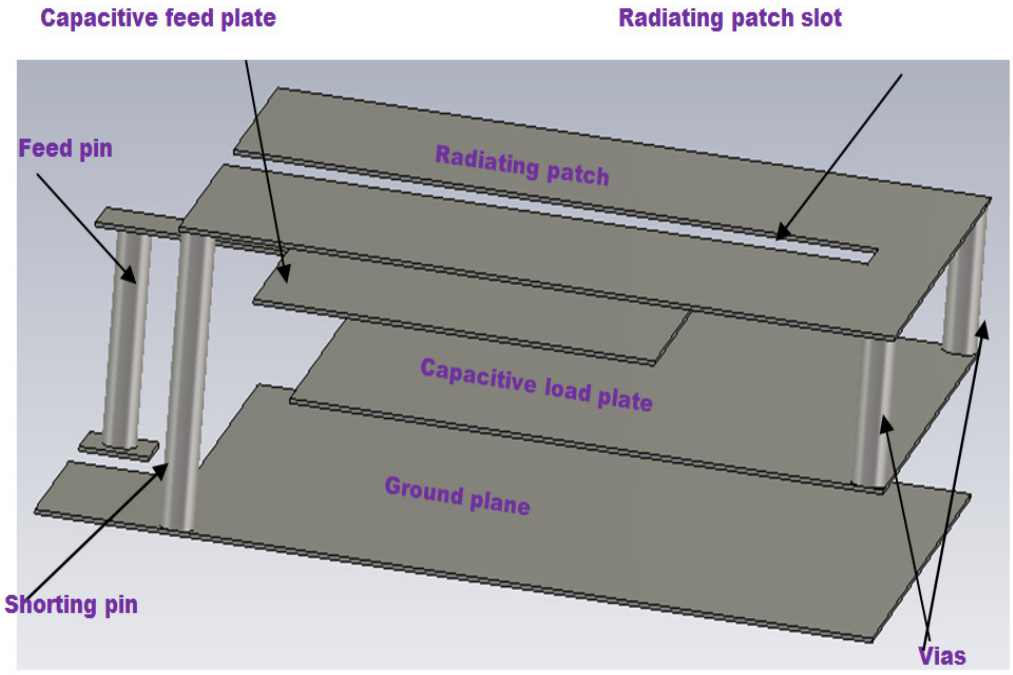
Capacitive feed plate
Radiating patch slot
Feed pin
Radiating patch
Capacitive load plate
Ground plane
Shorting pin
Vias

(a)

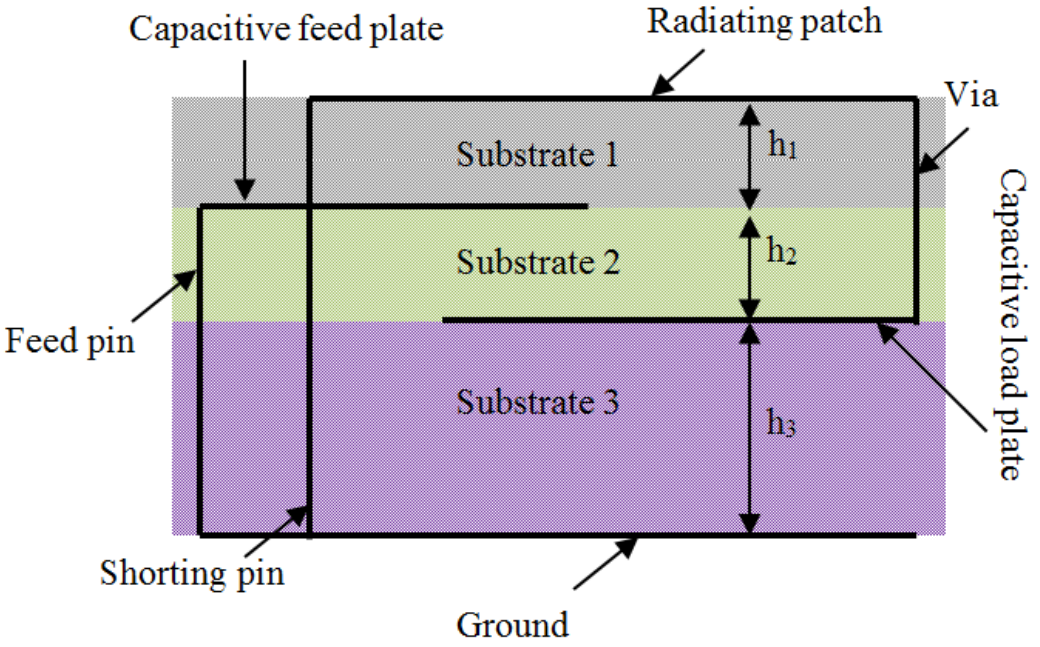
Capacitive feed plate
Radiating patch
Via
Substrate 1
h1
Substrate 2
h2
Feed pin
Substrate 3
h3
Capacitive load plate
Shorting pin
Ground

(b)

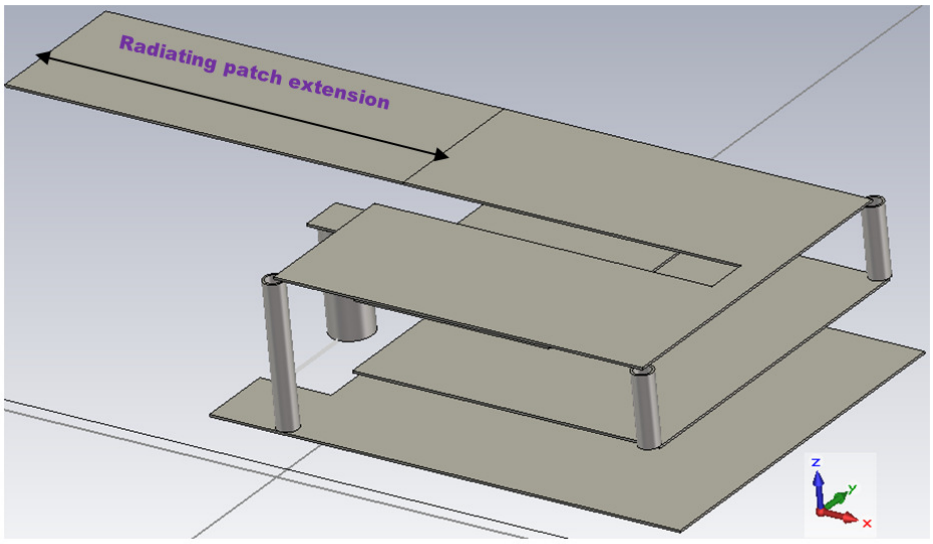

(c)

Fig. 7.1: The geometry of the designed implantable PIFA (a) 3D view (b) Side view (c) 3D of the antenna with the extended radiating patch for re-tuning.

A capacitive feed plate is printed on the lower surface of Substrate 1 and its area is 5.75mm×7.5mm. The FR4 Substrate 2 with the same thickness of 0.8mm is located below this feed plate. A capacitive load plate with an area of 6.0mm×8.0mm is printed on the bottom surface of this second substrate. The FR4 Substrate 3, with a height of 1.6mm, is located on the ground plane of the antenna. The area of the ground plane is 9.5mm×9.5mm. The top radiating patch and the capacitive load plate are connected through two vertical vias, each of them having a radius of 0.25mm. The radius of each via has been optimized by parametric optimization. Changing the area of the capacitive load plate will vary the capacitance between this plate and the ground plate. It is utilized for tuning the resonance frequency of the antenna. A vertical feed pin with an optimized radius of 0.25mm connected between the feed plate and the RF-module signal pin of the RFID circuit board. A shorting pin (SP) is located at the left corner of the radiating patch, connecting the radiating patch to the ground plane, and its height is 3.2mm.

Table 7.1: Antenna Environment Model Parameters

Name of antenna environment parameter	Symbol	Optimised value (mm)
Skin layer thickness	t_1	**2**
Fat layer thickness	t_2	**2**
Muscle layer thickness	t_4	**50**
Coating box height	t_3	**7.8**
Rat skin layer length	L_1	**200**
Fat layer length	L_1	**200**
Muscle layer length	L_1	**200**
Coating box length	L_2	**62**
Rat skin layer width	W_1	**60**
Fat layer width	W_1	**60**
Muscle layer width	W_1	**60**
Coating box width	W_2	**35**

The surrounding environment values of the antenna are tabulated in Table 7.1. The electrical parameters of the antenna environment are given in Table 7.2. The antenna is designed to fulfill the limitation of a small space allocated for antenna attachment on the RFID tag. In the design process, first, the antenna is encapsulated in a bio-compatible

material to isolate it from the tissue environment. Secondly, the coated antenna is placed in the muscle layer. Thirdly, the fat layer is placed on top of the coated antenna. Finally, rat skin is placed on top of the fat layer. The coated antenna is located at a position, equidistant from the side walls of the muscle layer.

Table 7.2: Electrical Parameters of Antenna Environment

Electrical parameters of antenna environment	Dielectric constant (ε_r)	Conductivity (σ)
Rat skin	**35 – 55**	**0.69**
Fat	**5.6**	**0.08**
Muscle	**58.8**	**0.84**
Coating	**3.9-4.7**	**0.001(tanδ)**

7.4 Parametric Study for Optimization

Simulations were performed by using commercial software (CST Microwave Design Studio) and numerical results are presented in this section. The thicknesses of the bio-compatible material (1.0mm) on the radiating patch of the antenna, the muscle layer (50mm) below the fat layer and fat layer (2mm) were fixed throughout the numerical calculations. When the skin permittivity of the rat is varied from 35 to 55, the optimum return loss is found at a resonance frequency of 920MHz and the bandwidth of the antenna at a10dB return loss is 15% (Fig. 7.2). If the relative permittivity of bio-compatible material is increased from 3.9 to 4.7, resonance frequency decreases gradually

(Fig. 7.3), but is well inside our band of interest (900MHz Australian ISM band). The bandwidth is still within 10% to 15% which covers desired bandwidth (~2%).

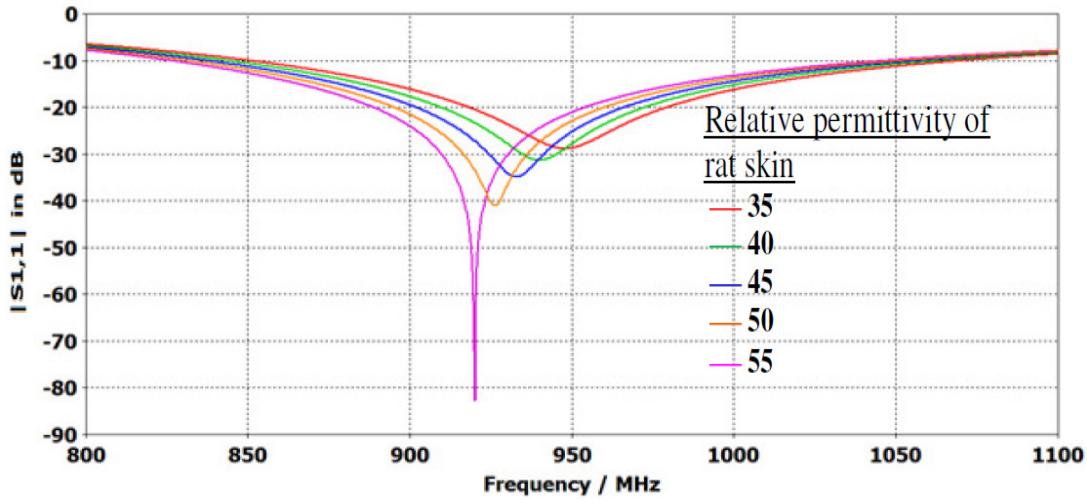

Fig. 7.2: Return loss of antenna with skin permittivity varied

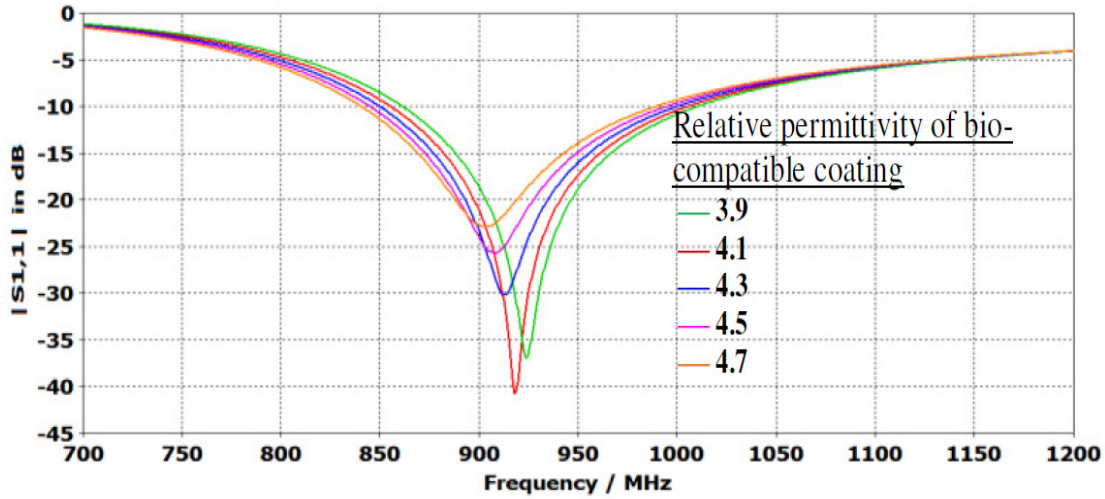

Fig. 7.3: Return loss when antenna and RFID tag's grounds are connected and permittivity of bi-compatible coating is varied (3.9-4.7)

The return loss of the antenna when its ground plane is not connected to RFID tag's ground plane and permittivity of bi-compatible material is varied between 3.9 and 4.4 is shown in Fig. 7.4. The antenna is not matched well when RFID tag's ground is not connected to the antenna ground.

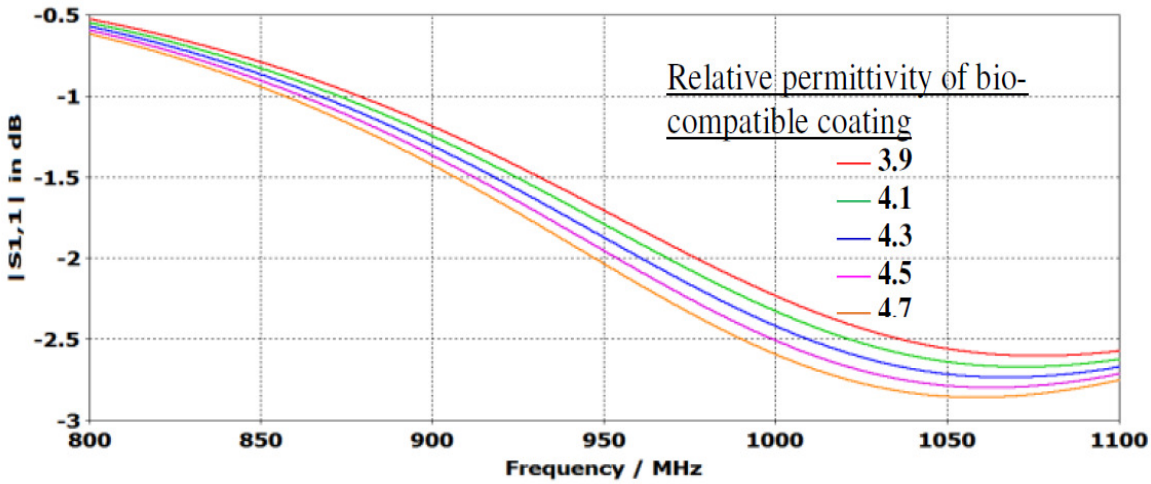

Fig. 7.4: Return loss when antenna and RFID tag's grounds are not connected and permittivity of coating is varied (3.9-4.7)

7.5 Implantable Antenna Fabrication

In order to validate the simulated results with measurements, three different multi-layered implantable PIFAs were fabricated. The first prototype of the implantable PIFA is shown in Fig. 7.5 and its overall dimensions are 30mm×13mm×3.2mm. The antenna is fabricated on a FR4 board substrate (dielectric constant = 4.3, loss tangent = 0.025). The U-shaped radiating patch dimensions are 9.5mm×8mm as shown in Fig. 7.5(a). A tuning slot is cut along the central line of the length and the optimised dimensions of the slot are 7.5mm×1mm. Fig. 7.5(b) shows the dimensions (30mm×13mm) of the ground plane of the antenna.

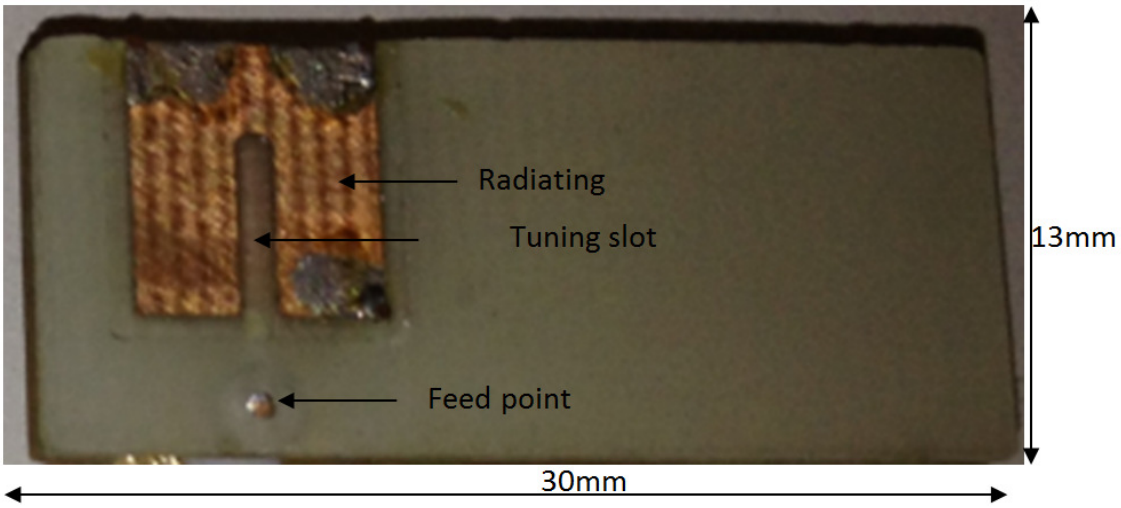

(a)

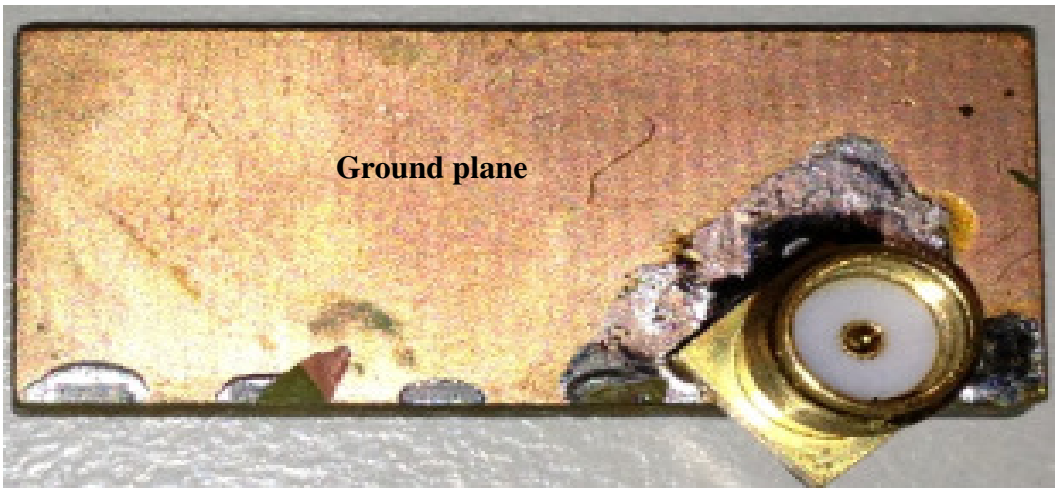

(b)

Fig. 7.5: First prototype of implantable PIFA antenna: (a) Radiating patch side (b) Ground plane side

The second prototype of the implantable PIFA is shown in Fig. 7.6 and its overall dimensions are 13mm×10mm×3.2mm. The antenna is fabricated on a FR4 board substrate (dielectric constant = 4.3, loss tangent = 0.025). The U-shaped radiating patch dimensions are 9.25mm×8.0mm as shown in Fig. 6(a). A tuning slot is cut along the

central line of the length and the optimized dimensions of the slot are 7.25mm×1mm. Fig. 7.6(b) shows the dimensions (9.5mm×9.5mm) of ground plane of the antenna.

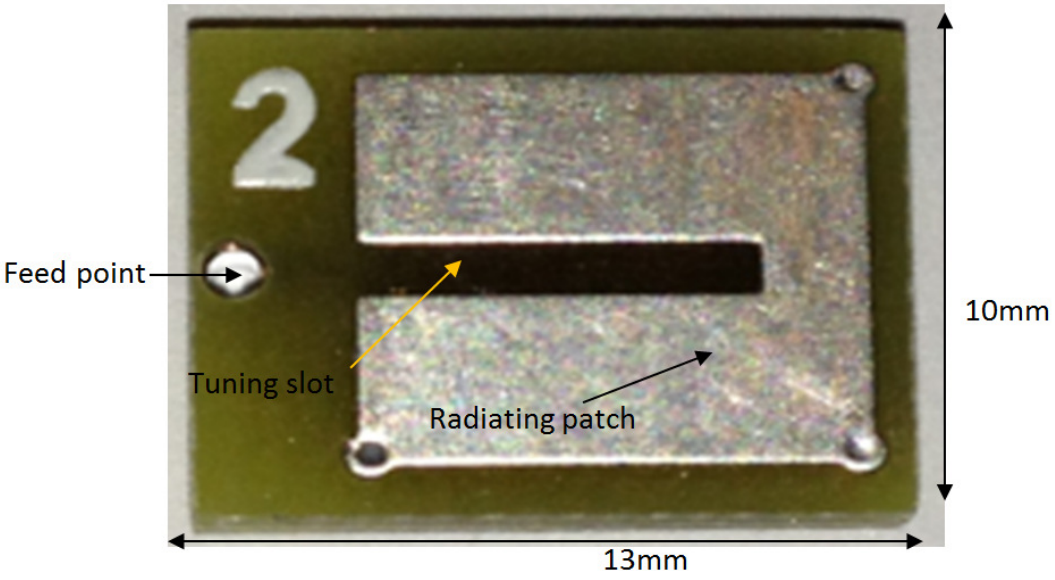

(a)

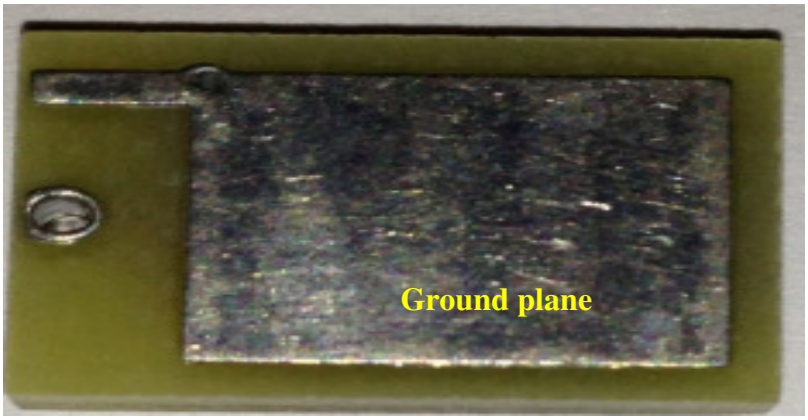

(b)

Fig. 7.6: Second prototype of implantable PIFA antenna: (a) Radiating patch side and (b) Ground plane side

The third prototype of the implantable PIFA is shown in Fig. 7.7 and its overall dimensions are 19.5mm×10mm×3.2mm. The antenna is fabricated on a FR4 board

substrate (dielectric constant = 4.3, loss tangent = 0.025). The J-shaped radiating patch dimensions are 19mm×8mm as shown in Fig. 7.7(a). A tuning slot is cut along the central line of the length and the optimised dimensions of the slot are 8.25mm×1mm. Fig. 7.7(b) shows the dimensions (9.5mm×9.5mm) of the ground plane of the antenna. The third prototype is an improved version of the second prototype in terms of retuning. One end of the U-shaped patch is extended to retune the antenna for Australian UHF ISM band. This extension makes the radiating patch a J-shaped structure.

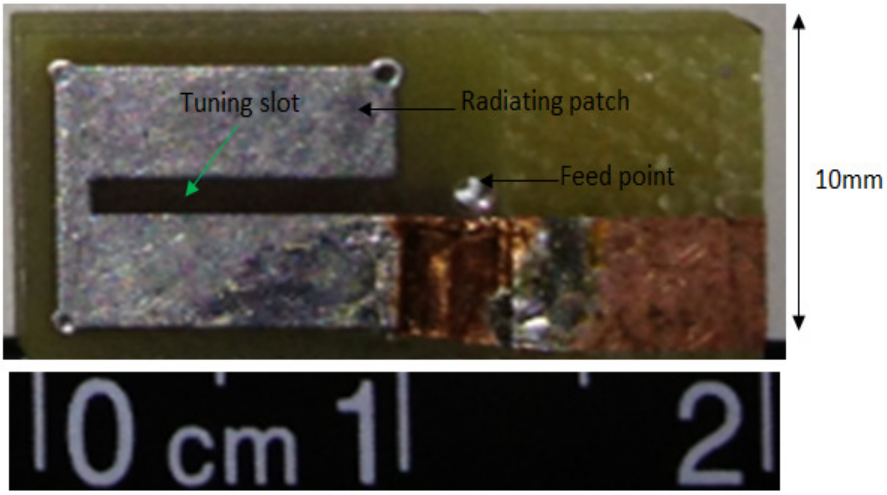

(a)

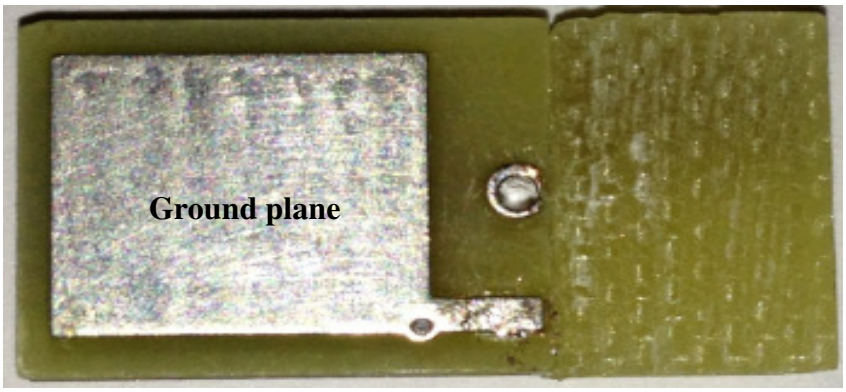

(b)

Fig. 7.7: Third prototype of implantable PIFA antenna: (a) Radiating patch side (b) Ground plane side

7.6 Experimental Setup and Measurement

To understand the surrounding environment of the S_{11} measurement setup, a photograph of the measurement laboratory is shown in Fig. 7.8. The experimental setup for input reflection coefficient measurement of the implantable PIFA is shown in Fig. 7.9. A Vector Network Analyzer (VNA) (HP 8720D) was used to measure the return loss (S_{11}) of the antenna. Firstly, calibration of the VNA is performed from 200MHz to 5000MHz to minimize the error in the measurements and then a S_{11} measurement is recorded. The S_{11} measurement was conducted in a typical laboratory environment instead of an anechoic chamber to avoid complexity. However, for radiation pattern measurements, an anechoic chamber was used. The measurement laboratory size is approximately 10m×10m×4m with brick walls and concrete floor. The measurement laboratory is located on the first floor of an L-shaped (brick-walled) 3-storied building. Some computers, oscilloscopes, signal generators, DC power supplies, VNAs etc. were in this measurement laboratory. The $|S_{11}|$ measurements of the antenna were performed in free space and then with the antenna covered by rat skin. However, before covering the antenna with rat skin, it was coated with bio-compatible material and placed on a typical foam plate as shown in Fig. 7.10. The experimental setup used to measure the radiation pattern (second prototype of implantable antenna) in the anechoic chamber in free space is shown in Fig. 7.11. The second prototype of the implantable antenna was coated with a biocompatible material, Sylgard (dielectric constant =2.7). Therefore, the radiation pattern measurement results shown in Fig. 7.18 represent the radiation of the coated implantable antenna (2^{nd} prototype) with no rat skin.

Fig. 7.8: Measurement laboratory in which $|S_{11}|$ of the antenna was measured

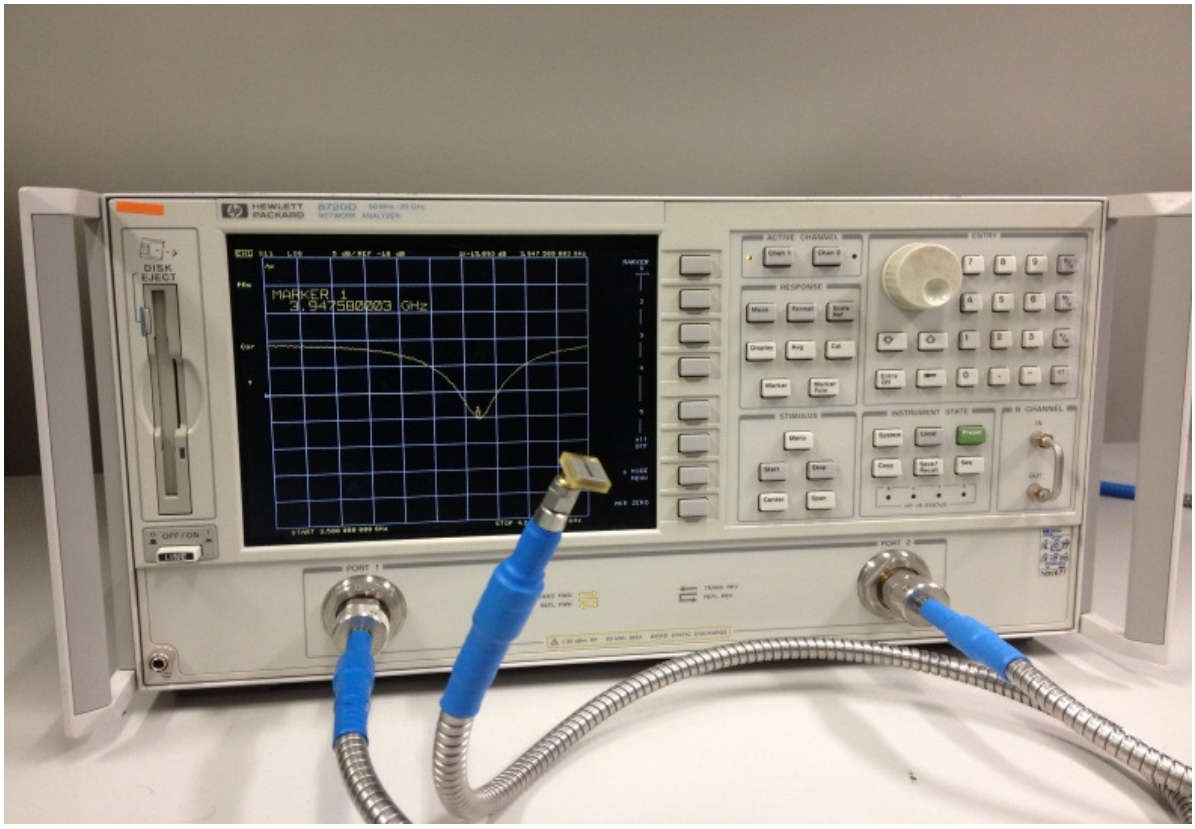

Fig. 7.9: Experimental setup to measure $|S_{11}|$ in free space

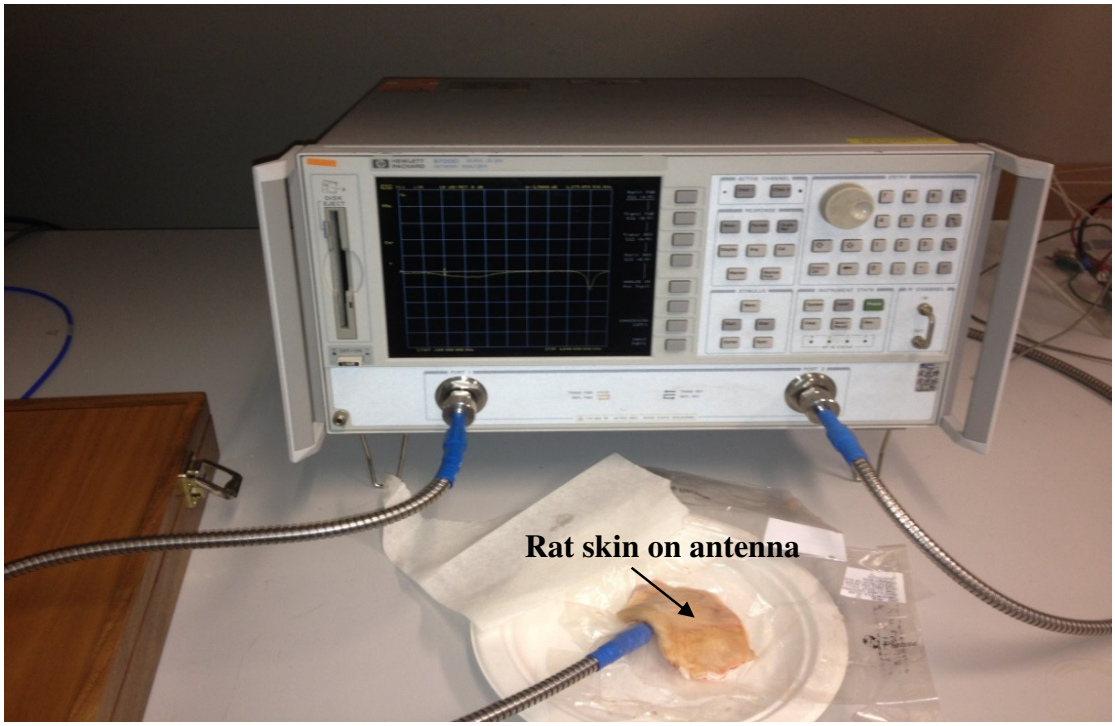

Fig. 7.10: Experimental setup to measure $|S_{11}|$ with rat skin

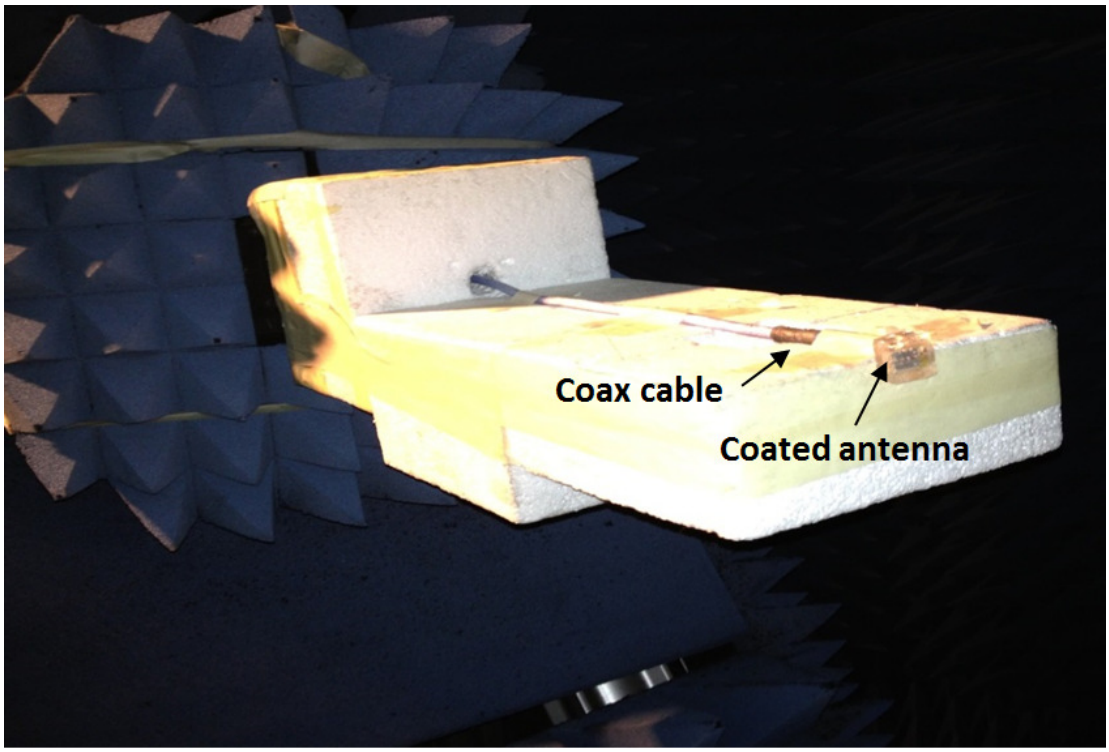

Fig. 7.11: Experimental setup to measure radiation pattern of coated implantable PIFA (2^{nd} prototype) in anechoic chamber (without rat skin)

In Fig. 7.12, predicted and measured $|S_{11}|$ are plotted when the antenna (1st and 2nd prototypes) is operating in free space. The second antenna prototype provides better performance since its ground is larger than the first prototype. The predicted and measured results of the first prototype do not agree at all. The difference in resonance frequency between the predicted and measured results is probably due to the fabrication error since manual fabrication process was applied in a local workshop. The resonance frequencies of the second antenna prototype are almost identical for predicted and measured results in free space, at about 3.94GHz, as shown in Fig. 7.12(b). Excellent agreement between the predicted and measured $|S_{11}|$ was obtained for this prototype that was carefully fabricated by an external workshop. The antenna was then coated with a readily available bio-compatible material (Sylgard 184, dielectric constant = 2.7) and placed under the skin of a rat. Fig. 7.13 shows the predicted and measured $|S_{11}|$ results when the coated antenna was covered by rat skin. Under rat skin, the measured $|S_{11}|$ is -9dB at 1250MHz while the predicted $|S_{11}|$ is just -2dB when the antenna is coated with Sylgard 184. Note that this antenna was originally designed to be coated with a higher permittivity biocompatible material. As shown by the blue curve in Fig. 7.13, its resonance frequency shifts down to the Australian UHF ISM band if the dielectric constant of the bio-compatible material is increased to 3.9. It is also seen that input reflection co-efficient of the antenna is improved to -23dB with the Sylgard's dielectric constant of 3.9. However, it was not possible to find such biocompatible material commercially.

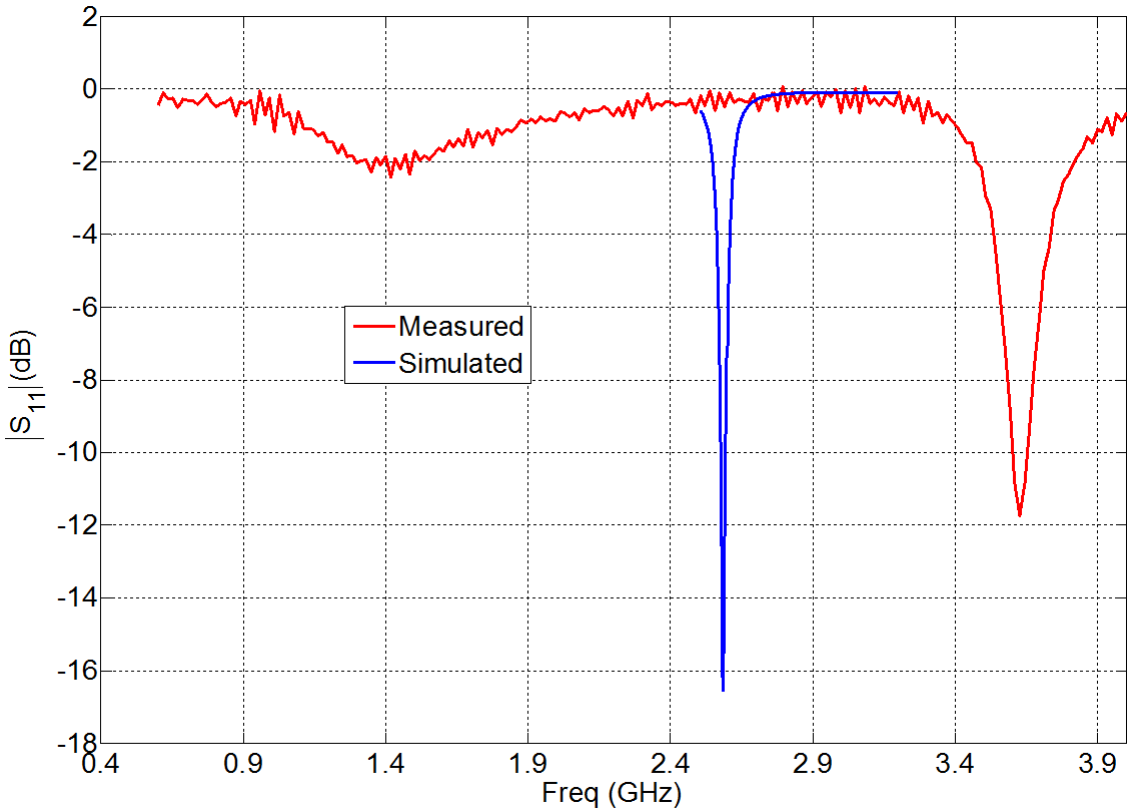

(a)

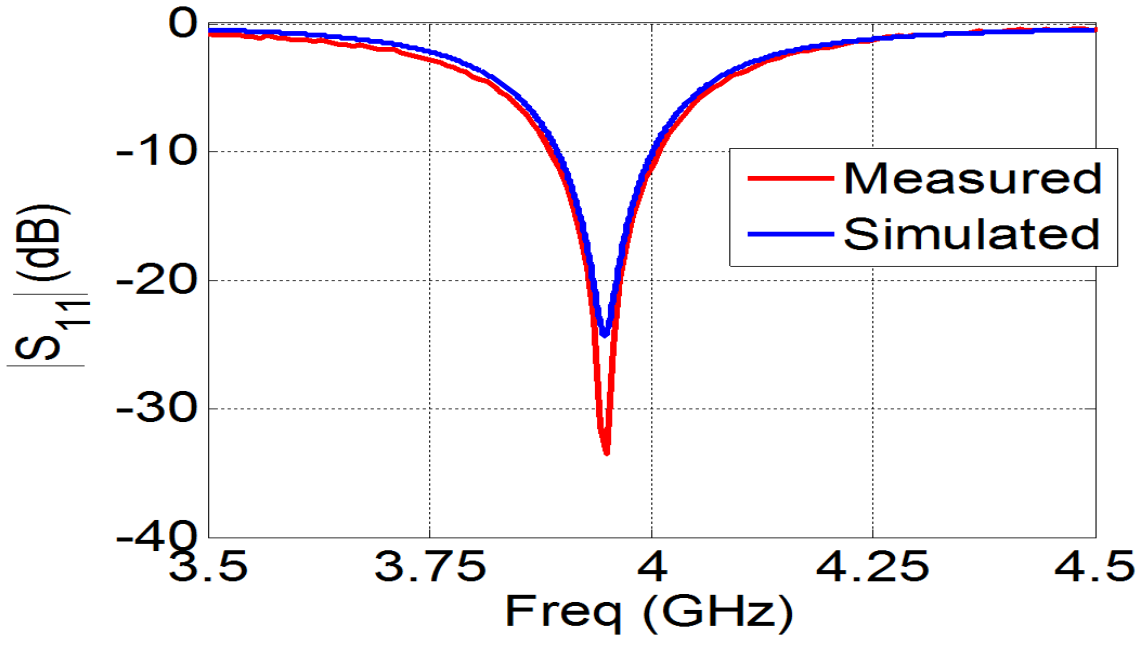

(b)

Fig. 7.12: Predicted and measured $|S_{11}|$ of fabricated PIFAs in free space: (a) Predicated and measured $|S_{11}|$ of 1st prototype and (b) Predicted and measured $|S_{11}|$ of 2nd prototype

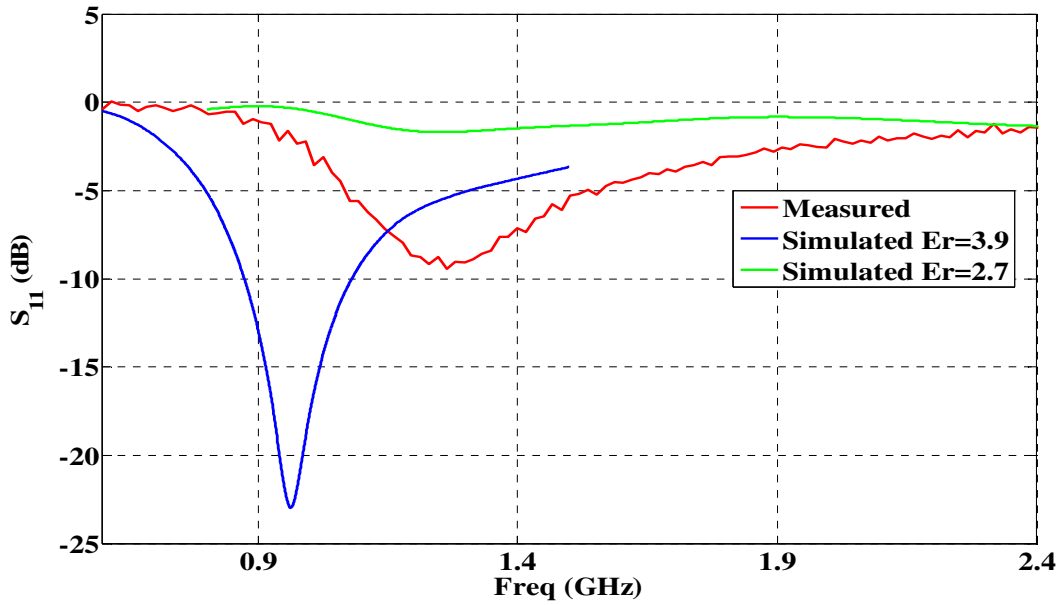

Fig. 7.13: Simulated and measured $|S_{11}|$ of fabricated PIFA when covered by rat skin (2^{nd} prototype)

The measured $|S_{11}|$ of the antenna 2^{nd} prototype suggests that the resonance frequency needs to be shifted down from 1250MHz to the UHF Australian ISM band (915-928MHz) for the operation of an implantable RF device. For this purpose, the easiest way to shift the resonance frequency down is to increase the length of the top radiating patch. The parametric study on the radiating patch length was conducted and the optimised value of the increased length was found to be 9.75mm. The third prototype of the implantable PIFA was fabricated and coated with a readily available bio-compatible material (MED 1134, dielectric constant = 2.8). The measured $|S_{11}|$ of the antenna in free space and in rat skin are shown in Fig. 7.14. They are found to be -7.5dB at 2.6GHz and -13dB at 920MHz, respectively. In this instance, the resonance frequency is within the Australian UHF ISM band. The bandwidth of the antenna at a10dB return loss is 120MHz (850-970MHz) or 13%, entirely covering the required UHF band of interest (1.5%) as shown in Fig. 7.15. The predicted and measured $|S_{11}|$ of the coated implantable PIFA

antenna (3rd prototype) is shown in Fig. 7.16. Predicted $|S_{11}|$ is in reasonable agreement with the measured result. However, the predicted bandwidth is larger (200MHz) than the measured one (120MHz) and the minimum value of $|S_{11}|$ is -14dB at 961MHz.

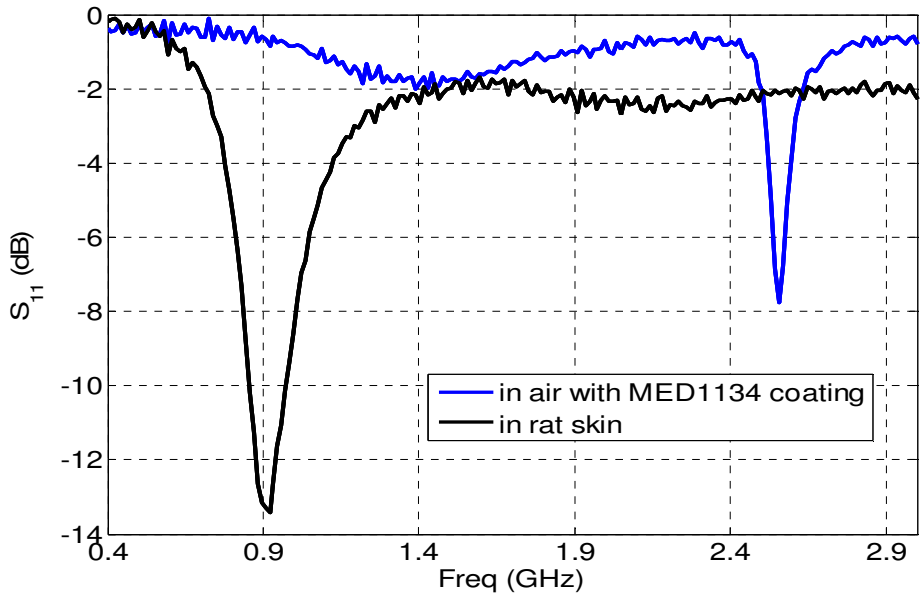

Fig. 7.14: Measured $|S_{11}|$ of modified antenna (3rd prototype) with MED 1134 biocompatible coating

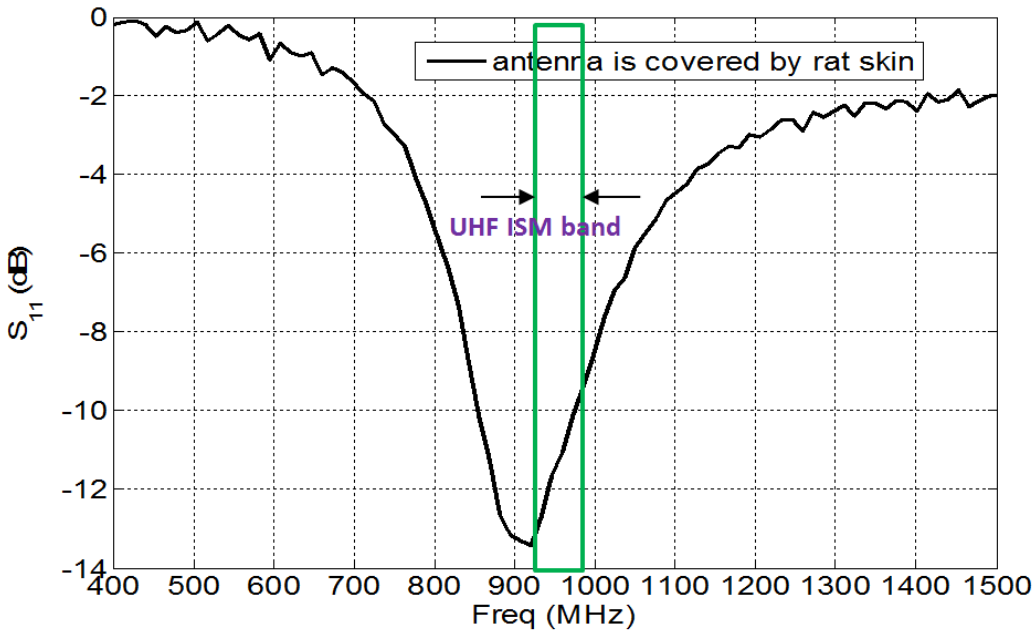

Fig. 7.15: Measured $|S_{11}|$ of modified coated antenna (3rd prototype) in rat skin

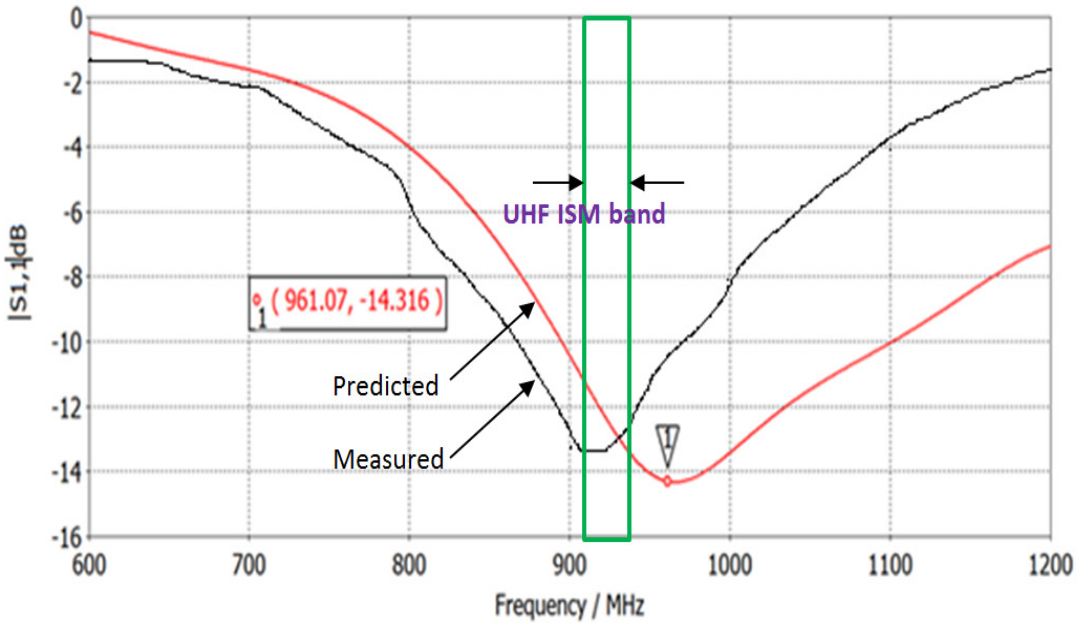

Fig. 7.16: Predicted and measured $|S_{11}|$of modified coated antenna (3rd prototype) in rat skin

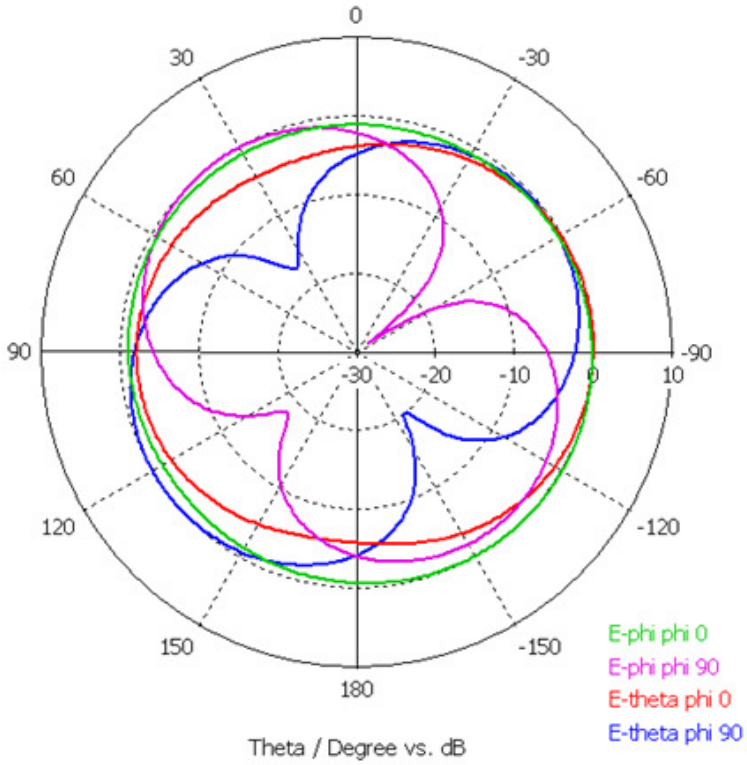

Fig. 7.17: Predicted radiation patterns in free space at 3.8 GHz (2nd prototype) with no rat skin. This is done to the antenna resonance frequency

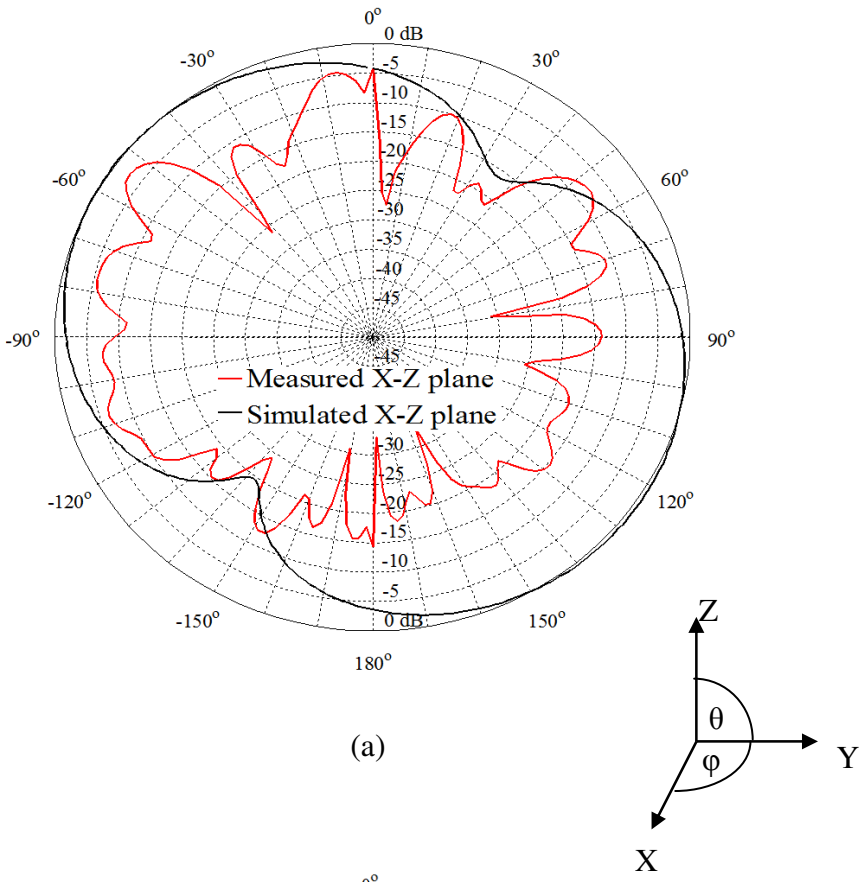

(a)

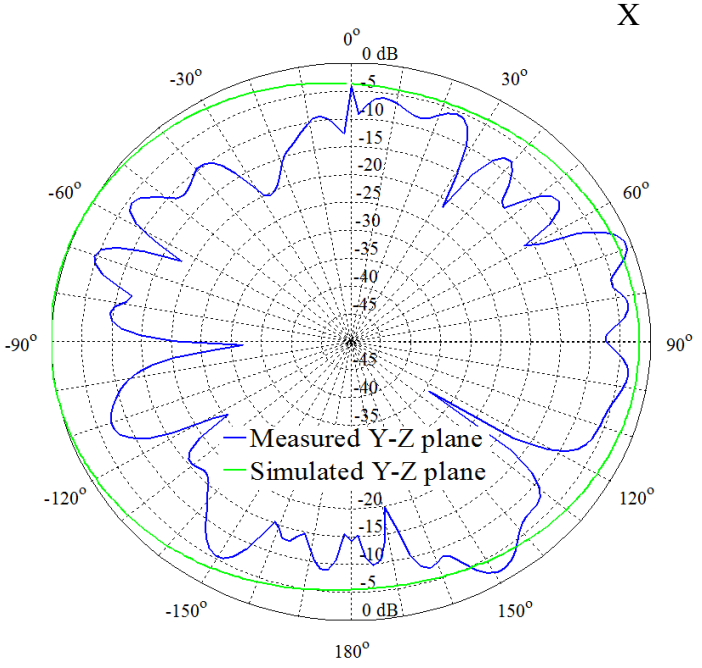

(b)

Fig. 7.18: Predicted and measured radiation patterns of the coated antenna (2^{nd} prototype) in free space at 3.8 GHz with no rat skin: (a) On $\varphi = 0^0$ plane and (b) On $\varphi = 90^0$ plane

The predicted radiation patterns in free space of the antenna (2^{nd} prototype) are shown in Fig. 7.17. The E_θ pattern on $\varphi = 0^0$ plane is almost omnidirectional as indicated by the green curve. On $\varphi = 90^0$ plane, the radiation (pink curve) is different and a null point is found at an angle of $\theta = -60^0$. Radiation patterns on $\theta = 0^0$ and $\theta = 90^0$ planes are also presented in Fig. 7.17. Predicted and measured results are compared in Fig. 18.

7.7 Read Range Measurement of Medical Data in the RFID Link

The coated implantable antenna was attached to the RFID tag PCB as shown in Fig. 7.19 as connected to RFID chip. The locations of the RF chip and the temperature sensor are indicated in the same figure. One of the challenges with this RFID tag is to appropriately connect the antenna ports with the signal and ground pads of the RF chip. The antenna has been designed and fabricated to meet this stringent requirement. In Fig. 7.20, the locations of the RF chip, the RF signal pad and the RF ground pad are shown on the RFID tag PCB layout. Fig. 7.21shows experimental setup for a RF link read range measurement of the system. A built-in temperature sensor is available on the RFID tag PCB and the inner side of the rat skin is placed on the temperature sensor. The RFID reader was connected to a laptop through a USB port as shown in Fig. 7.21, to monitor the temperature reading.

The experiment recorded the temperature reading as well as the absence or presence of the RFID tag in the range of the RFID reader. The RFID tag with the rat skin on top was placed at different locations around the RFID reader and “RFID tag found” or “RFID tag not found” messages were recorded in the laptop. When the RFID tag was found to be in the range of the RFID reader, temperature data stored in flash memory was transferred to the RFID reader and displayed by the laptop. One of the temperature readings is shown

in Fig. 7.22. A contour of read range is plotted and is illustrated in Fig. 7.23. The maximum read range of the RFID tag was found to be 0.8m. It is worth recalling that with the original commercial antenna, it was totally impossible to make any temperature reading when a rat skin is placed on the tag. This read range measurement ensures that our system prototype is functional in the Australian UHF ISM band. The RFID reader uses a UHF monopole antenna as shown in the system experimental setup (Fig. 7.21). The maximum temperature recorded by the proposed RFID system prototype was 25^0 C as shown in Fig. 7.22. The rat skin sample was stored in a refrigerator at Australian School of Advanced Medicine of our Macquarie University, Australia. The measurement was conducted within 15-30min after the collection of rat skin sample. Due to this reason, rat skin sample was cold and temperature sensor showed a sudden decrease of temperature reading. The RFID tag used in the communication read range measurement was an active tag since it takes its power supply from a button battery as shown in Fig. 7.19. Unlike a passive RFID tag an active RFID tag does not need a very strong signal from the RFID reader to power up the tag. However, in an active RFID tag, the battery needs to be replaced periodically and the tag is typically larger than a passive RFID tag.

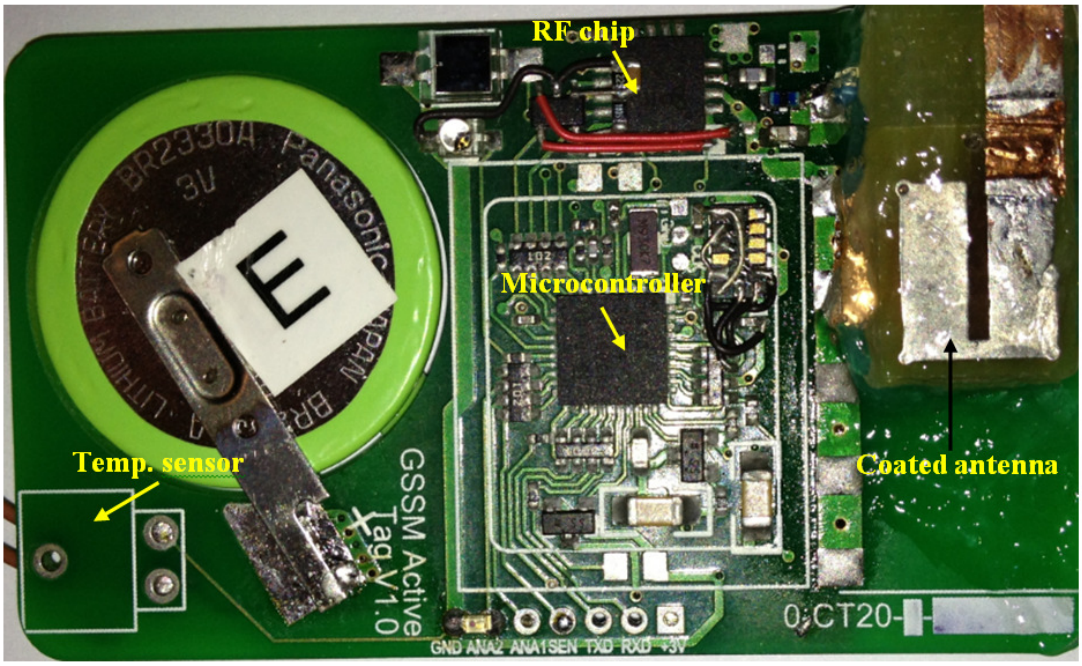

Fig. 7.19: Attachment of coated antenna (3rd prototype) to the RFID tag PCB

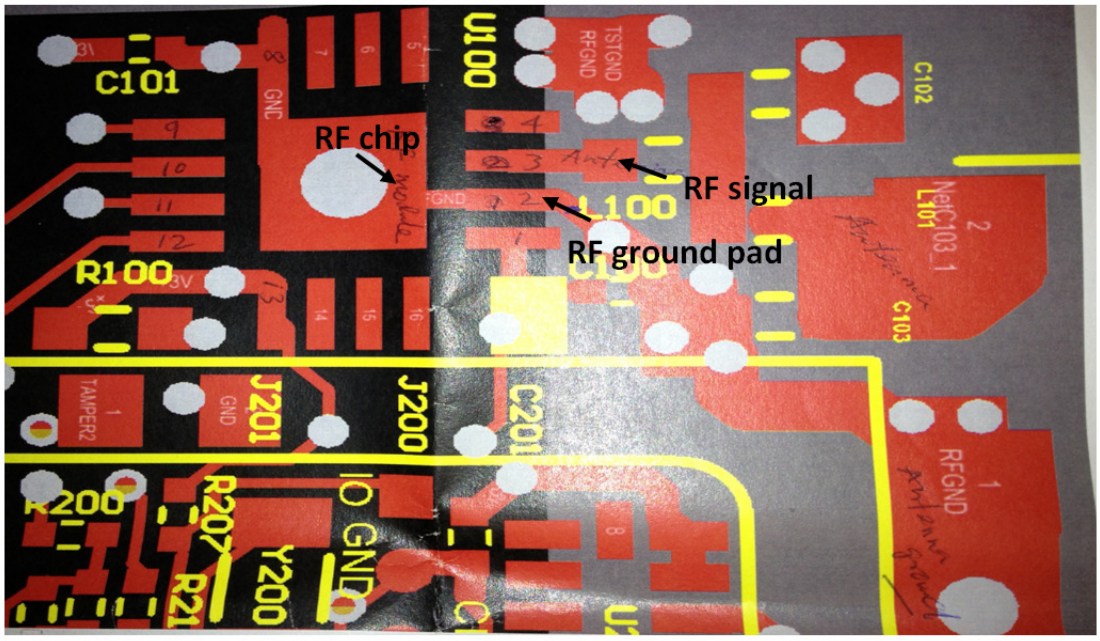

Fig. 7.20: Locations of the signal and ground pads of the RF chip on the RFID tag PCB

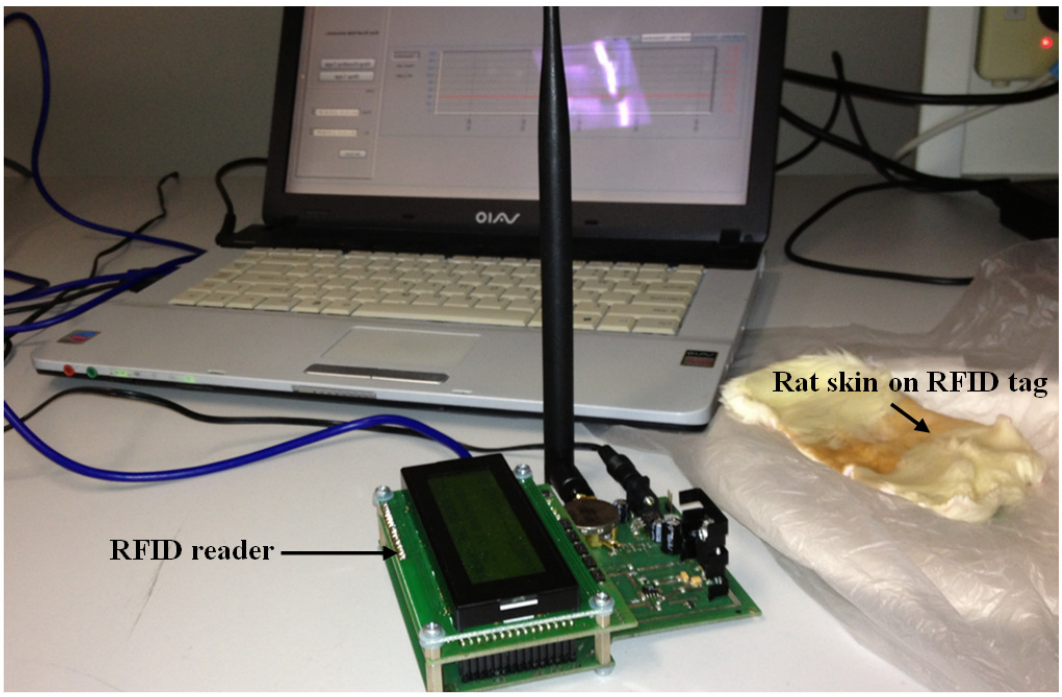

Fig. 7.21: Experimental setup for RF link read range measurement of the system

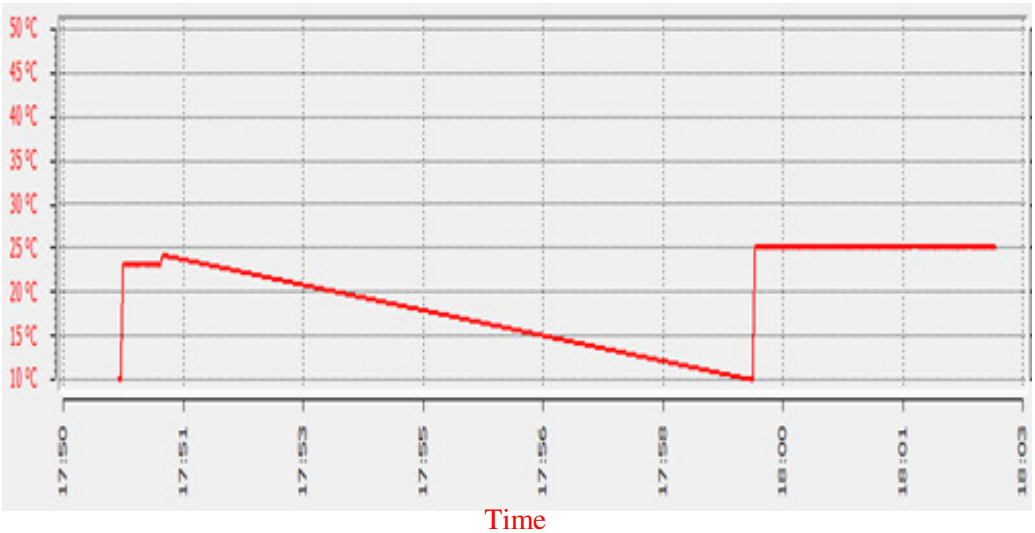

Fig. 7.22: Temperature reading of the implantable RFID system

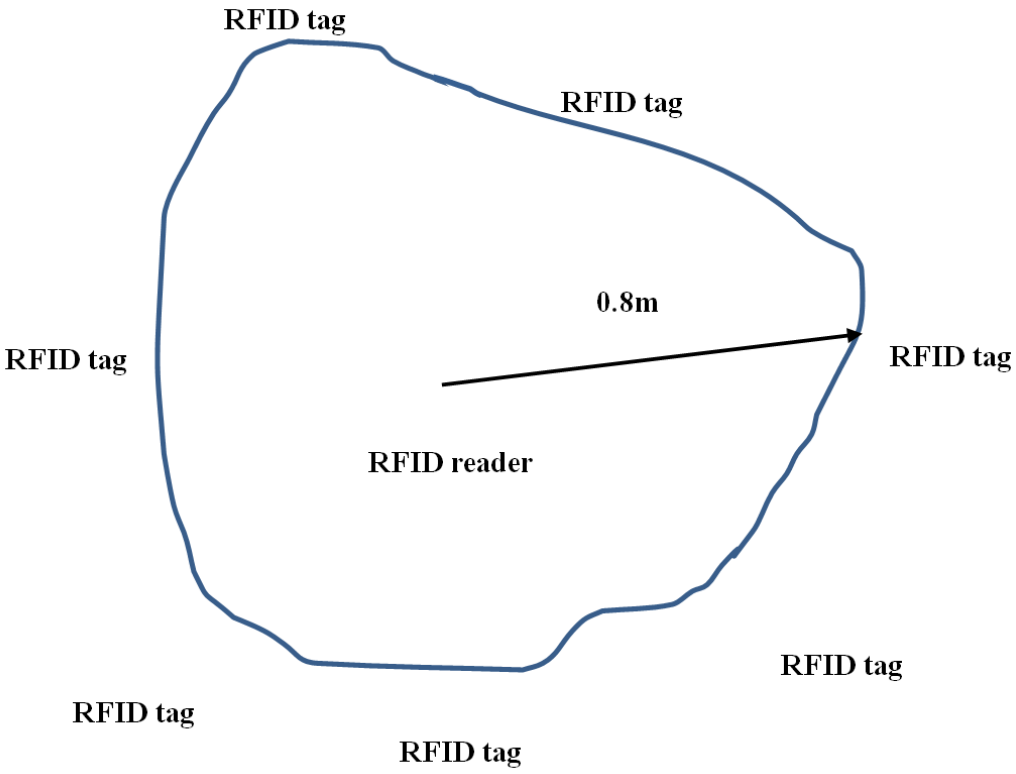

Fig. 7.23: Read range of the RFID system in the horizontal plane

7.8 Conclusion

A miniaturised implantable PIFA with a proximity feed technique was designed, fabricated, attached with an RFID tag and validated its reading range in the Australian UHF ISM band when placed under the skin of a rat. A measured bandwidth of 15% was obtained which covers the entire Australian UHF ISM band. The sensitivity of the antenna was verified by computer simulation, changing the thickness of rat skin on top of the bio-compatible material and it was found that the resonance frequency of the antenna was very stable. The designed miniature antenna was fabricated locally (initial prototype) and $|S_{11}|$ was measured but it failed to resonate in the desired Australian UHF ISM band once placed under the rat skin. This led us to develop an improved version of the implantable antenna (third antenna prototype coated with a biocompatible material, MED

1134). In this instance, measured and predicted results were in good agreement and the RFID system became operational in the UHF ISM band when the tag was placed under the rat skin. Muscle tissue of rat has negligible effect on the implantable antenna performance compared to biocompatible coating material and rat skin tissue. Hence, muscle tissue was not included in the measurement. Detuning of the resonance frequency of the antenna was observed using numerical simulations by varying the permittivity of the bio-compatible material (MED 1134) and it was never out of the desired ISM band. The bandwidth of the final prototype of the antenna is 15% when it is placed under the skin of a rat.

Chapter 8

Conclusion and Future Work

8.1 Conclusion

The designs and implementations of compact implantable PIFAs have been investigated with a focus on bio-telemetry applications. Firstly, effect of rat skin on the resonance frequency of a commercial antenna at MICS band was studied. The MS-fed and the CPW-fed antennas were tested and a 15%-20% decrease of resonance frequency was found for both feed configurations. These results suggest that, in order to maintain an efficient wireless link, the implantable antenna must be designed with the consideration of biological tissues surrounding the antenna. Slight resonance frequency shifting was observed due to aging effects of rat skin. The transmitted power (S_{21}) measurement confirmed that a large decrease in the resonance frequency may occur when the antenna is covered by fresh rat skin samples. In Chapter 4, a miniaturized subcutaneous partially-folded planar inverted-F antenna (PF-PIFA) was proposed for the wireless physiological data acquisition system to be operated in the Australian 900MHz ISM band (915-928MHz). The overall size of the antenna was $26\times19\times4.4mm^3$ and it was designed to be implanted just under the skin of a rat. The 10dB return-loss bandwidth of the antenna was 2.8% and it covered the Australian UHF ISM band.

Later, even smaller PIFAs were designed and antenna parameters were optimised through computer simulations when investigating the PIFA Design 1 in Chapter 5. It was found that potential variations in rat tissue did not produce a significant effect on antenna

matching and bandwidth. The antenna return loss was more sensitive to some antenna dimensional parameters and dielectric constant; the thickness of biocompatible coating material. Significant variations were observed when the dielectric constants of the substrate and the biocompatible coating were varied in a wide range. Lesser variations were found with the patch slot length and capacitive load plate length. The 10dB return-loss bandwidth of the PIFA Design 1 was predicted to be 8.5%. In Antenna Design 2, parameters of an implantable Hilbert PIFA were varied and the antenna performance was analyzed in rat tissue environment. Resonance frequency of the Antenna Design 2 was detuned due to the biocompatible coating around the antenna. The effect of the attachment of the antenna ground to the RFID tag PCB ground was studied. It was noticed that for better impedance matching the two grounds must be connected together. A 10dB return-loss bandwidth of ~3% (915-918MHz) was predicted. In Antenna Design 3, a J-shaped proximity feed PIFA was considered and the key antenna parameters were investigated. Despite the compactness of the antenna the optimised impedance bandwidth was greater than 5% (885-935MHz). The maximum radiation of the Antenna 3 was outwards through the rat skin and therefore it minimised the absorption loss in biological tissue.

All those antennas were designed for the space available on the RF chip side of the RFID tag PCB. In Chapter 6, the use of the space on the ground plane side of the tag PCB was considered and a compact PIFA antenna was designed for that purpose. It was observed that the bandwidth increased when the ground plane of antenna was connected to the ground plane of the RFID tag, leaving an optimized slot between two ground planes. The directivity of the antenna also improved when they are connected so. Thus,

the ground plane of the RFID tag was utilised to enhance the performance of the implantable antennas.

Finally, a miniaturized implantable PIFA antenna was designed with proximity feed technique. It had a much larger bandwidth of 15%, which covered the entire Australian UHF ISM band around 900MHz centre frequency. The sensitivity of the resonance frequency was assessed by changing the thickness of rat skin and found that the coated antenna was very stable. However, it failed to resonate in the desired UHF ISM band after implantation under the rat skin. This led to the development of an improved version for retuning the implantable antenna (final antenna prototype, coated with a biocompatible material, MED 1134). In this instance, measured and predicted results well matched and RFID system became operational at UHF ISM band. Sensitivity of resonance frequency of the antenna was monitored by varying the permittivity of bio-compatible (MED 1134) material and the antenna was always operating in the desired ISM band. This was validated by taking temperature reading between the RFID tag and RFID reader of the bio-telemetry system.

8.2 Opportunities for Future Research

The author realised that the outcome of the thesis has opened up some future research opportunities related to implantable antennas for RFID medical telemetry applications. Therefore, following directions research could be carried out in future for further advancement of the research on bio-telemetry applications.

- The RFID tag PCB utilised in this research has been designed and manufactured by the industry partner, considering free space communication and, therefore, it is

larger compared to the size of a rat or mouse. The tag may be re-designed to reduce its size leaving at least the same space for implantable antenna.

- RF bio-telemetry system validation showed that the maximum link coverage was 0.8m and this wireless medical data reading range can be improved further.

- It is also recommended that the implantable antenna with the RFID tag PCB should be validated in freely moving experimental rats for the bio-telemetry system. This will help to identify the variations between in vitro and in vivo measurements.

- An area of approximately 20mm×33mm is dedicated for the button battery used in the implantable RFID-tag PCB (60mm×33mm) which is one-third of the PCB size and therefore larger compared to the size of the RFID-tag. Energy harvesting possibility or smaller battery may be investigated for the RFID tag power supply. Alternatively, Power may be supplied to the RFID-tag by inductive coupling method.

- The RFID tag may be designed with a few sensors for multichannel physiological data transmission such as ECG, blood pressure, nerve activity to external base station. Even, single channel can be designed for the implantable RFID tag with multiplexing and demultiplexing technique to transmit multiple physiological signals from the body of animals.

Bibliography

[1] G.A.E. Vandenbosch and A.R. Van de Capelle, “Study of the capacitively fed microstrip antenna element”, IEEE Trans. Ant Prop., vol. 42, pp. 1648-1652, Dec. 1994.

[2] M. J. Alexander, “Capacitive matching of microstrip patch antennas,” in Proc. Inst. Elect. Eng., vol. 136, pt. H, no. 2, pp. 172-174, 1989.

[3] G. A. E. Vandenbosch, “Capacitive matching of microstrip antennas,” Electron. Lett., vol. 31, no. 18, pp. 1535-1536, 1995.

[4] K. Kagoshima, K. Tsunekawa, and A. Ando, “Analysis of a planar inverted F antenna fed by electromagnetic coupling,” Proc. of the Antennas and Propagation Society International Symposium(APSIS), Chicago,, Jul. 20-24, vol. 3, pp. 1702-1705, 1992.

[5] Suarez-Fajardo, J.O. Gomez-Sara and M. Ferrando-Bataller, “Broadband PIFA with Capacitive Feed,” Proc. Antenna and Propagation Society International Symposium, APSURSI ‘09, pp. 1- 4, 2009.

[6] T. Karacolak, R. Cooper, and E. Topsakal, “Electrical Properties of Rat Skin and Design of Implantable Antennas for Medical Wireless Telemetry,” IEEE Trans. Ant. Prop., vol. 57, no. 9, Sep. 2009.

[7] P. Cong, Wen H. Ko, and Darrin J. Young, “Wireless Batteryless Implantable Blood Pressure Monitoring Microsystem for Small Laboratory Animals,” IEEE Sensors J., vol. 10, no. 2, February 2010.

[8] M. S. Islam, K.P. Esselle, D. Bull, and P.M. Pilowsky, “Design of an Implantable Antenna to Acquire Physiological Signals in Rats,” Proc. IEEE Int’l. Symp. Antennas Propag., Chicago, IL, USA, July, 2012.

[9] S. R. Best and J. D. Morrow, “The effectiveness of space-filling fractal geometry in lowering resonant frequency,” IEEE Antennas Wireless Propag. Lett, vol. 1, pp.112–115, 2002.

[10] X. Chen, S. S. Naeini, and Y. Liu, “A down sized printed Hilbert antenna for UHF band,” Proc. IEEE Antennas and Propagation Society Int. Symp., vol. 2, pp. 581–584, Columbus, OH, 2003.

[11] V. T. Bai and S.K. Srivastaa, “Design and Simulation of Portable Telemedicine System for High Risk Cardiac Patients,” Proc. of World Academy of Science and Technology, vol. no. 18, Dec. 2006.

[12] C.M. Lee, T.-C. Yo, C.-H. Luo, C.-H. Tu and Y.-Z. Juang, ”Compact broadband stacked implantable antenna for biotelemetry with medical devices,” Electronics Letters, vol. 43, no. 12, 7th June 2007.

[13] T. Karacolak, R. Cooper, J. Butlar, S. Fisher and E. Topsakal, “In Vivo Verification of Implantable Antennas Using Rats as Model Animals,” IEEE Antennas and Wireless Propagation Letters, pp. 33-337 ,vol. 9, 2010.

[14] D.W. Ryoo, Y.S. Kim and J.W. Lee, “Wearable Systems for Service based on Physiological Signals,” Proc. IEEE Engineering in Medicine and Biology, Sept. 1-4, 2005.

[15] F.-J. Huang, C.-M. Lee, C.-L. Chang, L.-K. Chen, T.-C. Yo and C.-H. Luo, “Rectenna Application of Miniaturized Implantable Antenna Design for Triple-Band Biotelemetry Communication,” IEEE Trans. Antennas Propag., vol. 59, no. 7, Jul. 2011.

[16] M. S. Islam, K.P. Esselle, D. Bull, and P.M. Pilowsky, “A miniaturized implantable PIFA antenna for indoor wireless telemetry,” Proc. Int’l Conference on Electromagnetics in Advanced Applications, pp. 526-530, Cape Town, South Africa, Sept. 2012.

[17] M. S. Islam, K.P. Esselle, D. Bull, and P.M. Pilowsky, “Bandwidth enhancement of an implantable RFID tag antenna at 900 MHz ISM band for RF telemetry,” Proc. Int’l Symposium on Communications and Information Technologies, Gold Coast, Australia, Oct. 2012.

[18] L. Xu and M. Q.-H. Meng, "Effects of dielectric parameters of human body on radiation characteristics of ingestible wireless device at operating frequency of 430 MHz," IEEE Trans. Biomed. Eng., vol. 56, no. 8, pp. 2083–2094, Aug. 2009.

[19] T. Karacolak, A. Z. Hood, and E. Topsakal, "Design of a dual-band implantable antenna and development of skin mimicking gels for continuous glucose monitoring," IEEE Trans. Microw. Theory Tech., vol. 56, no. 4, pp. 1001–1008, Apr. 2008.

[20] J. Kim and Y. Rahmat-Samii, "Implanted antennas inside a human body: Simulations, designs and characterizations," IEEE Trans. Microw. Theory Tech., vol. 52, no. 8, pp. 1934–1943, Aug. 2005.

[21] R. Warty, M.-R. Tofighi, U. Kawoos, and A. Rosen, "Characterization of implantable antennas for intracranial pressure monitoring: Reflection by and transmission through a scalp phantom," IEEE Trans. Microw. Theory Tech., vol. 56, no. 10, pp. 2366–2376, Oct. 2008.

[22] A. Kiourti, M. Christopoulou, and K. S. Nikita, "Performance of a novel miniature antenna implanted in the human head for wireless biotelemetry," in Proc. IEEE Int. Symp. Antennas Propag, pp. 392–395, Spokane, WA, USA, July 2011.

[23] T. Dissanayake, K. P. Esselle, and Mehmet R. Yuce, "Dielectric Loaded Impedance Matching for Wideband Implanted Antennas," IEEE Trans. Microw. Theory Tech., vol. 57, no. 10, pp. 2480-2487 Oct. 2009.

[24] www.cochlear.com [Last Accessed : October 2013]

[25] ERC recommendation 70-3 relating to short range devices (SRD) in EUR. Postal Telecommunication Administrative Conf. Norway, CERPT/ERC 70-3, Annex 12, 1997.

[26] M.S. Zadeah, "Implantable Loop Antenna", M. App. Sc. thesis, Simon Fraser University, 2006.

[27] S. Curto, P. McEvoy, X. Bao and M. J. Ammann, "Compact Patch Antenna for Electromagnetic Interaction With Human Tissue at 434 MHz," IEEE Trans. Antennas Propag., vol. 57, no. 9, September 2009.

[28] T. Houzen , M. Takahashi, K. Saito and K. Ito, "Implanted Planar Inverted F-Antenna for Cardiac Pacemaker System," Proceedings of iWAT2008, Chiba, Japan, 2008.

[29] H. Lin, M. Takahashi, K. Saito, and K. Ito, ”Performance of Implantable Folded Dipole Antenna for In-Body Wireless Communication,” IEEE Trans. Antennas Propag. vol. 61, no. 3, March 2013.

[30] M. Rizk, “Reduction, Telemetry, and Processing of Neural Data for a Fully Implantable Data Acquisition System,” PhD Thesis, Department of Biomedical Engineering, Duke University, 2008.

[31] T. Akin and K. Najafi, “A telemetrically powered and controlled implantable neural recording system with CMOS interface circuitry,” IEEE Proceedings of the Mediterranean Electrotechnical Conference (MELECON) (Piscataway, New Jersey, USA), vol. 2, pp. 545-548, 1994.

[32] R.D. Beach, F.v. Kuster, and F. Moussy, “Subminiature implantable potentiostat and modified commercial telemetry device for remote glucose monitoring,” IEEE Transactions on Instrumentation and Measurement, vol. 48, pp. 1239-1245, December 1999.

[33] A. Boyer, M. Sawan, M. Abdel-Gawad, S. Robin, and M.M. Elhilali, “Implantable selective stimulator to improve bladder voiding: design and chronic experiments in dogs,” IEEE Transactions on Rehabilitation Engineering, pp. 464-470, December 2000.

[34] H.J. Park, H.W. Nam, B.S. Song, and J.H. Cho, “Design of miniaturized telemetry module for bi-directional wireless endoscopy,” IEICE Transactions on Fundamentals on Electronics, Communications and Computer Sciences, pp. 1487-1491, June 2003.

[35] M.C. Shults, R.K. Rhodes, S.J. Updike, B.J. Gilligan, and W.N. Reining, “A telemetry-instrumentation system for monitoring multiple subcutaneously implanted glucose sensors, IEEE Transactions on Biomedical Engineering,” vol. 41, pp. 937-942, October 1994.

[36] B. Smith, Z. Tang, M.W. Johnson, S. Pourmehdi, M.M. Gazdik, J.R. Buckett, and P.H. Peckham, “An externally powered, multichannel, implantable stimulator-telemeter for control of paralyzed muscle,” IEEE Transactions on Biomedical Engineering, vol. 45, pp. 463-475, 1998.

[37] J.A. Von Arx and K. Najafi, “A wireless single-chip telemetry-powered neural stimulation system,” IEEE International Solid-State Circuits Conference (ISSCC), pp. 214-215, 15-17 February 1999.

[38] J. Black, M. Wilkins, P. Atanasov, and E. Wilkins, "Integrated sensor-telemetry system for in vivo glucose monitoring," Sensors & Actuators, B: Chemical, vol. 31, pp. 147-153, 1996.

[39] T.A. Cook, K.W. Fernald, T.K. Miller, and J.J. Paulos, "A Custom Microprocessor for Implantable Telemetry Systems," Proceedings of Third Annual IEEE Symposium on Computer-Based Medical Systems, vol. 24, pp. 412-417, June 1990.

[40] T. Eggers, C. Marschner, U. Marschner, B. Clasbrummel, R. Laur, and J. Binder, "Advanced hybrid integrated low-power telemetric pressure monitoring system for biomedical applications," IEEE Proceedings of Microelectromechanical Systems (MEMS), pp. 329-334, 2000.

[41] C. Enokawa, Y. Yonezawa, H.Maki, and M. Aritomo, "A microcontroller-based implantable telemetry system for sympathetic nerve activity and ECG measurement," Proceedings of the 19th International Conference - IEEE/EMBS (Chicago, Illinois, USA), vol. 5, pp. 2232-2234, 30 October - 2 November 1997.

[42] S. Farshchi, I. Mody, and J.W. Judy, "A TinyOS-based wireless neural interface," Proceedings of the 26th Annual International Conference of the IEEE Engineering in Medicine and Biology Society (EMBS) (San Francisco, California, USA), pp. 4334-4337, September 1-5, 2004.

[43] K.W. Fernald, T.A. Cook, T.K. Miller III, and J.J. Paulos, "A Microprocessor-Based Implantable Telemetry System," IEEE Computer, vol. 24, pp. 23-30, March 1991.

[44] K.W. Fernald, B.A. Stackhouse, J.J. Paulos, and T.K. Miller, "A System Architecture for Intelligent Implantable Biotelemetry Instruments," Proceedings of the Annual International Conference of the IEEE Engineering in Medicine and Biology Society (EMBS), vol. 11, pp. 1411-1412, November 1989.

[45] Z. Hamici, R. Itti, and J. Champier, "A high-effciency power and data transmission system for biomedical implanted electronic devices," Measurement Science and Technology, vol. 7, pp. 192-201, 1996.

[46] T. Harpster, S. Hauvespre, B. Stark, A. Vosoughi, and K. Najafi, "A passive humidity monitoring system for in-situ remote wireless testing of micropackages," IEEE Proceedings of MicroElectroMechanical Systems (MEMS), pp. 335-340, 2000.

[47] P.J. Kettlewell, M.A. Mitchell, and I.R. Meeks, "An implantable radio-telemetry system for remote monitoring of heart rate and deep body temperature in poultry," Computers and Electronics in Agriculture, vol. 17, pp. 161-175, 1997.

[48] P. Atanasov, S. Yang, C. Salehi, A.L. Ghindilis, and E. Wilkins, "Short-term canine implantation of a glucose monitoring-telemetry device," Medical Engineering & Physics, vol. 18, pp. 632-640, 1996.

[49] P. Atanasov, S. Yang, C. Salehi, A.L. Ghindilis, E. Wilkins, and D. Schade, "Implantation of a refillable glucose monitoring-telemetry device," Biosensors & Bioelectronics, vol. 12, pp. 669-680, 1997.

[50] R.D. Beach and F. Moussy, "Implantable biosensor telemetry and interface using an optocoupler," Proceedings of the IEEE 25th Annual Northeast Bioengineering Conference, pp. 115-116, April 8-9, 1999.

[51] M. Clements, K. Vichienchom, W. Liu, C. Hughes, E. McGucken, C. DeMarco, J. Mueller, M. Humayun, E. De Juan, J.Weiland, and R. Greenberg, "An implantable neuro-stimulator device for a retinal prosthesis," Digest of Technical Papers - IEEE International Solid-State Circuits Conference, pp. 216-217, 1999.

[52] D.D. DLima, C.P. Townsend, S.W. Arms, B.A. Morris, and C.W. Colwell Jr, "An implantable telemetry device to measure intra-articular tibial forces," Journal of Biomechanics, vol. 38, pp. 299-304, February 2005.

[53] C.E. Harrigal and R.A. Walters, "The development of a microprocessor controlled implantable device," IEEE Proceedings of the 1990 Sixteenth Annual Northeast Bioengineering Conference, pp. 137-138, March 1990.

[54] C.E. Harrigal, R.A. Walters, and R. Reynolds, "An implanted device for stimulating paralyzed vocal chords," Proceedings of the Annual International Conference of the IEEE Engineering in Medicine and Biology Society (EMBS), pp. 1368-1369, 29 October - 1 November 1992.

[55] T.S. Lande, J.-T. Marienborg, and Y. Berg, "Neuromorphic cochlea implants," Proceedings of the IEEE International Symposium on Circuits and Systems (ISCAS) (Geneva, Switzerland), vol. 4, pp. 401-404, May 28-31, 2000.

[56] R. Lerch, E. Spiegel, R. Hakenes R. Kakerow, H. Kappert, H. Kohlhaas, N. Kordas, M. Buchmann, T. Franke, Y. Manoli, and J. Muller, "A programmable mixed-signal ASIC for data acquisition systems in medical implants," IEEE International Solid State Circuits Conference (Piscataway, New Jersey, USA), vol. 38, pp. 162- 163, 1995.

[57] M. Min, T. Parve, V. Kukk, and A. Kuhlberg, "An implantable analyzer of bio-impedance dynamics - mixed signal approach," IEEE Instrumentation and Measurement (Budapest, Hungary), pp. 38-43, May 21-23, 2001.

[58] J. Mouine, K.A. Ammar, and Z. Chtourou, "A completely programmable and very flexible implantable pain controller," Proceedings of the 22nd Annual EMBS International Conference (Chicago IL., USA), pp. 603-622, July 2000.

[59] M. Sawan, F. Duval, M.M. Hassouna, J.S. Li, and M.M. Elhilali, "A new bladder stimulator: hand-held controller and miniaturized implant; preliminary results on dogs," Biomedical Instrumentation & Technology, pp. 143-149, March - April 1993.

[60] P. S. Hall and Y. Hao, "Antennas and propagation for body centric acommunications," in Proc. Eur. Conf. Antenna Propag. (EuCAP '06), Nice, France, 430864, 2006.

[61] A. Sani, M. Rajab, R. Foster, andY.Hao, "Antennas and propagation of implanted RFIDs for pervasive healthcare applications," Proc. IEEE, vol. 98, no. 9, pp. 1648–1655, Sep. 2010.

[62] F. Merli et al., "Implanted antenna for biomedical applications," in Proc. IEEE Antennas Propag. Soc. Int. Symp., pp. 1–4, 2008.

[63] P. Soontornpipit, "Design of ImplantableAntennas for Communication with Medical Implants," M.S. thesis, Dept. Elect. Comput. Eng., Utah State Univ, Logan, UT, USA, 2002.

[64] P. Soontornpipit, C. M. Furse, and Y. C. Chung, "Design of implantable microstrip antennas for communication with medical implants," IEEE Trans. Microw. Theory Tech., vol. 52, no. 8, pp. 1944–1951, Aug. 2004.

[65] W. Xia, K. Saito, M. Takahashi, and K. Ito, "Performances of an implanted cavity slot antenna embedded in the human arm," IEEE Trans. Antennas Propag., vol. 57, no. 4, pp. 894–899, Apr. 2009.

[66] F. Merli, L. Bolomey, J.-F. Zurcher, E.Meurville, and A. K. Skrivervik, "Versatility and tunability of an implantable antenna for telemedicine," in Proc. Eur. Conf. Antenna Propag. (EuCAP '11), pp. 2487–2491, Apr. 2011.

[67] G. A. Thiele et al., "On the accuracy of the transmission line model of the folded dipole," IEEE Trans. Antennas Propag., vol. AP-28, no. 5, pp. 700–703, Sep. 1980.

[68] S. Hayashida et al., "A wideband folded loop antenna for handsets," IEICE Trans. Com., vol. J86-B, no. 9, pp. 1799–1805, Sep. 2003.

[69] Dielectric Properties of Body Tissues (IFAC), [Online]. Available: http://niremf.ifac.cnr.it/tissprop/

[70] Y. Uno, K. Saito, M. Takahashi, and K. Ito, "Structure of cylindrical tissue equivalent phantom for medical applications," in Proc. Int. Conf. Electromagn. Adv. Applicat. (ICEAA '10), Sydney, Australia, pp. 406–409, Sep. 2010.

[71] K. Ito, "Human body phantoms for evaluation of wearable and implantable antennas," in Proc. Eur. Conf. Antennas Propag. (EuCAP '07), pp. 1–6, 2007.

[72] ANT-403-SP data sheet, Antenna Factor, 159 Ort Lane, Merlin, OR 97532, Oct. 2008.

[73] Shi-Chang Gao, Le-Wei Li, Tat-Soon Yeo and Mook-Seng Leong, "Small Dual-Frequency Microstrip Antennas,"IEEE Trans. Veh. Technol., vol. 51, no. 1,pp.28-36, Jan. 2002.

[74] Linx Technologies, [Online]. Available: www.linxtechnologies.com

[75] M. S. Islam, Karu. P. Esselle, Ladislau M., David Bull. and Paul M. Pilowsky, "An Implantable Hilbert PIFA Antenna for an RFID- Based Telemetry System," ICEAA 2013, Turin, Italy, Sept. 2013.

[76] M. S. Islam, Karu. P. Esselle, Ladislau M., David Bull. and Paul M. Pilowsky, "An Implantable PIFA Antenna with a J-Shaped Proximity Feed for RFID Telemetry," ICECOM 2013, Croatia, Oct. 2013.

[77] M. K. T. Al-Nuaimi, "Mutual Coupling Evaluation of Dual-Miniaturized PIFA Antenna Array for MIMO Terminals," 11th European,Wireless Conference 2011 - Sustainable Wireless Technologies (European Wireless), pp. 1-4, 2011.

[78] M. Komulainen, M. Berg, H. Jantunen, E. T. Salonen, and C. Free, "A Frequency Tuning Method for a Planar Inverted-F Antenna," IEEE Transactions on Antennas and Propagation, vol. 56, pp. 944-950, 2008.

[79] C. R. Rowell and R. D. Murch, "A compact PIFA suitable for dual-frequency 900/1800- MHz operation," IEEE Transactions on Antennas and Propagation, vol. 46, pp. 596-598, 1998.

[80] C. Horng-Dean and T. Yu-Hung, "Low-Profile PIFA Array Antennas for UHF Band RFID Tags Mountable on Metallic Objects," IEEE Transactions on Antennas and Propagation, vol. 58, pp. 1087-1092, 2010.

[81] M. F. Abedin and M. Ali, "Modifying the ground plane and its effect on planar inverted- F antennas (PIFAs) for mobile phone handsets," IEEE Antennas and Wireless Propagation Letters, vol. 2, pp. 226-229, 2003.

[82] R. Hossa, A. Byndas, and M. E. Bialkowski, "Improvement of compact terminal antenna performance by incorporating open-end slots in ground plane," IEEE Microwave and Wireless Components Letters, vol. 14, pp. 283-285, 2004.

[83] B. B. Mandelbrot, "The Fractal Geometry of Nature," New York: W. H. Freeman. 1977.

[84] C. Puente, J. Romeu, R. Pous, J. Ramis, and A. Hijazo, "Small but Long Koch Fractal Monopole," Electronics Lett., vol. 34, no. 1, pp. 9-10, 1998.

[85] C. Puente, J. Romeu, R. Pous, X. Garcia, and F. Benitez, "Fractal Multiband Antenna Based on the Sierpinski Gasket," Electronics Lett., vol. 32, no. 1, pp. 1- 2, Jan. 1996.

[86] C. Puente, M. Navarro, J. Romeu, and R. Pous, "Variations on the Fractal Sierpinski Antenna Flare Angle," in Proc. IEEE AP-S Int. Symp. Dig. vol. 4, pp. 2340 - 2343, June 1998.

[87] C. Puente, J. Romeu, and A. Cardama, "The Koch Monopole: A Small Fractal Antenna," IEEE Trans. Antennas Propagat., vol. 48, no. 11, pp. 1773-81, Nov., 2000.

[88] D. H. Werner, A. R. Bretones, and B. R. Long, "Radiation Characteristics of Thin-Wire Ternary Fractal Trees," Electronics Lett., vol. 35, no. 8, pp. 609-10, 1999.

[89] S. R. Best, "A comparison of the resonant properties of small space-filling fractal antennas," IEEE Antennas Wireless Propagat. Lett., vol. 2, no. 1, pp.197–200, 2003.

[90] Z. Jinhui, A. Hoorfar, N. Engheta, "Peano antennas," IEEE Antennas Wireless Propagat. Lett., vol. 3, pp. 71-674, 2004.

[91] E. Khouly, H.Ghali, and S. A. Khamis, "High Directivity Antenna Using a Modified Peano Space-Filling Curve," IEEE Antennas Wireless Propagat. Lett., vol. 6, pp. 405-407, 2007.

[92] J. Anguera, C. Puente, E. Martinez, and E. Rozan, "The Fractal Hilbert Monopole: A two Dimensional Wire," Microwave Opt. Technol. Lett., vol. 36, no. 2, pp. 102-104, Jan. 20, 2003.

[93] K. J. Vinoy, "Fractal shaped antenna elements for wide and multi-band wireless applications," Ph.D. Dissertation, Pennsylvania State Univ., 2002.

[94] A.T.M. Sayem and M. Ali, "Characteristics of Miniaturized Microstrip-Fed Hilbert Slot Antenna," Progress in Electromagnetic Research, PIER 56, 1-18, 2006.

[95] Y. Kim and D. L. Jaggard, "The fractal random array", Proc. IEEE, vol. 74, issue 9, pp. 1278-1280, Sept. 1986.

[96] D. H. Werner, R. L. Haupt, and P. L. Werner, "Fractal antenna engineering: The theory and design of fractal antenna arrays," IEEE Antennas Propagat. Mag., vol. 41, no. 5, pp. 37–59, Oct. 1999.

[97] J. Zhu, A. Hoorfar, and N. Engheta, "Bandwidth, Cross-Polarization, and Feed- Point Characteristics of Matched Hilbert Antennas,'' IEEE Antennas Wireless Propagat. Lett., vol. 2, pp. 2-4, 2003.

[98] D. Gala, J. Soler, C. Puente, C. Borja, and J. Anguera, "Miniature Microstrip Patch Antenna Loaded With a Space-Filling Line Based on the Fractal Hilbert Curve," Microwave Opt. Technol. Let., vol. 38, no. 4, pp. 311-312, Aug. 2003.

[99] M. Z. Azad and M. Ali, "A Miniaturized Hilbert PIFA for Dual Band Mobile Wireless Applications," IEEE Antennas Wireless Propagat. Lett., vol. 4, pp. 59- 62, 2005.

[100] M. Z. Azad and M. Ali, "A Miniaturized Implantable Antenna for GPS Application,'' in Proc. IEEE AP-S Int. Symp. Dig., pp. 1103–1106, July 2006.

[101] Global Safety Solutions and Management Pty Ltd, [Online]. Available: www.gssm.com.au

[102] BCS International, [Online]. Available: www.bcsinnovations.com.au

[103] H. W. Son and G. Y. Choi, "Orthogonally proximity-coupled patch antenna for a passive RFID tag on metallic surfaces," Microw. Opt. Technol. Lett., vol. 49, no. 3, pp. 715–717, 2007.

[104] J. S. Kim, W. Choi, and G. Y. Choi, "UHF RFID tag antenna using two PIFAs embedded in metallic objects," Electron. Lett., vol. 44, no. 20, pp. 1181–1182, 2008.

[105] K. H. Kim, J. G. Song, D. H. Kim, H. S. Hu, and J. H. Park, "Fork-shaped RFID tag antenna mountable on metallic surfaces, "Electron. Lett. , vol. 43, no. 25, pp. 1400–1402, 2007.

[106] M. L. Ng, K. S. Leong, and P. H. Cole, "A small passive UHF RFID tag for metallic item identification," in Proc. Int. Tech. Conf. Circuits/Syst., Comput. Commun., pp. 141–144, Jul. 2006.

[107] C. Cho, H. Choo, and I. Park, "Design of planar RFID tag antenna for metallic objects," Electron. Lett., vol. 44, no. 3, pp. 175–177, 2008.

[108] S. L. Chen and K. H. Lin, "A slim RFID tag antenna design for metallic object applications, "IEEE Antennas Wireless Propag. Lett., vol. 7, pp.729–732, 2008.

[109] P. V. Nikitin, K. V. S. Rao, S. F. Lam, V. Pillai, R. Martinez, and H. Heinrich, "Power reflection coefficient analysis for complex impedances in RFID tag design," IEEE Trans. Microw. Theory Tech., vol. 53, no. 9, pp. 2721–2725, Sep. 2005.

[110] K. V. S. Rao, S. F. Lam, and P. V. Nikitin, "Wideband metal mount UHF RFID tag," in Proc. IEEE AP-S Int. Symp., pp. 1–4, 2008.

[111] H. Kwon and B. Lee, "Compact slotted planar inverted-F RFID tag mountable on metallic objects," Electron. Lett. , vol. 41, no. 24, pp. 1308–1310, 2005.